

KODIAQ-Z: METALS AND BARYONS IN THE COOL INTERGALACTIC AND CIRCUMGALACTIC GAS AT $2.2 \lesssim z \lesssim 3.6$

NICOLAS LEHNER,¹ CLAIRE KOPENHAFER,² JOHN M. O'MEARA,³ J. CHRISTOPHER HOWK,¹ MICHELE FUMAGALLI,^{4,5} J. XAVIER PROCHASKA,^{6,7} AYAN ACHARYYA,^{8,9,10} BRIAN W. O'SHEA,¹¹ MOLLY S. PEEPLES,^{8,9} JASON TUMLINSON,^{8,9} AND CAMERON B. HUMMELS¹²

¹Department of Physics, University of Notre Dame, Notre Dame, IN 46556

²Department of Physics and Astronomy, Department of Computational Mathematics, Science, and Engineering, Michigan State University, East Lansing, MI 48824

³W.M. Keck Observatory 65-1120 Mamalahoa Highway Kamuela, HI 96743

⁴Dipartimento di Fisica G. Occhialini, Università degli Studi di Milano Bicocca, Piazza della Scienza 3, 20126 Milano, Italy

⁵INAF - Osservatorio Astronomico di Trieste, via G. B. Tiepolo 11, 34143 Trieste, Italy

⁶UCO/Lick Observatory, Department of Astronomy & Astrophysics, University of California Santa Cruz, 1156 High Street, Santa Cruz, CA 95064

⁷Kavli Institute for the Physics and Mathematics of the Universe (WIP), 5-1-5 Kashiwanoha, Kashiwa, 277-8583, Japan

⁸Space Telescope Science Institute, 3700 San Martin Drive, Baltimore, MD 21218

⁹Department of Physics & Astronomy, Johns Hopkins University, 3400 N. Charles Street, Baltimore, MD 21218

¹⁰Research School of Astronomy and Astrophysics, Australian National University, Weston Creek, ACT 2611, Australia

¹¹Department of Computational Mathematics, Science, and Engineering, Department of Physics and Astronomy, National Superconducting Cyclotron Laboratory, Michigan State University, East Lansing, MI 48824

¹²Department of Astronomy, California Institute of Technology, Pasadena, CA 91125

ABSTRACT

We present the KODIAQ-Z survey aimed to characterize the cool, photoionized gas at $2.2 \lesssim z \lesssim 3.6$ in 202 H I-selected absorbers with $14.6 \leq \log N_{\text{HI}} < 20$, i.e., the gaseous interface between galaxies and the intergalactic medium (IGM). We find that the $14.6 \leq \log N_{\text{HI}} < 20$ gas at $2.2 \lesssim z \lesssim 3.6$ can be metal-rich gas ($-1.6 \lesssim [\text{X}/\text{H}] \lesssim -0.2$) as seen in damped Ly α absorbers (DLAs); it can also be very metal-poor ($[\text{X}/\text{H}] < -2.4$) or even pristine gas ($[\text{X}/\text{H}] < -3.8$) not observed in DLAs, but commonly observed in the IGM. For $16 < \log N_{\text{HI}} < 20$ absorbers, the frequency of pristine absorbers is about 1%–10%, while for $14.6 \leq \log N_{\text{HI}} \leq 16$ absorbers it is 10%–20%, similar to the diffuse IGM. Supersolar gas is extremely rare (< 1%) in this gas. The factor of several thousand spread from the lowest to highest metallicities and large metallicity variations (a factor of a few to > 100) between absorbers separated by less than $\Delta v < 500 \text{ km s}^{-1}$ imply that the metals are poorly mixed in $14.6 \leq \log N_{\text{HI}} < 20$ gas. We show that these photoionized absorbers contribute to about 10% of the cosmic baryons and 30% of the cosmic metals at $2.2 \lesssim z \lesssim 3.6$. We find the mean metallicity increases with N_{HI} , consistent with what is found in $z < 1$ gas. The metallicity of gas in this column density regime has increased by a factor ~ 8 from $2.2 \lesssim z \lesssim 3.6$ to $z < 1$, but the contribution of the $14.6 \leq \log N_{\text{HI}} < 19$ absorbers to the total metal budget of the universe at $z < 1$ is half that at $2.2 \lesssim z \lesssim 3.6$, indicating a substantial shift in the reservoirs of metals between these two epochs. We compare the KODIAQ-Z results to FOGGIE cosmological zoom simulations. The simulations show an evolution of $[\text{X}/\text{H}]$ with N_{HI} similar to our observational results. Very metal-poor absorbers with $[\text{X}/\text{H}] < -2.4$ at $z \sim 2$ –3 in these simulations are excellent tracers of inflows, while higher metallicity absorbers are a mixture of inflows and outflows.

Keywords: Circumgalactic medium (1879) — Damped Lyman-alpha systems — Intergalactic medium (813) — Lyman limit systems (981) — Metallicity (1031) — Quasar absorption line spectroscopy (1317)

1. INTRODUCTION

The intergalactic medium (IGM) and the circumgalactic medium (CGM) are massive reservoirs of baryons

(e.g., Fukugita et al. 1998; McQuinn 2016; Macquart et al. 2020) and major fuel sources for star formation in galaxies (e.g., Tumlinson et al. 2017). They play a vital role in the formation and evolution of galactic and large-scale structures in the universe. The empirical and theoretical characterizations of the CGM and IGM before, during, and after the peak of cosmic star formation ($z \sim 2$) are therefore of prime importance to understanding their role in the evolution of galaxies. Gathering data that can probe both the low and high redshift universe is critical for robustly constraining the evolution of these cosmic structures. This is also the best route to fully test always-improving cosmological simulations. Modern numerical simulations are now reaching new milestones in fidelity. Notably a new generation of simulations boasts unprecedented high spatial resolution, even in the more diffuse regions of the simulation boxes (e.g., van de Voort et al. 2019; Hummels et al. 2019; Peebles et al. 2019; Suresh et al. 2019). This allows for far more realistic modeling of the CGM and IGM and their inter-relationships with galaxies.

Over the last few years, our group has engaged in several H I-selected surveys at both low and high redshifts to target absorbers in the H I column density range $15 \lesssim \log N_{\text{HI}} \lesssim 19$. This column density interval spans a range of physical environments from the diffuse IGM (Ly α forest, hereafter LYAF) to the denser portions of the CGM and the edges of galaxy disks. Following Lehner et al. (2018), we describe absorbers as strong Ly α forest systems (SLFSs, $\log N_{\text{HI}} = 14.5\text{--}16.2$), as partial Lyman systems (pLLSs, $\log N_{\text{HI}} = 16.2\text{--}17.2$), or as Lyman limit systems (LLSs, $\log N_{\text{HI}} = 17.2\text{--}19$). Below this range is the LYAF ($\log N_{\text{HI}} \lesssim 14.5$) and above it are the super-LLSs (SLLSs, $19.0 - 20.3$, a.k.a. the sub-damped Ly α absorbers) and the damped Ly α absorbers (DLAs, ≥ 20.3). With overdensities between the diffuse IGM (probed by the LYAF) and galaxies (probed by DLAs), the SLFSs, pLLSs, and LLSs spanning $15 \lesssim \log N_{\text{HI}} \lesssim 19$ should be at the heart of the exchange of matter between galaxies, their CGM, and the diffuse IGM.

One of the main goals of our H I absorption surveys is to provide a census of the chemical enrichment of the absorbers with $14.6 \lesssim \log N_{\text{HI}} \lesssim 20$ over cosmic time (e.g., the COS CGM compedium, CCC, at low redshift—Lehner et al. 2018, 2019; Wotta et al. 2019, and see also Lehner et al. 2013; Wotta et al. 2016, the HD-LLS survey—Prochaska et al. 2015; Fumagalli et al. 2016b, the KODIAQ-Z survey—Lehner et al. 2016; this paper). The metallicity of the absorbers is a direct measure of their metal enrichment and a key diagnostic of their origins. The metallicity provides direct informa-

tion on how efficient (or not) galaxies are at enriching their immediate surroundings and beyond and on the level of metal mixing in the diffuse regions of the universe. The H I selection of our surveys provides a relatively unbiased way to obtain a census of the metallicity since selecting on hydrogen is sensitive to both very low and very high metallicities.

While pLLSs and LLSs have been found often in the CGM of galaxies at both low and high redshift (e.g., Lehner et al. 2009, 2013; Prochaska et al. 2017b; M. Berg et al. 2021, in prep.), there is growing evidence that at least some of the pLLSs and LLSs with very low metallicity may probe the denser IGM (very low metallicity being $[\text{X}/\text{H}] \lesssim -1.4$ at $z \lesssim 1$, M. Berg et al. 2021, in prep., and $[\text{X}/\text{H}] \lesssim -3$ at $2 \lesssim z \lesssim 3.5$, Fumagalli et al. 2011a, 2016a; Crighton et al. 2016; Lofthouse et al. 2020)¹. There are, however, also counter-examples at both low and high redshifts where very low metallicity absorbers are found in vicinity of galaxies (e.g., Ribaudo et al. 2011; Fumagalli et al. 2016a). Fully characterizing the metallicity distributions of the SLFSs, pLLSs, and LLSs at low and high z directly probes the metallicity enrichment (or lack of it) relative to galaxies and their inner regions probed by DLAs and SLLSs. This technique can also assess the amount of pristine gas in these overdense regions of the universe and how it compares to the more diffuse IGM probed by LYAF absorbers (Fumagalli et al. 2011a).

In previous papers, our group presented a sample of 261 $z < 1$ absorbers with $15 \lesssim \log N_{\text{HI}} \lesssim 19$ (Lehner et al. 2018, 2019; Wotta et al. 2019, hereafter, CCCI; CCC III; CCCII). This sample includes an unexpectedly large fraction of metal poor absorbers, many of which have metallicities $[\text{X}/\text{H}] < -2$ implying little chemical enrichment since $z \sim 2\text{--}3$.

The finding that metal-poor absorbers with $[\text{X}/\text{H}] \leq -1.4$ represents about half of the population of $z \lesssim 1$ absorbers with $15 \lesssim \log N_{\text{HI}} \lesssim 19$ was unanticipated. This is because neither the LYAF (owing, in retrospect, to a lack of sensitivity) nor the SLLSs/DLAs hinted at the presence and importance of such low-metallicity gas at low redshift. Although not fully appreciated at the time, there was, however, already some evidence of very low metallicity gas at low redshift based on individual studies of LLSs (Cooksey et al. 2008; Ribaudo et al. 2011, and see also Tripp et al. 2005 for a rare example of a primitive SLLS at $z \sim 0.06$). CCC also reveals that at $z < 1$ there is no evidence of pristine gas, implying

¹ For the metallicity, we use conventional squared-bracket notation $[\text{X}/\text{H}] \equiv \log N_{\text{X}}/N_{\text{H}} - \log(\text{X}/\text{H})_{\odot}$, where X is an α -element, unless otherwise stated.

> 99% gas with $15 \lesssim \log N_{\text{HI}} \lesssim 19$ has been polluted by $z \lesssim 1$, even if it is only at very low level. Low-redshift photoionized gas with $15 \lesssim \log N_{\text{HI}} \lesssim 19$ has a wide range of metallicities observed ($-3 \lesssim [\text{X}/\text{H}] \lesssim +0.4$) and can show large metallicity variations (factor up to 25) over small redshift/velocity separation ($\Delta v < 300 \text{ km s}^{-1}$), implying these absorbers sample a highly inhomogeneous medium probed by these absorbers. The CCC results beg the questions: are these properties unique to $z \lesssim 1$? how do they evolve from earlier times, across the peak of cosmic star formation at $z \sim 2.5$.

To address these questions, we present here the KODIAQ-Z survey (Keck Database of Ionized Absorbers toward Quasars), a survey designed to identify H I absorbers with $\log N_{\text{HI}} \gtrsim 14.5$ at $z > 2$ in Keck HIRES spectra available in the KODIAQ database (O’Meara et al. 2015, 2017) and determine their metallicities. Owing to the higher sensitivity of the Keck HIRES data than the Hubble Space Telescope (HST) COS Origins Spectrograph data, we can probe low N_{HI} absorbers at high redshift and still be sensitive to low metallicity gas. In fact, due to the new sensitivity gained with 8–10 m ground-based telescopes, early studies on the metal enrichment at high redshift largely focused mostly on IGM absorbers with $\log N_{\text{HI}} \lesssim 14.5$ (e.g., Songaila 1998; Ellison et al. 2000; Schaye et al. 2003; Aguirre et al. 2004; Simcoe et al. 2004). Our sample of H I-selected absorbers consists of 155 SLFs, 24 pLLSs, 16 LLSs, and 7 SLLSs at $2.2 \lesssim z \lesssim 3.6$, totaling 202 absorbers, 196 of them with $14.5 \lesssim \log N_{\text{HI}} \lesssim 19$. On account of the nature of the Keck HIRES data, the sample of pLLSs and LLSs has only marginally increased by a factor 1.3 compared to our earlier pilot survey (Lehner et al. 2016). However, in this paper, we undertake a systematic search and characterization of H I-selected SLFs.² In our analysis, we include the H I-selected absorbers from the HD-LLS survey (Prochaska et al. 2015; Fumagalli et al. 2016b), which adds another 46 LLSs, increasing the total sample to 241 absorbers with $14.5 \lesssim \log N_{\text{HI}} \lesssim 20$. The HD-LLS survey is directly complementary to KODIAQ-Z since most of the HD-LLS absorbers have $\log N_{\text{HI}} \gtrsim 17.5$ while KODIAQ-Z largely samples gas with lower N_{HI} .

The main goals of the present paper are to determine the metallicity distributions of these absorbers, assess how their metallicity changes with N_{HI} and z , and provide a robust limit on the amount of pristine gas at high redshift. We also present and discuss the physi-

cal properties of these absorbers and use these results to estimate the metal and baryon budgets of the cool photoionized CGM at $z \gtrsim 2.2$ –3.6. Our paper is organized as follows. In §2, we describe the survey design of KODIAQ-Z, the search of the H I-selected absorbers, and the sample of SLFs, pLLSs, and LLSs. In §3, we present the methods to derive the column densities of the metals and H I for each absorber, while in §4 we present basic statistical properties of our sample (z , N_{HI} , and the Doppler parameter b). In §5, we present ionization modeling of the KODIAQ-Z absorbers and assumptions for estimating their metallicity. Our main results on the metallicities of the H I-selected absorbers are presented in §6. In §7, we derive the physical properties of the absorbers, including their density (n_{H}), total column density (N_{H}), temperature, and linear scale ($l \equiv N_{\text{H}}/n_{\text{H}}$), and we model the neutral fraction as a function of N_{HI} in the range $14.6 \leq \log N_{\text{HI}} \leq 20$. In §8, we estimate the cosmic metal and baryon budgets of these absorbers. In §9, we compare the KODIAQ-Z results to the properties of the gas in cosmological zoom simulation from the Figuring Out Gas & Galaxies in Enzo (FOGGIE) project (Peeples et al. 2019; Corlies et al. 2020) and use these simulations to gain insight on the connection of the $14.5 \lesssim \log N_{\text{HI}} \lesssim 20$ gas depending on its metallicity with galaxies. In §10, we discuss the results, and in §11, we summarize our main conclusions.

2. SURVEY DESIGN, DATABASE, AND OBSERVATIONS

2.1. Sample Selection Criteria

Our survey is based on a search for H I absorption in the KODIAQ DR2 database (O’Meara et al. 2017) of 300 QSO spectra observed with HIRES. The QSOs useful for our survey lie at $2 \lesssim z_{\text{em}} \lesssim 4.5$, limiting the sample size to 235 QSOs. We also searched in the spectra of higher redshift ($z_{\text{em}} > 4.5$) QSOs, but the LYAF is too dense to allow us to reliably determine the H I and metal-line column densities at these redshifts. The lower redshift-threshold $z \gtrsim 2$ is required to have wavelength coverage of at least Ly α and Ly β .³ In each of the QSO spectra, we search for absorbers with H I column density $\log N_{\text{HI}} \gtrsim 14.5$. This contrasts with our KODIAQ-ZI survey where our search of H I absorbers was limited to absorbers with $\log N_{\text{HI}} \gtrsim 16.2$ (to match our initial lower z survey, L13) and was by no means a

² Simcoe et al. (2004) surveyed the metallicity of the IGM at $2.2 \lesssim z \lesssim 2.8$. While they focused on absorbers with $\log N_{\text{HI}} < 14.5$, they also included about 30–40 SLFs as part of their survey.

³ The Keck HIRES spectra are normalized and therefore we cannot rely on the break at the Lyman limit to estimate N_{HI} for the pLLSs and LLSs, relying solely on the Lyman series, and hence limiting the sample we can estimate accurately N_{HI} .

systematic and complete examination of the KODIAQ DR1 database (O’Meara et al. 2015).

A major difference (besides the redshift probed) with the low redshift survey CCC (CCCI) is that all the HIRES spectra are flux-normalized for the coaddition of the individual exposures and echelle orders (O’Meara et al. 2015, 2017). This makes determination of large-scale flux decrements (e.g., at the Lyman limit break or damping wings of DLAs) unreliable. Therefore, to estimate the H I column density we can rely only on the absorption observed in the Lyman-series transitions; specifically, the break at the Lyman limit for absorbers with $\log N_{\text{HI}} \gtrsim 16.5$ cannot be used. This limits the sample size of absorbers with $\log N_{\text{HI}} \gtrsim 17.2$ because it requires enough weak Lyman transitions that are not too contaminated to derive N_{HI} (see §3.2). For absorbers with $\log N_{\text{HI}} \gtrsim 18$, damping wings start to be observable in Ly α absorption, and therefore this transition can be used to derive N_{HI} depending on the level of contamination of the absorption from the LYAF. On the other hand, while CCC is limited to absorbers with $\log N_{\text{HI}} \gtrsim 15.3$ owing to the need to be sensitive to metallicities [X/H] $\lesssim -1$, the typically higher signal-to-noise ratios (SNRs) and higher spectral resolution of the Keck HIRES spectra allow us to probe lower N_{HI} , down to the LYAF threshold of about $\log N_{\text{HI}} \simeq 14.5$, and still be sensitive to metallicity with [X/H] $\lesssim -2$. Although with very high SNR Keck HIRES spectra, a strong limit ([X/H] $\lesssim -2$) on the metallicities can be placed down to $\log N_{\text{HI}} \simeq 13.6$ (e.g., Simcoe et al. 2004), our lower limit on N_{HI} was selected to correspond to the limit between the diffuse IGM and denser IGM/diffuse CGM. Following Schaye (2001a), a 14.5 dex limit on the H I column density corresponds to an overdensity of $\delta \gtrsim 5$ at $z \sim 2.8$ (about the average redshift of the absorbers in our sample, see §4.1).

2.2. Search for H I Absorbers in the KODIAQ database

To identify the strong H I absorption, we developed an automated search tool to help identify the Lyman series transitions from 1215 Å (Ly α) down to 917 Å. In Fig. 1, the colored profiles show single-component Voigt models for absorbers with a Doppler parameter $b = 25 \text{ km s}^{-1}$ and $\log N_{\text{HI}} = 15, 16, 17, 18$. That b -value is selected based on previous profile fitting of strong H I absorbers at similar redshifts (e.g., KODIAQ-ZI); as we will see below that choice is close *a posteriori* to the mean b value in our sample. We use these H I models to set the following criteria for our automatic search: 1) Ly α must have flux $F_\lambda \leq 0 \gtrsim 0.4 \text{ \AA}$ in contiguous pixels; 2) at the average velocity/redshift (v_c) of the identified Ly α , the flux in the Ly β absorption must also reach

$F_\lambda \leq 0$; 3) at v_c , we also require there is substantial absorption in at least Ly γ (and Ly δ if there is wavelength coverage of that transition). Additional conditions were added to ensure that when a DLA or a SLLS is present, the search-program would not continue to look for additional absorbers near the redshift of the DLA or SLLS. For this search, we therefore require for each QSO wavelength coverage of at least Ly α , Ly β , and Ly γ . However, since the damping wings of Ly α can be used to determine N_{HI} if $\log N_{\text{HI}} \gtrsim 18.5$, we also undertook a separate search that relies solely on Ly α where the flux $f_\lambda \simeq 0$ over a wavelength width of $\gtrsim 2 \text{ \AA}$. *A posteriori*, only a few of these very strong H I absorbers ended up in our sample owing to the fact that the KODIAQ spectra are normalized prior to coaddition, and the normalization was often not reliable enough to model the damping wings for these absorbers, especially the strong SLLSs and DLAs (DLAs being not an issue since they are not part of our survey).

For each candidate absorber, our search tool created a stack of H I transitions as shown on Fig. 1. Over 3000 candidates were created, many of these being false positives owing to the large contamination from the LYAF and other metal lines. That number is still small enough that a quick look to the stack of H I profiles could easily weed out most of the false positives using the Voigt models as a guide. This vetting led the sample to be reduced by more than a third to 949 candidate absorbers, for which we show their redshift distribution in Fig. 2. In this figure, we also show the redshift distribution of the QSOs. About 83% of the candidate absorbers are at $2.2 \leq z_{\text{abs}} \leq 3.6$; candidate absorbers at $z_{\text{abs}} \leq 2$ are detected solely based on Ly α .

To assemble our final sample for metallicity determinations, we considered both the ability to estimate N_{HI} and the coverage of metal ions (in order to be able to estimate the metallicity). For each candidate absorber, we therefore created another set of stack of velocity profiles with Ly α , Ly β , Ly δ , and some key metal transitions used in the estimation of the metallicity (including Si II, Si III, Si IV, C II, C III, C IV, Al II, Al III, Fe II, O I, and O VI) to assess if there is enough metal-ion coverage to determine the metallicity. After all the measurements are done (detailed in §3), the final sample size sample consists of 202 absorbers, i.e., $\approx 7\%$ of the candidates from the initial automatic search were absorbers where we could place a robust estimate on N_{HI} and metal-line column densities (including strong upper limits). The final KODIAQ-Z sample includes 155 SLFSs, 24 pLLSs, 16 LLSs, and 7 SLLSs.

2.3. Comparison Samples

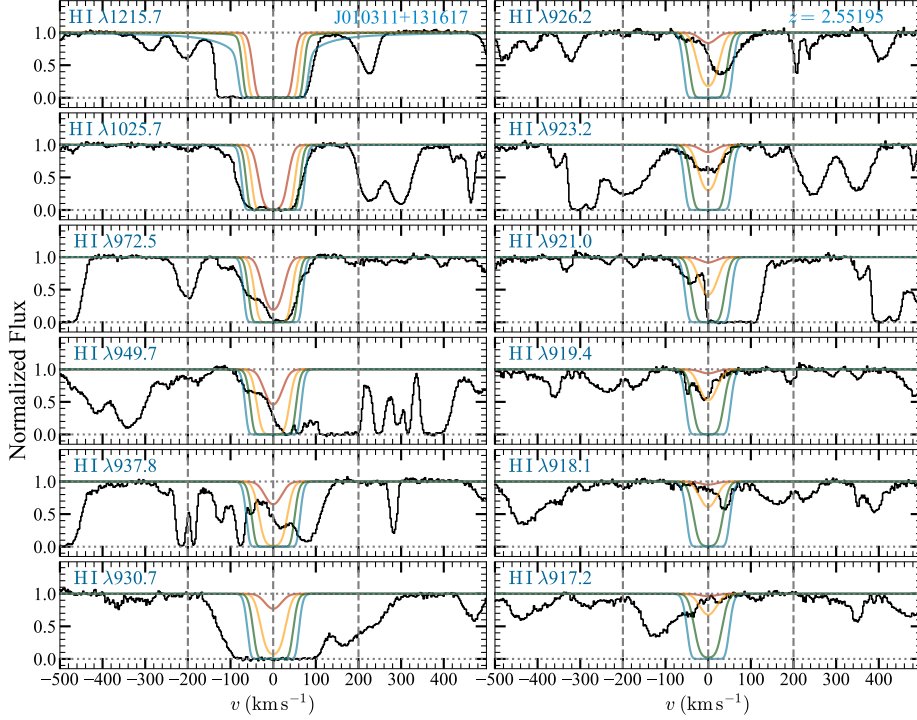


Figure 1. Example of an absorber identified by our automatic searching tool. For each identified candidate-absorber, a similar figure is created that shows the normalized spectra (in black) of the H I transitions from the 1215 to 917 Å transitions as function of the velocity in the redshift rest-frame. The colored profiles are Voigt profiles for an absorber with $b = 25 \text{ km s}^{-1}$ and $\log N_{\text{HI}} = 15, 16, 17, 18$ and are used to help assess the level of contamination in each transition. Ultimately for this candidate two absorbers were identified at $z = 2.55125$ and 2.55216 (corresponding to $v \simeq -50$ and $+17 \text{ km s}^{-1}$ in this figure).

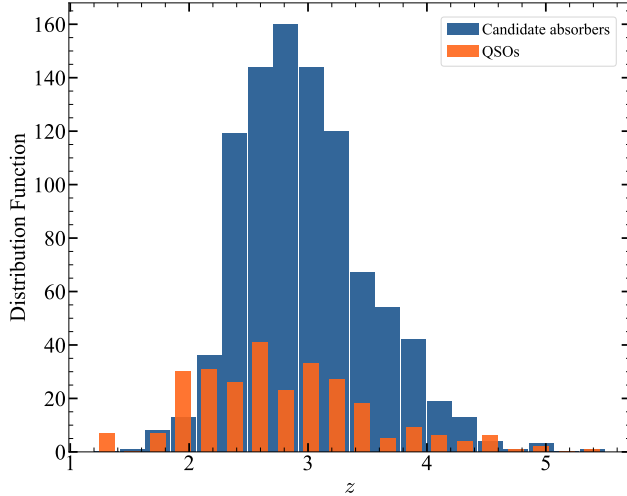


Figure 2. Distribution of the redshifts for the QSOs and the candidate absorbers from the automatic search in KODIAQ DR2.

One of the goals of our survey is to determine how the metallicity changes with N_{HI} at similar redshifts and between low and high z . For the low redshift, we use results from our CCC survey, including the compilation of H I absorbers at $\log N_{\text{HI}} \geq 19$ (see CCCI;

CCCI; CCCIII and references therein). At $z \gtrsim 2$, we use two surveys: 1) the HD-LLS survey (Prochaska et al. 2015; Fumagalli et al. 2016b), a survey of absorbers with $17.3 \leq \log N_{\text{HI}} < 20.3$ at $z = 2\text{--}4.39$, $\sim 95\%$ of the absorbers having H I column densities in the range $18 \leq \log N_{\text{HI}} < 20.3$ (which is directly complementary to KODIAQ-Z; HD-LLS also follows the same H I-selection); and 2) the DLA survey by Rafelski et al. (2012), hereafter the R12-DLA survey. The ease of access to the data while working in the early stage of KODIAQ-Z, including the metal and H I column densities for the HD-LLS, mostly dictated our use of these surveys. We note that the Magellan DLA survey by Jorgenson et al. (2013) has essentially the same metallicity distribution as R12-DLA in our redshift of interest $2.2 \lesssim z \lesssim 3.6$ (see below). The recent XQ-100 survey of SLLSs by Berg et al. (2021) shows also the same metallicity distributions as in HD-LLS.

For the R12-DLA, we adopt the metallicities from the α -elements (or Zn if not available). For the HD-LLS, we re-estimate all the metallicities using the same EUVB adopted in CCC in order to avoid mismatch in the comparisons of the metallicities although as we will show in §5.3, the systematic error arising from the EUVB in the photoionization modeling of the absorbers is much

smaller (in fact negligible) at $z > 2$ than at lower redshift, especially for the strong LLSs and SLLSs that are part of the HD-LLS survey.

3. ESTIMATION OF THE COLUMN DENSITIES

Our analysis follows closely that undertaken in CCC to estimate the column densities of H I and metal ions. Throughout we assume the atomic parameters (central wavelengths and f -values) listed in Morton (2003). For each absorber, we first attempt to estimate the H I column density since that step is necessary to estimate the metallicity of the absorbers. For H I, we use a combination of different methods (apparent optical depth–AOD–method Savage & Sembach 1991, curve-of-growth–COG–method, and Voigt profile fitting–PF–method), while for the metal ions, we use solely the AOD method. We employ several methods to estimate the H I column densities on the account that the contamination, blending, and saturation effects are more severe than for the metal lines (see Fig. 1).

3.1. Metal Column Densities

Although we only estimate the column densities of the metal species once the H I transitions were modeled (and hence the candidate absorber became a selected absorber), we first describe the metal lines as we use only the AOD method to extract the properties of the absorption. In this method, the absorption profiles are converted into apparent optical depth per unit velocity, $\tau_a(v) = \ln[F_c(v)/F_{\text{obs}}(v)]$, where $F_c(v)$ and $F_{\text{obs}}(v)$ are the modeled continuum and observed fluxes as a function of velocity. The AOD, $\tau_a(v)$, is related to the apparent column density per unit velocity, $N_a(v)$, through the relation $N_a(v) = 3.768 \times 10^{14} \tau_a(v)/(f\lambda(\text{\AA})) \text{ cm}^{-2} (\text{km s}^{-1})^{-1}$, where f is the oscillator strength of the transition and λ is the wavelength in Å. The total column density is obtained by integrating the profile over the pre-defined velocity interval, $N = \int_{v_{\min}}^{v_{\max}} N_a(v) dv$, where $[v_{\min}, v_{\max}]$ are the boundaries of the absorption. We computed the average line centroids through the first moment of the AOD $v_a = \int v \tau_a(v) dv / \int \tau_a(v) dv \text{ km s}^{-1}$. The velocity range over which the line was integrated was determined from weak H I transitions and metal line.

We emphasize that, as much as possible, the integration range ($[v_{\min}, v_{\max}]$) corresponds to a single absorbing H I complex as shown, e.g., in Fig. 3, but this does not mean necessarily the metal lines consist solely of a single component (often they are, but not always). For the absorbers considered in this survey, the main H I components can typically be separated when the difference between central velocities between two H I components are at least separated by $|\Delta v| \gtrsim 40 \text{ km s}^{-1}$ and

$\log N_{\text{HI}} \lesssim 18$. As we will see below the mean Doppler parameter of the H I components is around 27 km s^{-1} , corresponding to a temperature of $T < 4 \times 10^4 \text{ K}$, typical for photoionized gas. This means the thermal broadening is important and hence the H I lines are broader than the metal lines, i.e., there are H I transitions that can appear as a single component (at the observed spectral resolution) despite the metal ions showing multiple components over a velocity width of $\sim 50 \text{ km s}^{-1}$. In that case, we integrate the metal ions over a similar velocity width as the H I when that information is available from weak H I transitions; if the latter is not available (e.g., SLLS where weak H I transitions are not covered, which is the case for $\lesssim 5\%$ of the sample), we guide our analysis using the low ions or O I if it is detected, which are better tracers of denser regions probed by the strongest H I absorbers. In this latter case, we integrate over the entire profiles of the low ions that may have a single or several components; this velocity integration range dictates the integration range of the higher ions, even though they may extend well beyond the absorption seen in the low ions (see, e.g., Lehner et al. 2014).

As illustrated in Figs. 1 and 3, even deep in the LYAF, the original continuum placement (see O’Meara et al. 2015, 2017) is quite good and can be directly used in many cases to estimate the physical parameters of the absorption lines accurately. We therefore took full advantage that the Keck HIRES spectra are already normalized to use the AOD method in a fully automated way. For each identified absorber, we made typically two iterations to estimate the physical parameters of the lines (v_a , N_a , and equivalent width W_λ). In the first iteration, the velocity range is estimated based on the stack of velocities profiles used to preview the data. Our program created figures that show for each transition the normalized and apparent column density profiles (such as Fig. 3 in CCCI), allowing us to refine the integration velocity range and determine if the continuum needed any local refinement. In the second iteration, the refined velocity range is applied to the original or re-normalized spectra. If we determine that the continuum model needed to be re-estimated, we either use the automated Legendre polynomial fitting described in CCCI or selected by hand the continuum region to be fitted by low-order Legendre polynomials.

We integrate the equivalent widths using the same $[v_{\min}, v_{\max}]$ integration range adopted for the $N_a(v)$ profiles. The main use of the equivalent width for the metal lines in our survey is to determine if the absorption is detected at the $\geq 2\sigma$ level. If it is not, we quote a 2σ upper limit on the column density, which is simply defined as twice the 1σ error derived for the column den-

sity assuming the absorption line lies on the linear part of the curve of growth. The 1σ error is determined by integrating the spectrum over a similar velocity interval to that of a detected ion or very weak H I transition or otherwise $\pm 20 \text{ km s}^{-1}$ based on the typical smallest velocity intervals in other absorbers with weak detection of metals.

When an absorption feature is detected at $\geq 2\sigma$ significance, the next step is to assess if there are any contamination or saturation issues. The main ions detected in this work are C II, C III, C IV, Si II, Si III, Si IV, and O VI (see Fig. 3 and Appendix). Other ions are also considered such as Fe II, Fe III, Al II, Al III or atoms such as O I, but in most cases these are not detected (Fig. 3 and Appendix 11). For C IV $\lambda\lambda 1548, 1550$, Si IV $\lambda\lambda 1393, 1402$, and O VI $\lambda\lambda 1031, 1037$, Si II $\lambda\lambda 1193, 1260, 1304, 1526$, these are either doublets or ions with several transitions, and both contamination and saturation can be readily checked by comparing their $N_a(v)$ profiles. Ions with $\lambda \lesssim 1215 \text{ \AA}$ are more often likely to be contaminated than ions with transitions at longer wavelength owing to the dense LYAF at these redshifts. For example, for the absorber shown in Fig. 3, the C IV transitions are not contaminated, but the weak transition of O VI is. In contrast, the weakest H I absorber at about -55 km s^{-1} seen in Fig. 3 (that is not analyzed as part of this work because its H I column density is $\log N_{\text{HI}} < 14.5$) shows absorption in both transitions of each doublet of C IV and O VI. The C II ion has two transitions at 1334 and 1036 \AA , and we always check the latter transition if $\lambda 1334$ is detected; more often than not it is contaminated by the LYAF.

On the other hand, ions such as C III $\lambda 977$ and Si III $\lambda 1206$ are in the LYAF and have only a single transition. In this case, our strategy for assessing whether a given transition is contaminated by another unrelated absorber is based on a combination of visual inspection and comparison of the relevant quantities (e.g., mean velocity and apparent optical depth) with other transitions. Strong contamination can often be diagnosed visually, comparing both the central velocities of the peak optical depth and shape of the velocity structure of the absorption profiles across transitions from the same or similar ions.⁴ The mean velocities of the absorption profiles estimated from the integration of the absorption profiles can often point to strong contamination if the mean velocity from one transition is significantly different than others that are aligned. In the case of obvi-

⁴ Of course if the investigated ion is not in the same gas-phase than an ion that is uncontaminated (e.g., O VI in some cases), these criteria cannot be used.

ous contamination, the absorption feature is discarded. The only exceptions are as follows. If the contamination is very mild, only occurring in the wing of a relatively strong absorption, we changed slightly the velocity integration range to avoid the contaminated portion for that absorption feature. In cases where we are not sure that the absorption arises solely from the understudied metal ion (e.g., detection of C III but no coverage or detection of C IV or other ions), but the feature could very likely be produced by that ion based on the same velocity as that of H I and narrow absorption (as expected from a metal, low ion), we treat the column density from that ion as an upper limit in our ionization modeling⁵.

For most of the metal ions in our survey, saturation is not a major issue owing to the lower column H I densities than those of DLAs and even SLLSs (there are only 7 SLLSs in our sample and no DLA), lower metallicities on average than $z < 1$, and to the high spectral resolution of the Keck data. To determine if there is saturation, we proceed in a similar way that we did for the contamination assessment. Where there is no obvious sign of contamination and the absorption from the metal ion reaches zero flux, the absorption is automatically marked as a lower limit. The comparison of the AOD profiles for doublet ions or ions with multiple transitions can readily help determine whether there is saturation if the profiles do not match at the peak optical depth and if the apparent column density of the stronger transitions is systematically smaller than that of the weaker transitions.

For atomic or ionic transitions that have $\Delta \log(\lambda f) \simeq 0.3$ and the difference in apparent column densities of the weak and strong transitions is $\Delta(\log N_a) \equiv \log N_a^{\text{weak}} - \log N_a^{\text{strong}} \leq 0.13 \text{ dex}$ (see W16), we are able to correct for the mild saturation using the method described in Savage & Sembach (1991) and W16. In this case, we report the apparent column densities for each transition and then the adopted column density, corrected for saturation. In cases where we were not able to correct for saturation, we report the column density as a lower limit determined by the AOD method.⁶

For multiple transitions where there are no saturation or contamination issues, we give velocities and column densities as the weighted average. All the column densities, velocity integration ranges, averages velocities, and

⁵ This upper limit can be differentiated from a non-detection upper limit as the error bars of the former are not the standard non-detection upper limit errors $+0.18, -0.30 \text{ dex}$.

⁶ Contamination and saturation can be *a priori* both present at the same time and deceitful. However, it is unlikely to occur frequently over the same pixels, and therefore each can be disentangled reliably in most cases.

redshifts for the metal ions and H I (see §3.2) are summarized in Table 2. We also provide all the results in a machine readable format (see Appendix).

3.2. Determination of the H I Properties

To derive the metallicity, we can rely in all the cases on having column densities for several metal ions (detections and/or non-detections). However, to have information on the amount of hydrogen atoms, we rely solely on H I. The advantage with H I is that we can access, in most cases, to the entire Lyman series from 1215 Å all the way down to 913 Å (depending on wavelength coverage, redshift of the absorber, presence of a SLLS/DLA along the sightline, and strength of the absorption), spanning a difference in $f\lambda$ of over 2,700. However, the entire Lyman series is in the LYAF (and Ly β forest), and therefore many transitions can be and are often heavily contaminated, requiring a close look at all the H I absorption features to assess the level of contamination. Therefore our first task was to systematically look simultaneously at several H I profiles (from 1215 to 915 Å) to assess if there is enough information (i.e., portion of the profiles of H I transitions that are uncontaminated) to derive N_{HI} . If it was judged that the contamination could be dealt with, we proceeded by estimating the apparent column densities from the AOD profiles (and equivalent widths) and creating a mask of the H I profiles that are contaminated (i.e., flagging the pixels that are clearly contaminated), a mask that is then used in the PF (see below).

Owing to the LYAF contamination, each transition was manually handled, and we often also reassessed the continuum that can be more uncertain than in the redder part by modeling it with low-order Legendre polynomials. As mentioned above, we treated as much as possible an absorber as a single H I component. For the example shown in Fig. 3, there are two components separated by 65 km s^{-1} , which correspond to two absorbers at $z_{\text{abs}} = 2.55125$ and 2.55216 . We therefore integrated the AOD profiles over each component (for the absorber at $z_{\text{abs}} = 2.55125$, that corresponds to the velocity interval of about $[-30, 40] \text{ km s}^{-1}$). For absorbers with $\log N_{\text{HI}} \gtrsim 18$, this was not always possible especially if there is not coverage of the weaker Lyman series transitions (for these absorbers, the damping wings of Ly α and Ly β can be used to determine N_{HI} , see below). However, these absorbers are rare in our sample, $\lesssim 5\%$ (see below). For each transition, the AOD results are checked for contamination and/or saturation. For the transitions where there is no sign of contamination and/or saturation, we use a weighted-average of the in-

tegrated apparent column densities, which provides the N_{HI} estimates from the AOD method.

The equivalent widths, estimated along with the apparent column densities and average velocities, are used for the COG analysis, which employs a χ^2 minimization and χ^2 error derivation approach outlined by Sembach & Savage (1992). A single component COG is assumed. Our procedure solves for $\log N$ and b independently in estimating the errors. We started with all the H I transitions for which we estimated the equivalent widths and did not appear *a priori* to be contaminated based on the AOD analysis. We checked the results from the COG model and then removed only the transitions clearly departing from the model. We ran our COG program again with the new set of transitions to obtain the final estimate of N_{HI} with the COG method.

Using the normalized and masked H I spectra, we also Voigt-profile fit the H I transitions using an in-house PF program described in Lehner et al. (2011, 2014, 2018), which was updated and refined from Fitzpatrick & Spitzer (1997). A major difference from the previous methods is that the model profiles were convolved with the HIRES instrumental line-spread function, assumed to be Gaussian. The three parameters for each component i (typically $i = 1$, but in some cases $i = 2$ or 3 or in rare cases more)—column density (N_i), Doppler parameter (b_i), and central velocity (v_i)—are input as initial guesses and were subsequently varied to minimize χ^2 of the fit to all the fitted H I transitions. As for the COG, we started with all the H I transitions that did not appear *a priori* contaminated and iterated, removing any transitions that *a posteriori* appear contaminated (or sometimes revisiting the masked pixels). In Fig. 4, we show an example of profile fitting that consists of a two-component fit corresponding to the absorbers at $z_{\text{abs}} = 2.55125$ and 2.55216 . As it can be seen in each panel of Fig. 4, there is some evidence of contamination especially in the component at 65 km s^{-1} ($z_{\text{abs}} = 2.55216$), but even in that component there is enough information to derive robustly N_{HI} when using the different H I transitions simultaneously.

In general, there is a good agreement between these different methods to estimate N_{HI} for absorbers with $14.5 \lesssim \log N_{\text{HI}} \lesssim 17.2$. The three methods explore different parameters and different transitions, allowing us to robustly estimate N_{HI} . When multiple approaches are valid, we simply average the values from the different methods and propagate the errors accordingly. For systems with $\log N_{\text{HI}} \gtrsim 17.2$, the PF results are most of the times solely adopted as a consequence of the need to either fit the Ly α damping wings for absorbers with $\log N_{\text{HI}} \gtrsim 19$ or combination of weaker

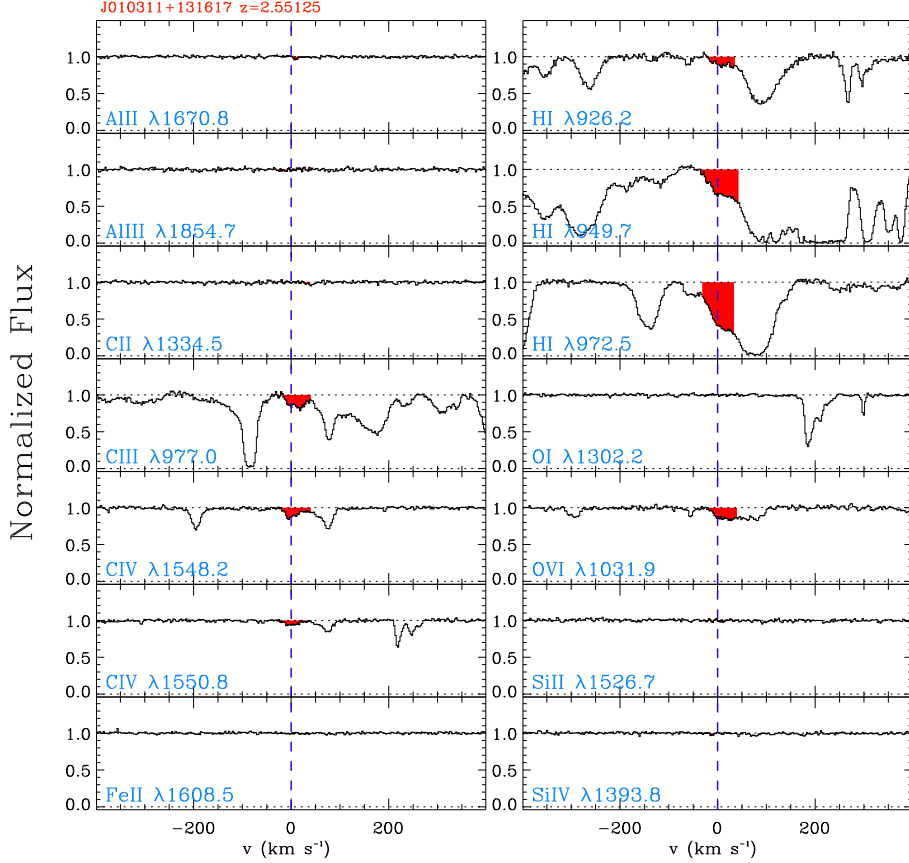


Figure 3. Example of normalized spectra against the rest-frame velocity of the absorber at $z = 2.55125$ toward J010311+131617 that show detection of H I, C III, C IV, and O VI (the integration range of the profiles are shown in red). Another absorber separated by 65 km s^{-1} is found at $z = 2.55216$; in this case the column densities can be estimated reliably in each component/absorber (see also Fig. 4)

and stronger H I transitions in order to correctly model the absorption that depends more strongly on both N and b in this regime. The eight systems with $17.5 \leq \log N_{\text{HI}} \leq 18.65$ require a more hands-on approach owing to having mostly saturated absorption in all the H I transitions and only weak damping features in Ly α . These were all analyzed as part of Lehner et al. (2014) and KODIAQ-ZI, and we refer the reader to these papers for a full description, noting, very conservative errors were adopted with a minimum error on the N_{HI} for any LLS of $\sigma_{\log N} = 0.15$ using this methodology. However, the metal lines associated with these absorbers were all reanalyzed as part of this work.

The adopted N_{HI} results are summarized in Table 2 and we also report in Table 3 the PF results, i.e., the velocities, Doppler parameters, and column densities, and errors associated with these quantities. In that table, the listed redshift corresponds to the adopted redshift (see above) and the third column indicates the component number for each absorber.

4. EMPIRICAL PROPERTIES OF THE KODIAQ-Z SURVEY

Before describing the ionization modeling of the absorbers, it is helpful to summarize the basic properties of the KODIAQ-Z survey, in particular in terms of N_{HI} and redshift distributions as we will compare our sample of absorbers to other surveys (such as surveys of stronger H I absorbers at similar redshift or absorbers with similar N_{HI} but at lower redshift). As we show below the N_{HI} and Doppler parameter distribution also motivate the use of photoionization in the ionization modeling to determine the metallicity of the absorbers.

4.1. H I Column Density and Redshift Distributions

In Fig. 5, we show the distributions of the absorber redshifts and H I column densities as well as the scatter plot between these two quantities. There are 202 absorbers in KODIAQ-Z and their full N_{HI} and z intervals are $14.43 \leq \log N_{\text{HI}} \leq 19.87$ and $2.23 \leq z_{\text{abs}} \leq 4.35$. However, 99% of the absorbers have $14.57 \leq \log N_{\text{HI}} \leq 19.87$ and $2.23 \leq z_{\text{abs}} \leq 3.57$ with means and standard deviations $\langle \log N_{\text{HI}} \rangle = 15.8 \pm 1.1$ (the median being

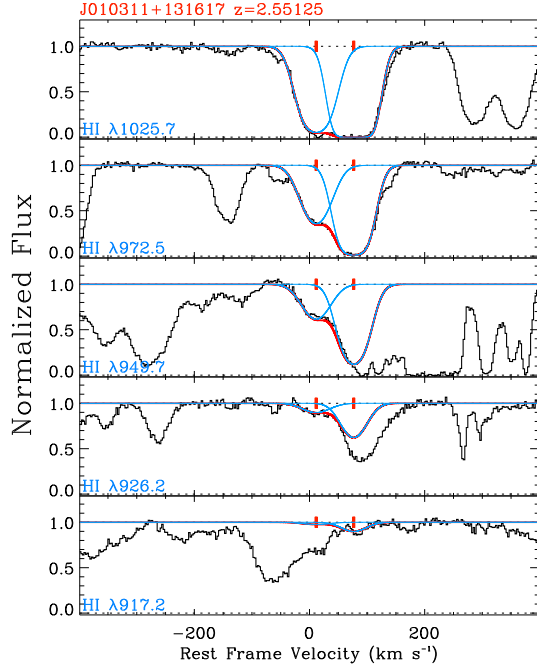


Figure 4. Example of the same absorber shown in Fig. 3 where we show the Voigt profile fit (in red the composite profile fit, and in blue each individual component) to the individual transitions of H I (black spectra). Despite some contamination in each transition, there is enough uncontaminated regions in each profile to estimate robustly the H I column density in each component.

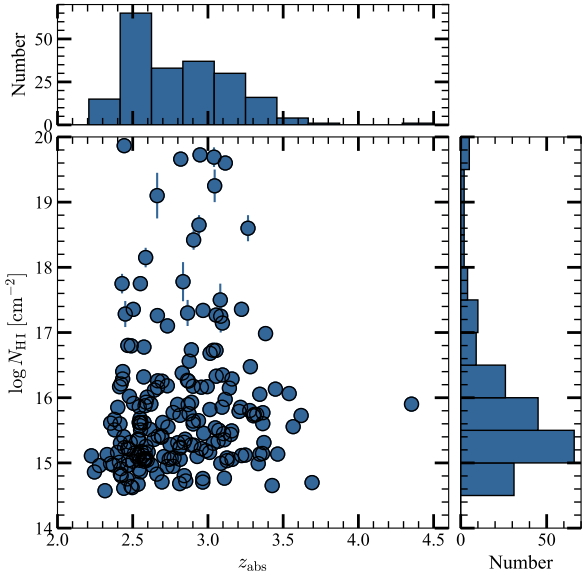


Figure 5. Distribution of the redshifts and H I column densities for the absorbers in the KODIAQ-Z sample. The top and right panels show the redshift and $\log N_{\text{HI}}$ distributions.

$\log N_{\text{HI}} = 15.5$) and $\langle z_{\text{abs}} \rangle = 2.79 \pm 0.31$ (the median being $z_{\text{abs}} = 2.75$), respectively. There is an evident peak in the redshift distribution at $2.4 \lesssim z_{\text{abs}} \lesssim 2.6$ where there are about 65 absorbers; otherwise between $z_{\text{abs}} \simeq 2.6$ and 3.35, the z -distribution is relatively flat with about 30–35 absorbers in each 0.2 redshift bin. This peak in the redshift distribution corresponds to redshifts where the optimal conditions are assembled to derive N_{HI} (access to the entire Lyman series transitions and smaller contamination from the LYAF): as z decreases below 2.4, the number of H I transitions diminishes rapidly; as z increases above 3.6, the level of contamination from the LYAF increases (and indeed at $3.5 \lesssim z_{\text{abs}} \lesssim 4.4$, only for 5 absorbers were we able to robustly derive N_{HI}). As alluded to before, we use two other main surveys at $z > 2$ for comparison with KODIAQ-Z: the HD-LLS survey (Prochaska et al. 2015; Fumagalli et al. 2016b) and the R12-DLA survey (Rafelski et al. 2012). Based on the redshift distribution of KODIAQ-Z, we limit these surveys to the redshift range $2.2 \leq z \lesssim 3.6$ when comparing the absorbers as a function of N_{HI} over the same redshift interval.

Owing to the selection of the absorbers, the N_{HI} distribution should follow to some extent the column density distribution of H I (Prochaska et al. 2014), which is why the N_{HI} distribution is not flat. From approximately 10^{15} to $10^{16.5} \text{ cm}^{-2}$, we see in Fig. 5 the expected drop in the number of absorbers as N_{HI} increases. At $\log N_{\text{HI}} < 15$, our sample is not complete as there is a sharp drop in the number of absorbers. This is because as N_{HI} decreases, we rely more and more on high S/N spectra in order to be sensitive to low metallicities, significantly reducing the sample. For absorbers with $16.5 \lesssim \log N_{\text{HI}} \lesssim 17.5$, we have to depend more on weak Lyman series transitions to estimate N_{HI} , limiting the number of absorbers especially as z increases beyond $z \gtrsim 3.2$. As described in §3.2, absorbers with $17.5 < \log N_{\text{HI}} \lesssim 18.65$ are rare because they are essentially on the flat part of the COG, dramatically restricting the number of absorbers where we can estimate N_{HI} . And indeed although absorbers with $18.7 \lesssim \log N_{\text{HI}} \lesssim 20$ should be less frequent than the previous category, there are more of these strong LLSSs/SLLSSs in our sample owing to that we can use the damping of Ly α and Ly β to derive N_{HI} (see also §3.2).

4.2. H I Column Density and Doppler Parameter Distributions

In Fig. 6, we compare the Doppler parameter, b , and N_{HI} derived from the profile fitting in the individual components of H I. There is no strong trend between b and N_{HI} , although broad components with $b > 40$

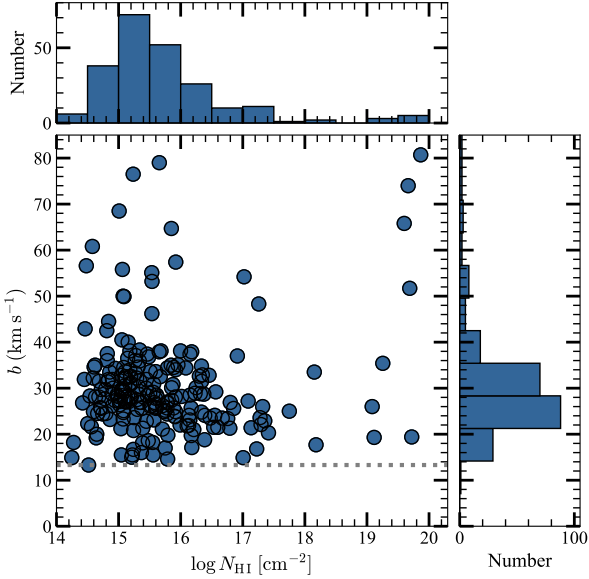


Figure 6. Distribution of the Doppler parameters (b) and H I column densities in the KODIAQ-Z sample obtained from the profile fitting of individual components. The right and top panels show the b and $\log N_{\text{HI}}$ distributions. The dotted line shows the lowest fitted b -value (corresponding $T \lesssim 10^4$ K); 90% of the components have $13.3 \leq b \leq 40 \text{ km s}^{-1}$. Note that for the Keck HIRES spectra, the instrumental b -value is about $4\text{--}5 \text{ km s}^{-1}$, well below the minimum b -value, i.e., narrower H I absorbers than $b < 12 \text{ km s}^{-1}$ could have been detected if present.

km s^{-1} are more frequent at $\log N_{\text{HI}} < 16$ ($b = 40 \text{ km s}^{-1}$ implies $T < 10^5$ K, which is the threshold b -value between broad and narrow H I absorbers as defined by Lehner et al. 2007).⁷ We, however, note that the majority of these broad components are found in more complex velocity profiles (2 or more components) and/or lower SNRs spectra, where a broad component reduces the χ^2 .

Considering the entire sample, the mean and standard deviation of b is $\langle b \rangle = 30 \pm 11 \text{ km s}^{-1}$ and median is 28 km s^{-1} . About 90% of the components have $13.3 \leq b \leq 40 \text{ km s}^{-1}$ where $\langle b \rangle = 27 \pm 6 \text{ km s}^{-1}$ and the median being 27 km s^{-1} . That latter value corresponds to a temperature of the gas of $T < 4 \times 10^4$ K, consistent with the gas being primarily photoionized. At $z < 1$ for the CCC absorbers, the results are remarkably similar since 91% of the profile-fitted absorbers have also $b < 40 \text{ km s}^{-1}$ and a mean of $28 \pm 8 \text{ km s}^{-1}$ (CCCI

⁷ The Doppler parameter for H I is related to the gas temperature via $b_{\text{HI}} = (2kT/m_{\text{H}} + b_{\text{nt}}^2)^{0.5}$, where k is the Boltzmann constant, T the temperature of the gas, m_{H} is the mass of hydrogen, and b_{nt} is the (unknown) non-thermal component to the broadening.

and Fig. 7 therein). This contrasts from the weaker LYAF absorbers with $\log N_{\text{HI}} \lesssim 14$ where the median and mean b -values are systematically larger by 15%–30% at $z \lesssim 0.5$ than at $1.5 \lesssim z \lesssim 3.6$, implying a larger fraction of the low- z IGM is hotter and/or more kinematically disturbed than the high- z IGM (Lehner et al. 2007).

5. DETERMINING THE METALLICITY OF THE ABSORBERS

5.1. Motivations for Photoionization Modeling

Several empirical studies at both low and high redshifts have shown that SLFSs, pLLSs, and LLSs have properties that are consistent with the gas being predominantly photoionized (Prochaska 1999; Prochaska et al. 2017b; L13; KODIAQ-ZI; CCCI; CCCII; Crighton et al. 2013; Fumagalli et al. 2016b; Cooper et al. 2021; Zahedy et al. 2021). In §4.2, we show the KODIAQ-Z absorbers have temperatures on average $T \lesssim 4 \times 10^4$ K, consistent with the gas being photoionized (the same result was found for the low redshift absorbers with similar N_{HI} , CCCI). As illustrated in the velocity profiles provided in the appendix, when detected metal ions such as the suite of carbon ions (C II, C III, C IV) or silicon ions (Si II, Si III, Si IV) align well with H I (although we emphasize again that sometimes metal ions owing to their smaller b can have more than 1 component within the breadth of the H I profiles even though the H I absorption can be fitted with a single component—that also implies that the thermal broadening is a large contributor to the broadening).

In contrast to the low redshift, for the ionizing radiation field and typical lower metallicities at $z \sim 2\text{--}3$ (about 0.1% solar or $[\text{X}/\text{H}] = -2$, see below, KODIAQ-ZI; HD-LLS), even strong transitions like C II $\lambda 1334$ and Si II $\lambda 1260$ are often not detected, so we have to rely more on intermediate (Si III, C III, Si IV) and high (C IV) ions to determine the metallicity. Because the current survey probes lower N_{HI} absorbers than our previous surveys at high redshift (Lehner et al. 2014; KODIAQ-ZI), we find that the O VI absorption can often be narrow and align with the absorption seen in H I (and other lower metal-ions if present). This contrasts from the very broad and strong O VI absorption frequently found in strong LLSs, SLLSs, and DLAs (Lehner et al. 2014). When O VI is narrow, it is used to constrain the photoionization models, and we find *a posteriori* that O VI is consistent with being produced by photoionization in many of these cases.

5.2. Photoionization Modeling

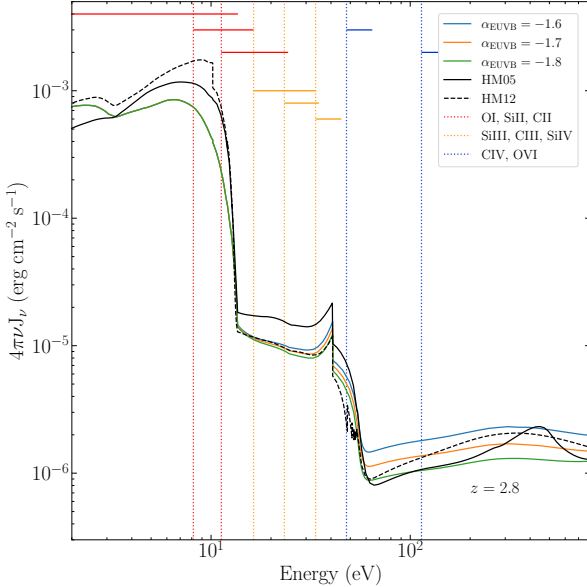


Figure 7. Comparison of the several spectral energy distributions for the ionizing background radiation field. The HM05 is adopted in this work, although we systematically compare it with the results from HM12. We also show the recent EUVB models from Khaire & Srianand (2019) for comparison. The key ions used to constrain the metallicities are shown where the dotted vertical bars show their minimum ionization energy while their range of ionization energy is shown with the horizontal bar.

To determine the metallicity for each absorber, we follow the same methodology and make similar assumptions described and discussed in CCC II and CCC III. As laid out in the previous section, owing to the higher redshift absorbers and the change in the EUVB, we include high ions in the photoionization modeling. We model the photoionization using Cloudy (version C13.02, see Ferland et al. 2013), assuming a uniform slab geometry in thermal and ionization equilibrium. In all cases the slab is illuminated with a Haardt–Madau EUVB radiation field from quasars and galaxies (HM05 and HM12, see Haardt & Madau 1996, 2001, 2012). We adopt HM05 (Haardt & Madau 2001, as implemented in Cloudy) as the fiducial radiation field for KODIAQ-Z to allow for a direct comparison with the CCC results at lower redshift. However, we also use the HM12 EUVB to explore systematics associated with uncertainties in the radiation field. In Fig. 7, we show the HM05 and HM12 EUVB at the average redshift of our survey ($z = 2.8$) along with the ionizing energy ranges for key ions used in KODIAQ-Z to constrain the metallicity of the absorbers. We also show in this figure the recent Khaire & Srianand (2019) EUVB models for their 3 favored slopes of the EUVB. While there are some differences between these EUVBs, these are not as large as at low z (Gibson

et al. 2021). And indeed we show *a posteriori* that the systematic errors arising from using a different EUVB are not as large as observed at $z \lesssim 1$. We note that for stronger absorbers ($\log N_{\mathrm{HI}} \gtrsim 18$) at $z \sim 3$, Fumagalli et al. (2016b) show that local ionizing sources did not affect much the metallicity estimates, and therefore we do not expect that local sources of (galactic) ionizing radiation would drastically change the metallicities in KODIAQ-Z. We adopt the same grid of Cloudy models summarized in Table 3 in CCC II.

The main variables for the photoionization models are the ionization parameter— $U \equiv n_{\gamma}/n_{\mathrm{H}} = H$, the ionizing photon density/total hydrogen number density (neutral + ionized)—and the metallicity, [X/H]. We assume solar relative—heavy element abundances from Asplund et al. (2009) but allow for possible variation between between C and α -elements (where α can be O or Si) since this ratio can be sensitive to nucleosynthesis effects (see, e.g., Cescutti et al. 2009; Mattsson 2010 for more detail). [C/ α] is therefore not necessarily solar in the gas probed by absorbers studied here (see Aguirre et al. 2004, and also Lehner et al. 2013; CCC II at $z < 1$).

To derive the metallicities, we compare the column densities for each absorber with a grid of photoionization models in a Bayesian context. We make use of the publicly available codes described in Fumagalli et al. (2016b, see also Prochaska et al. 2017b) and CCC II.⁸ We perform the MCMC analysis on an absorber-by-absorber basis. For each absorber we apply Gaussian priors on N_{HI} and redshift⁹. For all the absorbers, we first assume a flat prior on U . After examination of the model outputs (in particular convergence of walkers, comparison of predicted and observed column densities, and “corner plots” showing the posterior PDFs), we can assess which absorbers can be reliably modeled with this flat prior on U and which may require a Gaussian prior on $\log U$ to help the models converge (see below). Similarly, during this first iteration, we also determine which absorbers can be modeled with a flat prior on [C/ α] (i.e., for which we could estimate [C/ α]), which absorbers require [C/ α] = 0 (e.g., those with no detections for all the ions or no carbon ions), and which absorbers may require a Gaussian prior on [C/ α] (absorbers with poorly constraints on carbon ions and/or α -elements).

⁸ The code presented in Fumagalli et al. (2016b) and CCC II has been incorporated into the PyIGM Python package and is available at <https://github.com/pyigm/pyigm> (Prochaska et al. 2017a).

⁹ For the metal ions, the lower (upper) limits, the likelihoods are based on a rescaled Q-function (cumulative distribution function).

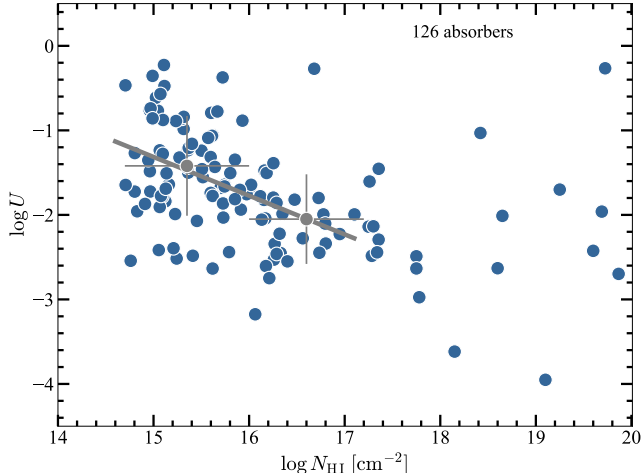


Figure 8. The $\log U$ median values as a function of N_{HI} for 126 absorbers in the KODIAQ-Z sample. The solid line shows a linear fit to the data with $14.6 \leq \log N_{\text{HI}} \leq 17.2$ (with a slope -0.46 ± 0.10 and intercept $+5.56$). The crosses show the mean values of the median values in each interval N_{HI} interval indicated by the horizontal bar.

When the constraints from the metal ions are not optimal, we adopt a Gaussian prior on $\log U$ (CCCII). These concern only SLFSs and pLLSs; the 16 LLSSs and 7 SLLSs have enough metal-ion constraints for the ionization models to converge. Fifty eight percent of the SLFSs and pLLSs do not require a Gaussian prior on $\log U$. In Fig. 8, we show the $\log U$ median values as a function of N_{HI} for the absorbers that can be modeled assuming a flat prior on $\log U$. As observed at low z , (CCCIII; CCCII), a strong anti-correlation is observed between the ionization parameter and N_{HI} , with a slope steeper by factor 2.3 compared to the low redshift absorbers. To characterize the distribution of $\log U$ appropriate for use as a Bayesian prior, we split the N_{HI} range into two bins, $14.4 \leq \log N_{\text{HI}} < 16$ and $16.2 \leq \log N_{\text{HI}} < 17.2$. In the former, 52% (75/143) can be modeled with a flat $\log U$ prior, while for the latter that number is 81% (30/37). In both cases, we find each PDF is well-fit with a normal distribution with $\langle \log U \rangle = -1.43 \pm 0.59$ and -2.06 ± 0.53 . We adopt these results for our Gaussian prior on $\log U$ in the $14.4 \leq \log N_{\text{HI}} < 16$ and $16.2 \leq \log N_{\text{HI}} < 17.2$ intervals, respectively.

For the Gaussian prior on $[\text{C}/\alpha]$, we similarly use absorbers with relatively good constraints from carbon and α -element ions to determine a mean and standard deviation of $\langle [\text{C}/\alpha] \rangle = -0.31 \pm 0.42$. We apply these for the Gaussian prior on the $[\text{C}/\alpha]$ ratio for absorbers with poorly-constrained $[\text{C}/\alpha]$. We note that for a few (13) absorbers, $[\text{C}/\alpha]$ is clustered around $-1 \lesssim [\text{C}/\alpha] \lesssim$

-0.9 . Not including those in the mean would of course increase the mean $[\text{C}/\alpha]$ value, but it would not change the posterior PDF of $[\text{C}/\alpha]$ for these absorbers. We discuss in §§5.6, 6.5 in more detail the $[\text{C}/\alpha]$ ratio.

We summarize the results of our photoionization modeling in Table 4 for all the absorbers in the KODIAQ-Z sample. For each absorber, we list the sightline name, the absorber redshift (z_{abs}), $\log N_{\text{HI}}$, metallicity, ionization parameter ($\log U$), and $[\text{C}/\alpha]$ ratio (when estimated). Each quantity is reported with the 68% CI and median values, except in the cases where we derive an upper or lower limit, in which case we report the 80% CI and median. We emphasize that these values are attempts to summarize the posterior PDFs provided by the MCMC sampling of the Cloudy models. While those PDFs can be well-behaved and nearly Gaussian, some are not as well behaved (see corner plots in the appendix).

For the HD-LLS absorbers used to compare with KODIAQ-Z, we apply the same overall methodology and same HM05 EUVB in the photoionization models in order to reduce any systematic errors between the two surveys. We, however, note that the absorption in absorber in the HD-LLS and KODIAQ-Z is not treated in the same way. In the HD-LLS survey, a velocity interval of $\pm 500 \text{ km s}^{-1}$ defines an absorber, which is driven by the methods to derive N_{HI} that use either the break at the Lyman limit or the damped wings from Ly α . For the metal lines, they sum the absorption components identified within that interval even though it is rarely larger than 200 km s^{-1} . As detailed in §3, we define an absorber using the Lyman series and as much as possible we consider the absorption component by component, so in a window of $\pm 200\text{--}500 \text{ km s}^{-1}$, KODIAQ-Z can have several absorbers. However, as N_{HI} increases and overlaps with the HD-LLS survey, i.e., for $\log N_{\text{HI}} \gtrsim 18$, we similarly lose our ability to derive the column densities in individual components, especially when we have information only from Ly α and Ly β . In these cases, we rely on the low ions to define the integration range in the intermediate and low ions. In our approach, we make the physically motivated assumption that the optical depths of the low ions follow that of the stronger H I absorption while the higher ions follow better weaker H I absorbers that may not contribute much to the total H I column—but the extra absorption in the higher metal-ions could dominate their column density (§3). However, *a posteriori* we will show that this different treatment does not lead to large different results.

5.3. Uncertainties on the Metallicities

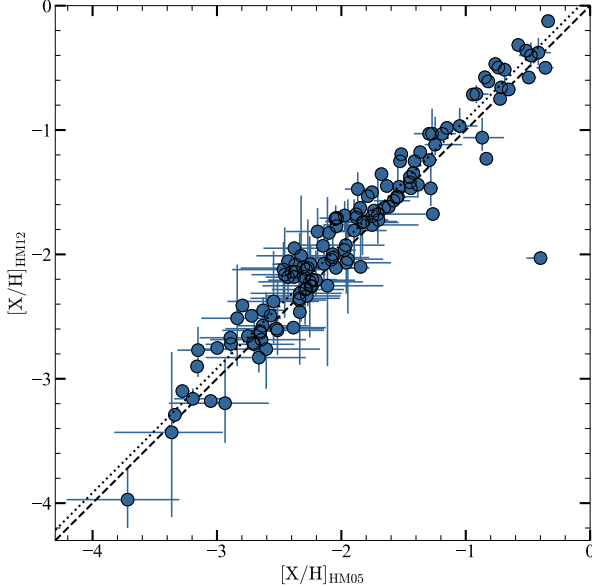


Figure 9. Comparison of the median metallicities (with 68% CI) of KODIAQ-Z derived using the HM12 and HM05 EUVBs. The dashed line is the 1:1 relationship. The dotted line shows the mean of the differences between the metallicities derived using HM12 and HM05.

All the errors for the output quantities (e.g., metallicity) reported in this work are statistical errors from the Bayesian MCMC ionization modeling. There are additional systematic and other uncertainties that we discuss here.

5.4. Ionizing Background

The first one is caused by the uncertainty in the ionizing EUVB as alluded to previously. At low redshift, CCCII shows that on average the metallicity is systematically shifted on average by about +0.4 dex for the SLFs/pLLS and +0.2 dex for the LLSs when the ionizing EUVB changes from HM05 to HM12. We have done a similar experiment with KODIAQ-Z and HD-LLS absorbers showing that the impact of the EUVB is overall smaller at high z than observed at low z . In Fig. 9, we show the comparison between the metallicities using HM12 and HM05 for the KODIAQ-Z absorbers where we did not apply a Gaussian prior on $\log U$ (that essentially removes all the limits, although including those would not change the results). The immediate conclusion from this figure is that the systematic differences between the metallicities derived using HM05 and HM12 are quite small and much smaller than observed at low z . On average considering all the absorbers, we find $\langle [X/H]_{\text{HM12}} - [X/H]_{\text{HM05}} \rangle = +0.10 \pm 0.17$. The difference is also not as systematic as low z since there are several cases where $[X/H]_{\text{HM12}} \leq [X/H]_{\text{HM05}}$.

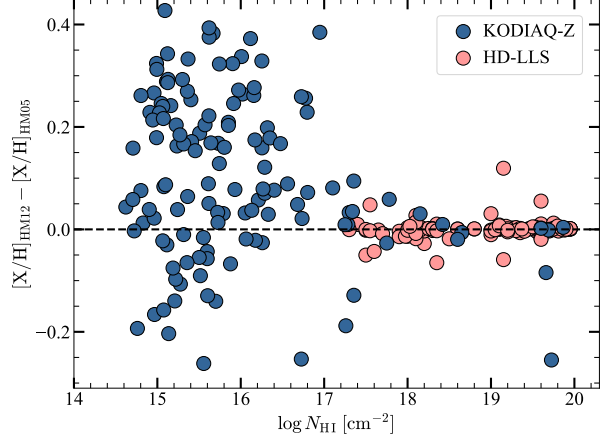


Figure 10. Difference between the median metallicities for the KODIAQ-Z and HD-LLS absorbers derived using the HM12 and HM05 EUVBs against the H I column densities of the absorbers.

As illustrated in Fig. 10 where the differences of the median metallicities between HM12 and HM05 vs. N_{HI} are shown for both the KODIAQ-Z and HD-LLS absorbers, that difference decreases with increasing N_{HI} as observed for the low redshift absorbers. In fact, for $\log N_{\text{HI}} \gtrsim 17.2$, $\langle [X/H]_{\text{HM12}} - [X/H]_{\text{HM05}} \rangle \simeq 0.0 \pm 0.1$, i.e., the HM12 and HM05 EUVBs essentially give the same metallicities and any small differences are essentially random. For the SLFs and pLLSs, $\langle [X/H]_{\text{HM12}} - [X/H]_{\text{HM05}} \rangle \simeq +0.12 \pm 0.15$. These results are not entirely surprising when considering the different EUVBs in Fig. 7 with their difference being smaller than at low z over similar ionizing energies (Gibson et al. 2021). Based on Fig. 7, the metallicities would not change much if we had used the more recent EUVBs from Khaire & Srianand (2019). For comparison with CCC, we adopt hereafter the results from the HM05 EUVB.

5.5. Multiple Ionization Phases

Throughout we also assume a single ionization phase. In cases where a higher ion (O VI in our survey) is clearly under produced by the photoionizing model, this ion is not included in the final model. In that latter case, this would be evidence for an absorber probing multiple gas-phases. As shown by Lehner et al. (2014), this can especially happen in the strong LLSs where O VI can be very strong and can rarely be modeled with a single gas-phase ionization model with the lower ions. In these cases, the velocity profiles of the O VI profiles are also very different from those of the lower ions (including C IV), strongly hinting at multiple gas-phases. However, as we explore lower N_{HI} absorbers in this present survey, we find in many cases that a single ionization gas-phase can match well the observed metal-ion column densities,

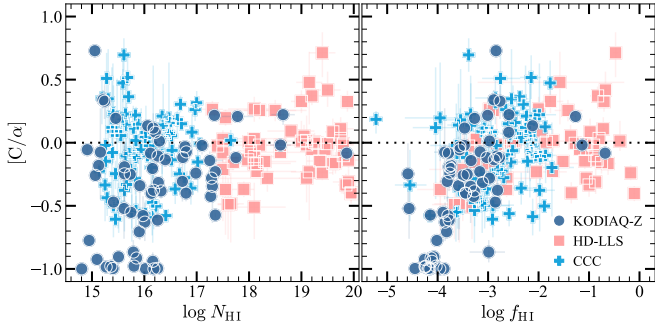


Figure 11. The ratio of $[C/\alpha]$ against the H I column density (left) and neutral fraction (right) from the KODIAQ-Z ($2.2 \lesssim z \lesssim 3.6$), HD-LLS ($2.2 \lesssim z \lesssim 3.6$), and CCC ($z \lesssim 1$) surveys. The median values of the $[C/\alpha]$ posterior PDFs are adopted as the central values with 68% CI.

including those of O VI. In these cases and in contrast to stronger H I absorbers, the absorption is also often quite simple (typically a single component) and the velocity profiles of the different metal ions align well with each other (including O VI when present) and with the H I velocity profiles. This, of course, does not necessarily mean that a more complex ionization structure might not be present, but a single gas-phase model is often sufficient to reproduce the observed column densities, especially in the SLFS and pLLS regimes. We adopt here therefore the simplest approach and assumption, a methodology also employed in CCC. Nevertheless, we note that at least at low redshift, the effects on the metallicities between single versus multiple gas-phase modelings typically lead to small changes in metallicities of the order of $< 0.1\text{--}0.2$ dex (Howk et al. 2009; Haislmaier et al. 2021). Therefore, we do not expect that considering a more complex ionization structures for the absorbers in our sample would drastically change the metallicities.

5.6. Non-solar Relative Abundances

Other uncertainties may arise from dust or non-solar relative abundances. Since carbon, silicon, and oxygen ions are typically used to constrain the ionization modeling at high redshift, we explicitly take account for possible non-solar $[C/\alpha]$ by letting this ratio vary in the range $-1 \leq [C/\alpha] \leq +1$. In Fig. 11, we show $[C/\alpha]$ as a function of N_{HI} (left panel) and the neutral fraction $f_{\text{HI}} \equiv N_{\text{HI}}/(N_{\text{HI}} + N_{\text{HII}})$ (right panel) for the KODIAQ-Z and HD-LLS absorbers. We also show in this figure the results from CCC at $z \lesssim 1$ (CCC III). For $[C/\alpha]\text{-}N_{\text{HI}}$, a Spearman rank-order test shows no strong evidence for a correlation between $[C/\alpha]$ and N_{HI} with a correlation coefficient $r_S = 0.14$ and a $p\text{-value} = 0.04$. On the other hand, the same statistical test shows a positive monotonic correlation between

$[C/\alpha]$ and f_{HI} with a correlation coefficient $r_S = 0.44$ and a $p\text{-value} \ll 0.05\%$. However, removing the 13 KODIAQ-Z absorbers with low $[C/\alpha] \lesssim -0.9$ eliminates any evidence of correlation between $[C/\alpha]$ and f_{HI} with a correlation coefficient $r_S = -0.05$ and a $p\text{-value} = 0.88$.

So far the CCC, HD-LLS, and KODIAQ-Z were treated as a single sample. Considering the samples individually would not change the conclusions for the lack of correlation between $[C/\alpha]$ and N_{HI} . However, while neither CCC nor HD-LLS shows any correlation between $[C/\alpha]$ and f_{HI} , for KODIAQ-Z, the Spearman rank-order test shows a strong positive monotonic correlation between $[C/\alpha]$ and f_{HI} with a correlation coefficient $r_S = 0.72$ and a $p\text{-value} \ll 0.05\%$. In that case, removing the 13 absorbers with low $[C/\alpha] \lesssim -0.9$ still yields $r_S = 0.55$ and a $p\text{-value} \ll 0.05\%$. Therefore in the KODIAQ-Z sample, $[C/\alpha]$ is more affected by ionization correction than in the other samples, most likely because often only C IV is detected (the limit on C II is often not very constraining and C III is often contaminated) and larger ionization correction are applied (for CCC, C II and C III are used to constrain $[C/\alpha]$, while for HD-LLS the ionization corrections are typically smaller). Based on CCC and HD-LLS where we always find $[C/\alpha] \geq -0.6$, $[C/\alpha]$ -values with $[C/\alpha] < -0.6$ are most likely predominantly caused by ionization rather than nucleosynthesis effects. Excluding the 13 absorbers with low $[C/\alpha] \lesssim -0.9$, we find that $\langle [C/\alpha] \rangle = -0.20 \pm 0.31$ in the KODIAQ-Z sample compared to $\langle [C/\alpha] \rangle = -0.05 \pm 0.30$ in the CCC survey and $\langle [C/\alpha] \rangle = -0.05 \pm 0.24$ in the HD-LLS survey. The similarity between CCC and HD-LLS is quite remarkable since different z , N_{HI} , and $[X/\text{H}]$ are probed. The 1σ dispersion is about the same in the three surveys, but on average the KODIAQ-Z sample has a systematic effect of -0.15 dex on $[C/\alpha]$ most likely caused by ionization. In conclusion, the variable C/α is important in that we can marginalize over that as a “nuisance” variable in order to get a better sense of the uncertainties in the metallicity, but it may not provide deep insights on the nucleosynthesis effects that may affect C/α (see also §6.5).

Finally, we note that for stronger LLSSs and SLLSSs as those in the HD-LLS survey (Fumagalli et al. 2016b), dust depletion is found to be a small effect for strong LLSSs and even SLLSSs at high z , and hence not very likely to have any appreciable effect on the metallicity estimates, especially considering the typical species—carbon, silicon, oxygen—used to constrain the ionization models are known not to be strongly depleted onto dust (e.g., Savage & Sembach 1996; Jenkins 2009; Jenkins & Wallerstein 2017).

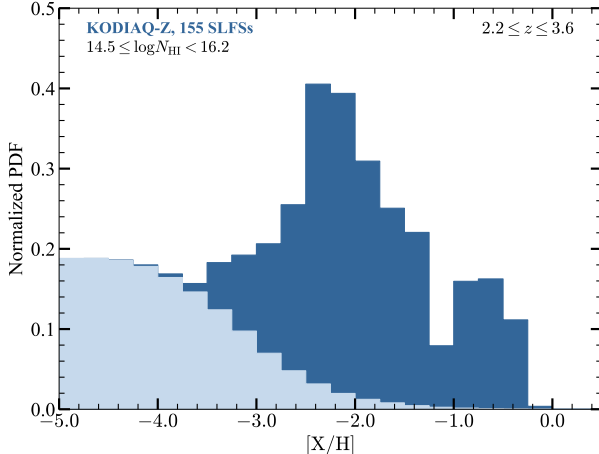


Figure 12. Posterior metallicity PDF of the SLFSs in the KODIAQ-Z sample. The light-colored regions indicate the contribution from the upper limits.

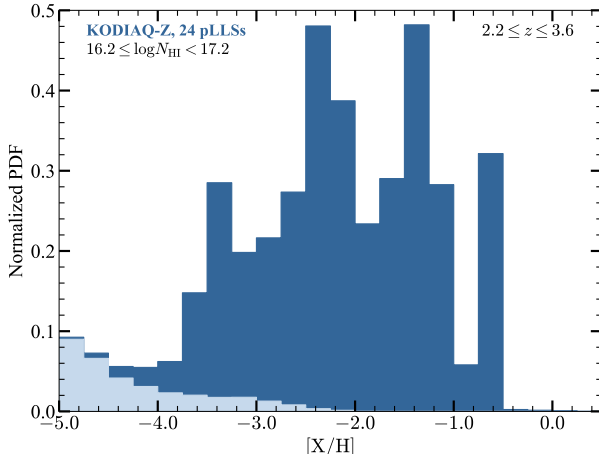


Figure 13. Posterior metallicity PDFs of the pLLSs in the KODIAQ-Z sample. The light-colored regions indicate the contribution from the upper limits.

6. METALLICITY OF THE IGM/CGM ABSORBERS AT $2.2 \lesssim z \lesssim 3.6$

6.1. Metallicity Distributions

In Figs. 12, 13, and 14, we show the posterior probability distribution functions (PDFs) of the metallicities of the SLFSs, pLLSs, and LLSs for KODIAQ-Z. In Fig. 14, we also overplot the LLSs from HD-LLS survey, showing similar PDFs between the two surveys, and hence implying we can combine both samples to improve the statistics for the LLSs. These posterior PDFs are constructed by combining the normalized metallicity PDFs of all of the absorbers within a given H I column density regime. In Table 4, we summarize the medians, means, standard deviations, and interquartile ranges (IQRs) for

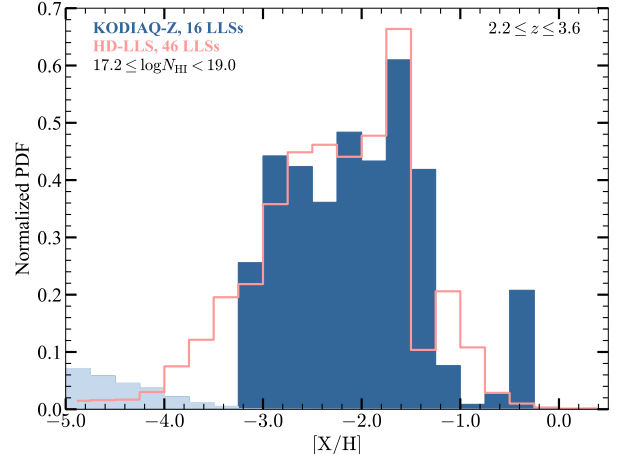


Figure 14. Comparison of the posterior metallicity PDFs of the LLSs in the KODIAQ-Z and HD-LLS sample. The light-colored regions indicate the contribution from the upper limits.

the various absorbers as well as a combination of these. We also include in this table the results for the HD-LLS, KODIAQ-Z+HD-LLS, and R12-DLA samples.

Considering first the SLFSs, the metallicity PDF is not unimodal. It is negatively skewed with a long and prominent tail extending well below $[X/H] < -3$. Its main peak is around the median value of -2.4 dex. The metallicity PDF of the SLFSs dips around -1.1 dex with a second weaker peak around -0.6 dex. The IQR is nearly 2 dex from -3.6 to -1.8 dex. As N_{HI} increases, the overall median metallicity increases and the IQR decreases. For pLLSs+LLSs, the median metallicity is -2.2 and IQR only ~ 1 dex from -2.8 to -1.7 dex. These features are distinctly illustrated in Fig. 15 where we compare the PDFs of the SLFSs and pLLSs+LLSs: there are more frequently pLLSs+LLSs in the metallicity range $-3.2 \lesssim [X/H] \lesssim -1.2$ than SLFSs, but SLFSs become more frequent at extremely low metallicity $[X/H] \lesssim -3.5$. Compared to the SLFS and pLLS PDFs, the LLS PDF is not as negatively skewed with about the same values for the mean and median.

For completeness and if one ignores the H I column density dependence of the metallicity PDFs between the SLFSs, pLLSs, and LLSs, we show in Fig. 16 the resulting metallicity PDF of the absorbers with $14.5 < \log N_{\text{HI}} < 19$ at $2.2 \lesssim z \lesssim 3.6$. Since the SLFSs are about 2/3 of the sample, the metallicity PDF of the $14.5 < \log N_{\text{HI}} < 19$ absorbers is not too different to that of the SLFSs with a similarly skewed distribution toward low metallicities, but also a second weaker peak around -0.6 dex.

6.2. Metallicity vs. N_{HI}

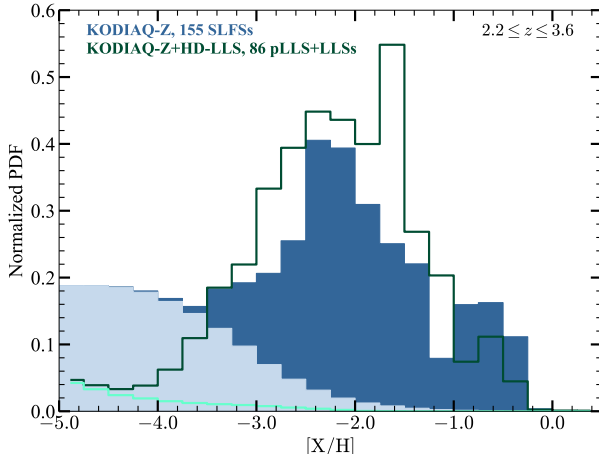


Figure 15. Comparison of the posterior metallicity PDFs of the SLFSs (KODIAQ-Z) and pLLSs+LLSs (KODIAQ-Z+HD-LLS). The light-colored regions indicate the contribution from the upper limits.

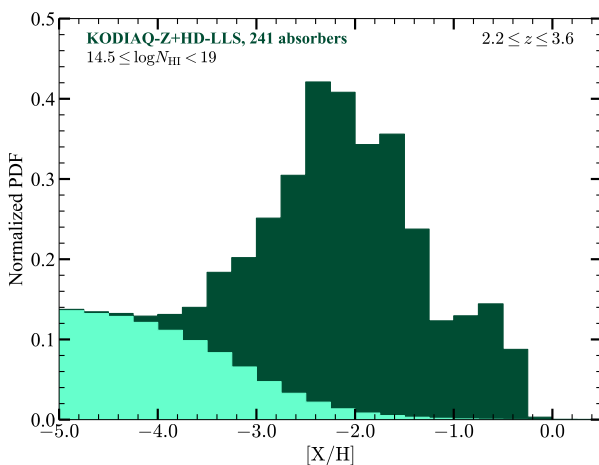


Figure 16. Posterior metallicity PDF of the absorbers with $14.5 \leq \log N_{\text{HI}} < 19$ in the combined sample of KODIAQ-Z and HD-LLS. The light-colored regions indicate the contribution from the upper limits.

As shown in the previous section, there is already evidence for an overall increase of the metallicities with N_{HI} in the range $14.5 \leq \log N_{\text{HI}} \leq 19$. We now explore further how the metallicity varies with N_{HI} considering the higher N_{HI} absorbers (the SLLSs and DLAs). From Table 4, the trend described above with increasing median/mean metallicity with increasing N_{HI} continues to apply in the SLLS and DLA regimes. The IQR and standard deviation for the SLLSs are about similar to that of pLLSs+LLSs, but those for the DLAs are substantially smaller (the IQR is 0.65 dex smaller than that of the SLFSs). The negative skewness is also less pronounced for the SLLSs and absent for the DLAs. In fact,

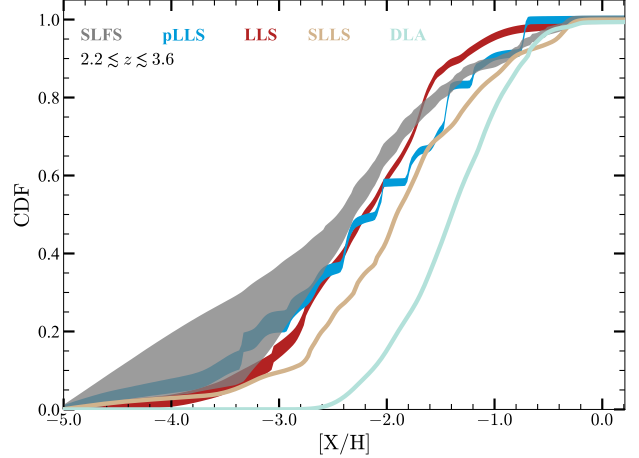


Figure 17. Cumulative probabilities of the SLFS, pLLS, LLS, SLLS, and DLA metallicity PDFs. The SLFSs and pLLSs are from KODIAQ-Z, the LLSs and SLLSs from KODIAQ-Z and HD-LLS, and the DLAs from R12-DLA.

the DLA metallicity PDF, contrary to the PDFs of the other weaker absorbers, is fully consistent with a Gaussian distribution according to the Kolmogorov–Smirnov (KS) test with a p -value $\ll 0.1\%$ (see also Rafelski et al. 2012).

These conclusions are strengthened considering the cumulative distribution functions (CDFs) of the metallicity PDFs (see CCCII for the description of the estimation of the CDFs including upper and lower limits). We show in Fig. 17 the metallicity CDFs for the SLFSs, pLLSs, LLSs, SLLSs, and DLAs. With only 24 pLLSs, this regime remains the least sampled. Nevertheless, the CDF confirms the overall evolution of the metallicities as N_{HI} increases: very metal poor (VMP) absorbers with $[X/\text{H}] \leq -2.4$ are more likely to be found in the SLFS, pLLS, LLS regimes than in the SLLS or DLA regime ($[X/\text{H}]_{\text{VMP}} = -2.4$ is the 2σ lower bound of the DLA metallicities). Notably the median metallicity of the SLFS is right at that threshold of $[X/\text{H}]_{\text{VMP}} = -2.4$, implying that 50% of these absorbers are VMP while only $< 5\%$ of the DLAs may be VMP by definition.

Thus far, we have separately analyzed the absorbers in different N_{HI} categories. However, we can also simply plot the metallicities of the absorbers as a function of N_{HI} , which is shown in Fig. 18. This has the obvious advantage that one does not have to make an *a priori* differentiation between the different absorbers in classes of H I column densities. For the SLFSs, pLLSs, LLSs, and SLLSs with well-constrained metallicities (i.e., not including the lower and upper limits), the central values represent the median of the posterior PDFs, and the error bars represent the 68% CI. For the upper and lower limits, the down and upward triangles give the 90th and

10^{th} quantiles while the vertical bar gives the 80% CI. For the DLAs, the best estimates with their 1σ error bars are shown. The horizontal dashed line at $[\text{X}/\text{H}] = 0$ represents solar metallicity. The horizontal dotted line at $[\text{X}/\text{H}] = -2.4$ represents the VMP limit as defined above. Note that the lack of data between $\log N_{\text{HI}} = 20$ and 20.3 is purely artificial, resulting from our grid of photoionization models stopping at $\log N_{\text{HI}} = 20$.

Fig. 18 further demonstrates the striking metallicity changes as a function of N_{HI} . Absorbers with $[\text{X}/\text{H}] \gtrsim -2.4$ are observed at any N_{HI} , but absorbers with $[\text{X}/\text{H}] < -2.4$ are observed only at $\log N_{\text{HI}} \lesssim 19.8$. While the VMP definition implies this is VMP gas for DLAs, for low N_{HI} absorbers the VMP definition is the median value for SLFSs and not even 1σ below the median of pLLSs and LLSs. As already pointed out above, the frequency of VMP absorbers also increases as N_{HI} decreases, which is quantitatively summarized in Table 6. We therefore also define extremely metal-poor absorbers as absorbers with $[\text{X}/\text{H}] < -3$, which are mostly observed at some level in absorbers with $\log N_{\text{HI}} \lesssim 18$, see Table 6.¹⁰ Extremely metal-poor absorbers have metallicities that are so low that only Pop III stars may have contaminated them if they have some metals (see, e.g., Frebel et al. 2007; Crighton et al. 2015).

We finally note that the metallicity dip around -1.1 dex observed especially in the SLFS metallicity PDF is also evident in the non-binned distribution shown in Fig. 18. In that figure, there is a lack of data points at $-1.1 \lesssim [\text{X}/\text{H}] \lesssim -1$ for H I column density absorbers with $14.5 \lesssim \log N_{\text{HI}} \lesssim 16.4$. This is reminiscent of the metallicity dip at a similar value of $[\text{X}/\text{H}] \simeq -1$ observed in the pLLS+LLS PDF at $0.45 \lesssim z \lesssim 1$ (CCC III, and see §6.3 for the cosmic evolution of the metallicity).

6.3. Cosmic Evolution of the Metallicity

In Lehner et al. (2016), for the first time, we studied the redshift evolution of the metallicity absorbers with $16.2 \lesssim \log N_{\text{HI}} < 19$, but with a much smaller sample at both low and high z . The samples of absorbers at all surveyed z have increased at least by a factor 8 and provide far more robust results. Furthermore, we also now sample at low and high z the N_{HI} regimes below $\log N_{\text{HI}} \lesssim 16.2$. In Fig. 19, we show the metallicity PDFs at low ($z < 1$) and high ($2.2 \leq z \leq 3.6$) redshift for H I-selected absorbers with $15 \lesssim N_{\text{HI}} < 19$. There is some overlap between the two distributions

¹⁰ We emphasize that VMP DLAs with $[\text{X}/\text{H}] < -2.4$ exist at $z \sim 2\text{--}4$, but are found only in targeted searches (e.g., Cooke et al. 2011, 2016)—they are uncommon and they do not show in sample as small as presented here since they are only $< 5\%$ of the population.

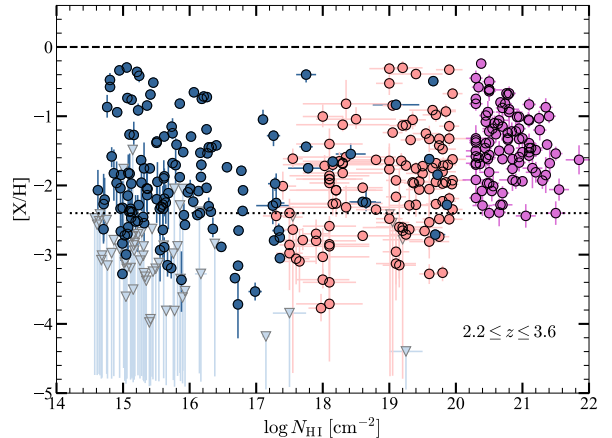


Figure 18. Metallicities of the SLFSs ($14.5 < \log N_{\text{HI}} < 16.2$), pLLSs ($16.2 \leq \log N_{\text{HI}} < 17.2$), LLSs ($17.2 \leq \log N_{\text{HI}} < 19$), SLLSs ($19 \leq \log N_{\text{HI}} < 20.3$), and DLAs ($\log N_{\text{HI}} \geq 20.3$) at $2.2 \lesssim z \lesssim 3.6$ as a function of N_{HI} . The blue data from the KODIAQ-Z survey (this paper). The orange data are from the HD-LLS survey (Fumagalli et al. 2016b) but we re-estimated the metallicities of these absorbers following the same EUVB and methodology as in KODIAQ-Z. The purple data (DLAs) are from Rafelski et al. (2012).

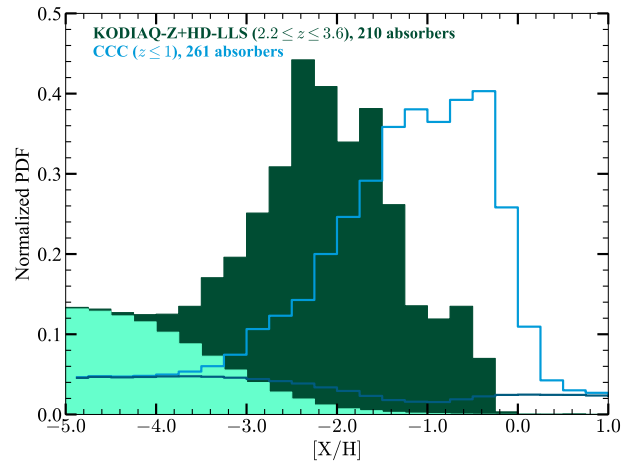


Figure 19. Comparison of the posterior metallicity PDFs of the absorbers with $15 \leq \log N_{\text{HI}} < 19$ at high and low redshifts. The light-colored regions indicate the contribution from the upper limits. For CCC, The light colored histogram indicates the contributions from upper and lower limits.

between $-3 \lesssim [\text{X}/\text{H}] \lesssim -1.4$, but evidently there are more absorbers with $[\text{X}/\text{H}] \lesssim -2$ at high z while many more with $[\text{X}/\text{H}] > -1.2$ at $z < 1$. In fact the latter value corresponds to the median metallicity at $z < 1$ for $16.2 \lesssim \log N_{\text{HI}} < 19$ absorbers, and only 10% of the high redshift absorbers have metallicities $[\text{X}/\text{H}] \geq -1.2$. The medians and means at $z < 1$ are about +1 dex higher than at $2.2 \leq z \leq 3.6$. Both distributions are

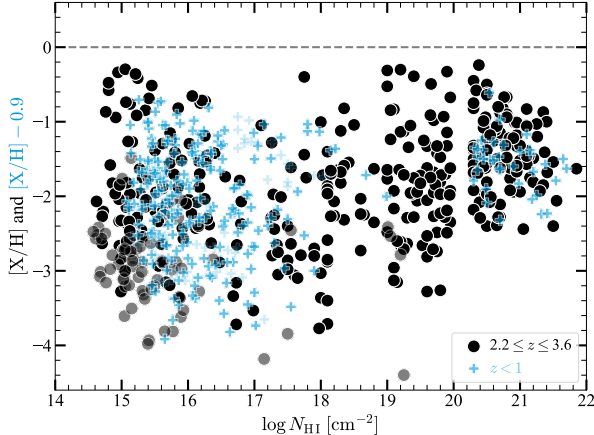


Figure 20. The metallicity as a function of N_{HI} at low z (CCC) and high z (KODIAQ-Z, HD-LLS, R12-DLA). For the $z < 1$ absorbers, we subtract the metallicity of each absorber by 0.9 dex (see text for more details). For the black circles, lighter symbols are upper limits on the metallicity. For the blue crosses, lighter symbols are upper limits if $[X/\text{H}] \leq -1$ and lower limits if $[X/\text{H}] > -1$. For clarity, we did not plot the error bars (which are available in Fig. 18 and Fig. 9 of CCC III for the low redshift sample). Median metallicities are plotted, but that we treat upper and lower limits as Fig. 18, i.e., the lower and upper values represent the 10th and 90th percentiles, respectively.

negatively skewed with similar IQRs $\simeq 1.5$ at low and high z .

In Fig. 20, we compare the metallicities of the absorbers (following the same methodology used to produce Fig. 18) at $z < 1$ and $2.2 \leq z \leq 3.6$ over the H I column density range $14.5 \lesssim N_{\text{HI}} < 22$. For the low redshift redshift absorbers, we shifted the metallicity by -0.9 dex, which is about the average difference between the mean/median metallicity of the absorbers at low and high z (-0.8 dex for DLAs, and -1 dex for lower N_{HI} absorbers). The notable feature from this figure is that despite different metallicity behaviors at low and high H I column densities, the offset metallicities and the overall dispersion at low and high z show striking overlap at any given N_{HI} (where there is a good sampling in both datasets). A closer look reveals a small excess of higher metallicity absorbers in the SLFS, SLLS, and DLA regimes at high z (i.e., a slightly larger dispersion of the metallicity distribution). However, overall the major change between $2.2 \leq z \leq 3.6$ and $z < 1$ absorbers is an increase of their metallicity by a factor ~ 8 .

In Fig. 21, we now show the metallicities as a function of the redshift for the absorbers included in CCC, HD-LLS, and KODIAQ-Z (for clarity we do not show the R12-DLA sample in this figure). For the HD-LLS

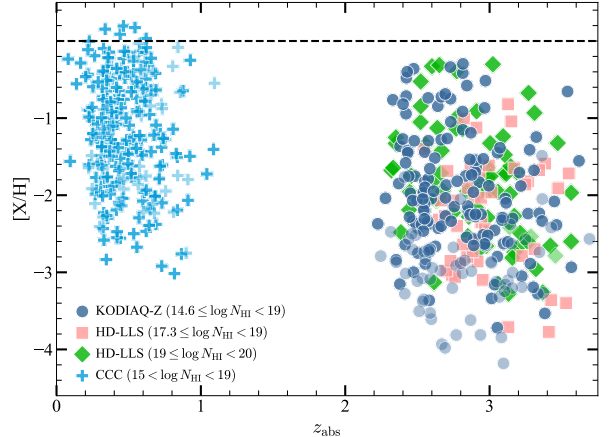


Figure 21. The metallicity of different absorbers as a function of the redshift. For HD-LLS and KODIAQ-Z surveys, lighter symbols are upper limits on the metallicity. For CCC, lighter symbols are upper limits if $[X/\text{H}] \leq -1$ and lower limits if $[X/\text{H}] > -1$. Median metallicities are plotted for the CCC, KODIAQ-Z, and HD-LLS surveys, but we treat upper and lower limits as Fig. 18, i.e., the lower and upper values represent the 10th and 90th percentiles, respectively.

sample, we differentiate the LLSs and SLLSs. This figure strengthens the previous conclusions, showing the overall increase in metallicities as z decreases. At $z < 1$, there is a substantial fraction of $\log N_{\text{HI}} < 19$ absorbers with $-0.15 \lesssim [X/\text{H}] \lesssim +0.15$, while these are mostly absent at higher redshift. On the other hand, at $z < 1$ there is no evidence of population of absorbers with $[X/\text{H}] \lesssim -3$, while there is at $2.2 \leq z \leq 3.6$. As already noted by Lehner et al. (2016) with a much smaller sample, while the VMP threshold increases by 1 dex over $2.2 \leq z \leq 3.6$ to $z < 1$ (the 5% quantile of DLA metallicities from -2.4 to -1.4 dex), a similar fraction of about 50% of $\log N_{\text{HI}} \lesssim 18$ VMP absorbers at low and high z lie in the respective VMP regime.

In Fig. 21, there is also some evidence that the metallicity distribution somewhat changes around $z \sim 2.85$. Considering the KODIAQ-Z and HD-LLS sample with $\log N_{\text{HI}} < 19$ absorbers at $z > 2.85$, the fraction of absorbers with $[X/\text{H}] \geq -1$ is very small ($4/112 \simeq 3.6\%$) while at $z \leq 2.85$ it is a factor ~ 4 larger ($17/130 \simeq 13.1\%$). To explore that potential of the change of the metallicity with z , in Fig. 22, we show the comparison between the metallicity CDFs of the absorbers with $14.5 \leq \log N_{\text{HI}} < 19$ from KODIAQ-Z and HD-LLS above and below several redshift thresholds, $z_{\text{th}} = 2.8, 2.9, 3.0$. The large number of absorbers with $[X/\text{H}] \gtrsim -1$ at $z \lesssim 2.9$ compared to higher z is further demonstrated in this figure. However, this figure also shows that at $z \gtrsim 2.9$, and in particular at $z \geq 3.0$, there is a much larger fraction of metal-poor absorbers with

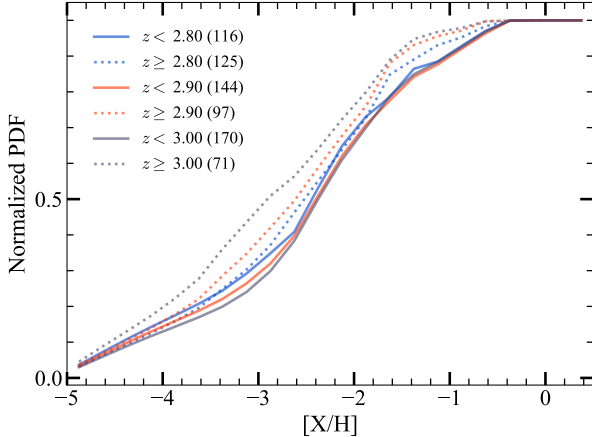


Figure 22. Comparison of the metallicity CDFs of the absorbers in KODIAQ-Z and HD-LLS with $14.5 \leq \log N_{\text{HI}} < 19$ above and below a given redshift threshold, $z_{\text{th}} = 2.8, 2.9, 3.0$. The numbers between parentheses indicate the number of absorbers in each redshift interval.

$[\text{X}/\text{H}] - 2.8$ than at lower redshifts, demonstrating that within the redshift interval $2.2 \lesssim z \lesssim 3.6$, there is a change in the metallicity PDFs with an overall increase of the metallicity at $2.2 \lesssim z < 2.8$ compared to $2.8 \lesssim z \lesssim 3.6$.

6.4. Metallicity Variation over Small Velocity Scales

Owing to the treatment of the absorbers where we separate individual H I components as much as possible (see §3), our KODIAQ-Z survey provides also information on the metallicity variation over small redshift/velocity separation between absorbers. Following CCCIII, we define here paired absorbers as absorbers that are closely separated in redshift space so that $\Delta v \equiv |(z_{\text{abs}}^2 - z_{\text{abs}}^1)/(1 + z_{\text{abs}}^1) c| < 500 \text{ km s}^{-1}$. We have a sample of 37 such paired absorbers.

In Fig. 23, we show in the left panel the absolute metallicity difference ($\Delta[\text{X}/\text{H}]$) between the higher and lower median metallicities of the paired absorbers against their absolute velocity separation and in the right panel the histogram distribution of $\Delta[\text{X}/\text{H}]$. As observed at low z (CCC III), we find no obvious relation between Δv and the level of the metallicity variation. At any velocity separation, there is a large scatter from about 0.2 dex to > 2 dex. Using the survival method to account for the lower limits (Feigelson & Nelson 1985), we estimate a mean $\langle \Delta[\text{X}/\text{H}] \rangle = 1.20 \pm 0.16$ (error on the mean) and the IQR in $\Delta[\text{X}/\text{H}]$ is $[0.38, 1.81]$. There appear to be two main clusters of data separated at $\Delta[\text{X}/\text{H}] \simeq 1$ with about 50% of the sample in each bin and with a mean $\langle \Delta[\text{X}/\text{H}] \rangle = 0.39 \pm 0.05$ and 2.15 ± 0.13 below and above this limit, respectively. Therefore for the about half of the paired absorbers, there is evidence

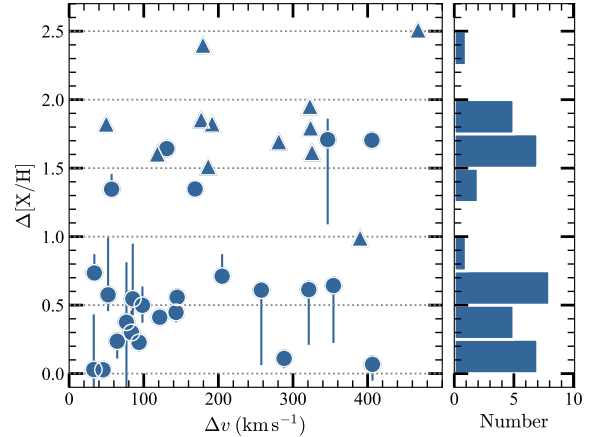


Figure 23. *Left:* scatter plot of the difference between the higher and lower median metallicities for the closely-redshift separated absorbers (a.k.a. paired-absorbers) as a function of their absolute velocity difference. For the lower limits (blue triangles), we use the lower bound of the 80% CI to be the most conservative. *Right:* distribution of the metallicity differences between paired-absorbers.

for metallicity variations over $\Delta v \lesssim 500 \text{ km s}^{-1}$ of a factor 2–3 and for the other half of a factor > 140 .

Owing to the large metallicity variation over $\Delta v \lesssim 500 \text{ km s}^{-1}$, *a posteriori* it is justified to treat these paired absorbers as individual absorbers. The other direct consequence is, when possible, components in absorbers should be treated individually to derive the true metallicity of the gas rather than a column-density weighted average metallicity between very different types of gaseous components, a consequence first inferred by Prochter et al. (2010) at similar redshifts for one LLS and then in the CCC survey at $z < 1$ for 30 paired-absorbers (CCC II; CCC III; see also Kacprzak et al. 2019; Zahedy et al. 2021). We discuss the implication of these findings in §10.4 in more detail.

6.5. The $[\text{C}/\alpha]$ ratio as a Function of the Metallicity

In the photoionization modeling of the absorbers to determine their metallicities, the $[\text{C}/\alpha]$ ratio is allowed to vary in the range $-1 \lesssim [\text{C}/\alpha] \lesssim +1$ to take into account possible nucleosynthesis effects that likely arise from the time-lag in the production between α -elements and carbon (e.g., Cescutti et al. 2009; Mattsson 2010). The general trend between $[\text{C}/\alpha]$ and $[\alpha/\text{H}]$ seen in stars (e.g., Akerman et al. 2004; Fabbian et al. 2010) and SLLSs/DLAs (e.g., Pettini et al. 2008; Penprase et al. 2010; Cooke et al. 2011) is a decrease of $[\text{C}/\alpha]$ from about $[\text{C}/\alpha] \simeq 0$ (up to $+0.2$ dex) at $[\alpha/\text{H}] \gtrsim 0$ to $[\text{C}/\alpha] \simeq -0.6$ at $[\alpha/\text{H}] \simeq -0.5$ where $[\text{C}/\alpha]$ plateaus around that metallicity value up to a metallicity of

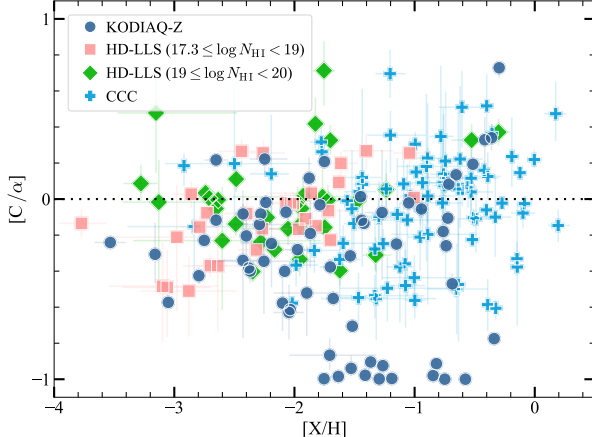


Figure 24. The $[C/\alpha]$ ratio against the metallicity of the absorbers from the KODIAQ-Z ($2.2 \lesssim z \lesssim 3.6$), HD-LLS ($2.2 \lesssim z \lesssim 3.6$), and CCC ($z \lesssim 1$) surveys. The median values of the $[C/\alpha]$ and $[X/H]$ posterior PDFs are adopted with 68% CI. Note that $[C/\alpha]$ -values with $[C/\alpha] < -0.6$ are most likely predominantly caused by ionization corrections rather than nucleosynthesis effects (see text for more details).

$[\alpha/H] \simeq -2$ where an upturn is observed in $[C/\alpha]$ with an increase of $[C/\alpha]$ to $[C/\alpha] \gtrsim +0.2$ at $[\alpha/H] \leq -2.8$.

As discussed in CCC III at low redshift and Lehner et al. (2016) at high redshift, the SLFSs, pLLSs, and LLSs do not quite follow this overall trend. In fact, little trend is observed between $[C/\alpha]$ and $[\alpha/H]$ for these absorbers with a large scatter in $[C/\alpha]$ at any metallicity. While no obvious trend is observed between $[C/\alpha]$ and $[\alpha/H]$ for these absorbers, CCC III note three characteristics: 1) a lower floor level for the distribution at about $[C/\alpha] \simeq -0.6$, similar to that observed for the stars, H II regions, and SLLSs/DLAs; 2) an upper ceiling of the distribution at $[C/\alpha] \simeq +0.5$, but with a concentration of data around $0 < [C/\alpha] \sim +0.3$, similar again to the highest values observed in stars, H II regions, and SLLSs/DLAs; and 3) a tentative upturn in $[C/\alpha]$ at $[X/H] \lesssim -2$, which would be similar to the one observed in stars and SLLSs/DLAs.

With KODIAQ-Z and our re-modeling of the HD-LLS absorbers, we can now revisit these conclusions with a much larger sample at high redshift, especially in the low metallicity regime. In Fig. 24, we show $[C/\alpha]$ as a function of $[X/H]$ for all the absorbers in KODIAQ-Z, HD-LLS, and CCC where the relative abundance and metallicity are simultaneously constrained. In that figure, we use different symbols to differentiate LLSs from SLLSs in the HD-LLS survey (there is only one SLLS in KODIAQ-Z with information on $[C/\alpha]$, see Fig. 11, which we did not highlight in Fig. 24). Excluding the 13 absorbers with $[C/\alpha] \lesssim -0.9$ (because those are more largely af-

fected by ionization, see 5.3 and below), the addition of the KODIAQ-Z and HD-LLS data confirm the first two characteristics described above and summarized in CCC III. However, at $[X/H] \lesssim -2$, there is no clear upturn in $[C/\alpha]$ for the absorbers with $\log N_{\text{HI}} < 19$, although the scatter in the $[C/\alpha]$ distribution becomes smaller. On the other hand, considering the SLLSs from HD-LLS (diamond symbols in Fig. 24), the upturn in $[C/\alpha]$ is apparent when the metallicity becomes smaller than $[X/H] \lesssim -2.2$.

Since the derived ratio of $[C/\alpha]$ is controlled by both ionization corrections and nucleosynthesis effects, it is plausible that the ionization corrections are washing away some of the trends that would appear if only nucleosynthesis effects were at play (as for example for the DLAs). In §5.6, we show that $[C/\alpha]$ in the KODIAQ-Z sample is more affected by ionization than in the two other samples in view of the correlation between $[C/\alpha]$ and f_{HI} . However, no such correlation is observed in CCC and HD-LLS, and the overall dispersion is similar in these three surveys. The mean values for $[C/\alpha]$ in CCC and HD-LLS are also the same (see §5.6), despite widely different ionization correction levels. Therefore the $[C/\alpha]$ ratio with $[C/\alpha] > -0.6$ determined from the ionization modeling does not seem to have a strong dependence with the level of the ionization correction. Nevertheless, the ionization correction essentially adds noise in the $[C/\alpha]$ distribution at the level of ± 0.3 dex at any N_{HI} and metallicity, which is large enough to hide subtle changes of $[C/\alpha]$ with $[X/H]$ at the expected level of 0.2–0.5 dex. Hence, the scatter observed in Fig. 24 must be largely caused by ionization while the range $-0.6 \lesssim [C/\alpha] \lesssim +0.5$ where most of the absorbers lie may be controlled by nucleosynthesis effects based on its similarity observed in DLAs, stars, and H II regions.

7. PHYSICAL PROPERTIES OF THE SLFSs, PLLSs, LLSs, AND SLLSs AT $2.2 \lesssim z \lesssim 3.6$

The photoionization models discussed in §5 also predict the physical properties of the absorbers. In particular, these include the neutral fraction of the gas (f_{HI}), the density of the gas (n_{H}), the total H column density ($N_{\text{H}} \equiv N_{\text{HI}} + N_{\text{HII}}$), the length-scale of the cloud ($l \equiv n_{\text{H}}/N_{\text{H}}$), and the temperature of the gas (T). These can in turn be used to constrain the cosmological baryon and metal budgets for the absorbers (Fumagalli et al. 2016b; CCC III). A caveat to keep in mind and discussed at length in Fumagalli et al. (2016b) is that there is a degeneracy between the density and intensity of the radiation field. This dependency produces much less robust inference on the density and sizes of absorbers than for the metallicity, which depends only on the shape of the

radiation field. We also remind the reader that only photoionization by the EUVB has been used in this work, and it is quite plausible that more than one ionization process is at play, which would also affect more the physical quantities discussed in this section.

7.1. Densities, H Column Densities, Temperatures, and Length Scales

We summarize the physical quantities (n_{H} , N_{H} , l , and T) derived from our modeling for the KODIAQ-Z sample in Table 7. Values of $\log n_{\text{H}}$ with a trailing colon represents absorbers for which we adopted a Gaussian prior on $\log U$, and therefore on $\log n_{\text{H}}$. In Table 8, we summarize the statistical properties of the physical properties derived for the entire sample (median, mean, and dispersion of N_{HI} , n_{H} , N_{H} , l , and T) and a restricted sample where only a flat prior on $\log U$ was used. Comparing the results from Table 8 between the entire and restricted samples, it is apparent that the results are not statistically different. We emphasize that most of the pLLSs, LLSs, SLLSs did not require a Gaussian prior on $\log U$. However, for about 45% of the pLLSs, we had to use a Gaussian prior on $\log U$, and the results are essentially the same in both sample. Hereafter, we therefore consider the results from the entire sample. In Fig. 25, we show the posterior PDFs of N_{H} , and n_{H} , and l for the SLLSs and LLSs (using results from KODIAQ-Z and HD-LLS) in the top two rows and the pLLSs and SLFSs (from KODIAQ-Z) in the bottom two rows. These PDFs contrast remarkably from the metallicity PDFs with much narrower distributions.

Temperatures of ionized gas predicted by Cloudy are based on the balance of atomic heating (photoionization) and cooling (recombination and collisional effects). As such, temperatures are dependent on the radiation field shape and intensity, density, and metallicity of the models. The distribution of predicted temperatures has overall small dispersion, and there is a clear trend of decreasing temperatures as N_{HI} increases of about 0.1 dex decreases between each absorber category from the SLFSs, pLLSs, LLSs, to SLLSs (see Table 8). For the SLFSs, the average temperature is around 3×10^4 K, while it is a factor 2 less on average for the SLLS. In §4.2, we show that for about 90% of the H I components $\langle b \rangle = 27 \pm 6 \text{ km s}^{-1}$. This places an upper limit on the temperature from the observations of $T < 4 \times 10^4$ K, consistent with the ionization modeling. It also implies that for the SLFSs, on average the thermal broadening component is somewhat larger than the non-thermal component, while for the other absorbers, non-thermal motions take over the thermal ones. Compared to the CCC III, the predicted temperatures of the $z < 1$ SLFSs,

pLLSs, and LLSs are about a factor 1.4 times smaller than at $2.2 \lesssim z \lesssim 3.6$.

Considering the SLFSs, pLLSs, and LLSs, the total H column densities decrease with decreasing N_{HI} , but their distributions overlap within 1σ dispersion (that are large for these quantities, see Table 8 and Fig. 25). The differences between the mean $\log N_{\text{HI}}$ for SLFSs compared with the pLLSs and the pLLSs to the LLSs are a factor 4 and 28, respectively. In contrast, the differences in total H are significantly smaller with differences of a factor ~ 4 and 6.5 between the SLFSs and pLLSs and pLLSs and LLSs, respectively. Thus, despite their lower N_{HI} values, the contribution of pLLSs and SLFSs to the total mass and baryon budgets are higher compared with the LLSs than their H I columns would suggest, especially since they are more numerous (e.g., Prochaska et al. 2014 and see §8). The N_{H} column densities for SLLSs are similar to those for LLSs, N_{H} is about the same even though N_{HI} is on average a factor 34 smaller for the LLSs than for SLLSs. Given the higher incidence of LLSs, they make a larger contribution to the cosmic baryon budget than the SLLSs. Compared to CCC III, N_{H} at the $z < 1$ SLFSs, pLLSs, and LLSs are about a factor $\sim 10\text{--}15$ smaller than at $2.2 \lesssim z \lesssim 3.6$.

The estimated hydrogen densities increase as N_{HI} increases. The SLLSs has the largest dispersion on n_{H} , which is caused by a long tail at low and high n_{H} values (see Fig. 25). While there is an increase in n_{H} with increasing N_{HI} , the bulk of the hydrogen density for the pLLSs, LLS, and LLSs are within about $\log n_{\text{H}} \simeq -3.4$ and -1.8 , while for SLFSs it is between $\log n_{\text{H}} \simeq -4.2$ and -2.5 . At $z \sim 2.8$ (the mean redshift of KODIAQ-Z), the mean cosmic density is about $\bar{n}_{\text{H}} \simeq 10^{-5} \text{ cm}^{-3}$ (Schaye 2001b). The pLLSs, LLSs, and SLLSs therefore probe over-densities of $\delta \equiv n_{\text{H}}/\bar{n}_{\text{H}} - 1 \sim 40\text{--}1600$ while for the lower column SLFSs $\delta \sim 5\text{--}320$. A large part of the observed pLLSs, LLSs, and SLLSs largely probe virialized (mini)halos ($\delta > 100$, Schaye 2001b). For SLFSs, there is more a mixture of systems probing over-densities below and above 60, at the transition between the IGM and virialized halos (Schaye 2001b). Compared to the CCC III, n_{H} at the $z < 1$ SLFSs, pLLSs, LLSs, SLLSs are about a factor $\sim 1.5\text{--}2.5$ smaller than at $2.2 \lesssim z \lesssim 3.6$. However, owing to the redshift dependence of the mean cosmic density that is $\propto ((1+z)/4)^3$ (Schaye 2001b), the density contrast at $z < 1$ for the SLFSs and other stronger H I absorbers is always $\delta > 100$, even for the lower densities probed by SLFSs (although we note that at $z < 1$, only $\log N_{\text{HI}} > 15$ SLFSs could be probed).

The length-scales, which are directly related to n_{H} and N_{H} , have the largest dispersion among all these physical

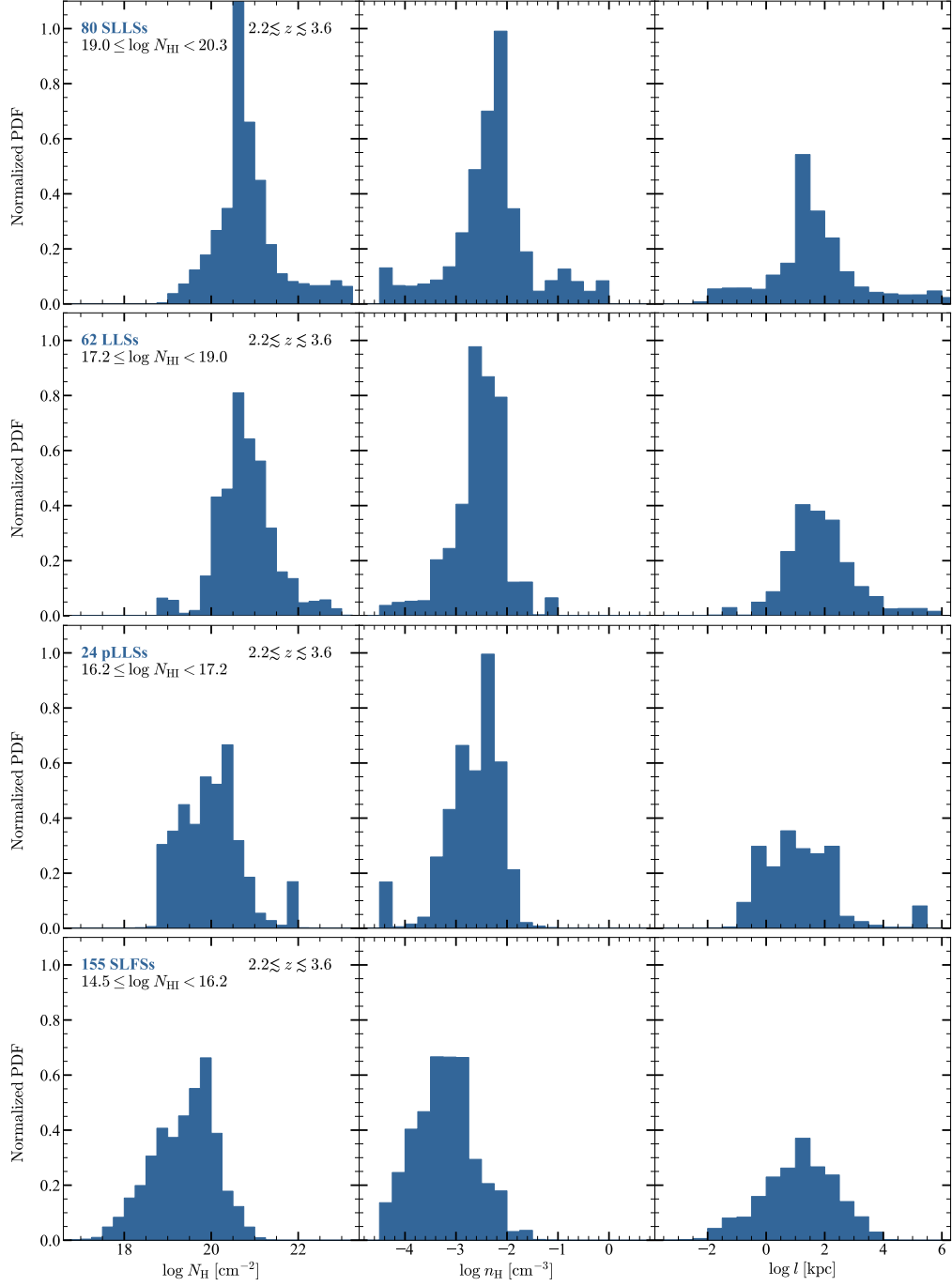


Figure 25. Posterior PDFs of the total H column density (*left*), H density (*middle*), and path-length (*right*) for SLLSs, LLSs, pLLSs, and SLFSs for the entire sample from the KODIAQ-Z survey and HD-LLSs.

quantities. For the SLFSs and pLLSs, the interquartile range (IQR) of length-scale of the absorbers is about $4 \lesssim l \lesssim 150$ kpc. For the LLSs, IQR for l is $18 \lesssim l \lesssim 288$ kpc and for the SLLSs it is $8 \lesssim l \lesssim 80$ kpc. In contrast at $z < 1$, the IQR of length-scale of these absorbers is $0.3 \lesssim l \lesssim 3.2$ kpc (CCC III). At $2.2 \lesssim z \lesssim 3.6$, the SLFSs, pLLSs, LLSs, and even the SLLSs may probe a variety of structures from gas embedded in virialized ha-

los to large-scale structures. Recent MUSE galaxy surveys show strong hints that at least LLSs may probe a wide variety of environments at $z > 2$, including gaseous filaments, CGM of galaxies, or intra-group gas (e.g., Fumagalli et al. 2016a, 2017; Lofthouse et al. 2020).

7.2. Neutral Fractions

The behaviour of the neutral fraction with N_{HI} can be used to constrain the cosmic baryon and metal budgets (see §8). In Fig. 26, we show the neutral fraction of the absorbers estimated from the Cloudy models as a function of N_{HI} from $\log N_{\text{HI}} \simeq 14.6$ to 20 from KODIAQ-Z and HD-LLS (see §5.2, and see also the recent work for the SLLSs from Berg et al. 2021). There is a clear correlation between f_{HI} and N_{HI} . This is confirmed by the Spearman rank-order test that shows a strong positive monotonic correlation between f_{HI} and N_{HI} with a correlation coefficient $r_S = 0.9$ and a p -value $\ll 0.05\%$. However, the slope of the correlation is shallower between the SLFS, pLLS, LLS regimes compared to the LLS, SLLS regimes. The dashed red line in Fig. 26 is a linear fit to the data with $14.6 \leq \log N_{\text{HI}} < 19$, yielding $\log f_{\text{HI}} = (0.51 \pm 0.04) \log N_{\text{HI}} - 12.00$. The slope is quite similar to that found at $z < 1$ for absorbers with $15.1 \leq \log N_{\text{HI}} < 19$ (CCC III). The dash-dotted magenta line is a linear fit to the data with $17.2 < \log N_{\text{HI}} \leq 20$, $\log f_{\text{HI}} = (1.00 \pm 0.08) \log N_{\text{HI}} - 20.76$, which is consistent with the linear fit derived in the HD-LLS survey for the LLSs+SLLSs (Fumagalli et al. 2016b).

To model this overall trend between f_{HI} and N_{HI} , we use a Gaussian process (GP) model, providing a generic supervised learning method designed to solve a regression. We refer the reader to Appendix F in Lehner et al. (2020) for more details about this method, but in short, the advantage of this method is that the prediction interpolates the observations in a nonparametric way and is probabilistic so that empirical confidence intervals can be computed. We use the Python GAUSSIAN PROCESS REGRESSION package within SCIKIT-LEARN (Pedregosa et al. 2011; Buitinck et al. 2013) to model the data with a squared-exponential kernel (the use of a more complex kernel like a Matern kernel would yield similar results when using similar bounds). The overall scatter in the data is typically much larger than the errors on single data point, and we use the 1σ dispersion derived for SLFSs, pLLSs, LLSs, and SLLSs to inform the GP model of the intrinsic scatter in the data (this can be understood as a prior factor to smooth out the scatter of the data). The black curve in Fig. 26 is the GP model with the dark area showing the standard deviation determined by the GP model. There is a large overlap with the two linear fits, but the GP fit has the advantage of providing a global model to the data without *a priori* selecting manually the inflection point in the curve. The black curve is well-fitted by a third order polynomial, $\log f_{\text{HI}} = -0.0104x^3 + 0.6268x^2 - 11.62x + 64.23$ (where $x = \log N_{\text{HI}}$).

8. COSMOLOGICAL BUDGETS

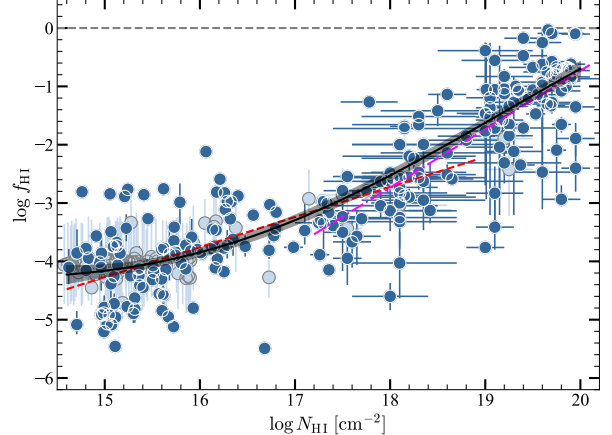


Figure 26. The neutral fraction of H I versus N_{HI} using the KODIAQ-Z and HD-LLS surveys. The median values of the posterior PDFs are adopted with 68% CI. Light blue data were estimated using a Gaussian prior on $\log U$, while the other data have a flat prior on $\log U$. The black curve is a GP-derived model to the entire N_{HI} range shown in the figure (the dark area corresponds to the dispersion derived from the GP model). The dashed red line is a linear fit to the data with $14.6 \leq \log N_{\text{HI}} < 19$ (i.e., the SLFSs, pLLSs, and LLSs). The dash-dotted magenta line is a linear fit to the data with $17.2 < \log N_{\text{HI}} \leq 20$ (i.e., the LLSs and SLLSs). For all the models, we consider only data with a flat prior on $\log U$ (although the results are similar if the entire dataset was considered instead).

8.1. Cosmological Baryon Budget

Observations of the LYAF show that about 80%–90% of the baryons at $2 < z < 4$ are found in the cool photoionized phase of IGM (e.g., Rauch et al. 1997; Weinberg et al. 1997; Kim et al. 2001). In Lehner et al. (2014), we show that the photo- and collisionally-ionized gas found in $\tau_{\text{LL}} > 1$ systems is very likely the second largest contributor to the baryon budget at $z \sim 2$ –3. However, this result could be affected by small-number statistics as Lehner et al. sample included only 7 LLSs and 8 SLLSs. Our earlier study also did not consider the baryon contributions from the SLFSs and pLLSs. Here we review the impact of the cool, photoionized gas in these absorbers on the cosmic baryon budget at $2.2 \lesssim z \lesssim 3.6$.

The mass gas density relative to the critical density, Ω_g , can be estimated via (e.g., Tytler 1987; Lehner et al. 2007; O’Meara et al. 2007; Prochaska et al. 2010; CCC III):

$$\Omega_g = \frac{\mu_H m_H H_0}{\rho_c c} \int \frac{N_{\text{HI}}}{f_{\text{HI}}} \mathcal{F}(N_{\text{HI}}) dN_{\text{HI}}, \quad (1)$$

where $m_H = 1.673 \times 10^{-24}$ g is the mass of hydrogen, $\mu_H = 1.3$ corrects for the presence of helium, $c = 2.9979 \times 10^{10}$ cm s $^{-1}$ is the speed of light, $\rho_c =$

$3H_0^2/(8\pi G) = 8.62 \times 10^{-30} \text{ g cm}^{-3}$ is the $z = 0$ critical density, $H_0 = 2.20 \times 10^{-18} \text{ s}^{-1}$ is the Hubble constant,¹¹ and $\mathcal{F}(N_{\text{HI}})$ is the column density distribution function. For $\mathcal{F}(N_{\text{HI}})$, we adopt the spline function model from Prochaska et al. (2014) at $z \approx 2.5$ (see their Table 2 and Fig. 7). For the neutral fraction, f_{HI} , we adopt the GP model from §7.2. Integrating the above equation over the different N_{HI} regimes of the SLFSs, pLLSs, LLSs, and SLLSs, we find that $\Omega_g \simeq (2.7, 1.1, 1.4, 1.1) \times 10^{-3}$ for the SLFSs, pLLSs, LLSs, and SLLSs, respectively. The contributions of Ω_g to the total baryon density are $\Omega_g/\Omega_b \simeq 5.5\%, 2.2\%, 2.8\%, 2.3\%$ for the SLFSs, pLLSs, LLSs, and SLLSs, respectively ($\Omega_b = 0.0486$, Planck Collaboration et al. 2016). The values for the LLSs and SLLSs are consistent with the ranges in Lehner et al. (2014) (their Table 6, column with Si IV).¹²

Importantly these estimates do not include a contribution from the highly ionized, hotter gas that is not photoionized. Lehner et al. (2014) found that the O VI collisionally ionized gas in LLSs and SLLSs could contribute to 0.4–10% to baryonic budget. As noted in §5.1, for the pLLSs and SLFSs, we often find that the O VI absorption is narrow and aligns with the absorption seen in H I (and other lower metal-ions if they are detected), i.e., the properties of the O VI are quite different as N_{HI} decreases to $\log N_{\text{HI}} < 17$ compared to stronger H I absorbers. The observed column densities for these narrow O VI components are also well-reproduced by single-phase photoionization models as those described in §5 where the source of the ionizing photons is EUVB. Providing a full description of the O VI associated with the KODIAQ-Z absorbers is beyond the scope of this paper, but based on a visual inspection of the profiles and our ionization modeling, very broad, strong O VI absorbers associated with SLFSs and pLLSs are rare, whereas they are common in LLSs, SLLSs, and even DLAs. Therefore the contribution of broad, strong O VI associated with SLFSs and pLLSs to the cosmic baryon budget is very likely small.

The photoionized gas associated with pLLSs, LLSs, and SLLSs combined therefore contribute $\Omega_g/\Omega_b \simeq 7\%$ and the SLFSs contribute to another 5.5% to the total baryon budget.¹³ In contrast, the neutral gas that

¹¹ We adopt here the Planck 2015 results (Planck Collaboration et al. 2016).

¹² Although we remind the reader that here the SLLSs include only absorbers with $19 \leq \log N_{\text{HI}} \leq 20$ owing to the grid of ionization models stopping at $\log N_{\text{HI}} = 20$.

¹³ We separate the SLFSs from the other absorbers because, e.g., Kim et al. (2001) included those in the LYAF contribute where they estimate that 90% of all baryons reside in the LYAF at $1.5 < z < 4$.

is mostly found in DLAs yield only $\Omega_g/\Omega_b \simeq 2\%$ at $z \sim 2\text{--}5$. (e.g., Prochaska et al. 2005; Wolfe et al. 2005; Lehner et al. 2014; Péroux & Howk 2020). At $z < 1$, CCC III find fractional contributions to baryonic budget for the SLFSs, pLLSs, and LLSs that are about 10 times smaller. At $z < 1$, the SLFSs, pLLSs, and LLSs are probing much larger overdensities, and at these redshifts only $\sim 5\%$ of the baryons are thought to be in the CGM of galaxies (Shull et al. 2012).

8.2. Cosmological Metal Budget

The metal density of the absorbers can be estimated with the baryon density via $\Omega_m = \Omega_g Z$, where $Z = 10^{[\text{X}/\text{H}]} Z_\odot$ is the metallicity of the gas in mass units and $Z_\odot = 0.0142$ is the bulk solar metallicity in mass units from Asplund et al. (2009). For the metallicity, we use the linear mean metallicities in about 0.5 dex bin of N_{HI} from $\log N_{\text{HI}} = 14.5$ to $\log N_{\text{HI}} = 20$. We note that the linear mean metallicities for SLFSs, pLLSs, and LLSs are $0.035, 0.032, 0.028 Z_\odot$, respectively. We find $\Omega_m = (1.4, 4.7, 5.9) \times 10^{-7}$ for the SLFSs, pLLSs, and LLSs, respectively. The latter value is consistent with that derived by Fumagalli et al. (2016b), $\Omega_m = 5.1 \times 10^{-7}$. It is not surprising that our value is somewhat larger since KODIAQ-Z added a few LLSs on the high metallicity side, including one with $[\text{X}/\text{H}] \simeq -0.4$ (see, e.g, Fig. 18) and since the estimate of Ω_m that depends on the mean linear metallicity is much more sensitive to the positive tail end of the logarithmic metallicity PDF. Since we do not have SLLSs with $\log N_{\text{HI}} > 20$ in our sample, we use the result from the HD-LLS survey where Fumagalli et al. (2016b) derived $\Omega_m = 1.6 \times 10^{-6}$ for the SLLSs. For reasons (sample variance, using the arithmetic mean) discussed in detail in Fumagalli et al., these values are uncertain by a factor ~ 3 (see also discussion in Berg et al. 2021). We note that the comoving metal-mass density can be estimated via $\rho_m = \Omega_m/\rho_c$ (e.g., Péroux & Howk 2020). Therefore, for the combined photoionized SLFSs, pLLSs, and LLSs, we find $\rho_m = 1.5 \times 10^5 \text{ M}_\odot \text{ cMpc}^{-3}$, while combined with the SLLSs, this increases to $3.5 \times 10^5 \text{ M}_\odot \text{ cMpc}^{-3}$.

The total expected cosmic metal density from the output of stars at $z \sim 2.8$ is about $\Omega_m^{\text{exp}} \simeq 9 \times 10^{-6}$ or expressed in terms of cosmic metal mass density $\rho_m^{\text{exp}} \simeq 10^6 \text{ M}_\odot \text{ cMpc}^{-3}$ (Péroux & Howk 2020). Péroux & Howk (2020) also recently estimated for the DLAs, i.e., for the neutral gas, that $\Omega_m \simeq 3.5 \times 10^{-6}$ and for the dust $\Omega_m \simeq 1 \times 10^{-6}$ at $2.2 \lesssim z \lesssim 3.6$, i.e., about 40% of the metals are in the neutral gas and about 10% are in form of dust at $2.2 \lesssim z \lesssim 3.6$. The SLLSs account for 17%, while the SLFSs, pLLSs, and LLSs account for 1.5%, 5.1%, 6.4%, and all combined they account for

about 30% of the metals at $2.2 \lesssim z \lesssim 3.6$. We note that the recent estimates from Péroux & Howk (2020) for the SLLSs and LLSs are about within 1σ errors from those derived here and Fumagalli et al. (2016b). As for the baryons, another contribution is from the hot O VI gas associated with LLSs, SLLSs, and DLAs that can contribute another $\gtrsim 7\%$ (Lehner et al. 2014).

While most of the baryons at $2.2 \lesssim z \lesssim 3.6$ are in the LYAF, this is not the case for the metals since the DLAs, dust, SLLSs, LLSs, pLLSs, and SLFSs contribute to about 90% of the cosmic metal budget. Direct estimates of the metal budgets in the LYAF are uncertain owing to ionization correction and the fact that some of the metals are not solely associated with $\log N_{\text{HI}} \gtrsim 14.5$ absorbers. Using the recent results on Ω_{CIV} from D’Odorico et al. (2013, 2010) (but see also, e.g., Schaye et al. 2003; Simcoe et al. 2004; Songaila 2005) and correcting their estimate from C IV to carbon and carbon to the total metal content yields $\Omega_m \gtrsim 3.4 \times 10^{-7}$ at $z \sim 2.8$ for the “IGM” or about $\gtrsim 4\%$ of the total cosmic metal budget (although we note this may include contributions from higher H I column density absorbers than LYAF absorbers). Overall the ionized universe probed by absorbers $\log N_{\text{HI}} < 20$ contains about 40% of the metals at $2.2 \lesssim z \lesssim 3.6$. Combining these results with those from Péroux & Howk (2020), the majority of metals are in the neutral and ionized gas at $z \sim 2.8$.

At $z < 1$, $\Omega_m = (4.6, 6.5, 25.9) \times 10^{-7}$ for the SLFSs, pLLSs, and LLSs, respectively, (CCC III).¹⁴ In terms of comoving mass density, the combined SLFSs, pLLSs, and LLSs at $z < 1$ have $\rho_m = 4.7 \times 10^5 \text{ M}_\odot \text{ cMpc}^{-3}$. Therefore the amount of metals in SLFSs, pLLSs, and LLSs has increased by a factor 3 from $z \simeq 2.2\text{--}3.6$ to $z \lesssim 1$. However, the total expected cosmic metal density at $z \sim 0.5$ is about $\Omega_m^{\text{exp}} \simeq 6 \times 10^{-5}$ or cosmic metal mass density $\rho_m^{\text{exp}} \simeq 8 \times 10^6 \text{ M}_\odot \text{ cMpc}^{-3}$ (Péroux & Howk 2020), a factor 7 larger than at $z \sim 2.8$. This implies that the (photoionized) metals associated with the SLFSs, pLLSs, and LLSs account for about 6% of the cosmic metal budget at low redshift, a factor 2 times lower than the contribution of the same absorbers at $2.2 \lesssim z \lesssim 3.6$. As shown by Péroux & Howk (2020), the majority of the metals at low redshift remain in galaxies (including stars), in their vicinity, and in the

hot intra-cluster medium, demonstrating a major shift in the distribution of the metals from 2.3 Gyr to $\gtrsim 9$ Gyr post-Big Bang.

9. COMPARISON TO THE FOGGIE SIMULATIONS

9.1. Motivation and Methodology

In this section we compare the KODIAQ-Z metallicity measurements as a function of H I column density to the simulated CGM from the FOGGIE project (Peeples et al. 2019, and <https://foggie.science/>). This project is comprised of cosmological zoom simulations of six Milky Way-like halos. While KODIAQ-Z selects for absorbers without knowing their galaxy associations, absorbers with the highest column densities probe overdensities that are consistent with being virialized (mini)halos of galaxies (see §7.1 and §9.3). The FOGGIE simulations let us address whether or not the metallicity-H I column density distribution seen in KODIAQ-Z could be explained by only the CGM and nearby IGM of progenitors to Milky Way-mass galaxies.

Many groups, including FOGGIE, have recently shown that better spatial resolution in the simulated CGM leads to a natural development of small clouds (van de Voort et al. 2019; Peeples et al. 2019; Rhodin et al. 2019; Suresh et al. 2019), largely because once the cooling length of the gas is resolved the gas can cool and condense into smaller structures (Humels et al. 2019; Zheng et al. 2020). Importantly for comparisons to observables such as metallicity, improved spatial resolution in the low-density gas also reduces the artificial mixing of metals, thereby allowing gas to remain at “high” and “low” metallicities even in the CGM; that is, while the median metallicities do not change much, the scatter about that median increases with improved resolution (Corlies et al. 2020). In the FOGGIE cosmological zoom-in simulations analyzed here the CGM resolution at $z = 2$ is 91 proper pc in the cooler gas, with a coarsest resolution of 365 proper pc. (The resolutions are correspondingly a factor of 0.85 and 0.75 smaller at $z = 2.5$ and $z = 3$, owing to the spatial resolution being at a fixed comoving size). This spatial resolution profile enables both the development of small relatively-dense and cool clouddlets and for the hotter, more rarefied, generally more metal-rich gas to be well-resolved. Our analysis uses the $z = 2, 2.5$, and 3 outputs for each of the six FOGGIE halos. As presented in Simons et al. (2020), these halos are selected to be “Milky Way-like” in that they are roughly $\sim 10^{12} \text{ M}_\odot$ at $z = 0$ and have no mergers of mass ratios more than 1:10 after $z = 2$ (see also Zheng et al. 2020 and Lochhaas et al. 2021 for the full histories and $z = 0$ properties of the Tempest, Squall, and Maelstrom halos). While the KODIAQ-Z

¹⁴ In CCC III, we inadvertently used the mean logarithmic metallicity, instead of the linear mean, which does not change the value for the LLSs, but does for the SLFSs and pLLSs, which are, respectively, $0.177Z_\odot$ and $0.197Z_\odot$. This increases Ω_m by a factor 5 for these absorbers. As the LLSs dominate the metal budget, the effect on the total Ω_m for the SLFSs, pLLSs, and LLSs is only an increase by a factor 1.3, i.e., $\Omega_m \simeq 3.7 \times 10^{-6}$ for these absorbers at $z < 1$.

absorbers are not selected to be associated with Milky Way-like halos, galaxy halos of this size account for most of the stellar mass in the universe and therefore most of the chemical enrichment.

We extracted H I absorbers from each sightline using the Synthetic Absorption Line Surveyor Application (SALSA, Boyd et al. 2020) and its Simple Procedure for Iterative Cloud Extraction (SPICE) method. Across all six FOGGIE galaxies, we found 8825 H I absorbers at $z = 3$, 8207 at $z = 2.5$, and 7694 at $z = 2$, for a total of 24,726 H I absorbers. SPICE identifies absorbers based on H I number density, without the need for synthetic spectra. First, a number density cutoff is determined such that 80% of the total column density lies above the cutoff¹⁵. An interval is defined encompassing the sightline’s cells that lie above this cutoff. This interval is then masked, and a new number density cutoff is found. The intervals from these two generations are then combined if they overlap along the line of sight and their average line-of-sight velocities are within 10 km s^{-1} of each other. These steps are repeated until the total column density of the remaining, unmasked cells falls below $\log N_{\text{HI}} = 12$. SALSA then calculates the total column density and column-density weighted average metallicity of each identified absorber.

While KODIAQ-Z is an H I-selected survey, we also extracted C IV and Si IV absorbers from these same sightlines in order to assess how our sample of simulated absorbers would differ if we also required the presence of metal absorption. Carbon and silicon are not tracked by the FOGGIE simulations, so they are inferred from the metallicity field assuming solar abundances. Their ionization states are estimated using the Trident code (Hummels, Smith, & Silvia 2017), based on a table of Cloudy equilibrium models (Ferland et al. 2013) using the Haardt & Madau (2012) UV background with self-shielding (Emerick et al. 2019). We pair our H I and metal absorbers based on their position within the simulations and their velocities. To be paired, the two absorbers must be within the same sightline, within 100 pc of each other, and have line-of-sight velocities within 10 km s^{-1} of each other. Pairing absorbers in this way is robust to minor changes in distance and velocity. Of our 24,736 H I absorbers at redshifts 2, 2.5, and 3, 1189 have an associated C IV absorber and 358 are associated with an Si IV absorber.

¹⁵ Adjusting this cutoff has a slight effect on the total number of absorbers but does not significantly impact the resulting distribution of properties. Using a 70% threshold results in a 6% drop in the number of H I absorbers, and a 90% threshold a 11% increase.

9.2. Comparison of the Metallicities

The column density and average metallicity of our extracted FOGGIE H I absorbers are shown in Fig. 27. The plot bounds and dotted and dashed lines are the same as in Fig. 18. The left panel shows all H I absorbers in cyan, with the observational samples overplotted. Gray-scale contours have been added to illustrate the structure of the scatter plot where the density of points is highest. For the rightmost panel, no metallicity limit or metal line requirement has been imposed on the H I absorbers. The middle panel only shows H I absorbers that are close to a C IV or Si IV absorber in position and velocity space, which—due to column density limits on our selection—is analogous to requiring a C IV or Si IV detection with column densities $> 10^{12} \text{ cm}^{-2}$. This limits the metallicity of the H I absorbers to $[\text{X}/\text{H}] \gtrsim -2.4$, which is the limit defining the metal-poor regime for KODIAQ-Z. Imposing requirements on metal line detection can therefore limit the observed metallicity range (reinforcing the idea that a H I-selection is required to probe the entire metallicity distribution). It should be noted that the gradual increase in the absorber metallicity as N_{HI} decreases seen in the middle panel is caused by the column density requirement of $\log N_{\text{X}} > 12$ placed on the simulated C IV and Si IV absorbers. The far right-panel in this figure compares probability densities for the full, C IV-paired, and Si IV-paired H I absorber populations in FOGGIE.

There is a broad agreement between the FOGGIE H I absorbers and those seen by the KODIAQ-Z, HDLLS, and R12-DLA surveys. Both the observed and simulated absorbers follow similar trends in metallicity with N_{HI} . Table 9 gives the median, mean, standard deviation, and IQR range on the metallicity for different classes of H I absorber, which can be compared to the observed populations in Table 5 (although note that the observations probe a larger redshift range). Both the mean and median metallicities increase with N_{HI} , with the spread tending to decrease as N_{HI} increases. This is remarkable because neither EAGLE nor FIRE zoom simulations could reproduce the similar trend seen at low redshift (CCC II; CCC III). In Fig. 28, we compare the metallicity CDFs for the various absorbers at $2 \lesssim z \lesssim 3$ in the FOGGIE simulations and observations, further demonstrating the similar trends of increasing metallicity with increasing N_{HI} .¹⁶ However, this figure

¹⁶ The FOGGIE H I absorbers can have metallicity as low as $\log(Z/Z_{\odot}) = -8$ (the FOGGIE metallicity floor). There are absorbers with $\log(Z/Z_{\odot}) < -5$ classified as SLFs and pLLSs. These absorbers are not excluded from the CDFs in Fig. 28, so these CDFs do not start at zero.

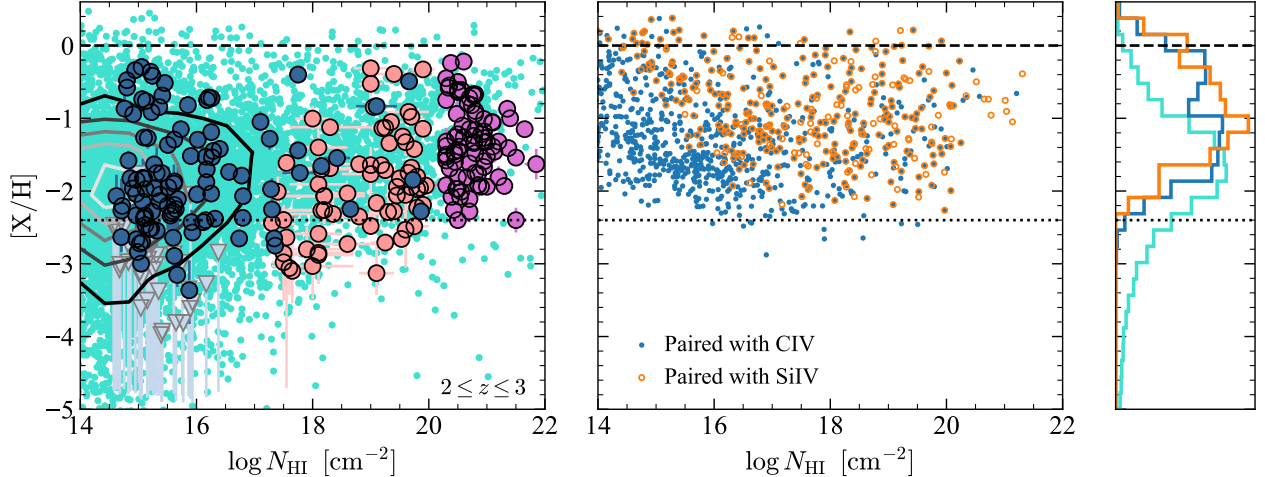


Figure 27. Metallicities of the H I absorbers extracted from the FOGGIE cosmological zoom-in simulations (Peeples et al. 2019; Simons et al. 2020). On the left, all H I absorbers (cyan) are compared to the KODIAQ-Z, HD-LLS, R12-DLA surveys (where we limit these surveys to $2 \leq z \leq 3$ to match the FOGGIE redshift range). Contours have been added where the density of cyan scatter plot points is highest. In the middle panel, we only show H I absorbers that have been paired with a C IV (blue filled circles) or Si IV (orange open circles) absorber, analogous to requiring detection of C IV or Si IV with $\log N_x > 12$. Probability densities of both the full FOGGIE H I absorber population (cyan) and the subset with paired metal absorbers (blue and orange) are shown on the right. The dashed and dotted lines are the solar and VMP metallicity levels, respectively.

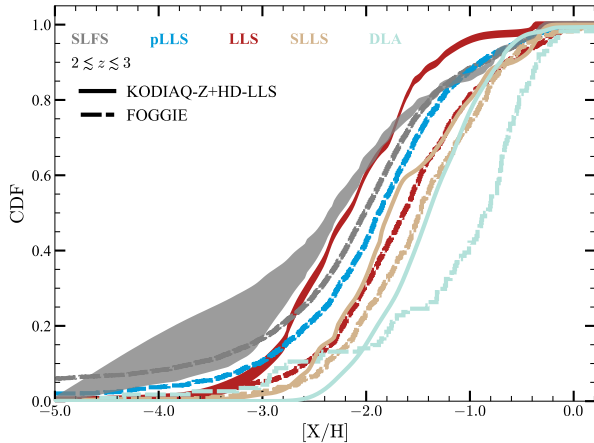


Figure 28. Comparison of the metallicity CDFs for the different categories of absorbers in the KODIAQ-Z+HD-LLS+R12 observations and FOGGIE simulations at $2 \leq z \leq 3$ (the sample of pLLSs in this redshift interval for the observation sample is too small to produce a reliable CDF and therefore is not shown here).

also shows that the metallicity of the FOGGIE absorbers is higher than that seen in the observations (even though their IQR or standard deviations are similar), especially for the LLSs and DLAs.

The FOGGIE absorbers therefore mimic the general trend seen in the observations, where higher H I column density regimes are dominated by higher metallicities. In FOGGIE, however, the metallicity at which a particular H I regime is most prevalent is higher than seen in

the observational data. FOGGIE's SLFSs have a higher metallicity than both the observed SLFSs and the observed LLSs. Moreover, the FOGGIE LLSs more closely match the CDF of the observed SLLSs. Similarly, the FOGGIE SLLS CDF is closer in metallicity to the observed DLAs. The FOGGIE DLAs have a substantial higher metallicity (the FOGGIE median metallicity is 0.5 dex higher or a factor 3 higher than in the R12-DLA sample).

The metallicities used for the FOGGIE absorbers are conceptually slightly different from the metallicities derived in KODIAQ-Z and other spectral surveys, in that the metallicities reported for FOGGIE are the column density-weighted average of the gas cells identified as the absorber rather than the result of a fit to single-phase ionization models. However, Marra et al. (2021) show that these two approaches, when applied to the same physical system, do not lead to large discrepancies in the average metallicity of the gas. The precise metallicities of FOGGIE's absorbers likely depend strongly on its implementation of supernova feedback, and these would be expected to differ slightly (e.g., be generally lower or higher) for different implementations. Yet despite FOGGIE's overall higher metallicity, the general similarity between the observed and simulated absorbers in Figure 27 seems to be a good indication that the *trends* observed in the KODIAQ-Z, HD-LLS, and DLA surveys can in principle be explained by CGM and nearby IGM gas around typical galaxies at these redshifts.

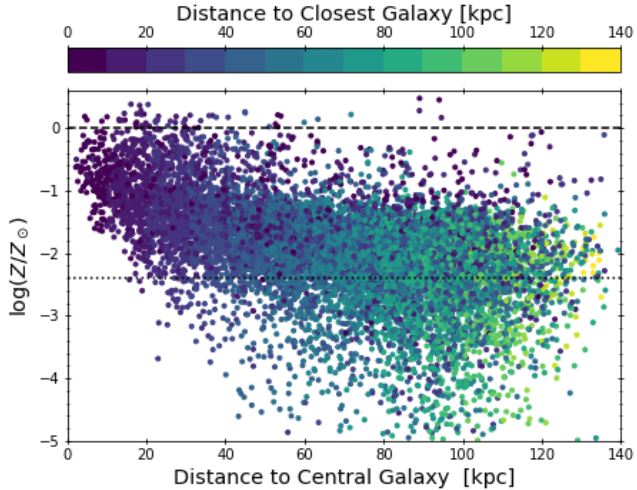


Figure 29. Metallicities of the FOGGIE H I absorbers versus their distance from the central galaxy, colored by the distance to their closest galaxy. Possible “closest galaxies” include the central and all satellites with more than 1% of the central’s stellar mass. High metallicity absorbers far from the central galaxy tend to be close to a satellite galaxy. Dashed and dotted lines are the same as in Figure 18

9.3. Insights from FOGGIE Simulations

Given some similarities in the metallicity trends with N_{HI} between our samples of observed and simulated absorbers, we can use the FOGGIE simulations to shed light on the origin(s) of these absorbers and their connection to galaxies. From the empirical results from KODIAQ-Z, the overdensities (at least for the pLLSs, LLSs, and SLLSs) imply that these absorbers should largely probe gas within virialized (mini)halos (see §7.1). The Keck Baryonic Structure Survey (KBSS) also shows that at $z \sim 2-3$ there is a strong incidence of absorbers with $\log N_{\text{HI}} > 14.5$ with galaxies at transverse physical distance $\lesssim 300$ kpc and velocity separation between the absorber and galaxy redshifts $\lesssim 300 \text{ km s}^{-1}$ (Rudie et al. 2012). This connection is not observed for lower N_{HI} absorbers, also implying some connection between $\log N_{\text{HI}} > 14.5$ absorbers and galaxies. On the other hand, recent MUSE IFU observations also show at least some LLSs may probe IGM filaments (Fumagalli et al. 2016a; Lofthouse et al. 2020). With the FOGGIE simulations, we can explore the origins of these absorbers without observational constraints due to, e.g., due to brightness limit of the galaxies. It is possible, however, that biases due to the selection criteria of the FOGGIE galaxies as Milky Way-like analogues at $z = 0$ could bias the results in some way. Importantly, we can also explore if and how the origins may depend on the metal enrichment of the absorbers.

Each of the central FOGGIE galaxies is surrounded by a number of satellites at $z = 2-3$. These satellite galaxies likely contribute to the enrichment seen in our absorbers, and it is worth determining whether a given absorber is more likely to be associated with such a satellite than with the central galaxy. Including only those satellites with at least 1% of the central galaxy’s stellar mass, we identify which galaxy each absorber is physically closest to. In Fig. 29, we compare the absorber metallicities to their distance from the central galaxy and the distance to their closest galaxies, be that a satellite or the central galaxy. Generally, distance to an absorber’s closest galaxy increases with distance from the central galaxy, which is the behavior we expect for absorbers whose closest galaxy is the central galaxy. Metallicity also tends to decrease with increasing distance from the central galaxy. Yet, there are important exceptions to these two trends: some absorbers are far from the central galaxy yet close to a satellite, and these absorbers span the range of extracted metallicites. This includes some absorbers distant from the central galaxy that have metallicity close to and above solar. Therefore, not all high metallicity absorbers should be assumed to be associated with the central galaxy.

In Figs. 30 and 31, we select FOGGIE absorbers that are inflowing toward or outflowing from the central galaxy. This separation is made based on the angle between an absorber’s 3D velocity vector and its position vector, both of which are calculated in the rest frame of the relevant central FOGGIE galaxy. Outflowing gas must have an angle $\theta > 60^\circ$, while inflowing absorbers must have $\theta < 120^\circ$. This is equivalent to $\hat{v} \cdot \hat{r} = \cos \theta = \pm 0.5$. This cut prevents gas that is neither strongly inflowing nor outflowing from being selected.

Fig. 30 shows the metallicity and H I column densities of our inflowing (blue) and outflowing (red) FOGGIE absorbers. PDFs are also included for these two quantities, with both metallicity PDFs repeated in the upper and lower panels for comparison. The inflowing absorbers dominate by number, but both categories have similar H I column distributions with absorbers becoming more numerous at lower H I column densities. The outflowing absorbers skew towards the high metallicity end of the distribution. This is not surprising, as in FOGGIE winds are launched by the same supernova feedback that also enriches the surrounding gas. There is a plateau in the outflowing metallicity distribution around $-2 \lesssim \log Z/Z_\odot \lesssim -1$, which may be tracing older outflows that have slowed and mixed with the ambient CGM. These absorbers number significantly less than the inflowing absorbers at the same metallicity, however, so it would be difficult for observations to dis-

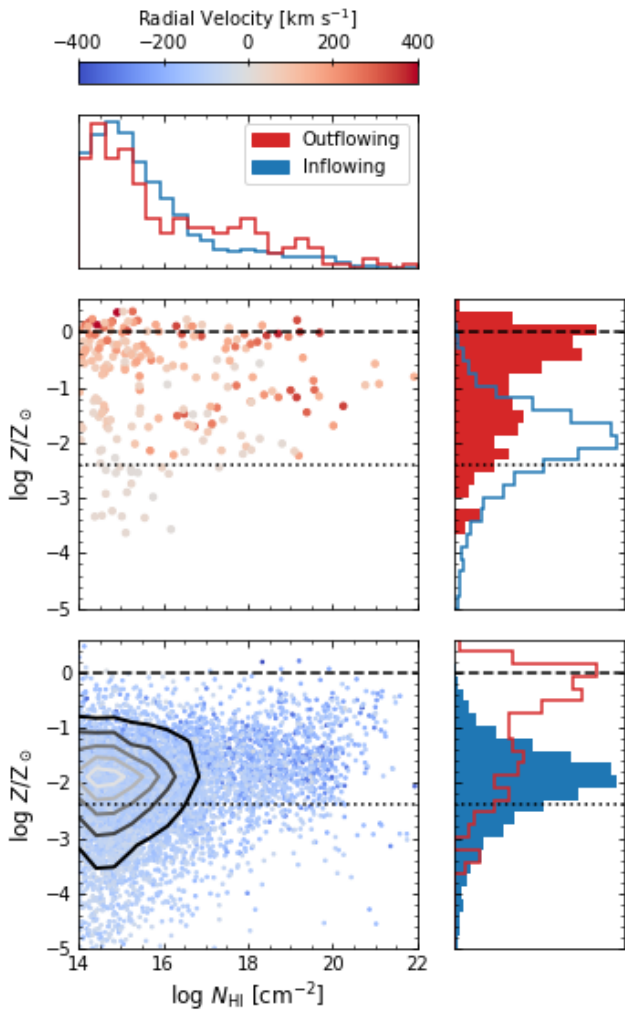


Figure 30. Metallicities of the FOGGIE H I absorbers in Figure 27, split into outflowing (red) and inflowing (blue) based on $|\hat{v} \cdot \hat{r}| > 0.5$ in the frame of the host central galaxy. Saturation shows the magnitude of the radial velocity. Probability densities are provided as histograms along the side and top. Both metallicity distributions are repeated in the side panels, with the filled histogram corresponding to the adjacent scatter plot. Contours have been added to show where the density of inflowing absorbers is highest.

entangle these less enriched outflows. The inflowing absorbers follow a more symmetric metallicity distribution, with a peak about 0.5 dex above the metal-poor limit for KODIAQ-Z; though, as stated above, the FOGGIE absorbers generally tend to have higher metallicities than seen in the random sightlines observed by KODIAQ-Z. The inflowing absorbers also extend to the lowest metallicities. Even though Fig. 29 reveals that some absorbers may be closer to a satellite than to the central galaxy, the trends in Fig. 30 are unchanged when the absorbers are limited to those whose closest galaxy is the central.

The biggest difference is that there are no outflowing absorbers with $\log Z/Z_\odot < -2.4$.

Although the outflowing absorbers dominate the high end of the metallicity PDF, they are far outnumbered by the inflowing absorbers even at the highest metallicities. This is largely due to the selection on H I and the underlying physics included in the FOGGIE simulations. There is very little cool gas that would form H I within the outflows as these are driven only by thermal pressure. Simulations with additional non-thermal pressure sources such as magnetic fields and cosmic rays (Butsky & Quinn 2018; Ji et al. 2020) demonstrate an increase in H I at large radii within the CGM. It is therefore quite likely that the number of H I absorbers classified as either inflowing or outflowing following our definition would change if these physical processes were included in the FOGGIE simulations, though it is likely that the numbers would still favor inflowing gas.

With Fig. 31, we look at the metallicity and velocity of the FOGGIE absorbers as a function of their distance from the central simulated galaxy. We also compare the absorbers to the underlying gas distributions. This distribution compiles together the gas in all 18 FOGGIE outputs we sampled. Probability densities are shown for the metallicity and radial distributions, and the mean metallicity of the gas is shown with a black line. Colors indicate the mean radial velocity at that metallicity and radius; we note that, unlike with the absorbers, the gas radial velocity has no selection based on the angle toward or away from the galaxy.

First, we consider outflowing material: outflowing absorbers with the highest metallicities tend to be at or within the virial radius of these central halos, which at $z = 2\text{--}3$ is about 30–50 kpc, and have the highest velocities. These velocities are generally higher than what is seen in the gas at similar radii and metallicities, and appears consistent with fast-moving enriched material launched by stellar feedback. On the other hand, high metallicity gas can be found even beyond the virial radius, implying that galactic outflows become more diffuse as they travel farther away from the galaxy. The outflowing absorbers with the lowest metallicity are found well outside the virial radius, and their velocities are comparable to the gas in this regime. This supports the interpretation that these absorbers come from previously ejected gas.

Inflowing absorbers can be found at all radii, with their metallicity generally increasing the closer they are to their central galaxy, similar to the outflowing gas. The velocity of these inflowing absorbers is also higher near the galaxy. The FOGGIE zoom simulations contain several satellite and pre-merger galaxies that are

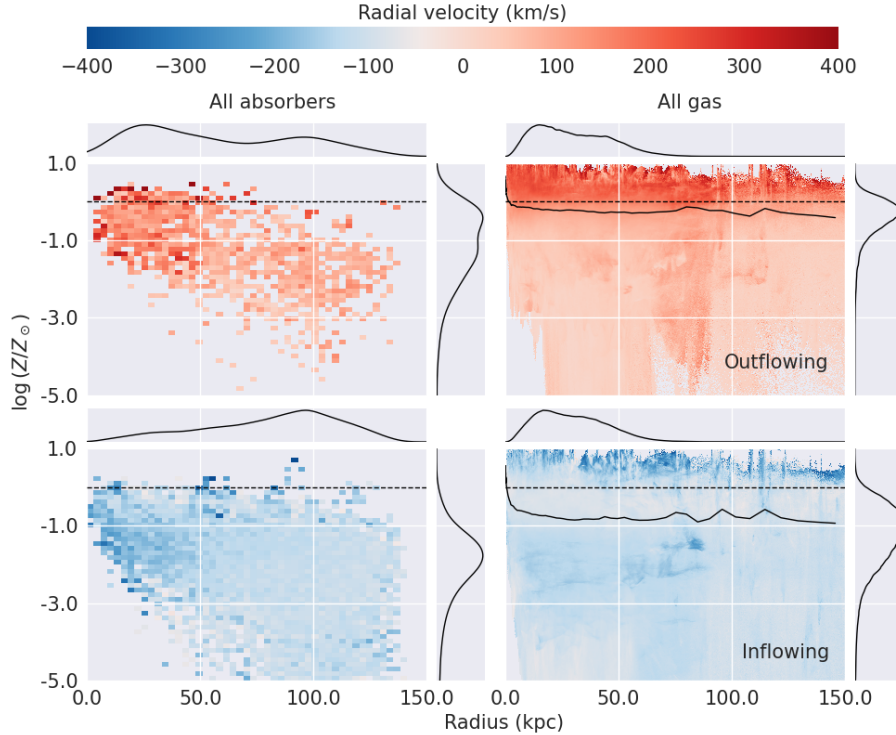


Figure 31. On the left, the metallicities of outflowing (red) and inflowing (blue) FOGGIE absorbers are binned versus their distance from their host central galaxies, colored by the average radial velocity for that bin. On the right, the gas in all eighteen FOGGIE snapshots is shown in the same configuration. The mean metallicity ($\log(Z/Z_{\odot})$) is marked with a black line. The dashed line indicates the solar metallicity level. Probability densities are shown at the top and sides of each panel.

producing their own enriched outflows, which explains why high metallicity absorbers can be found at large distances from the central galaxy. These absorbers do not appear to reflect the fastest inflowing gas, which has very high metallicity and can again be found at all radii.

Together, Figs. 30 and 31 imply that, given a set of H I-selected observed absorbers that are known or assumed to be associated with a galaxy system, most of these absorbers are likely to be inflowing towards a central galaxy. The precise number of inflowing and outflowing absorbers predicted by simulation will depend on the included physics, especially non-thermal pressure sources, though inflowing absorbers will likely still dominate. This dominance is true across column densities and metallicities, as satellites and nearby companions enrich gas flowing towards the central galaxy. Whether inflowing or outflowing, more enriched absorbers are more likely to be located physically close to the central galaxy.

10. DISCUSSION

10.1. Bridging the LYAF and DLAs

The history of metallicity in the universe provides an important constraint on models of galaxy formation and evolution. The metals in the universe represent a fossil

record of star formation; characterizing how the metallicities change with H I column density (and hence overdensities or densities) yields information on the transport of metals and efficiency of that transport from the densest to the most diffuse regions of the universe. At high redshift, much of the effort has focused on the metal enrichment of the most diffuse regions probed by the LYAF (e.g., Cowie et al. 1995; Songaila 1998; Ellison et al. 2000; Schaye et al. 2000, 2003; Aguirre et al. 2004; Simcoe et al. 2004; Simcoe 2011) and the densest regions of the universe probed by DLAs (e.g., Pettini et al. 1997, 1999; Prochaska 1999; Prochaska et al. 2003; Rafelski et al. 2012; Jorgenson et al. 2013). The HD-LLS survey (Prochaska et al. 2015; Fumagalli et al. 2016b, and see also Berg et al. 2021 for the XQ-100 survey of SLLSs) has surveyed lower H I column density absorbers mostly in the range $17.8 \lesssim \log N_{\text{HI}} < 20.3$. With KODIAQ-Z (this work, and earlier KODIAQ surveys Lehner et al. 2014, 2016), we bridge the gap between the DLA/SLLS regimes and the LYAF.¹⁷

¹⁷ We show in §6.3 that similar trends of the metallicities with N_{HI} are observed at low and high redshifts in the range $15 \lesssim \log N_{\text{HI}} \lesssim 22$. However, the current UV observations at low z do not have sensitivity to probe much lower metallicities than $[\text{X}/\text{H}] < -1$ in the LYAF at $z < 1$ (this would need to await a

In §6.2, we show that the scatter of absorber metallicities at $[X/H] \geq -2.4$ is quite similar for the DLAs and the $14.6 \lesssim \log N_{\text{HI}} \lesssim 20$ regime, i.e., metal enriched gas is observed not only in the densest regions (in or near galaxies) but has also spread to the more diffuse regions down to overdensities $\delta \lesssim 10$ (see Fig. 18). However, as N_{HI} decreases below $\log N_{\text{HI}} \lesssim 14.4$ (diffuse IGM), most of the absorbers have metallicities $[X/H] \lesssim -1.6$ (see Fig. 5 in Simcoe et al. 2004), while gas with $-1.6 \lesssim [X/H] \lesssim -0.2$ is commonly observed over the entire range $14.6 \lesssim \log N_{\text{HI}} \lesssim 22$. Therefore the diffuse IGM probed by LYAF absorbers has not been enriched at the same level as stronger H I absorbers.

In contrast, for metallicities $[X/H] \lesssim -2.4$, blind surveys of DLAs do not reveal a significant population of VMP DLAs (e.g., Rafelski et al. 2012; Jorgenson et al. 2013). Yet, VMP absorbers are regularly observed at $\log N_{\text{HI}} \lesssim 20$, and their frequency increases with decreasing N_{HI} (see Table 6 and Fig. 18). These VMP absorbers are of course also observed in the LYAF. The median metallicity of the LYAF at $z \sim 2.5$ is around $[X/H] = -2.8$ (Simcoe et al. 2004; Simcoe 2011 and see also, e.g., Ellison et al. 2000; Schaye et al. 2003; Aguirre et al. 2004), which is a factor 2.5 lower than the median metallicity of the SLFSs at $\langle z \rangle \simeq 2.8$ (Table 4). However, owing to sensitivity issues, the lowest metallicities found for LYAF absorbers are around $[X/H] \sim -3.5$, while our survey reveals a population of absorbers with $[X/H] < -3.5$ that is nearly and completely metal-free (see §10.2, and also Fumagalli et al. 2011a; Lehner et al. 2016). Simcoe et al. (2004) estimated that about 70%–80% of the LYAF has been enriched to $[X/H] \gtrsim -3$, but 20–30% might be chemically pristine gas at low densities, which is about the same as the fraction of SLFSs with $[X/H] < -3$.

Therefore, gas in the intermediate overdensity regime between the DLAs and LYAF has metallicities that are found in both the most diffuse and densest region of the universe. Gas probed by absorbers with $14.6 \lesssim \log N_{\text{HI}} \lesssim 20$ has a much larger dispersion in metallicity than observed either in $\log N_{\text{HI}} \lesssim 14.4$ or ≥ 20.3 gas. The simultaneous presence of abundant pristine, metal-rich, intermediate metallicity gas is unique to the H I column density range $14.6 \lesssim \log N_{\text{HI}} \lesssim 20$. Below we discuss in more details these various levels of chemical enrichment and the mixing of metals in the $14.6 \lesssim \log N_{\text{HI}} \lesssim 20$ range.

future ~6-m UV space-based telescope), and we cannot yet assess the full range of metallicities for absorbers with $\log N_{\text{HI}} < 15$ at $z < 1$. Therefore, we keep our discussion focused on the high redshift universe.

10.2. Pristine Gas

From the KODIAQ-Z survey and CCC at low redshift, we find that there is an abundance of VMP absorbers in relatively high overdensity (except for the DLAs by definition). While the metallicities have increased by about a factor 8–10 from $2.2 \lesssim z \lesssim 3.6$ to $z < 1$, the fractions of VMP absorbers are strikingly similar at low and high redshifts in $\log N_{\text{HI}} < 19$ absorbers. On the other hand, owing to the overall increase of the metallicity from $2.2 \lesssim z \lesssim 3.6$ to $z < 1$, it is not surprising that extremely metal poor gas with $[X/H] < -3.5$ or even < -3.0 is scant at $z < 1$ (CCCIII). With KODIAQ-Z, we determine that the fractions of SLFSs and pLLSs with $[X/H] < -3.5$ and < -3.0 are about 3%–10% and 15%–25% (90% confidence intervals, see Table 6). Combining KODIAQ-Z and HD-LLS, similar numbers are derived for the LLSs. For the SLLSs, the fractions of absorbers with these metallicities are smaller by about a factor 2.

The pristine LLSs reported by Fumagalli et al. (2011a) at $z \sim 3.5$ have $[X/H] < -3.8$ and < -4.2 , but at the time of this discovery it was impossible to say how common this population was. With KODIAQ-Z, we can revisit this question (see also Lehner et al. 2016). The lowest metallicity where some metals are detected is around $[X/H] \lesssim -3.8$ in KODIAQ-Z (see Fig. 18). We use that value of $[X/H] \simeq -3.8$ to separate pristine (no metal) from metal-enriched (even at very low levels) absorbers. Considering Fig. 18, we can separate the population of H I absorbers into two broad categories owing to the impact that upper limits on $[X/H]$ can have for interpreting the frequency of pristine absorbers:

1) For absorbers with $16 \leq \log N_{\text{HI}} \leq 20$, there are only 11 upper limits on $[X/H]$: 3 out 179 these absorbers have $[X/H] < -3.8$, implying a frequency of pristine absorbers in the range 0.7%–4.2% (90% CI) in this column density interval. This number cannot increase by much more than a factor ~2 including data with higher upper limits. Even if all the upper limits represent pristine gas for absorbers with $\log N_{\text{HI}} \geq 16$, this would increase the frequency of pristine absorbers to only 3.7%–9.6% (90% CI). Hence, the fraction of pristine $\log N_{\text{HI}} \geq 16$ absorbers (i.e., gas with overdensities $\delta \gtrsim 50$ –100) is at least 1% and at most 10% at $2.2 \lesssim z \lesssim 3.6$.

2) The second regime is for absorbers with $14.6 \lesssim \log N_{\text{HI}} < 16$ where the upper limits on the metallicities are much more numerous. Taking strictly $[X/H] < -3.8$, there are 4 absorbers out of 142, implying a frequency of pristine absorbers of 1.3%–6.1% (90% CI), a similar percentage to that of absorbers with higher N_{HI} . However, if all the $\log N_{\text{HI}} < 16$ absorbers with upper limits such as $[X/H] < -3$ probe pristine absorbers,

then the frequency of pristine $\log N_{\text{HI}} < 16$ absorbers would increase to 13.3%–23.9% (90% CI). This would be similar to the possible population of metal-free LYAF absorbers at similar redshifts (see previous section and Simcoe et al. 2004). The fraction of pristine gas in overdensities $\delta \gtrsim 50$ –100 at $2.2 \lesssim z \lesssim 3.6$ is therefore at the level of a few percent, while for smaller overdensities it is likely in the range 10%–20%.

The frequency of mock absorbers with $[\text{X}/\text{H}] < -3.8$ in the FOGGIE simulations is very similar to the frequencies found in KODIAQ-Z, despite the FOGGIE absorbers on average have higher metallicities than observed. In contrast, cruder resolution simulations show a tendency to have over-enriched pLLSs and LLSs (see discussion in Fumagalli et al. 2011a). In the EAGLE HiRes cosmological hydrodynamical simulations, Rahmati & Oppenheimer (2018) find a fraction of pristine gas with $[\text{X}/\text{H}] < -3.8$ of about 10% in the pLLS and LLS regimes. However, contrary to FOGGIE and the observations reported here or at low redshift (CCC II; CCC III), the EAGLE simulations show little change of the metallicity with N_{HI} (see also CCC II; CCC III); the FIRE simulations also show similar results (Hafen et al. 2017). Consistent with the lack of N_{HI} dependence, these simulations find a significant population of $[\text{X}/\text{H}] < -3$ DLAs that is not observed. This highlights some issues in simulations that may be related to the implementation of feedback physics, but is probably also related to insufficient resolution in the more diffuse gas. As discussed in §9.2, low-metallicity inflowing gas is able to naturally get much closer to the galaxy when the CGM structures are resolved than in the standard-resolution simulations because the metals are not forced to over-mix in the regions around galaxies (see also Peebles et al. 2019; van de Voort et al. 2019; Hummels et al. 2019; Suresh et al. 2019). As discussed in §9.3 and shown in Figs. 29, 30, 31, the pristine and the VMP absorbers predominantly probe inflowing cool gas (see, also Hafen et al. 2017; Rahmati & Oppenheimer 2018; Suresh et al. 2019), consistent with the idea that these absorbers are ideal candidates for the cold-mode accretion (e.g., Kereš et al. 2005; Dekel et al. 2009; Fumagalli et al. 2011b).

10.3. Extreme Metallicities and Metal-rich gas

The metal-enriched diffuse gas constitutes a record of the transport of metals from the densest to the most diffuse regions of the universe. In §10.1, we discuss that while the LYAF shows evidence for metal enrichment, it is not enriched to levels seen in higher H I column absorbers have. Metallicities in the range $-1.6 \lesssim [\text{X}/\text{H}] \lesssim -0.2$ are commonly observed over the

entire range $14.6 \lesssim \log N_{\text{HI}} \lesssim 22$, but not in the LYAF. Therefore, at $2.2 \lesssim z \lesssim 3.6$, galaxies have not yet polluted the diffuse IGM with metals at the same level as denser regions of the universe.

In Lehner et al. (2016), we reported the discovery of one supersolar pLLS at $z \simeq 2.5$ with $[\text{X}/\text{H}] \simeq +0.2$.¹⁸ Besides its metallicity, this pLLS is unique on several other levels including the detection of O I, its small physical (0.35 pc), relatively high density ($n_{\text{H}} \simeq 0.2 \text{ cm}^{-3}$), and multiphase nature, with C IV having a very different velocity profile compared to the low ions (see Fig. 14 in Lehner et al. 2016). We argued in that paper that its high metallicity and multiphase nature strongly suggest that it directly probes an active outflow from a protogalaxy at $z \simeq 2.5$. At $z \sim 1.8$, Prochaska et al. (2006) uncovered two supersolar SLLSs, suggesting that these metal-rich absorbers may represent a significant metal reservoir in the young universe.

However, the HD-LLS survey does not report any supersolar SLLS (see Fig. 18), and the XQ-100 survey only reports one supersolar SLLS at $z \sim 2.5$ (see Fig. 2 in Berg et al. 2021; we exclude poorly-constrained upper limits on the metallicity that are above solar in that survey). Adding that supersolar pLLS to the KODIAQ-Z+HD-LLS survey would imply that only 1 out 242 absorbers has a supersolar metallicity at $2.2 \lesssim z \lesssim 3.6$, i.e., $0.41\%^{+1.42\%}_{-0.32\%}$ (90% CI) of the absorbers have $[\text{X}/\text{H}] > 0$. None is found in the R12-DLA either, implying that the fraction of supersolar absorbers in the H I column density range $14.6 \lesssim \log N_{\text{HI}} < 22$ at $2.2 \lesssim z \lesssim 3.6$ drops to $0.29\%^{+1.00\%}_{-0.23\%}$. Supersolar metallicity absorbers are therefore very rare at $2.2 \lesssim z \lesssim 3.6$ for any N_{HI} absorber.

At low redshift, the situation is quite different, with at least 2%–6% of supersolar absorbers at $z < 1$ (see Fig. 21, and CCC III). This number could increase by a factor ~ 3 if a harder EUVB was used instead of the HM05 EUVB to model the absorbers (at low redshift the effect of the EUVB is more important, see CCC II and §5). This increase of supersolar absorbers is consistent with the overall increase of the metallicities by a factor 8–10 from $2.2 \lesssim z \lesssim 3.6$ to $z < 1$ (see Fig. 20).

The larger fraction of metal-enriched and even supermetallicity absorbers at low redshift indicates a much larger volume of the universe has been exposed to metal pollution than at $2.2 \lesssim z \lesssim 3.6$. Ferrara et al. (2000) developed a model that predicts at $z < 1$ essentially all absorbers should have associated metal absorption, and

¹⁸ The HIRES spectrum of this QSO was not released in KODIAQ DR2 and therefore is not part of the present KODIAQ-Z survey.

the spread in metallicity should be less than 1 dex. This is not case. Even at $z < 1$, the enrichment of the most diffuse gas in the universe is still very inhomogeneous in view of the nearly 3 dex spread in metallicities at $z < 1$ for absorbers with $15 \lesssim \log N_{\text{HI}} \lesssim 19$ (see Fig. 21 and next section).

10.4. Inhomogeneous Metal Mixing

There is ample of evidence for inhomogeneous abundances in H I column density $14.6 \lesssim \log N_{\text{HI}} \lesssim 20$ gas where the metallicities range from pristine ($[\text{X}/\text{H}] < -4$) to about $[\text{X}/\text{H}] \simeq -0.2$ dex, a factor at 6,000 spread from the lowest to highest metallicities. Similar results are found at $z < 1$, but a factor somewhat smaller with 1,000 variation between the highest and lowest metallicities (CCC III and Fig. 21). However, our results also show there is inhomogeneous metal mixing in single halos as directly evidenced by the large variation in metallicity in closely redshift-separated absorbers (see Fig. 23). Such large metallicity variation over small redshift separations was initially reported by Prochter et al. (2010) between a SLFS, a pLLS, and a LLS at $z \sim 3.5$ separated in velocities along the same QSO from about 130 to 180 km s⁻¹ where the metallicity differences were a factor 3, 40, and 158. Now with a sample of 37 paired absorbers, we find similarly large metallicity variations between absorbers separated by less than $\Delta v < 500$ km s⁻¹ along a given QSO sightline where about half of paired absorbers have metallicity variations of a factor 2–3 and for the other half of a factor > 140 . It is plausible that the smaller variations may be related to the variation within a halo, while the large variations to gas in inter-halos.

Thus, within the overdensities of a few to several hundreds, the gas probed by absorbers with $14.6 \lesssim \log N_{\text{HI}} \lesssim 20$ is chemically inhomogeneous where both metal-poor and metal-rich gas are observed. This again appears unique to the $14.6 \lesssim \log N_{\text{HI}} \lesssim 20$ column density range. While for DLAs determining the metallicity in individual components is complicated since the H I velocity structure cannot be recovered over $\Delta v < 500$ km s⁻¹, the metallicity spread for the DLAs is much smaller than observed at $14.6 \lesssim \log N_{\text{HI}} \lesssim 20$ (see 10.1). It is also much smaller for the LYAF (e.g., Simcoe et al. 2004), implying overall a more chemically homogeneous gas in the LYAF and DLA regimes. Therefore, in and quite near galaxies, in the gas traced by DLAs, the metal enrichment from supernovae is quite efficient, but beyond the immediate vicinity of the galaxies, the volume filling factor for metals must be low, which is consistent with models of metal ejection from supernovae that is

not expected to be efficient and confined to small regions (e.g., Ferrara et al. 2000; Scannapieco 2005).

11. SUMMARY AND CONCLUDING REMARKS

Using the KODIAQ DR2 data from the KOA (O’Meara et al. 2015), we have built a sample of 202 H I-selected absorbers with $14.6 \leq \log N_{\text{HI}} \leq 20$ at $2.2 \leq z \leq 3.6$ comparable in size to our companion survey, CCC, at $z < 1$. The H I selection and the H I column density range both ensure that no bias is introduced in the metallicity distribution of these absorbers, i.e., we are sensitive to any absorbers with $[\text{X}/\text{H}] \gtrsim -3.5$. The H I selection also provides a clean separation of the absorbers based on H I column density, which is largely used to separate the LYAF, absorbers with $\log N_{\text{HI}} \lesssim 14.5$ (IGM), from the denser regions of the universe probed by stronger H I absorbers. By definition, the SLFSs all have over-densities $\delta > 3$ in our sample ($z = 3.6$, the maximum redshift in our statistical sample corresponds to this δ value using the analytical expression in Schaye 2001b). In contrast, a metal-selection using C IV or O VI can include a wide range of H I column density absorbers from the LYAF to the pLLS regime.

In the KODIAQ-Z survey, we have 155 SLFSs, 24 pLLSs, 16 LLSs, and also 7 SLLSs, for a total of 202 absorbers. To increase the number of LLSs and SLLSs in our sample, we use the H I-selected absorbers from the HD-LLS survey that have a H I column density range $17.2 \leq \log N_{\text{HI}} \leq 20$, but a majority have $17.7 \lesssim \log N_{\text{HI}} \leq 20$ (Prochaska et al. 2015; Fumagalli et al. 2016b). We also use the results from survey from Rafelski et al. (2012) to study the metallicity changes with N_{HI} in the DLA regime. For both of these surveys, we restrict them survey to absorbers at $2.2 \leq z \leq 3.6$, unless otherwise stated.

For all the absorbers with $\log N_{\text{HI}} \lesssim 20$ in the KODIAQ-Z and HD-LLS, we derive the posterior PDFs of the metallicities and other physical quantities using a Bayesian formalism that employs a MCMC sampling of a grid of Cloudy photoionization models (where we assume photons from the HM05 EUVB provide the source of photoionization). This follows directly from the methodology used in HD-LLS (Fumagalli et al. 2016b) and CCC (CCC II; CCC III). For absorbers with less than ideal constraints (about half of the SLFS sample and a few pLLSs), we adopt the “low-resolution” method developed at low redshift by Wotta et al. (2016) and refined in CCC II to estimate the metallicities. Using SLFSs and pLLSs with reliable constraints from the metal ions, we find that $\log U$ can be reasonably well modeled by a Gaussian for the SLFSs and pLLSs, which

can then be used reliably as a prior in the Bayesian MCMC modeling. We explore the effects of changing the EUVB from HM05 and HM12 to estimate the metallicities (Figs. 9, 10), and we find that the changes in the metallicities between these two EUVBs are negligible for the absorbers with $\log N_{\text{HI}} \gtrsim 17.2$. For the SLFSs and pLLSs, the effect is only an increase of $+0.12 \pm 0.15$. The effect from changing the EUVBs on the metallicities is therefore much smaller than at $z < 1$.

Our main findings on the properties of our statistical sample of H I selected absorbers with $14.6 \leq \log N_{\text{HI}} \leq 20$ at $2.2 \leq z \leq 3.6$ can be summarized as follows.

1. From the comparison of the absorption profiles and the width of the profiles, we conclude that singly, doubly, triply ionized species (e.g., Si II, Si III, Si IV, C II, C IV) and H I often trace the same gas in absorbers with $\log N_{\text{HI}} < 19$. For SLFSs and pLLSs, we also find that when O VI absorption is present, it has often a similar velocity structure than lower ions, i.e., the O VI absorption is commonly narrow in these absorbers. This contrasts remarkably from the O VI that is frequently strong and broad when detected in absorbers with $\log N_{\text{HI}} \gtrsim 17.8$.

2. From the profile fitting of the H I transitions, we show that 90% of the components have $13.3 \leq b \leq 40 \text{ km s}^{-1}$ with a mean $\langle b \rangle = 27 \pm 6 \text{ km s}^{-1}$. This implies a temperature of the gas of $T < 4 \times 10^4 \text{ K}$, consistent with the gas being primarily photoionized.

3. We find that a single-phase photoionization model is appropriate to match the column densities of the low ions to high ions (including O VI) for the majority of the SLFSs and pLLSs. For the LLSs and SLLSs, when O VI is detected, a single-phase photoionization model cannot commonly reproduce the observed O VI column density, implying that as N_{HI} increases, the multiple gas-phase nature becomes more important.

4. In our ionization models, $[\text{C}/\alpha]$ is allowed to vary in the range $[-1, +1]$ to accommodate for non-solar relative abundances between carbon and α -elements caused by nucleosynthesis effects. This approach allows us to have a better sense of the uncertainties in the metallicity caused by the variability of C/α . Overall, we find that $[\text{C}/\alpha]$ is in the range $-0.6 \lesssim [\text{C}/\alpha] \lesssim +0.5$ as observed in other environments (DLAs, stars, H II regions), but robustly studying the variation of $[\text{C}/\alpha]$ with $[\text{X}/\text{H}]$ for these absorbers is hindered by the ionization corrections that add too much noise in the $[\text{C}/\alpha]$ distribution, hiding any subtle changes between $[\text{C}/\alpha]$ with $[\text{X}/\text{H}]$ that are expected to be at the level of a factor 2–3.

5. The 155 H I-selected SLFSs ($14.6 \leq \log N_{\text{HI}} < 16.2$) probe a wide range of metallicities from $[\text{X}/\text{H}] < -4$ to $[\text{X}/\text{H}] \simeq -0.2$. The metallicity posterior PDF is negatively skewed with a prominent tail extending well below $[\text{X}/\text{H}] < -3$. It has a main peak around the median value $[\text{X}/\text{H}] \simeq -2.4$ and another smaller peak around -0.6 dex solar (the dip around -1.1 is observed in both binned and unbinned data).

6. The 24 H I-selected pLLSs ($16.2 \leq \log N_{\text{HI}} < 17.2$) probe a range of metallicity from $[\text{X}/\text{H}] < -4.2$ to about $[\text{X}/\text{H}] \simeq -1$. The sample is too small to robustly characterize the distribution and the lack of pLLSs with $[\text{X}/\text{H}] > -1$ could be mainly due to small-number statistics. However, both the median (-2.1 dex) and IQR metallicities imply an overall increase in metallicities compared to the SLFSs despite the lack of $[\text{X}/\text{H}] > -1$ pLLSs.

7. Our sample of H I-selected LLSs ($17.2 \leq \log N_{\text{HI}} < 19$) consists of 16 absorbers that we combine with the HD-LLS survey to reach a size sample of 62 LLSs. The full range and median of the LLS metallicity PDF are quite similar to that of the pLLSs. Combining the pLLSs+LLSs, the median metallicity is -2.2 and IQR only 1 dex compared to -2.42 and 2 dex, respectively, for the SLFSs. The pLLSs+LLSs are more frequent in the metallicity range $-3.2 \lesssim [\text{X}/\text{H}] \lesssim -1.2$ but less frequent at very low metallicity $[\text{X}/\text{H}] \lesssim -3.5$ than the SLFSs, showing there is a shift in the metallicity enrichment properties of these absorbers below and above $\log N_{\text{HI}} \simeq 16.2$ (at $2.2 \leq z \leq 3.6$, this corresponds to overdensities of $\delta \simeq 140$ – 50).

8. Combining the 7 SLLSs from KODIAQ-Z and 73 SLLSs from HD-LLS ($19 \leq \log N_{\text{HI}} \leq 20$) and using the R12-DLA sample of 101 DLAs ($\log N_{\text{HI}} \geq 20.3$), the overall metallicity trend observed with N_{HI} continues in these regimes: the median/mean metallicity increases and IQR decreases with increasing N_{HI} . For the SLLSs, the median and IQR metallicities -1.9 and 1.1 dex, while these are -1.4 and 0.65 dex for the DLAs. DLAs have therefore rarely gas with $[\text{X}/\text{H}] < -2.4$, while at $\log N_{\text{HI}} \lesssim 20$, VMP absorbers are not rare at $2.2 \leq z \leq 3.6$.

9. The fractions of extremely metal-poor systems with $[\text{X}/\text{H}] < -3.5$ for the pLLSs, pLLSs, LLSs are about the same, around 3–10% (90% confidence interval). For the SLLSs, it is most likely somewhat smaller with a fraction in the range 0.3–5.4%. Yet, the most metal poor absorber in our sample is a SLLS with $\log N_{\text{HI}} = 19.25 \pm 0.25$ and $[\text{X}/\text{H}] < -4.4$ with a cosmic overdensity of several thousands.

10. We find that (pristine) gas clouds with no metals down to limit $[X/H] < -3.8$ constitutes about 1%–10% of the $16 < \log N_{\text{HI}} < 20$ absorbers at $2.2 \leq z \leq 3.6$, and increases to 10%–20% for $14.6 \leq \log N_{\text{HI}} \leq 16$ absorbers, the latter being similar to the amount of pristine gas found in the diffuse IGM. On the other hand, supersolar absorbers at any N_{HI} at $2.2 \lesssim z \lesssim 3.6$ are very uncommon (< 1%).
11. Using paired absorbers with velocity separations of $\Delta v \lesssim 500 \text{ km s}^{-1}$ along the same QSO sightlines, we find there is a large scatter in the metallicity from about 0.2 dex to > 2 dex. For about half of the paired absorbers, there is evidence for metallicity variations over $\Delta v \lesssim 500 \text{ km s}^{-1}$ of a factor 2–3, while for the other half of a factor > 140. It is plausible that the smaller variations correspond to the change within a single galaxy halo, while the large variations to differences between galaxy halos. Both the large metallicity range and metallicity variation between paired absorbers imply that the transport of metals from their formation sites (galaxies) into the CGM and the IGM is very inhomogeneous.
12. The photoionized gas associated with pLLSs, LLSs, and SLLSs contribute to the cosmic baryon budget to $\Omega_g/\Omega_b \simeq 7\%$ and the SLFSs contribute to another 5.5%. From the first KODIAQ survey (Lehner et al. 2014), the O VI-bearing hot collisionally ionized gas associated with LLSs and SLLSs is likely to contribute to about the same level. These are the second largest contributors to the cosmic baryon budget at high redshift behind the LYAF.
13. We show that about 2%, 5%, 7% of the metals ever produced at $2.2 \lesssim z \lesssim 3.6$ are in photoionized gas associated with SLFSs, pLLSs, and LLSs, respectively. The SLLSs account for another 18%, and therefore about 30% of the metals at $2.2 \lesssim z \lesssim 3.6$ in photoionized absorbers with $14.6 \leq \log N_{\text{HI}} < 20.3$. Combining the SLFSs, pLLSs, LLSs, and SLLSs, their comoving metal mass density of the photoionized gas probed by these absorbers is $\rho_m = 3.5 \times 10^5 \text{ M}_\odot \text{ cMpc}^{-3}$. Another possible 5%–20% of the cosmic metal budget may also be in form of highly ionized metals in gas with $\log N_{\text{HI}} \gtrsim 17.8$ (Lehner et al. 2014).
- To study their cosmic evolution, we combine our results with the CCC survey that explores the properties of similar absorbers at $z < 1$ (CCC I; CCC II; CCC III). The cosmic evolution of absorbers from $2.2 \lesssim z \lesssim 3.6$ to $z \lesssim 1$ with $\log N_{\text{HI}} \gtrsim 15$ is summarized as follows.
14. We find that from $2.2 \leq z \leq 3.6$ to $z < 1$, there is an overall increase of the metallicity of the gas probed by SLFSs, pLLSs, LLSs, SLLSs, and DLAs by a factor ~ 8 .
15. While the metallicity threshold for the VMP absorbers increases by about 1 dex from $2.2 \leq z \leq 3.6$ to $z < 1$, a similar fraction of about 50% of absorbers with $\log N_{\text{HI}} \lesssim 18$ are VMP at low and high z .
16. Although there is plenty of *primitive* gas around $z \lesssim 1$ galaxies that has largely not been polluted, the fraction of pristine SLFSs, pLLSs, LLSs with $[X/H] < -3$ at $z \lesssim 1$ is < 1% at the 90% confidence level over the range $15 < \log N_{\text{HI}} < 19$. In contrast 10%–25% of similar absorbers at $2.2 \lesssim z \lesssim 3.6$ have $[X/H] < -3$, implying that although the transport of metals outside galaxies is still very inhomogeneous at $z < 1$, all regions with $\log N_{\text{HI}} \gtrsim 15$ have been polluted to some level by $z < 1$.
17. The hydrogen column density (N_{H}) is a factor 10–15 smaller at $z < 1$ than at $2.2 \lesssim z \lesssim 3.6$, and therefore the contribution to baryonic budget from the SLFSs, pLLSs, and LLSs are about 10 times smaller at $z < 1$ than at $2.2 \lesssim z \lesssim 3.6$.
18. The photoionized metals associated with the SLFSs, pLLSs, and LLSs take about 6% of the cosmic metal budget at low redshift. This is about a factor 2 decrease compared the contribution of the same absorbers at $2.2 \lesssim z \lesssim 3.6$, i.e., at low redshift most of the metals are found in or near galaxies and in the intra-cluster medium (see Péroux & Howk 2020). This is a major change in the distribution of metals in the universe from $z \sim 2.8$ to $z \sim 0.5$.
- We set our empirical results in the context of the cosmological zoom simulations using simulations from the FOGGIE project, and the main conclusions from that study are as follows.
19. Contrary to cruder resolution simulations (especially in the CGM), a striking feature of the FOGGIE cosmological zoom simulations is that the behavior of the metallicity as a function of N_{HI} is broadly similar to the observed empirical relationship: as N_{HI} increases the overall metallicity increases and the dispersion of the metallicity decreases. However, as other cosmological simulations, FOGGIE appears to have too many metals at any N_{HI} (e.g., supersolar metallicity gas is not uncommon in these simulations, but observationally it is), implying that metals are more homogeneously distributed than observed.
20. In the FOGGIE simulations, outflowing absorbers with the highest metallicities tend to be at or within the virial radius of these central halos and probe active

or recent galaxy outflows, while outflowing absorbers with the lowest metallicity are found well outside the virial radius of the central galaxies and therefore the remnants of ejected gas. On the other hand, inflowing absorbers can be found at all radii, with their metallicity generally increasing the closer they are to their central galaxy. Very metal-poor absorbers with $[X/H] < -2.4$ are excellent probe inflowing gas in these simulations.

ACKNOWLEDGEMENTS

We are grateful to Anna Wright for providing the satellite catalogs used in Fig. 29 based on the methods of (Pontzen & Tremmel 2018). The main support for this research was made by NASA through the Astrophysics Data Analysis Program (ADAP) grant NNX16AF52G. Additional support was provided by NSF grant award number 1516777. Support for the development of the Cloudy ionization models was provided by NASA through grants HST-AR-12854 and HST-AR-15634 from the Space Telescope Science Institute, which is operated by the Association of Universities for Research in Astronomy, Incorporated, under NASA contract NAS5-26555. CC and BWO acknowledge support by NSF grants no. AST-1517908 and AST-1908109 and NASA ATP grants NNX15AP39G and 80NSSC18K1105. This project has received funding from the European Research Council (ERC) under the European Union’s Horizon 2020 research and innovation programme (grant agreement No 757535). This work has been supported by Fondazione Cariplo, grant No 2018-2329. All the data presented in this work were obtained from KODIAQ DR1 and DR2, which was funded through NASA ADAP grants NNX10AE84G

and NNX16AF52G along with NSF award number 1516777. This research has made use of the Keck Observatory Archive (KOA), which is operated by the W. M. Keck Observatory and the NASA Exoplanet Science Institute (NExScI), under contract with the National Aeronautics and Space Administration. The authors wish to recognize and acknowledge the very significant cultural role and reverence that the summit of Maunakea has always had within the indigenous Hawaiian community. The photoionization modeling was supported by the Notre Dame Center for Research Computing through the Grid Engine software and, together with the Notre Dame Cooperative Computing Lab, through the HTCondor software. Analysis of the FOGGIE simulations used the resources of the Michigan State University High Performance Computing Center, operated by the Institute for Cyber-Enabled Research. The FOGGIE calculations were performed using the publicly-available Enzo code (Bryan et al. 2014; Brummel-Smith et al. 2019) and analyzed using yt (Turk et al. 2011), both of which are the products of the collaborative effort of many independent scientists from numerous institutions around the world.

Software: Astropy (Astropy Collaboration et al. 2018), emcee (Foreman-Mackey et al. 2013), Matplotlib (Hunter 2007), PyIGM (Prochaska et al. 2017a), scikit-learn (Pedregosa et al. 2011; Buitinck et al. 2013), Enzo (Bryan et al. 2014; Brummel-Smith et al. 2019), yt (Turk et al. 2011), Trident (Hummels et al. 2017), SALSA (Boyd et al. 2020)

Facilities: Keck(HIRES)

REFERENCES

- Aguirre, A., Schaye, J., Kim, T.-S., et al. 2004, ApJ, 602, 38
 Akerman, C. J., Carigi, L., Nissen, P. E., Pettini, M., & Asplund, M. 2004, A&A, 414, 931
 Asplund, M., Grevesse, N., Sauval, A. J., & Scott, P. 2009, ARA&A, 47, 481
 Astropy Collaboration, Price-Whelan, A. M., Sipőcz, B. M., et al. 2018, AJ, 156, 123
 Berg, T. A. M., Fumagalli, M., D’Odorico, V., et al. 2021, MNRAS, 502, 4009
 Boyd, B., Silvia, D., O’Shea, B., et al. 2020, The Journal of Open Source Software, 5, 2581
 Brummel-Smith, C., Bryan, G., Butsky, I., et al. 2019, The Journal of Open Source Software, 4, 1636
 Bryan, G. L., Norman, M. L., O’Shea, B. W., et al. 2014, ApJS, 211, 19
 Buitinck, L., Louppe, G., Blondel, M., et al. 2013, in ECML PKDD Workshop: Languages for Data Mining and Machine Learning, 108–122
 Butsky, I. S., & Quinn, T. R. 2018, ApJ, 868, 108
 Cescutti, G., Matteucci, F., McWilliam, A., & Chiappini, C. 2009, A&A, 505, 605
 Cooke, R., Pettini, M., Steidel, C. C., Rudie, G. C., & Nissen, P. E. 2011, MNRAS, 417, 1534
 Cooke, R. J., Pettini, M., Nollett, K. M., & Jorgenson, R. 2016, ApJ, 830, 148
 Cooksey, K. L., Prochaska, J. X., Chen, H.-W., Mulchaey, J. S., & Weiner, B. J. 2008, ApJ, 676, 262
 Cooper, T. J., Rudie, G. C., Chen, H.-W., et al. 2021, MNRAS, 508, 4359

- Corlies, L., Peebles, M. S., Tumlinson, J., et al. 2020, ApJ, 896, 125
- Cowie, L. L., Songaila, A., Kim, T.-S., & Hu, E. M. 1995, AJ, 109, 1522
- Crighton, N. H. M., Hennawi, J. F., Simcoe, R. A., et al. 2015, MNRAS, 446, 18
- Crighton, N. H. M., O'Meara, J. M., & Murphy, M. T. 2016, MNRAS, 457, L44
- Crighton, N. H. M., Bechtold, J., Carswell, R. F., et al. 2013, MNRAS, 433, 178
- Dekel, A., Birnboim, Y., Engel, G., et al. 2009, Nature, 457, 451
- D'Odorico, V., Calura, F., Cristiani, S., & Viel, M. 2010, MNRAS, 401, 2715
- D'Odorico, V., Cupani, G., Cristiani, S., et al. 2013, MNRAS, 435, 1198
- Ellison, S. L., Songaila, A., Schaye, J., & Pettini, M. 2000, AJ, 120, 1175
- Emerick, A., Bryan, G. L., & Mac Low, M.-M. 2019, MNRAS, 482, 1304
- Fabbian, D., Khomenko, E., Moreno-Insertis, F., & Nordlund, Å. 2010, ApJ, 724, 1536
- Feigelson, E. D., & Nelson, P. I. 1985, ApJ, 293, 192
- Ferland, G. J., Porter, R. L., van Hoof, P. A. M., et al. 2013, RMxAA, 49, 137
- Ferrara, A., Pettini, M., & Shchekinov, Y. 2000, MNRAS, 319, 539
- Fitzpatrick, E. L., & Spitzer, Jr., L. 1997, ApJ, 475, 623
- Foreman-Mackey, D., Hogg, D. W., Lang, D., & Goodman, J. 2013, PASP, 125, 306
- Frebel, A., Johnson, J. L., & Bromm, V. 2007, MNRAS, 380, L40
- Fukugita, M., Hogan, C. J., & Peebles, P. J. E. 1998, ApJ, 503, 518
- Fumagalli, M., Cantalupo, S., Dekel, A., et al. 2016a, MNRAS, 462, 1978
- Fumagalli, M., O'Meara, J. M., & Prochaska, J. X. 2011a, Science, 334, 1245
- . 2016b, MNRAS, 455, 4100
- Fumagalli, M., Prochaska, J. X., Kasen, D., et al. 2011b, MNRAS, 418, 1796
- Fumagalli, M., Mackenzie, R., Trayford, J., et al. 2017, MNRAS, 471, 3686
- Gibson, J. L. andLehner, N., Oppenheimer, B. D., Howk, J. C. B. D., Cooksey, K. L., & Fox, A. J. 2021, ApJ, submitted
- Haardt, F., & Madau, P. 1996, ApJ, 461, 20
- Haardt, F., & Madau, P. 2001, in Clusters of Galaxies and the High Redshift Universe Observed in X-rays, ed. D. M. Neumann & J. T. V. Tran, 64
- . 2012, ApJ, 746, 125
- Hafen, Z., Faucher-Giguère, C.-A., Anglés-Alcázar, D., et al. 2017, MNRAS, 469, 2292
- Haislmaier, K. J., Tripp, T. M., Katz, N., et al. 2021, MNRAS, 502, 4993
- Howk, J. C., Ribaudo, J. S., Lehner, N., Prochaska, J. X., & Chen, H.-W. 2009, MNRAS, 396, 1875
- Hummels, C. B., Smith, B. D., & Silvia, D. W. 2017, ApJ, 847, 59
- Hummels, C. B., Smith, B. D., Hopkins, P. F., et al. 2019, ApJ, 882, 156
- Hunter, J. D. 2007, Computing in Science and Engineering, 9, 90
- Jenkins, E. B. 2009, ApJ, 700, 1299
- Jenkins, E. B., & Wallerstein, G. 2017, ApJ, 838, 85
- Ji, S., Chan, T. K., Hummels, C. B., et al. 2020, MNRAS, 496, 4221
- Jorgenson, R. A., Murphy, M. T., & Thompson, R. 2013, MNRAS, 435, 482
- Kacprzak, G. G., Pointon, S. K., Nielsen, N. M., et al. 2019, ApJ, 886, 91
- Kereš, D., Katz, N., Weinberg, D. H., & Davé, R. 2005, MNRAS, 363, 2
- Khaire, V., & Srianand, R. 2019, MNRAS, 484, 4174
- Kim, T. S., Cristiani, S., & D'Odorico, S. 2001, A&A, 373, 757
- Lehner, N., O'Meara, J. M., Fox, A. J., et al. 2014, ApJ, 788, 119
- Lehner, N., O'Meara, J. M., Howk, J. C., Prochaska, J. X., & Fumagalli, M. 2016, ApJ, 833, 283
- Lehner, N., Prochaska, J. X., Kobulnicky, H. A., et al. 2009, ApJ, 694, 734
- Lehner, N., Savage, B. D., Richter, P., et al. 2007, ApJ, 658, 680
- Lehner, N., Wotta, C. B., Howk, J. C., et al. 2018, ApJ, 866, 33
- . 2019, ApJ, 887, 5
- Lehner, N., Zech, W. F., Howk, J. C., & Savage, B. D. 2011, ApJ, 727, 46
- Lehner, N., Howk, J. C., Tripp, T. M., et al. 2013, ApJ, 770, 138
- Lehner, N., Berek, S. C., Howk, J. C., et al. 2020, ApJ, 900, 9
- Lochhaas, C., Tumlinson, J., O'Shea, B. W., et al. 2021, arXiv e-prints, arXiv:2102.08393
- Lofthouse, E. K., Fumagalli, M., Fossati, M., et al. 2020, MNRAS, 491, 2057
- Macquart, J. P., Prochaska, J. X., McQuinn, M., et al. 2020, Nature, 581, 391

- Marra, R., Churchill, C. W., Doughty, C., et al. 2021, MNRAS, 508, 4938
- Mattsson, L. 2010, A&A, 515, A68
- McQuinn, M. 2016, ARA&A, 54, 313
- Morton, D. C. 2003, ApJS, 149, 205
- O'Meara, J. M., Lehner, N., Howk, J. C., et al. 2017, AJ, 154, 114
- O'Meara, J. M., Prochaska, J. X., Burles, S., et al. 2007, ApJ, 656, 666
- O'Meara, J. M., Lehner, N., Howk, J. C., et al. 2015, AJ, 150, 111
- Pedregosa, F., Varoquaux, G., Gramfort, A., et al. 2011, Journal of Machine Learning Research, 12, 2825
- Peeples, M. S., Corlies, L., Tumlinson, J., et al. 2019, ApJ, 873, 129
- Penprase, B. E., Prochaska, J. X., Sargent, W. L. W., Toro-Martinez, I., & Beeler, D. J. 2010, ApJ, 721, 1
- Péroux, C., & Howk, J. C. 2020, ARA&A, 58, 363
- Pettini, M., Ellison, S. L., Steidel, C. C., & Bowen, D. V. 1999, ApJ, 510, 576
- Pettini, M., Smith, L. J., King, D. L., & Hunstead, R. W. 1997, ApJ, 486, 665
- Pettini, M., Zych, B. J., Steidel, C. C., & Chaffee, F. H. 2008, MNRAS, 385, 2011
- Planck Collaboration, Ade, P. A. R., Aghanim, N., et al. 2016, A&A, 594, A13
- Pontzen, A., & Tremmel, M. 2018, ApJS, 237, 23
- Prochaska, J. X. 1999, ApJL, 511, L71
- Prochaska, J. X., Gawiser, E., Wolfe, A. M., Castro, S., & Djorgovski, S. G. 2003, ApJL, 595, L9
- Prochaska, J. X., Herbert-Fort, S., & Wolfe, A. M. 2005, ApJ, 635, 123
- Prochaska, J. X., Madau, P., O'Meara, J. M., & Fumagalli, M. 2014, MNRAS, 438, 476
- Prochaska, J. X., O'Meara, J. M., Fumagalli, M., Bernstein, R. A., & Burles, S. M. 2015, ApJS, 221, 2
- Prochaska, J. X., O'Meara, J. M., Herbert-Fort, S., et al. 2006, ApJL, 648, L97
- Prochaska, J. X., O'Meara, J. M., & Worseck, G. 2010, ApJ, 718, 392
- Prochaska, J. X., Tejos, N., Wotta, C. B., et al. 2017a, pyigm/pyigm: Initial release for publications, UCSC, doi:10.5281/zenodo.1045480
- Prochaska, J. X., Werk, J. K., Worseck, G., et al. 2017b, ApJ, 837, 169
- Prochter, G. E., Prochaska, J. X., O'Meara, J. M., Burles, S., & Bernstein, R. A. 2010, ApJ, 708, 1221
- Rafelski, M., Wolfe, A. M., Prochaska, J. X., Neeleman, M., & Mendez, A. J. 2012, ApJ, 755, 89
- Rahmati, A., & Oppenheimer, B. D. 2018, MNRAS, 476, 4865
- Rauch, M., Miralda-Escudé, J., Sargent, W. L. W., et al. 1997, ApJ, 489, 7
- Rhodin, N. H. P., Agertz, O., Christensen, L., Renaud, F., & Fynbo, J. P. U. 2019, MNRAS, 488, 3634
- Ribaudo, J., Lehner, N., Howk, J. C., et al. 2011, ApJ, 743, 207
- Rudie, G. C., Steidel, C. C., & Pettini, M. 2012, ApJL, 757, L30
- Savage, B. D., & Sembach, K. R. 1991, ApJ, 379, 245
- . 1996, ARA&A, 34, 279
- Scannapieco, E. 2005, ApJL, 624, L1
- Schaye, J. 2001a, ApJL, 562, L95
- . 2001b, ApJ, 559, 507
- Schaye, J., Aguirre, A., Kim, T.-S., et al. 2003, ApJ, 596, 768
- Schaye, J., Theuns, T., Rauch, M., Efstathiou, G., & Sargent, W. L. W. 2000, MNRAS, 318, 817
- Sembach, K. R., & Savage, B. D. 1992, ApJS, 83, 147
- Shull, J. M., Smith, B. D., & Danforth, C. W. 2012, ApJ, 759, 23
- Simcoe, R. A. 2011, ApJ, 738, 159
- Simcoe, R. A., Sargent, W. L. W., & Rauch, M. 2004, ApJ, 606, 92
- Simons, R. C., Peeples, M. S., Tumlinson, J., et al. 2020, ApJ, 905, 167
- Songaila, A. 1998, AJ, 115, 2184
- . 2005, AJ, 130, 1996
- Suresh, J., Nelson, D., Genel, S., Rubin, K. H. R., & Hernquist, L. 2019, MNRAS, 483, 4040
- Tripp, T. M., Jenkins, E. B., Bowen, D. V., et al. 2005, ApJ, 619, 714
- Tumlinson, J., Peeples, M. S., & Werk, J. K. 2017, ARA&A, 55, 389
- Turk, M. J., Smith, B. D., Oishi, J. S., et al. 2011, The Astrophysical Journal Supplement Series, 192, 9
- Tytler, D. 1987, ApJ, 321, 49
- van de Voort, F., Springel, V., Mandelker, N., van den Bosch, F. C., & Pakmor, R. 2019, MNRAS, 482, L85
- Weinberg, D. H., Miralda-Escudé, J., Hernquist, L., & Katz, N. 1997, ApJ, 490, 564
- Wolfe, A. M., Gawiser, E., & Prochaska, J. X. 2005, ARA&A, 43, 861
- Wotta, C. B., Lehner, N., Howk, J. C., et al. 2019, ApJ, 872, 81
- Wotta, C. B., Lehner, N., Howk, J. C., O'Meara, J. M., & Prochaska, J. X. 2016, ApJ, 831, 95
- Zahedy, F. S., Chen, H.-W., Cooper, T. M., et al. 2021, MNRAS, 506, 877

Zheng, Y., Peebles, M. S., O'Shea, B. W., et al. 2020, ApJ,
896, 143

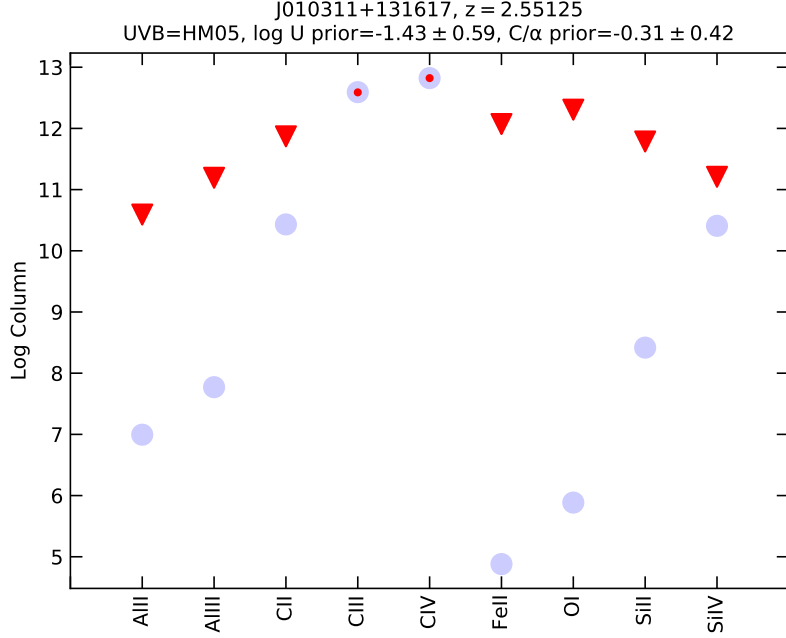


Figure A1. Example of a MCMC comparison plot for the absorber at $z = 2.55125$ toward J010311+131617. It shows the measured column densities for each ion (red) and the predicted column densities from the median MCMC model (blue). Downward triangles show upper limits.

APPENDIX

[Note: owing to their sizes, supplemental files are available on request. They will be easily accessible when the paper is published.]

In this Appendix, we provide information regarding the supplemental files. For each KODIAQ-Z absorber, we produced a figure as shown in Fig. 3 where we plot the normalized profiles of metals and some H I transitions for which we estimated the column densities (supplemental figure fA3.pdf). The red portion in each profile shows the velocity range of the absorption over which the velocity profile was integrated to derive the column densities and average velocity. The vertical dashed lines mark the zero velocity. We also provide for each KODIAQ-Z absorber (and sometimes paired or multiple closely redshift spaced absorbers) a set of figures as Fig. 4 where the Voigt profile fits (in red the composite profile fit, and in blue each individual component fit) to the individual transitions of H I (black spectra) are shown (supplemental figure fA4.pdf).

Next, we provide the visualization results from the MCMC Bayesian photoionization modeling. For each KODIAQ-Z absorber, we provide the comparison plots between the observations and models and corner plots as shown in Figs. A1 and A2, respectively (supplemental figures fA5.pdf and fA6.pdf). The example shown in these figures is one of the absorbers shown in Fig. 3. In Fig. A1, we compare the measured column densities for each ion (red) and the predicted column densities from the median MCMC model (blue). Triangles (when present) show lower limits (i.e., saturated transitions), while downward triangles show upper limits. Red data points with error bars (sometimes smaller than the circles) denote well-constrained column densities. From the corner or comparison plots, one can determine readily which modeling was used: (1) if there is no entry for $\log U$ ($\log U$ prior = False), then a flat prior on the ionization parameter was used; (2) if a value to $\log U$ is given, then a Gaussian prior on $\log U$ was used with the listed mean and dispersion values; (3) if $[C/\alpha]$ is present, the absence of value indicates that a flat prior was used, otherwise a Gaussian prior was used on that ratio with the listed mean and dispersion values. The EUVB used in the modeling is also provided (in this case, HM05). Finally, the comparison plots show which ions were used in the ionization modeling.

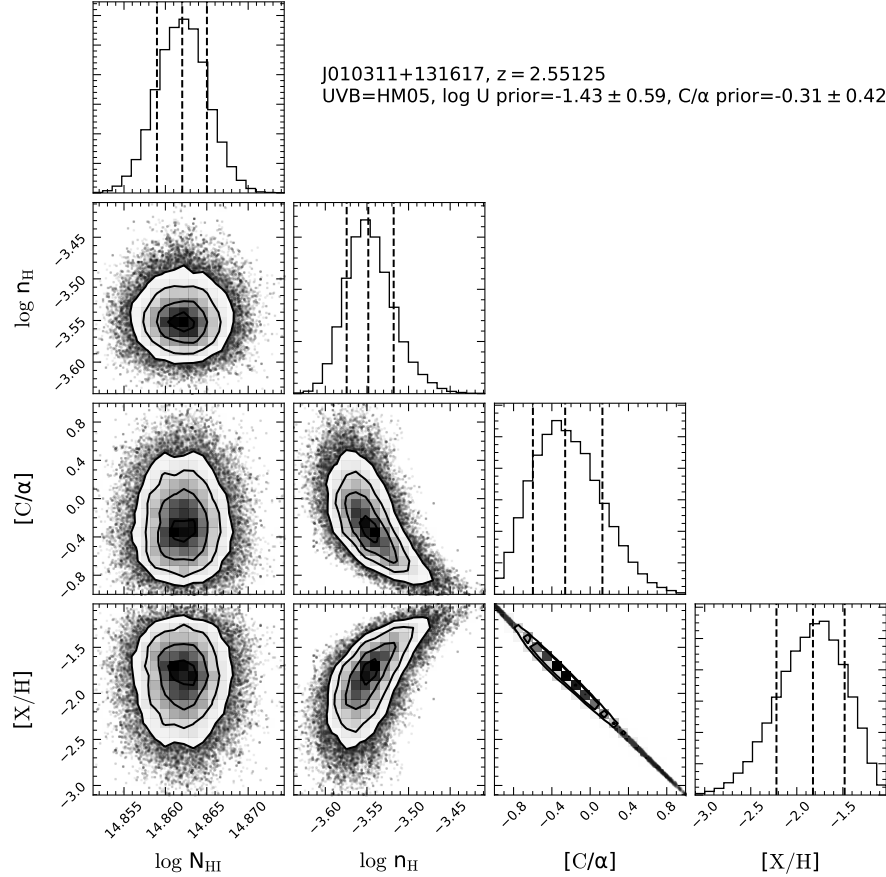


Figure A2. Example of a MCMC corner plot for the absorber at $z = 2.55125$ toward J010311+131617. The histograms along the diagonal show the PDFs for N_{HI} , hydrogen number density (n_{H}), $[\text{C}/\alpha]$, and metallicity, respectively. The contour plots below the diagonal show the joint posterior PDFs of the given row and column. For this absorber, there is not enough constraint on the metal column densities to derive the metallicity and $[\text{C}/\alpha]$ without using priors (see Fig. A1).

Table 1. Sample Summary

Target	z_{em}	λ_{min}	λ_{max}	SNR ₉₃₅	SNR ₁₁₇₀	SNR ₁₄₅₀	Decker	Obs.
		(Å)	(Å)					
J002127-020333	2.596	3365	6198	10	12	10	C1	0
J003501-091817	2.418	3123	5979	7	18	19	C5	0
J004530-261709	3.440	3972	8542	10	17	15	C1	0
J005700+143737	2.643	3366	6198	5	9	8	C1	0
J010311+131617	2.721	3122	8566	54	76	84	C5	1
J010806+163550	2.652	3047	8158	34	101	29	C5	1
J010925-210257	3.226	3304	6179	19	19	14	C5	0
J011150+140141	2.470	3132	6030	4	7	6	C5	0
J012156+144823	2.870	3243	7512	30	87	79	C5	1
J014516-094517	2.729	3022	7522	77	112	100	C5	1
J015741-010629	3.564	3937	6294	10	19	-1	C5	1
J020950-000506	2.828	3022	9218	32	53	48	C1	1
J023359+004938	2.522	3174	6032	4	8	5	C1	0
J025905+001121	3.365	3805	6858	9	82	57	C1	1
J030341-002321	3.175	3535	7222	22	33	34	C5	1
J033900-013318	3.197	3685	7719	10	24	21	C5	1
J045213-164012	2.684	3100	6024	30	50	36	C5	1
J064204+675835	3.177	3469	6620	42	132	142	C5	1
J073149+285448	3.675	4160	8767	13	24	18	C5	0
J074521+473436	3.220	3574	6841	55	172	133	C5	1
J074749+443417	4.435	4849	9572	8	10	6	C1	1
J080117+521034	3.235	4043	6829	-1	100	104	C5	1
J081240+320808	2.711	3330	8771	26	45	74	C1	1
J082107+310751	2.625	3057	5980	24	38	33	C1	1
J083102+335803	2.427	3122	5979	6	15	16	C5	0
J090033+421546	3.290	3545	11691	14	52	67	C5	1
J093337+284532	3.425	3847	6933	3	47	28	C5	1
J093643+292713	2.923	2995	5869	10	13	10	C1	0
J094202+042244	3.275	3363	6200	39	42	26	C1	0
J095852+120245	3.297	3608	9800	35	45	36	C5	1
J100841+362319	3.125	3541	7992	23	47	27	C5	1
J101155+294141	2.652	3048	8921	74	118	17	C5	1
J101447+430030	3.125	3500	7268	39	103	47	C5	1
J101723-204658	2.545	3127	5980	24	37	36	C1	0
J102009+104002	3.167	3615	7352	23	45	42	C5	1
J104018+572448	3.408	3793	6656	15	18	12	C5	0
J105756+455553	4.137	3927	9175	66	152	92	C5	1
J113418+574204	3.521	3972	8534	18	26	23	C5	0
J113508+222715	2.886	3433	7240	19	40	43	C1	1
J120006+312630	2.989	3435	6178	16	61	62	C5	1
J121930+494052	2.633	3026	8958	45	72	15	C5	1
J124610+303131	2.560	3189	6085	10	16	16	C1	0
J130411+295348	2.850	2995	5870	14	20	16	C1	0
J131215+423900	2.566	3101	7647	24	34	34	C5	1
J134328+572147	3.034	3074	6468	11	19	12	C1	1
J134544+262506	2.031	3500	6385	-1	17	26	C5	0

Table 1 continued

Table 1 (*continued*)

Target	z_{em}	λ_{min}	λ_{max}	SNR ₉₃₅	SNR ₁₁₇₀	SNR ₁₄₅₀	Decker	Obs.
		(Å)	(Å)					Flag
J135038–251216	2.534	3108	5980	19	46	39	C1	1
J142438+225600	3.620	3569	7720	71	287	188	C5	1
J143316+313126	2.940	3244	6095	36	46	34	C5	0
J144453+291905	2.660	2995	7602	74	122	102	C5	1
J155152+191104	2.843	2995	7646	80	243	302	C5	1
J160455+381201	2.551	3105	7065	22	69	96	C1	1
J160843+071508	2.877	3077	8687	23	46	39	C1	1
J162557+264448	2.601	3101	9673	8	18	25	C5	1
J170100+641209	2.734	3060	9093	65	185	183	C5	1
J171227+575507	3.008	3451	6340	29	47	35	C5	1
J173352+540030	3.424	3734	8543	42	49	43	C5	1
J193957–100241	3.787	3569	7450	75	92	-1	C5	1
J212912–153841	3.268	3571	6975	25	51	21	C5	1
J220852–194400	2.573	3022	7626	42	88	59	C5	1
J222256–094636	2.926	3214	6095	10	18	13	C1	0
J234628+124859	2.573	3022	12723	48	181	95	C5	1
J234856–104131	3.172	3101	5979	15	19	-1	C5	0

NOTE— The median SNR is calculated by $\text{SNR} = 1.0/\sigma$ per pixel within $\pm 5\text{\AA}$ (where σ is the error on the normalized flux) of three rest wavelengths. A -1 in one of the SNR column indicates there is no wavelength coverage where the SNR is estimated. The pixels are a constant 2.1 km s^{-1} for pre-2004 observations or 2.6 km s^{-1} for post-2004 observations and for coadditions of observations mixing pre- and post-2004 data (see O’Meara et al. 2017). The observation flag “1” in the last column indicates if there was more than one run or a single run (“0”) (see Table 2 in O’Meara et al. 2017). The decker setup corresponds to the following resolution: C1: $R = 45,000$; C5: $R = 34,000$.

Table 2. Summary of the Column Densities of the KODIAQ-Z Absorbers

Target	z_{abs}	Ion	v_1	v_2	v	σ_v	$\log N$	$\sigma_{\log N}^1$	$\sigma_{\log N}^2$	Detection	Reliability	Unique
			(km s $^{-1}$)	(km s $^{-1}$)	(km s $^{-1}$)		[cm $^{-2}$]	Flag	Flag			
J002127–020333	2.54918	Al II	-50.0	50.0	999.0	999.0	11.625	0.176	0.301	-1	3	1
J002127–020333	2.54918	C II	-50.0	50.0	999.0	999.0	13.379	0.176	0.301	-1	3	1
J002127–020333	2.54918	C IV	-50.0	50.0	0.4	3.9	13.175	0.058	0.066	0	2	1
J002127–020333	2.54918	Fe II	-50.0	50.0	999.0	999.0	13.228	0.176	0.301	-1	3	1
J002127–020333	2.54918	H I	-50.0	50.0	-2.4	2.7	15.680	0.019	0.022	0	2	1
J002127–020333	2.54918	N I	-50.0	50.0	999.0	999.0	13.329	0.176	0.301	-1	3	1
J002127–020333	2.54918	N V	-50.0	50.0	999.0	999.0	12.658	0.176	0.301	-1	3	1
J002127–020333	2.54918	O I	-50.0	50.0	999.0	999.0	13.860	0.176	0.301	-1	3	1
J002127–020333	2.54918	O VI	-50.0	50.0	-10.0	5.2	13.418	0.068	0.081	0	1	1
J002127–020333	2.54918	S II	-50.0	50.0	999.0	999.0	13.674	0.176	0.301	-1	3	1
J002127–020333	2.54918	S III	-50.0	50.0	999.0	999.0	13.533	0.176	0.301	-1	3	1
J002127–020333	2.54918	Si II	-50.0	50.0	999.0	999.0	11.778	0.176	0.301	-1	3	1
J002127–020333	2.54918	Si IV	-50.0	50.0	999.0	999.0	12.172	0.176	0.301	-1	3	1
J003501–091817	2.35342	C II	-50.0	50.0	999.0	999.0	12.470	0.180	0.300	-1	3	2
J003501–091817	2.35342	C IV	-50.0	50.0	999.0	999.0	12.410	0.180	0.300	-1	3	2
J003501–091817	2.35342	Fe II	-50.0	50.0	999.0	999.0	12.850	0.180	0.300	-1	3	2
J003501–091817	2.35342	H I	-50.0	50.0	0.6	4.0	15.610	0.040	0.050	0	2	2

Table 2 continued

Table 2 (*continued*)

Target	z_{abs}	Ion	v_1	v_2	v	σ_v	$\log N$	$\sigma_{\log N}^1$	$\sigma_{\log N}^2$	Detection	Reliability	Unique
			(km s $^{-1}$)	(km s $^{-1}$)	(km s $^{-1}$)	[cm $^{-2}$]	Flag	Flag	ID			
J003501-091817	2.35342	O I	-50.0	50.0	999.0	999.0	12.980	0.180	0.300	-1	3	2
J003501-091817	2.35342	S II	-50.0	50.0	999.0	999.0	13.280	0.180	0.300	-1	3	2
J003501-091817	2.35342	Si II	-50.0	50.0	999.0	999.0	11.420	0.180	0.300	-1	3	2
J003501-091817	2.35342	Si IV	-50.0	50.0	999.0	999.0	11.990	0.180	0.300	-1	3	2
J004530-261709	2.81907	Al III	-110.0	60.0	-38.2	5.4	12.400	0.050	0.050	0	3	3
J004530-261709	2.81907	C IV	-230.0	130.0	-28.6	1.4	14.200	0.010	0.010	0	3	3
J004530-261709	2.81907	Fe II	-110.0	60.0	-19.0	0.9	14.330	0.010	0.010	0	2	3
J004530-261709	2.81907	H I	-1000.0	1000.0	-1.8	164.5	19.660	0.010	0.010	0	3	3
J004530-261709	2.81907	Zn II	-110.0	60.0	-3.6	14.1	12.060	0.100	0.140	0	1	3
J004530-261709	3.24823	Al II	-70.0	40.0	999.0	999.0	11.230	0.180	0.300	-1	3	4
J004530-261709	3.24823	Al III	-70.0	40.0	-27.9	9.4	12.010	0.100	0.140	-1	3	4
J004530-261709	3.24823	C II	-70.0	40.0	999.0	999.0	12.530	0.180	0.300	-1	3	4
J004530-261709	3.24823	C IV	-70.0	40.0	999.0	999.0	12.250	0.180	0.300	-1	3	4
J004530-261709	3.24823	H I	-70.0	40.0	-3.7	1.3	15.120	0.010	0.010	0	2	4
J004530-261709	3.24823	O I	-70.0	40.0	999.0	999.0	12.770	0.180	0.300	-1	3	4
J004530-261709	3.24823	Si II	-70.0	40.0	999.0	999.0	12.430	0.180	0.300	-1	3	4
J004530-261709	3.24823	Si IV	-70.0	40.0	999.0	999.0	12.210	0.180	0.300	-1	3	4
J004530-261709	3.36517	Al III	-30.0	30.0	999.0	999.0	11.590	0.180	0.300	-1	3	5
J004530-261709	3.36517	C II	-30.0	30.0	999.0	999.0	12.370	0.180	0.300	-1	3	5
J004530-261709	3.36517	Fe II	-30.0	30.0	999.0	999.0	12.620	0.180	0.300	-1	3	5
J004530-261709	3.36517	H I	-58.3	55.2	5.5	2.3	15.770	0.010	0.020	0	2	5
J004530-261709	3.36517	O I	-30.0	30.0	999.0	999.0	12.850	0.180	0.300	-1	3	5
J004530-261709	3.36517	Si II	-30.0	30.0	999.0	999.0	11.250	0.180	0.300	-1	3	5
J004530-261709	3.36517	Si IV	-30.0	30.0	999.0	999.0	11.850	0.180	0.300	-1	3	5
J005700+143737	2.54721	Al II	-30.0	30.0	999.0	999.0	11.550	0.180	0.300	-1	3	6
J005700+143737	2.54721	C II	-30.0	30.0	999.0	999.0	13.490	0.180	0.300	-1	3	6
J005700+143737	2.54721	C III	-30.0	30.0	999.0	999.0	12.320	0.180	0.300	-1	3	6
J005700+143737	2.54721	C IV	-30.0	30.0	999.0	999.0	12.540	0.180	0.300	-1	3	6
J005700+143737	2.54721	Fe II	-30.0	30.0	999.0	999.0	13.040	0.180	0.300	-1	3	6
J005700+143737	2.54721	H I	-150.3	71.9	-21.7	1.7	15.040	0.010	0.010	0	3	6
J005700+143737	2.54721	N I	-30.0	30.0	999.0	999.0	13.480	0.180	0.300	-1	3	6
J005700+143737	2.54721	O I	-30.0	30.0	999.0	999.0	13.180	0.180	0.300	-1	3	6
J005700+143737	2.54721	Si II	-30.0	30.0	999.0	999.0	11.680	0.180	0.300	-1	3	6
J005700+143737	2.54721	Si IV	-30.0	30.0	999.0	999.0	12.150	0.180	0.300	-1	3	6
J010311+131617	2.54303	Al II	-35.0	35.0	999.0	999.0	10.629	0.176	0.301	-1	3	7
J010311+131617	2.54303	Al III	-35.0	35.0	999.0	999.0	11.554	0.176	0.301	-1	3	7
J010311+131617	2.54303	C II	-35.0	35.0	999.0	999.0	11.825	0.176	0.301	-1	3	7
J010311+131617	2.54303	C IV	-35.0	35.0	1.7	0.2	13.270	0.004	0.004	0	3	7
J010311+131617	2.54303	H I	-58.8	55.5	0.7	0.2	15.621	0.002	0.002	0	3	7
J010311+131617	2.54303	O VI	-35.0	35.0	2.5	0.3	13.688	0.006	0.007	0	1	7
J010311+131617	2.54303	S VI	-35.0	35.0	999.0	999.0	12.048	0.176	0.301	-1	3	7
J010311+131617	2.54303	Si II	-35.0	35.0	999.0	999.0	11.770	0.176	0.301	-1	3	7
J010311+131617	2.54303	Si IV	-35.0	35.0	999.0	999.0	11.215	0.176	0.301	-1	3	7
J010311+131617	2.55125	Al II	-30.0	40.0	999.0	999.0	10.592	0.176	0.301	-1	3	8
J010311+131617	2.55125	Al III	-30.0	40.0	999.0	999.0	11.193	0.176	0.301	-1	3	8
J010311+131617	2.55125	C II	-30.0	40.0	999.0	999.0	11.870	0.176	0.301	-1	3	8
J010311+131617	2.55125	C III	-30.0	40.0	12.7	0.7	12.589	0.015	0.016	0	1	8

Table 2 continued

Table 2 (*continued*)

Target	z_{abs}	Ion	v_1	v_2	v	σ_v	$\log N$	$\sigma_{\log N}^1$	$\sigma_{\log N}^2$	Detection	Reliability	Unique
			(km s $^{-1}$)	(km s $^{-1}$)	(km s $^{-1}$)	[cm $^{-2}$]	Flag	Flag	ID			
J010311+131617	2.55125	C IV	-30.0	40.0	6.4	0.5	12.822	0.012	0.012	0	3	8
J010311+131617	2.55125	Fe II	-30.0	40.0	999.0	999.0	12.071	0.176	0.301	-1	3	8
J010311+131617	2.55125	H I	-24.7	36.5	9.1	0.1	14.862	0.003	0.003	0	3	8
J010311+131617	2.55125	O I	-30.0	40.0	999.0	999.0	12.306	0.176	0.301	-1	3	8
J010311+131617	2.55125	O VI	-30.0	40.0	14.5	0.7	13.348	0.014	0.014	0	1	8
J010311+131617	2.55125	Si II	-30.0	40.0	999.0	999.0	11.786	0.176	0.301	-1	3	8
J010311+131617	2.55125	Si IV	-30.0	40.0	999.0	999.0	11.209	0.176	0.301	-1	3	8
J010311+131617	2.55216	Al II	-40.0	25.0	999.0	999.0	10.590	0.176	0.301	-1	3	9
J010311+131617	2.55216	Al III	-40.0	25.0	999.0	999.0	11.171	0.176	0.301	-1	3	9
J010311+131617	2.55216	C II	-40.0	25.0	-39.7	13.7	11.976	0.138	0.204	-1	3	9
J010311+131617	2.55216	C III	-40.0	25.0	-0.3	0.2	13.143	0.005	0.005	0	1	9
J010311+131617	2.55216	C IV	-40.0	25.0	-6.6	0.3	13.091	0.006	0.006	0	3	9
J010311+131617	2.55216	Fe II	-40.0	25.0	1.7	11.0	12.105	0.163	0.263	-1	3	9
J010311+131617	2.55216	H I	-30.8	38.6	-1.6	0.2	15.505	0.007	0.007	0	3	9
J010311+131617	2.55216	O I	-40.0	25.0	999.0	999.0	12.288	0.176	0.301	-1	3	9
J010311+131617	2.55216	O VI	-40.0	25.0	-9.7	0.5	13.417	0.012	0.012	0	1	9
J010311+131617	2.55216	Si II	-40.0	25.0	999.0	999.0	12.019	0.176	0.301	-1	3	9
J010311+131617	2.55216	Si IV	-40.0	25.0	999.0	999.0	11.508	0.176	0.301	-1	3	9
J010806+163550	2.31582	Al II	-30.0	30.0	999.0	999.0	11.147	0.176	0.301	-1	3	10
J010806+163550	2.31582	Al III	-30.0	30.0	999.0	999.0	11.725	0.176	0.301	-1	3	10
J010806+163550	2.31582	C IV	-30.0	30.0	999.0	999.0	12.009	0.176	0.301	-1	3	10
J010806+163550	2.31582	Fe II	-30.0	30.0	999.0	999.0	12.510	0.176	0.301	-1	3	10
J010806+163550	2.31582	H I	-70.0	60.0	-11.1	0.3	14.574	0.004	0.004	0	2	10
J010806+163550	2.31582	O VI	-30.0	30.0	999.0	999.0	12.720	0.176	0.301	-1	3	10
J010806+163550	2.31582	Si II	-30.0	30.0	999.0	999.0	10.988	0.176	0.301	-1	3	10
J010806+163550	2.31582	Si IV	-30.0	30.0	999.0	999.0	11.109	0.176	0.301	-1	3	10
J010806+163550	2.46164	Al II	-30.0	30.0	-4.6	6.1	11.283	0.133	0.193	-1	3	11
J010806+163550	2.46164	Al III	-30.0	30.0	999.0	999.0	12.102	0.176	0.301	-1	3	11
J010806+163550	2.46164	C II	-30.0	30.0	999.0	999.0	11.713	0.176	0.301	-1	3	11
J010806+163550	2.46164	C IV	-30.0	30.0	999.0	999.0	12.064	0.176	0.301	-1	3	11
J010806+163550	2.46164	Fe II	-30.0	30.0	999.0	999.0	12.551	0.176	0.301	-1	3	11
J010806+163550	2.46164	H I	-68.6	58.8	1.7	0.2	14.754	0.002	0.002	0	3	11
J010806+163550	2.46164	Si II	-30.0	30.0	999.0	999.0	12.210	0.176	0.301	-1	3	11
J010806+163550	2.46164	Si IV	-30.0	30.0	999.0	999.0	11.677	0.176	0.301	-1	3	11
J010806+163550	2.48359	Al III	-35.0	35.0	999.0	999.0	11.811	0.176	0.301	-1	3	12
J010806+163550	2.48359	C II	-35.0	35.0	-3.6	5.4	12.034	0.102	0.134	-1	3	12
J010806+163550	2.48359	C III	-35.0	35.0	13.5	0.6	12.944	0.013	0.013	0	1	12
J010806+163550	2.48359	C IV	-35.0	35.0	3.0	0.7	13.336	0.015	0.016	0	3	12
J010806+163550	2.48359	Fe II	-35.0	35.0	999.0	999.0	12.504	0.176	0.301	-1	3	12
J010806+163550	2.48359	Fe III	-35.0	35.0	999.0	999.0	12.435	0.176	0.301	-1	3	12
J010806+163550	2.48359	H I	-71.9	58.8	1.6	0.5	15.315	0.010	0.010	0	3	12
J010806+163550	2.48359	O I	-35.0	35.0	999.0	999.0	12.123	0.176	0.301	-1	3	12
J010806+163550	2.48359	S II	-35.0	35.0	999.0	999.0	12.633	0.176	0.301	-1	3	12
J010806+163550	2.48359	Si II	-35.0	35.0	999.0	999.0	10.753	0.176	0.301	-1	3	12
J010806+163550	2.50561	Al II	-30.0	30.0	-8.6	8.4	11.107	0.174	0.295	-1	3	13
J010806+163550	2.50561	Al III	-30.0	30.0	999.0	999.0	11.743	0.176	0.301	-1	3	13
J010806+163550	2.50561	C II	-30.0	30.0	999.0	999.0	11.740	0.176	0.301	-1	3	13

Table 2 continued

Table 2 (*continued*)

Target	z_{abs}	Ion	v_1	v_2	v	σ_v	$\log N$	$\sigma_{\log N}^1$	$\sigma_{\log N}^2$	Detection	Reliability	Unique
			(km s $^{-1}$)	(km s $^{-1}$)	(km s $^{-1}$)	[cm $^{-2}$]	Flag	Flag	ID			
J010806+163550	2.50561	C IV	-30.0	30.0	1.0	3.4	12.459	0.078	0.096	0	2	13
J010806+163550	2.50561	Fe II	-30.0	30.0	999.0	999.0	12.363	0.176	0.301	-1	3	13
J010806+163550	2.50561	H I	-50.7	47.5	-2.6	0.4	15.914	0.004	0.003	0	3	13
J010806+163550	2.50561	O I	-30.0	30.0	999.0	999.0	12.081	0.176	0.301	-1	3	13
J010806+163550	2.50561	Si II	-30.0	30.0	999.0	999.0	11.257	0.176	0.301	-1	3	13
J010806+163550	2.50561	Si IV	-30.0	30.0	2.9	7.4	11.526	0.144	0.217	0	1	13
J010925-210257	2.96546	C II	-35.0	25.0	999.0	999.0	12.732	0.176	0.301	-1	3	14
J010925-210257	2.96546	C III	-35.0	25.0	999.0	999.0	12.031	0.176	0.301	-1	3	14
J010925-210257	2.96546	C IV	-35.0	25.0	999.0	999.0	12.338	0.176	0.301	-1	3	14
J010925-210257	2.96546	H I	-61.0	40.6	-7.3	0.3	14.706	0.007	0.008	0	3	14
J010925-210257	2.96546	N I	-35.0	25.0	999.0	999.0	12.720	0.180	0.300	-1	3	14
J010925-210257	2.96546	O I	-35.0	25.0	999.0	999.0	12.681	0.176	0.301	-1	3	14
J010925-210257	2.96546	O VI	-35.0	25.0	-8.7	3.2	13.115	0.079	0.096	0	1	14
J010925-210257	2.96546	S II	-35.0	25.0	999.0	999.0	13.863	0.176	0.301	-1	3	14
J010925-210257	2.96546	S IV	-35.0	25.0	999.0	999.0	13.125	0.176	0.301	-1	3	14
J010925-210257	2.96546	Si II	-35.0	25.0	999.0	999.0	11.904	0.176	0.301	-1	3	14
J010925-210257	2.96546	Si IV	-35.0	25.0	999.0	999.0	11.901	0.176	0.301	-1	3	14
J010925-210257	3.14253	C II	-30.0	30.0	999.0	999.0	12.525	0.176	0.301	-1	3	15
J010925-210257	3.14253	H I	-45.8	32.7	-1.4	3.6	16.147	0.013	0.013	0	3	15
J010925-210257	3.14253	O I	-30.0	30.0	999.0	999.0	13.001	0.176	0.301	-1	3	15
J010925-210257	3.14253	S II	-30.0	30.0	999.0	999.0	13.676	0.176	0.301	-1	3	15
J010925-210257	3.14253	Si II	-30.0	30.0	999.0	999.0	12.741	0.176	0.301	-1	3	15
J010925-210257	3.14253	Si IV	-30.0	30.0	999.0	999.0	11.943	0.176	0.301	-1	3	15
J011150+140141	2.42374	Al II	-30.0	30.0	999.0	999.0	11.740	0.176	0.301	-1	3	16
J011150+140141	2.42374	C II	-30.0	30.0	999.0	999.0	13.131	0.176	0.301	-1	3	16
J011150+140141	2.42374	C IV	-30.0	30.0	999.0	999.0	12.636	0.176	0.301	-1	3	16
J011150+140141	2.42374	Fe II	-30.0	30.0	999.0	999.0	13.222	0.176	0.301	-1	3	16
J011150+140141	2.42374	H I	-37.0	37.0	0.9	2.0	14.803	0.019	0.021	0	3	16
J011150+140141	2.42374	N I	-30.0	30.0	999.0	999.0	13.630	0.176	0.301	-1	3	16
J011150+140141	2.42374	N II	-30.0	30.0	999.0	999.0	13.109	0.176	0.301	-1	3	16
J011150+140141	2.42374	N V	-30.0	30.0	999.0	999.0	12.834	0.176	0.301	-1	3	16
J011150+140141	2.42374	O I	-30.0	30.0	999.0	999.0	13.313	0.176	0.301	-1	3	16
J011150+140141	2.42374	O VI	-30.0	30.0	6.0	6.0	13.470	0.125	0.177	0	1	16
J011150+140141	2.42374	S II	-30.0	30.0	999.0	999.0	13.480	0.176	0.301	-1	3	16
J011150+140141	2.42374	S III	-30.0	30.0	999.0	999.0	13.525	0.176	0.301	-1	3	16
J011150+140141	2.42374	Si II	-30.0	30.0	-2.3	6.2	11.766	0.142	0.213	-1	3	16
J011150+140141	2.42374	Si III	-30.0	30.0	-19.8	5.4	12.054	0.084	0.104	0	1	16
J011150+140141	2.42374	Si IV	-30.0	30.0	999.0	999.0	12.561	0.176	0.301	-1	3	16
J012156+144823	2.41837	Al II	-12.0	17.0	999.0	999.0	10.519	0.176	0.301	-1	3	17
J012156+144823	2.41837	C IV	-12.0	17.0	5.5	0.5	12.353	0.023	0.024	0	3	17
J012156+144823	2.41837	Fe II	-12.0	17.0	999.0	999.0	11.765	0.176	0.301	-1	3	17
J012156+144823	2.41837	Fe III	-12.0	17.0	7.4	4.9	12.516	0.168	0.279	-1	3	17
J012156+144823	2.41837	H I	-75.0	55.0	-16.2	0.5	14.829	0.005	0.008	0	2	17
J012156+144823	2.41837	Si II	-12.0	17.0	999.0	999.0	11.604	0.176	0.301	-1	3	17
J012156+144823	2.41837	Si III	-12.0	17.0	999.0	999.0	10.877	0.176	0.301	-1	3	17
J012156+144823	2.41837	Si IV	-12.0	17.0	3.5	1.6	11.175	0.072	0.087	0	2	17
J012156+144823	2.46812	C IV	-32.0	0.1	-19.9	0.7	12.244	0.030	0.032	0	3	18

Table 2 continued

Table 2 (*continued*)

Target	z_{abs}	Ion	v_1	v_2	v	σ_v	$\log N$	$\sigma_{\log N}^1$	$\sigma_{\log N}^2$	Detection	Reliability	Unique
			(km s $^{-1}$)	(km s $^{-1}$)	(km s $^{-1}$)	[cm $^{-2}$]	Flag	Flag	ID			
J012156+144823	2.46812	H I	-71.9	49.0	-11.1	0.4	14.962	0.010	0.010	0	2	18
J012156+144823	2.46812	O I	-32.0	0.1	999.0	999.0	12.096	0.176	0.301	-1	3	18
J012156+144823	2.46812	S III	-32.0	0.1	999.0	999.0	12.830	0.176	0.301	-1	3	18
J012156+144823	2.46812	Si II	-32.0	0.1	999.0	999.0	11.591	0.176	0.301	-1	3	18
J012156+144823	2.46812	Si IV	-32.0	0.1	999.0	999.0	10.871	0.176	0.301	-1	3	18
J012156+144823	2.53765	Al II	-40.0	-10.0	999.0	999.0	10.322	0.176	0.301	-1	3	19
J012156+144823	2.53765	C II	-40.0	-10.0	999.0	999.0	11.368	0.176	0.301	-1	3	19
J012156+144823	2.53765	C III	-40.0	-10.0	-24.1	0.8	12.505	0.034	0.036	0	1	19
J012156+144823	2.53765	C IV	-40.0	-10.0	-24.6	0.5	12.166	0.025	0.027	0	3	19
J012156+144823	2.53765	H I	-91.5	29.4	-19.5	0.4	15.124	0.004	0.005	0	2	19
J012156+144823	2.53765	O VI	-40.0	-10.0	999.0	999.0	12.224	0.176	0.301	-1	3	19
J012156+144823	2.53765	Si II	-40.0	-10.0	999.0	999.0	11.379	0.176	0.301	-1	3	19
J012156+144823	2.53765	Si IV	-40.0	-10.0	-24.6	2.7	11.228	0.108	0.143	0	2	19
J012156+144823	2.62486	Al II	-20.0	20.0	3.7	2.8	10.645	0.084	0.105	-1	3	20
J012156+144823	2.62486	C II	-20.0	20.0	999.0	999.0	11.566	0.176	0.301	-1	3	20
J012156+144823	2.62486	C III	-20.0	20.0	-8.1	3.5	11.909	0.095	0.122	0	1	20
J012156+144823	2.62486	C IV	-20.0	20.0	-36.7	19.1	11.648	0.137	0.202	0	2	20
J012156+144823	2.62486	Fe II	-20.0	20.0	999.0	999.0	11.847	0.176	0.301	-1	3	20
J012156+144823	2.62486	H I	-104.6	42.5	-18.1	0.4	14.966	0.008	0.006	0	2	20
J012156+144823	2.62486	O I	-20.0	20.0	999.0	999.0	11.858	0.176	0.301	-1	3	20
J012156+144823	2.62486	Si II	-20.0	20.0	999.0	999.0	10.711	0.176	0.301	-1	3	20
J012156+144823	2.62486	Si IV	-20.0	20.0	999.0	999.0	11.077	0.180	0.300	-1	3	20
J012156+144823	2.66022	Al II	-20.0	20.0	999.0	999.0	10.650	0.176	0.301	-1	3	21
J012156+144823	2.66022	C II	-20.0	20.0	999.0	999.0	11.555	0.176	0.301	-1	3	21
J012156+144823	2.66022	C IV	-20.0	20.0	999.0	999.0	11.350	0.176	0.301	-1	3	21
J012156+144823	2.66022	Fe II	-20.0	20.0	999.0	999.0	12.022	0.176	0.301	-1	3	21
J012156+144823	2.66022	H I	-30.0	40.0	3.7	0.3	14.828	0.021	0.022	0	3	21
J012156+144823	2.66022	N V	-20.0	20.0	999.0	999.0	11.980	0.176	0.301	-1	3	21
J012156+144823	2.66022	O I	-20.0	20.0	999.0	999.0	11.874	0.176	0.301	-1	3	21
J012156+144823	2.66022	Si II	-20.0	20.0	999.0	999.0	11.241	0.176	0.301	-1	3	21
J012156+144823	2.66022	Si IV	-20.0	20.0	-7.0	3.4	11.266	0.096	0.123	-1	3	21
J012156+144823	2.66241	Al II	-50.0	60.0	2.0	0.2	12.838	0.003	0.003	0	1	22
J012156+144823	2.66241	C II	-50.0	60.0	1.3	0.2	14.817	0.006	0.006	-2	1	22
J012156+144823	2.66241	C IV	-50.0	60.0	14.8	0.1	13.784	0.002	0.002	0	3	22
J012156+144823	2.66241	Fe II	-50.0	60.0	20.6	0.4	14.025	0.009	0.009	0	1	22
J012156+144823	2.66241	H I	-100.0	80.0	-4.6	8.4	19.100	0.350	0.350	0	3	22
J012156+144823	2.66241	O I	-50.0	60.0	-2.8	0.1	14.620	0.001	0.001	0	3	22
J012156+144823	2.66241	O VI	-50.0	60.0	17.4	0.7	13.890	0.009	0.009	0	1	22
J012156+144823	2.66241	S VI	-50.0	60.0	-7.5	9.5	12.727	0.109	0.146	0	1	22
J012156+144823	2.66241	Si II	-50.0	60.0	-2.2	0.1	13.892	0.001	0.001	0	3	22
J012156+144823	2.66241	Si III	-50.0	60.0	10.9	4.7	14.050	0.001	0.001	-2	1	22
J012156+144823	2.66241	Si IV	-50.0	60.0	13.9	0.1	13.463	0.002	0.002	0	1	22
J012156+144823	2.66416	Al II	-20.0	25.0	0.9	0.1	12.320	0.000	0.000	0	1	23
J012156+144823	2.66416	C II	-20.0	25.0	1.9	0.0	14.210	0.010	0.010	0	3	23
J012156+144823	2.66416	C IV	-20.0	25.0	3.9	0.1	13.590	0.000	0.000	0	3	23
J012156+144823	2.66416	Fe II	-20.0	25.0	-5.1	2.6	12.430	0.070	0.090	0	1	23
J012156+144823	2.66416	Fe III	-20.0	25.0	-2.2	1.0	13.230	0.030	0.030	0	1	23

Table 2 continued

Table 2 (*continued*)

Target	z_{abs}	Ion	v_1	v_2	v	σ_v	$\log N$	$\sigma_{\log N}^1$	$\sigma_{\log N}^2$	Detection	Reliability	Unique
			(km s $^{-1}$)	(km s $^{-1}$)	(km s $^{-1}$)	[cm $^{-2}$]	Flag	Flag	ID			
J012156+144823	2.66416	H I	-20.0	25.0	0.0	0.7	17.260	0.100	0.100	0	3	23
J012156+144823	2.66416	N I	-20.0	25.0	999.0	999.0	12.010	0.180	0.300	-1	3	23
J012156+144823	2.66416	N II	-20.0	25.0	2.4	0.5	13.280	0.010	0.010	0	1	23
J012156+144823	2.66416	O I	-20.0	25.0	2.2	0.2	13.430	0.010	0.010	0	1	23
J012156+144823	2.66416	O VI	-20.0	25.0	2.9	0.2	14.190	0.010	0.010	0	1	23
J012156+144823	2.66416	Si II	-20.0	25.0	2.7	0.0	13.070	0.000	0.000	0	3	23
J012156+144823	2.66416	Si IV	-20.0	25.0	5.9	0.1	12.970	0.000	0.000	0	3	23
J012156+144823	2.66593	Al II	-25.0	14.0	-5.5	0.5	11.523	0.021	0.022	0	1	24
J012156+144823	2.66593	C II	-25.0	14.0	-6.1	0.1	13.295	0.005	0.005	0	3	24
J012156+144823	2.66593	C III	-25.0	14.0	-5.5	1.4	13.927	0.085	0.106	-2	1	24
J012156+144823	2.66593	C IV	-25.0	14.0	-7.2	0.0	13.579	0.002	0.002	0	3	24
J012156+144823	2.66593	Fe II	-25.0	14.0	999.0	999.0	11.976	0.176	0.301	-1	3	24
J012156+144823	2.66593	Fe III	-25.0	14.0	-6.1	1.0	13.097	0.036	0.040	0	1	24
J012156+144823	2.66593	H I	-35.0	20.0	-6.0	0.3	16.259	0.023	0.024	0	3	24
J012156+144823	2.66593	N I	-25.0	14.0	999.0	999.0	12.441	0.176	0.301	-1	3	24
J012156+144823	2.66593	O I	-25.0	14.0	999.0	999.0	11.906	0.176	0.301	-1	3	24
J012156+144823	2.66593	O VI	-25.0	14.0	-6.4	0.3	13.747	0.010	0.011	0	1	24
J012156+144823	2.66593	Si II	-25.0	14.0	-7.4	0.1	12.275	0.006	0.006	0	3	24
J012156+144823	2.66593	Si III	-25.0	14.0	-4.9	0.1	13.286	0.014	0.014	-2	1	24
J012156+144823	2.66593	Si IV	-25.0	14.0	-6.2	0.0	13.211	0.003	0.003	0	3	24
J012156+144823	2.81222	C II	-20.0	20.0	999.0	999.0	11.591	0.176	0.301	-1	3	25
J012156+144823	2.81222	C IV	-20.0	20.0	999.0	999.0	11.491	0.176	0.301	-1	3	25
J012156+144823	2.81222	Fe II	-20.0	20.0	999.0	999.0	11.992	0.176	0.301	-1	3	25
J012156+144823	2.81222	H I	-91.5	26.1	-20.0	0.2	14.683	0.002	0.002	0	3	25
J012156+144823	2.81222	N I	-20.0	20.0	999.0	999.0	11.665	0.176	0.301	-1	3	25
J012156+144823	2.81222	N II	-20.0	20.0	999.0	999.0	12.058	0.176	0.301	-1	3	25
J012156+144823	2.81222	O I	-20.0	20.0	999.0	999.0	12.048	0.176	0.301	-1	3	25
J012156+144823	2.81222	O VI	-20.0	20.0	-1.0	2.9	12.408	0.095	0.122	-1	3	25
J012156+144823	2.81222	S II	-20.0	20.0	999.0	999.0	12.396	0.176	0.301	-1	3	25
J012156+144823	2.81222	S III	-20.0	20.0	999.0	999.0	12.634	0.176	0.301	-1	3	25
J012156+144823	2.81222	Si II	-20.0	20.0	999.0	999.0	10.529	0.176	0.301	-1	3	25
J012156+144823	2.81222	Si III	-20.0	20.0	999.0	999.0	10.649	0.176	0.301	-1	3	25
J012156+144823	2.81222	Si IV	-20.0	20.0	999.0	999.0	10.971	0.176	0.301	-1	3	25
J014516-094517	2.49969	Al II	-20.0	20.0	999.0	999.0	10.381	0.176	0.301	-1	3	26
J014516-094517	2.49969	C II	-20.0	20.0	-2.7	5.5	11.592	0.164	0.268	-1	3	26
J014516-094517	2.49969	C IV	-20.0	20.0	999.0	999.0	11.425	0.176	0.301	-1	3	26
J014516-094517	2.49969	H I	-63.1	18.5	-14.1	0.1	15.026	0.001	0.001	0	3	26
J014516-094517	2.49969	O VI	-20.0	20.0	-10.4	5.1	12.164	0.147	0.223	-1	3	26
J014516-094517	2.49969	Si II	-20.0	20.0	999.0	999.0	11.079	0.176	0.301	-1	3	26
J014516-094517	2.49969	Si IV	-20.0	20.0	999.0	999.0	10.996	0.176	0.301	-1	3	26
J014516-094517	2.58808	C II	-20.0	20.0	-4.6	4.2	11.788	0.124	0.174	-1	3	27
J014516-094517	2.58808	C IV	-20.0	20.0	-5.8	1.5	12.030	0.044	0.049	0	3	27
J014516-094517	2.58808	H I	-47.6	58.2	-10.0	0.1	15.065	0.001	0.001	0	3	27
J014516-094517	2.58808	N I	-20.0	20.0	999.0	999.0	11.882	0.176	0.301	-1	3	27
J014516-094517	2.58808	N II	-20.0	20.0	-13.9	8.3	11.851	0.154	0.240	-1	3	27
J014516-094517	2.58808	O I	-20.0	20.0	999.0	999.0	12.073	0.176	0.301	-1	3	27
J014516-094517	2.58808	Si II	-20.0	20.0	3.4	5.5	10.631	0.162	0.263	-1	3	27

Table 2 continued

Table 2 (*continued*)

Target	z_{abs}	Ion	v_1	v_2	v	σ_v	$\log N$	$\sigma_{\log N}^1$	$\sigma_{\log N}^2$	Detection	Reliability	Unique
			(km s $^{-1}$)	(km s $^{-1}$)	(km s $^{-1}$)	[cm $^{-2}$]	Flag	Flag	ID			
J014516–094517	2.58808	Si III	−20.0	20.0	999.0	999.0	10.725	0.176	0.301	−1	3	27
J014516–094517	2.58808	Si IV	−20.0	20.0	999.0	999.0	11.030	0.176	0.301	−1	3	27
J014516–094517	2.66513	Al II	−30.0	30.0	999.0	999.0	10.970	0.176	0.301	−1	3	28
J014516–094517	2.66513	C II	−30.0	30.0	−0.3	2.0	12.369	0.046	0.052	0	1	28
J014516–094517	2.66513	C IV	−30.0	30.0	−2.0	0.2	13.061	0.005	0.005	0	3	28
J014516–094517	2.66513	Fe II	−30.0	30.0	999.0	999.0	12.078	0.176	0.301	−1	3	28
J014516–094517	2.66513	H I	−46.7	21.5	2.2	0.1	16.156	0.001	0.001	0	3	28
J014516–094517	2.66513	N I	−30.0	30.0	999.0	999.0	12.321	0.176	0.301	−1	3	28
J014516–094517	2.66513	O I	−30.0	30.0	−9.2	4.8	12.496	0.095	0.123	−1	3	28
J014516–094517	2.66513	S II	−30.0	30.0	−1.2	5.3	12.749	0.109	0.147	−1	3	28
J014516–094517	2.66513	S IV	−30.0	30.0	999.0	999.0	12.253	0.176	0.301	−1	3	28
J014516–094517	2.66513	Si II	−30.0	30.0	22.0	13.8	10.725	0.150	0.231	−1	3	28
J014516–094517	2.66513	Si III	−30.0	30.0	2.3	0.4	11.997	0.009	0.010	0	1	28
J014516–094517	2.66513	Si IV	−30.0	30.0	3.3	1.5	11.884	0.035	0.038	0	3	28
J014516–094517	2.66911	Al II	−20.0	20.0	999.0	999.0	10.822	0.176	0.301	−1	3	29
J014516–094517	2.66911	C II	−20.0	20.0	999.0	999.0	11.636	0.176	0.301	−1	3	29
J014516–094517	2.66911	C III	−20.0	20.0	7.6	4.0	11.344	0.120	0.166	−1	3	29
J014516–094517	2.66911	C IV	−20.0	20.0	8.8	5.0	11.559	0.122	0.170	−1	3	29
J014516–094517	2.66911	Fe II	−20.0	20.0	999.0	999.0	12.076	0.176	0.301	−1	3	29
J014516–094517	2.66911	H I	−72.4	27.1	−24.9	0.1	15.412	0.001	0.001	0	3	29
J014516–094517	2.66911	O I	−20.0	20.0	999.0	999.0	12.039	0.176	0.301	−1	3	29
J014516–094517	2.66911	S II	−20.0	20.0	999.0	999.0	12.409	0.176	0.301	−1	3	29
J014516–094517	2.66911	S IV	−20.0	20.0	999.0	999.0	12.164	0.176	0.301	−1	3	29
J014516–094517	2.66911	Si II	−20.0	20.0	999.0	999.0	11.769	0.176	0.301	−1	3	29
J014516–094517	2.66911	Si IV	−20.0	20.0	999.0	999.0	11.068	0.176	0.301	−1	3	29
J014516–094517	2.69212	C II	−20.0	20.0	999.0	999.0	11.623	0.176	0.301	−1	3	30
J014516–094517	2.69212	C III	−20.0	20.0	999.0	999.0	11.167	0.176	0.301	−1	3	30
J014516–094517	2.69212	C IV	−20.0	20.0	999.0	999.0	11.416	0.176	0.301	−1	3	30
J014516–094517	2.69212	Fe II	−20.0	20.0	999.0	999.0	11.934	0.176	0.301	−1	3	30
J014516–094517	2.69212	H I	−57.0	2.0	−28.7	0.1	15.395	0.001	0.001	0	3	30
J014516–094517	2.69212	N V	−20.0	20.0	−3.5	4.0	11.936	0.136	0.199	−1	3	30
J014516–094517	2.69212	S II	−20.0	20.0	999.0	999.0	12.916	0.176	0.301	−1	3	30
J014516–094517	2.69212	Si II	−20.0	20.0	999.0	999.0	10.561	0.176	0.301	−1	3	30
J014516–094517	2.69212	Si IV	−20.0	20.0	999.0	999.0	11.049	0.176	0.301	−1	3	30
J014516–094517	2.69430	C II	−20.0	20.0	999.0	999.0	11.670	0.176	0.301	−1	3	31
J014516–094517	2.69430	C IV	−20.0	20.0	−2.1	1.2	12.027	0.042	0.046	0	3	31
J014516–094517	2.69430	Fe II	−20.0	20.0	999.0	999.0	11.944	0.176	0.301	−1	3	31
J014516–094517	2.69430	H I	−52.0	39.7	−4.1	0.1	14.708	0.001	0.003	0	3	31
J014516–094517	2.69430	N V	−20.0	20.0	999.0	999.0	11.458	0.176	0.301	−1	3	31
J014516–094517	2.69430	O I	−20.0	20.0	999.0	999.0	12.066	0.176	0.301	−1	3	31
J014516–094517	2.69430	S II	−20.0	20.0	999.0	999.0	12.417	0.176	0.301	−1	3	31
J014516–094517	2.69430	Si II	−20.0	20.0	999.0	999.0	10.556	0.176	0.301	−1	3	31
J014516–094517	2.69430	Si IV	−20.0	20.0	999.0	999.0	11.033	0.176	0.301	−1	3	31
J014516–094517	2.70685	C II	−35.0	20.0	999.0	999.0	11.701	0.176	0.301	−1	3	32
J014516–094517	2.70685	C III	−35.0	20.0	−7.0	0.2	12.781	0.006	0.006	0	1	32
J014516–094517	2.70685	C IV	−35.0	20.0	−10.6	0.2	12.913	0.006	0.006	0	3	32
J014516–094517	2.70685	Fe II	−35.0	20.0	999.0	999.0	12.080	0.176	0.301	−1	3	32

Table 2 continued

Table 2 (*continued*)

Target	z_{abs}	Ion	v_1	v_2	v	σ_v	$\log N$	$\sigma_{\log N}^1$	$\sigma_{\log N}^2$	Detection	Reliability	Unique
			(km s $^{-1}$)	(km s $^{-1}$)	(km s $^{-1}$)	[cm $^{-2}$]	Flag	Flag	ID			
J014516–094517	2.70685	Fe III	−35.0	20.0	999.0	999.0	12.174	0.176	0.301	−1	3	32
J014516–094517	2.70685	H I	−55.0	47.0	−8.4	0.1	15.097	0.001	0.001	0	3	32
J014516–094517	2.70685	N I	−35.0	20.0	14.8	12.1	12.544	0.160	0.256	0	2	32
J014516–094517	2.70685	N II	−35.0	20.0	999.0	999.0	11.961	0.176	0.301	−1	3	32
J014516–094517	2.70685	N III	−35.0	20.0	999.0	999.0	11.979	0.176	0.301	−1	3	32
J014516–094517	2.70685	N V	−35.0	20.0	−7.9	5.3	11.651	0.125	0.176	0	2	32
J014516–094517	2.70685	O I	−35.0	20.0	999.0	999.0	12.924	0.176	0.301	−1	3	32
J014516–094517	2.70685	O VI	−35.0	20.0	−11.6	0.2	13.524	0.004	0.004	0	3	32
J014516–094517	2.70685	S II	−35.0	20.0	999.0	999.0	12.521	0.176	0.301	−1	3	32
J014516–094517	2.70685	Si II	−35.0	20.0	999.0	999.0	10.759	0.176	0.301	−1	3	32
J014516–094517	2.70685	Si III	−35.0	20.0	−6.5	5.2	10.768	0.122	0.171	−1	3	32
J014516–094517	2.70685	Si IV	−35.0	20.0	999.0	999.0	11.071	0.176	0.301	−1	3	32
J015741–010629	3.36274	C II	−20.0	20.0	999.0	999.0	12.464	0.176	0.301	−1	3	33
J015741–010629	3.36274	Fe III	−20.0	20.0	999.0	999.0	12.849	0.176	0.301	−1	3	33
J015741–010629	3.36274	H I	−57.0	46.0	−12.1	1.0	15.145	0.013	0.016	0	2	33
J015741–010629	3.36274	O I	−20.0	20.0	999.0	999.0	12.622	0.176	0.301	−1	3	33
J015741–010629	3.36274	Si II	−20.0	20.0	999.0	999.0	11.234	0.176	0.301	−1	3	33
J015741–010629	3.36274	Si IV	−20.0	20.0	999.0	999.0	11.886	0.176	0.301	−1	3	33
J020950–000506	2.41125	Al II	−10.0	29.0	999.0	999.0	10.679	0.176	0.301	−1	3	34
J020950–000506	2.41125	Al III	−10.0	29.0	999.0	999.0	11.657	0.176	0.301	−1	3	34
J020950–000506	2.41125	Fe II	−10.0	29.0	999.0	999.0	11.574	0.176	0.301	−1	3	34
J020950–000506	2.41125	H I	−90.9	73.8	−17.5	0.3	15.009	0.006	0.006	0	3	34
J020950–000506	2.41125	O I	−10.0	29.0	999.0	999.0	13.393	0.176	0.301	−1	3	34
J020950–000506	2.41125	Si II	−10.0	29.0	999.0	999.0	10.954	0.176	0.301	−1	3	34
J020950–000506	2.41125	Si IV	−10.0	29.0	999.0	999.0	10.920	0.176	0.301	−1	3	34
J020950–000506	2.41125	Zn II	−10.0	29.0	999.0	999.0	11.745	0.176	0.301	−1	3	34
J020950–000506	2.57449	Al II	−18.0	30.0	−3.9	1.4	11.391	0.035	0.038	0	1	35
J020950–000506	2.57449	Al III	−18.0	30.0	999.0	999.0	11.432	0.176	0.301	−1	3	35
J020950–000506	2.57449	C II	−18.0	30.0	5.1	0.2	13.147	0.007	0.007	0	1	35
J020950–000506	2.57449	C IV	−18.0	30.0	1.9	0.1	13.863	0.003	0.003	0	3	35
J020950–000506	2.57449	Fe II	−18.0	30.0	999.0	999.0	11.593	0.176	0.301	−1	3	35
J020950–000506	2.57449	H I	−32.2	29.7	4.1	0.2	16.777	0.002	0.004	0	3	35
J020950–000506	2.57449	O VI	−18.0	30.0	4.0	0.2	13.792	0.005	0.005	0	3	35
J020950–000506	2.57449	Si II	−18.0	30.0	4.4	0.7	11.923	0.022	0.023	0	3	35
J020950–000506	2.57449	Si IV	−18.0	30.0	4.4	0.1	13.203	0.003	0.003	0	3	35
J020950–000506	2.57449	Zn II	−18.0	30.0	999.0	999.0	11.725	0.176	0.301	−1	3	35
J020950–000506	2.64137	Al II	−16.0	15.0	999.0	999.0	10.955	0.176	0.301	−1	3	36
J020950–000506	2.64137	C II	−16.0	15.0	999.0	999.0	11.631	0.176	0.301	−1	3	36
J020950–000506	2.64137	C IV	−16.0	15.0	−3.0	0.1	13.578	0.004	0.005	0	3	36
J020950–000506	2.64137	Fe II	−16.0	15.0	999.0	999.0	11.501	0.176	0.301	−1	3	36
J020950–000506	2.64137	H I	−25.6	17.0	−11.2	0.3	15.360	0.003	0.003	0	3	36
J020950–000506	2.64137	N I	−16.0	15.0	999.0	999.0	12.820	0.176	0.301	−1	3	36
J020950–000506	2.64137	O I	−16.0	15.0	999.0	999.0	11.952	0.176	0.301	−1	3	36
J020950–000506	2.64137	Si II	−16.0	15.0	999.0	999.0	10.836	0.176	0.301	−1	3	36
J020950–000506	2.64137	Si III	−16.0	15.0	−2.3	0.8	11.553	0.039	0.042	0	1	36
J020950–000506	2.64137	Si IV	−16.0	15.0	−3.9	0.4	12.252	0.021	0.022	0	3	36
J020950–000506	2.64137	Zn II	−16.0	15.0	999.0	999.0	11.317	0.176	0.301	−1	3	36

Table 2 continued

Table 2 (*continued*)

Target	z_{abs}	Ion	v_1	v_2	v	σ_v	$\log N$	$\sigma_{\log N}^1$	$\sigma_{\log N}^2$	Detection	Reliability	Unique
			(km s $^{-1}$)	(km s $^{-1}$)	(km s $^{-1}$)	[cm $^{-2}$]	Flag	Flag	ID			
J020950-000506	2.76903	Al III	-15.0	15.0	999.0	999.0	11.317	0.176	0.301	-1	3	37
J020950-000506	2.76903	C IV	-15.0	15.0	999.0	999.0	11.508	0.176	0.301	-1	3	37
J020950-000506	2.76903	Fe II	-15.0	15.0	-3.8	3.7	11.651	0.143	0.215	-1	3	37
J020950-000506	2.76903	H I	-33.2	32.1	-1.8	0.1	15.773	0.002	0.002	0	3	37
J020950-000506	2.76903	N I	-15.0	15.0	999.0	999.0	11.756	0.176	0.301	-1	3	37
J020950-000506	2.76903	N II	-15.0	15.0	999.0	999.0	12.158	0.176	0.301	-1	3	37
J020950-000506	2.76903	O I	-15.0	15.0	999.0	999.0	12.176	0.176	0.301	-1	3	37
J020950-000506	2.76903	O VI	-15.0	15.0	1.1	3.8	12.009	0.163	0.264	-1	3	37
J020950-000506	2.76903	S III	-15.0	15.0	999.0	999.0	12.360	0.176	0.301	-1	3	37
J020950-000506	2.76903	Si II	-15.0	15.0	999.0	999.0	10.544	0.176	0.301	-1	3	37
J020950-000506	2.76903	Si III	-15.0	15.0	999.0	999.0	10.597	0.176	0.301	-1	3	37
J020950-000506	2.76903	Si IV	-15.0	15.0	999.0	999.0	11.241	0.176	0.301	-1	3	37
J023359+004938	2.48836	Al II	-15.0	15.0	999.0	999.0	11.586	0.176	0.301	-1	3	38
J023359+004938	2.48836	C II	-15.0	15.0	999.0	999.0	12.706	0.176	0.301	-1	3	38
J023359+004938	2.48836	C III	-15.0	15.0	999.0	999.0	12.220	0.176	0.301	-1	3	38
J023359+004938	2.48836	C IV	-15.0	15.0	999.0	999.0	12.427	0.176	0.301	-1	3	38
J023359+004938	2.48836	Fe II	-15.0	15.0	999.0	999.0	13.116	0.176	0.301	-1	3	38
J023359+004938	2.48836	H I	-68.3	32.4	-14.8	1.2	14.640	0.018	0.020	0	3	38
J023359+004938	2.48836	N I	-15.0	15.0	999.0	999.0	13.129	0.176	0.301	-1	3	38
J023359+004938	2.48836	N II	-15.0	15.0	999.0	999.0	12.902	0.176	0.301	-1	3	38
J023359+004938	2.48836	O I	-15.0	15.0	999.0	999.0	13.137	0.176	0.301	-1	3	38
J023359+004938	2.48836	O VI	-15.0	15.0	999.0	999.0	12.870	0.176	0.301	-1	3	38
J023359+004938	2.48836	S II	-15.0	15.0	999.0	999.0	13.532	0.176	0.301	-1	3	38
J023359+004938	2.48836	S IV	-15.0	15.0	999.0	999.0	13.318	0.176	0.301	-1	3	38
J023359+004938	2.48836	Si II	-15.0	15.0	999.0	999.0	11.662	0.176	0.301	-1	3	38
J023359+004938	2.48836	Si III	-15.0	15.0	999.0	999.0	11.447	0.176	0.301	-1	3	38
J023359+004938	2.48836	Si IV	-15.0	15.0	999.0	999.0	12.121	0.176	0.301	-1	3	38
J025905+001121	3.08204	C II	-15.0	15.0	999.0	999.0	11.813	0.176	0.301	-1	3	39
J025905+001121	3.08204	C IV	-15.0	15.0	999.0	999.0	11.923	0.176	0.301	-1	3	39
J025905+001121	3.08204	Fe II	-15.0	15.0	999.0	999.0	12.231	0.176	0.301	-1	3	39
J025905+001121	3.08204	H I	-15.0	15.0	0.0	2.0	17.500	0.250	0.250	0	3	39
J025905+001121	3.08204	O I	-15.0	15.0	999.0	999.0	11.715	0.176	0.301	-1	3	39
J025905+001121	3.08204	O VI	-15.0	15.0	2.9	2.7	12.660	0.112	0.151	-1	3	39
J025905+001121	3.08204	Si II	-15.0	15.0	999.0	999.0	11.569	0.176	0.301	-1	3	39
J025905+001121	3.08204	Si III	-15.0	15.0	-0.4	0.7	11.837	0.030	0.033	-1	3	39
J025905+001121	3.08204	Si IV	-15.0	15.0	999.0	999.0	11.394	0.176	0.301	-1	3	39
J025905+001121	3.08465	C II	-57.0	20.0	-5.7	1.9	12.888	0.029	0.031	0	1	40
J025905+001121	3.08465	C IV	-57.0	20.0	-16.6	0.3	13.650	0.006	0.006	0	3	40
J025905+001121	3.08465	Fe II	-57.0	20.0	999.0	999.0	12.423	0.176	0.301	-1	3	40
J025905+001121	3.08465	H I	-57.0	20.0	-22.5	2.5	17.250	0.250	0.250	0	3	40
J025905+001121	3.08465	O I	-57.0	20.0	-22.5	2.5	12.633	0.046	0.051	-1	3	40
J025905+001121	3.08465	Si II	-57.0	20.0	999.0	999.0	11.971	0.176	0.301	-1	3	40
J025905+001121	3.08465	Si III	-57.0	20.0	-15.2	1.6	13.453	0.030	0.032	0	1	40
J025905+001121	3.08465	Si IV	-57.0	20.0	-19.8	0.3	13.108	0.006	0.006	0	3	40
J025905+001121	3.12722	C II	-15.0	15.0	999.0	999.0	11.726	0.176	0.301	-1	3	41
J025905+001121	3.12722	C III	-15.0	15.0	4.1	1.7	12.248	0.071	0.086	-1	3	41
J025905+001121	3.12722	C IV	-15.0	15.0	-8.5	3.9	11.792	0.115	0.156	-1	3	41

Table 2 continued

Table 2 (*continued*)

Target	z_{abs}	Ion	v_1	v_2	v	σ_v	$\log N$	$\sigma_{\log N}^1$	$\sigma_{\log N}^2$	Detection	Reliability	Unique
			(km s $^{-1}$)	(km s $^{-1}$)	(km s $^{-1}$)	[cm $^{-2}$]	Flag	Flag	ID			
J025905+001121	3.12722	Fe II	-15.0	15.0	999.0	999.0	12.195	0.176	0.301	-1	3	41
J025905+001121	3.12722	H I	-56.2	35.7	-11.1	0.7	15.035	0.009	0.008	0	3	41
J025905+001121	3.12722	O I	-15.0	15.0	999.0	999.0	12.202	0.176	0.301	-1	3	41
J025905+001121	3.12722	Si II	-15.0	15.0	999.0	999.0	11.780	0.176	0.301	-1	3	41
J025905+001121	3.12722	Si III	-15.0	15.0	999.0	999.0	10.948	0.176	0.301	-1	3	41
J025905+001121	3.12722	Si IV	-15.0	15.0	999.0	999.0	11.196	0.176	0.301	-1	3	41
J025905+001121	3.22368	C III	-15.0	15.0	5.2	2.6	12.067	0.096	0.123	-1	3	42
J025905+001121	3.22368	C IV	-15.0	15.0	4.7	4.6	11.822	0.142	0.212	-1	3	42
J025905+001121	3.22368	H I	-47.7	29.3	-10.8	0.5	15.113	0.005	0.005	0	3	42
J025905+001121	3.22368	O I	-15.0	15.0	999.0	999.0	12.195	0.176	0.301	-1	3	42
J025905+001121	3.22368	O VI	-15.0	15.0	12.7	4.7	12.622	0.119	0.165	-1	3	42
J025905+001121	3.22368	Si II	-15.0	15.0	999.0	999.0	10.381	0.176	0.301	-1	3	42
J025905+001121	3.22368	Si IV	-15.0	15.0	999.0	999.0	11.331	0.176	0.301	-1	3	42
J025905+001121	3.30796	C II	-45.0	25.0	999.0	999.0	11.964	0.176	0.301	-1	3	43
J025905+001121	3.30796	C III	-45.0	25.0	-5.7	0.4	13.519	0.013	0.014	0	1	43
J025905+001121	3.30796	C IV	-59.4	28.7	-4.9	0.6	13.236	0.012	0.012	0	3	43
J025905+001121	3.30796	H I	-56.3	18.8	-8.8	0.9	15.744	0.012	0.011	0	3	43
J025905+001121	3.30796	O I	-45.0	25.0	999.0	999.0	12.594	0.176	0.301	-1	3	43
J025905+001121	3.30796	Si II	-45.0	25.0	999.0	999.0	11.931	0.176	0.301	-1	3	43
J025905+001121	3.30796	Si IV	-45.0	25.0	-6.9	1.5	12.277	0.032	0.035	0	3	43
J030341-002321	2.44326	Al II	-22.0	20.0	-0.3	0.7	11.855	0.026	0.028	0	1	44
J030341-002321	2.44326	Al III	-22.0	20.0	0.8	4.6	11.419	0.136	0.198	0	2	44
J030341-002321	2.44326	C II	-22.0	20.0	-1.3	0.2	14.108	0.011	0.012	0	1	44
J030341-002321	2.44326	C IV	-22.0	20.0	-5.7	0.4	13.091	0.012	0.012	0	3	44
J030341-002321	2.44326	Fe II	-22.0	20.0	-0.2	1.5	13.088	0.050	0.056	0	1	44
J030341-002321	2.44326	H I	-719.4	399.6	-4.2	1.1	19.866	0.010	0.010	0	3	44
J030341-002321	2.44326	O I	-22.0	20.0	2.4	0.2	14.530	0.014	0.014	0	1	44
J030341-002321	2.44326	Si II	-22.0	20.0	1.6	0.2	13.331	0.008	0.008	0	3	44
J030341-002321	2.44326	Si IV	-22.0	20.0	-6.4	1.6	12.278	0.048	0.054	0	1	44
J030341-002321	2.93700	C II	-15.0	15.0	-0.7	3.6	11.996	0.144	0.217	-1	3	45
J030341-002321	2.93700	C III	-15.0	15.0	999.0	999.0	11.642	0.176	0.301	-1	3	45
J030341-002321	2.93700	C IV	-15.0	15.0	999.0	999.0	12.091	0.176	0.301	-1	3	45
J030341-002321	2.93700	Fe II	-15.0	15.0	999.0	999.0	12.335	0.176	0.301	-1	3	45
J030341-002321	2.93700	Fe III	-15.0	15.0	999.0	999.0	12.555	0.176	0.301	-1	3	45
J030341-002321	2.93700	H I	-76.2	43.2	-17.4	0.6	15.648	0.006	0.006	0	2	45
J030341-002321	2.93700	O I	-15.0	15.0	999.0	999.0	12.164	0.176	0.301	-1	3	45
J030341-002321	2.93700	S VI	-15.0	15.0	999.0	999.0	12.081	0.176	0.301	-1	3	45
J030341-002321	2.93700	Si II	-15.0	15.0	999.0	999.0	11.551	0.176	0.301	-1	3	45
J030341-002321	2.93700	Si IV	-15.0	15.0	999.0	999.0	11.525	0.176	0.301	-1	3	45
J030341-002321	2.94069	C II	-23.0	26.0	6.8	0.1	14.070	0.005	0.005	0	1	46
J030341-002321	2.94069	C IV	-23.0	26.0	-0.1	0.2	13.931	0.007	0.007	0	3	46
J030341-002321	2.94069	Fe II	-23.0	26.0	999.0	999.0	12.486	0.176	0.301	-1	3	46
J030341-002321	2.94069	H I	-23.0	26.0	7.5	1.0	18.650	0.150	0.300	0	3	46
J030341-002321	2.94069	O I	-23.0	26.0	7.5	1.0	13.163	0.028	0.030	0	1	46
J030341-002321	2.94069	Si II	-23.0	26.0	6.6	0.1	13.160	0.009	0.009	0	3	46
J030341-002321	2.94069	Si IV	-22.0	26.0	2.8	0.3	13.875	0.003	0.003	0	3	46
J030341-002321	2.95653	C II	-40.0	40.0	999.0	999.0	12.263	0.176	0.301	-1	3	47

Table 2 continued

Table 2 (*continued*)

Target	z_{abs}	Ion	v_1	v_2	v	σ_v	$\log N$	$\sigma_{\log N}^1$	$\sigma_{\log N}^2$	Detection	Reliability	Unique
			(km s $^{-1}$)	(km s $^{-1}$)	(km s $^{-1}$)	[cm $^{-2}$]	Flag	Flag	ID			
J030341–002321	2.95653	C IV	−40.0	40.0	−3.6	0.3	13.632	0.007	0.007	0	3	47
J030341–002321	2.95653	H I	−39.2	61.7	−1.7	0.6	16.161	0.010	0.010	0	3	47
J030341–002321	2.95653	O I	−40.0	40.0	999.0	999.0	12.404	0.176	0.301	−1	3	47
J030341–002321	2.95653	Si II	−40.0	40.0	999.0	999.0	12.195	0.176	0.301	−1	3	47
J030341–002321	2.95653	Si III	−40.0	40.0	−2.0	0.8	12.540	0.016	0.017	0	1	47
J030341–002321	2.95653	Si IV	−40.0	40.0	−1.7	1.3	12.689	0.025	0.027	0	3	47
J030341–002321	2.99495	C IV	−79.0	33.2	−18.9	0.8	13.546	0.012	0.012	0	1	48
J030341–002321	2.99495	H I	−66.6	37.5	−13.8	0.4	16.170	0.004	0.004	0	3	48
J030341–002321	2.99495	O I	−68.0	40.0	999.0	999.0	12.571	0.176	0.301	−1	3	48
J030341–002321	2.99495	O VI	−68.0	40.0	−37.5	2.3	13.805	0.028	0.030	0	1	48
J030341–002321	2.99495	S VI	−68.0	40.0	999.0	999.0	12.319	0.176	0.301	−1	3	48
J030341–002321	2.99495	Si III	−68.0	40.0	−6.7	0.7	12.708	0.011	0.011	0	1	48
J030341–002321	2.99495	Si IV	−68.2	34.1	−8.9	2.2	12.452	0.036	0.039	0	3	48
J030341–002321	3.10354	C II	−15.0	15.0	3.9	4.8	12.054	0.165	0.269	−1	3	49
J030341–002321	3.10354	C IV	−15.0	15.0	−3.0	2.9	12.085	0.101	0.132	−1	3	49
J030341–002321	3.10354	H I	−30.0	40.0	−1.4	0.7	15.449	0.010	0.011	0	3	49
J030341–002321	3.10354	O I	−15.0	15.0	999.0	999.0	12.531	0.176	0.301	−1	3	49
J030341–002321	3.10354	Si II	−15.0	15.0	999.0	999.0	10.817	0.176	0.301	−1	3	49
J030341–002321	3.10354	Si III	−15.0	15.0	999.0	999.0	11.000	0.176	0.301	−1	3	49
J030341–002321	3.10354	Si IV	−15.0	15.0	−0.8	3.6	11.647	0.144	0.217	−1	3	49
J030341–002321	3.10937	C II	−15.0	15.0	1.9	2.1	12.329	0.091	0.115	−1	3	50
J030341–002321	3.10937	C III	−15.0	15.0	8.6	5.5	11.715	0.169	0.279	−1	3	50
J030341–002321	3.10937	C IV	−15.0	15.0	999.0	999.0	11.789	0.176	0.301	−1	3	50
J030341–002321	3.10937	H I	−57.3	28.6	−11.5	0.2	14.766	0.005	0.004	0	3	50
J030341–002321	3.10937	O I	−15.0	15.0	999.0	999.0	12.467	0.176	0.301	−1	3	50
J030341–002321	3.10937	O VI	−15.0	15.0	0.9	3.1	12.532	0.114	0.155	−1	3	50
J030341–002321	3.10937	Si II	−15.0	15.0	999.0	999.0	10.841	0.176	0.301	−1	3	50
J030341–002321	3.10937	Si III	−15.0	15.0	999.0	999.0	11.001	0.176	0.301	−1	3	50
J030341–002321	3.10937	Si IV	−15.0	15.0	7.6	5.1	11.501	0.161	0.258	−1	3	50
J030341–002321	3.15168	C II	−15.0	15.0	999.0	999.0	12.078	0.176	0.301	−1	3	51
J030341–002321	3.15168	H I	−38.7	28.5	−3.5	0.2	15.436	0.003	0.004	0	3	51
J030341–002321	3.15168	O I	−15.0	15.0	999.0	999.0	12.481	0.176	0.301	−1	3	51
J030341–002321	3.15168	O VI	−15.0	15.0	−0.3	1.2	12.808	0.062	0.072	−1	3	51
J030341–002321	3.15168	Si II	−15.0	15.0	999.0	999.0	10.882	0.176	0.301	−1	3	51
J030341–002321	3.15168	Si III	−15.0	15.0	2.0	2.1	11.331	0.083	0.103	−1	3	51
J030341–002321	3.15168	Si IV	−15.0	15.0	10.0	5.0	11.643	0.142	0.213	−1	3	51
J033900–013318	3.11542	C II	−50.0	50.0	1.3	1.3	14.744	0.003	0.003	−2	1	52
J033900–013318	3.11542	C IV	−50.0	50.0	−4.8	0.2	13.926	0.004	0.004	0	3	52
J033900–013318	3.11542	Fe II	−50.0	50.0	5.5	2.8	13.359	0.042	0.046	0	1	52
J033900–013318	3.11542	Fe III	−50.0	50.0	2.7	1.8	13.958	0.030	0.032	0	1	52
J033900–013318	3.11542	H I	−510.5	350.1	−28.3	22.3	19.600	0.050	0.050	0	3	52
J033900–013318	3.11542	N II	−50.0	50.0	2.4	1.4	13.825	0.021	0.022	0	1	52
J033900–013318	3.11542	O I	−50.0	50.0	−3.4	0.3	14.667	0.018	0.019	0	3	52
J033900–013318	3.11542	S II	−50.0	50.0	−19.5	12.1	13.303	0.138	0.203	0	2	52
J033900–013318	3.11542	Si II	−50.0	50.0	0.7	0.3	13.957	0.011	0.011	0	3	52
J033900–013318	3.11542	Si IV	−50.0	50.0	−5.1	0.2	13.668	0.006	0.006	0	3	52
J045213–164012	2.39910	Al II	−42.0	30.0	999.0	999.0	10.768	0.176	0.301	−1	3	53

Table 2 continued

Table 2 (*continued*)

Target	z_{abs}	Ion	v_1	v_2	v	σ_v	$\log N$	$\sigma_{\log N}^1$	$\sigma_{\log N}^2$	Detection	Reliability	Unique
			(km s $^{-1}$)	(km s $^{-1}$)	(km s $^{-1}$)	[cm $^{-2}$]	Flag	Flag	ID			
J045213-164012	2.39910	C IV	-42.0	30.0	-4.5	0.3	13.514	0.007	0.007	0	3	53
J045213-164012	2.39910	Fe II	-42.0	30.0	999.0	999.0	12.447	0.176	0.301	-1	3	53
J045213-164012	2.39910	H I	-88.7	53.6	-15.7	0.4	15.161	0.004	0.004	0	3	53
J045213-164012	2.39910	N I	-42.0	30.0	999.0	999.0	12.744	0.176	0.301	-1	3	53
J045213-164012	2.39910	O I	-42.0	30.0	-2.5	4.1	12.697	0.076	0.092	-1	3	53
J045213-164012	2.39910	S VI	-42.0	30.0	999.0	999.0	12.311	0.176	0.301	-1	3	53
J045213-164012	2.39910	Si IV	-42.0	30.0	-3.9	5.0	11.856	0.095	0.122	0	1	53
J045213-164012	2.44044	Al II	-15.0	15.0	999.0	999.0	10.642	0.176	0.301	-1	3	54
J045213-164012	2.44044	C II	-15.0	15.0	999.0	999.0	11.787	0.176	0.301	-1	3	54
J045213-164012	2.44044	C IV	-15.0	15.0	999.0	999.0	11.770	0.176	0.301	-1	3	54
J045213-164012	2.44044	Fe II	-15.0	15.0	999.0	999.0	12.253	0.176	0.301	-1	3	54
J045213-164012	2.44044	Fe III	-15.0	15.0	999.0	999.0	12.445	0.176	0.301	-1	3	54
J045213-164012	2.44044	H I	-37.9	57.0	4.0	0.2	14.611	0.004	0.004	0	3	54
J045213-164012	2.44044	O I	-15.0	15.0	999.0	999.0	12.723	0.176	0.301	-1	3	54
J045213-164012	2.44044	Si II	-15.0	15.0	999.0	999.0	11.640	0.176	0.301	-1	3	54
J045213-164012	2.44044	Si IV	-15.0	15.0	999.0	999.0	11.245	0.176	0.301	-1	3	54
J045213-164012	2.53542	Al II	-15.0	15.0	999.0	999.0	10.855	0.176	0.301	-1	3	55
J045213-164012	2.53542	C II	-15.0	15.0	-7.9	4.6	12.058	0.133	0.193	-1	3	55
J045213-164012	2.53542	C III	-15.0	15.0	10.4	3.6	11.670	0.134	0.195	-1	3	55
J045213-164012	2.53542	C IV	-15.0	15.0	999.0	999.0	11.737	0.176	0.301	-1	3	55
J045213-164012	2.53542	Fe II	-15.0	15.0	999.0	999.0	12.036	0.176	0.301	-1	3	55
J045213-164012	2.53542	H I	-65.5	38.0	-14.5	0.2	14.674	0.004	0.002	0	3	55
J045213-164012	2.53542	O I	-15.0	15.0	999.0	999.0	12.218	0.176	0.301	-1	3	55
J045213-164012	2.53542	O VI	-15.0	15.0	-2.5	2.1	12.844	0.084	0.105	-1	3	55
J045213-164012	2.53542	Si II	-15.0	15.0	999.0	999.0	10.567	0.176	0.301	-1	3	55
J045213-164012	2.53542	Si IV	-15.0	15.0	-0.7	3.3	11.483	0.122	0.171	-1	3	55
J064204+675835	2.86842	Al II	-15.0	15.0	2.9	2.6	10.959	0.132	0.191	-1	3	56
J064204+675835	2.86842	C II	-15.0	15.0	999.0	999.0	11.928	0.176	0.301	-1	3	56
J064204+675835	2.86842	C III	-15.0	15.0	8.1	1.4	12.177	0.051	0.058	-1	3	56
J064204+675835	2.86842	C IV	-15.0	15.0	999.0	999.0	11.926	0.176	0.301	-1	3	56
J064204+675835	2.86842	H I	-89.2	71.8	11.6	1.0	15.894	0.008	0.004	0	2	56
J064204+675835	2.86842	O I	-15.0	15.0	-4.7	2.9	12.861	0.127	0.180	-1	3	56
J064204+675835	2.86842	Si II	-15.0	15.0	999.0	999.0	11.824	0.176	0.301	-1	3	56
J064204+675835	2.86842	Si III	-15.0	15.0	7.1	0.9	11.569	0.034	0.036	-1	3	56
J064204+675835	2.86842	Si IV	-15.0	15.0	999.0	999.0	11.370	0.176	0.301	-1	3	56
J064204+675835	2.90469	Al II	-55.0	25.0	-19.5	0.3	12.904	0.008	0.008	0	1	57
J064204+675835	2.90469	C II	-55.0	25.0	-17.3	0.6	14.674	0.015	0.016	-2	1	57
J064204+675835	2.90469	C IV	-55.0	25.0	-14.1	0.1	14.278	0.004	0.004	0	3	57
J064204+675835	2.90469	Fe II	-55.0	25.0	-28.9	1.3	13.598	0.021	0.022	0	1	57
J064204+675835	2.90469	H I	-55.0	25.0	-14.3	4.4	18.420	0.150	0.300	0	3	57
J064204+675835	2.90469	O I	-55.0	25.0	-20.9	0.2	13.985	0.004	0.004	0	1	57
J064204+675835	2.90469	O VI	-55.0	25.0	-14.5	0.1	14.493	0.002	0.002	0	3	57
J064204+675835	2.90469	Si II	-55.0	25.0	-24.9	0.1	14.130	0.010	0.010	0	2	57
J064204+675835	2.90469	Si IV	-55.0	25.0	-14.9	0.2	14.190	0.080	0.080	0	2	57
J064204+675835	3.01338	C II	-15.0	15.0	999.0	999.0	12.141	0.176	0.301	-1	3	58
J064204+675835	3.01338	C IV	-15.0	15.0	5.4	1.4	12.807	0.060	0.070	-1	3	58
J064204+675835	3.01338	Fe II	-15.0	15.0	999.0	999.0	12.314	0.176	0.301	-1	3	58

Table 2 continued

Table 2 (*continued*)

Target	z_{abs}	Ion	v_1	v_2	v	σ_v	$\log N$	$\sigma_{\log N}^1$	$\sigma_{\log N}^2$	Detection	Reliability	Unique
			(km s $^{-1}$)	(km s $^{-1}$)	(km s $^{-1}$)	[cm $^{-2}$]	Flag	Flag	ID			
J064204+675835	3.01338	H I	-51.3	74.5	4.9	0.4	15.819	0.004	0.005	0	2	58
J064204+675835	3.01338	O I	-15.0	15.0	999.0	999.0	12.456	0.176	0.301	-1	3	58
J064204+675835	3.01338	Si II	-15.0	15.0	999.0	999.0	12.025	0.176	0.301	-1	3	58
J064204+675835	3.01338	Si IV	-15.0	15.0	-0.1	2.3	11.656	0.094	0.121	-1	3	58
J064204+675835	3.06746	C II	-15.0	15.0	999.0	999.0	11.496	0.176	0.301	-1	3	59
J064204+675835	3.06746	C IV	-15.0	15.0	999.0	999.0	11.298	0.176	0.301	-1	3	59
J064204+675835	3.06746	H I	-39.8	48.2	0.8	0.1	15.332	0.004	0.008	0	3	59
J064204+675835	3.06746	O I	-15.0	15.0	-9.7	7.4	12.062	0.139	0.205	-1	3	59
J064204+675835	3.06746	Si II	-15.0	15.0	999.0	999.0	11.645	0.176	0.301	-1	3	59
J064204+675835	3.06746	Si IV	-15.0	15.0	999.0	999.0	10.830	0.176	0.301	-1	3	59
J073149+285448	3.42673	Al II	-15.0	15.0	999.0	999.0	11.120	0.176	0.301	-1	3	60
J073149+285448	3.42673	Al III	-15.0	15.0	999.0	999.0	11.871	0.176	0.301	-1	3	60
J073149+285448	3.42673	C II	-15.0	15.0	2.9	3.5	12.418	0.157	0.249	-1	3	60
J073149+285448	3.42673	C IV	-15.0	15.0	999.0	999.0	12.015	0.176	0.301	-1	3	60
J073149+285448	3.42673	Fe II	-15.0	15.0	999.0	999.0	12.412	0.176	0.301	-1	3	60
J073149+285448	3.42673	H I	-50.0	50.0	-11.6	0.4	14.653	0.009	0.007	0	3	60
J073149+285448	3.42673	O I	-15.0	15.0	999.0	999.0	12.419	0.176	0.301	-1	3	60
J073149+285448	3.42673	Si II	-15.0	15.0	999.0	999.0	11.180	0.176	0.301	-1	3	60
J073149+285448	3.42673	Si IV	-15.0	15.0	999.0	999.0	11.705	0.176	0.301	-1	3	60
J074521+473436	2.85216	Al II	-15.0	15.0	999.0	999.0	10.389	0.176	0.301	-1	3	61
J074521+473436	2.85216	C II	-15.0	15.0	999.0	999.0	11.179	0.176	0.301	-1	3	61
J074521+473436	2.85216	C IV	-35.0	35.0	-0.6	1.1	12.270	0.023	0.025	0	1	61
J074521+473436	2.85216	H I	-48.3	49.2	6.1	0.1	14.723	0.004	0.004	0	3	61
J074521+473436	2.85216	Si II	-15.0	15.0	999.0	999.0	11.422	0.176	0.301	-1	3	61
J074521+473436	2.85216	Si IV	-15.0	15.0	999.0	999.0	10.872	0.176	0.301	-1	3	61
J074521+473436	2.96558	C II	-50.0	100.0	-22.4	5.2	12.602	0.033	0.036	0	1	62
J074521+473436	2.96558	C IV	-50.0	100.0	-22.9	1.1	12.868	0.007	0.008	0	3	62
J074521+473436	2.96558	Fe II	-50.0	100.0	999.0	999.0	12.004	0.176	0.301	-1	3	62
J074521+473436	2.96558	H I	-40.3	45.4	-0.6	0.1	14.761	0.002	0.004	0	3	62
J074521+473436	2.96558	Si IV	-50.0	100.0	999.0	999.0	11.375	0.176	0.301	-1	3	62
J074521+473436	3.03515	C II	-27.0	40.0	-9.2	11.1	11.657	0.147	0.223	-1	3	63
J074521+473436	3.03515	C IV	-27.0	40.0	1.8	0.3	12.785	0.006	0.006	0	3	63
J074521+473436	3.03515	Fe II	-27.0	40.0	11.8	3.8	12.136	0.079	0.096	-1	3	63
J074521+473436	3.03515	H I	-22.2	64.8	18.1	0.2	16.727	0.014	0.014	0	3	63
J074521+473436	3.03515	O I	-27.0	40.0	999.0	999.0	11.830	0.176	0.301	-1	3	63
J074521+473436	3.03515	O VI	-27.0	40.0	999.0	999.0	12.471	0.176	0.301	-1	3	63
J074521+473436	3.03515	Si II	-27.0	40.0	999.0	999.0	11.627	0.176	0.301	-1	3	63
J074521+473436	3.03515	Si III	-25.0	42.0	10.9	2.8	12.109	0.068	0.080	0	1	63
J074521+473436	3.03515	Si IV	-27.0	40.0	6.7	1.4	11.906	0.030	0.032	0	1	63
J074521+473436	3.05358	C II	-20.0	20.0	999.0	999.0	11.404	0.176	0.301	-1	3	64
J074521+473436	3.05358	C IV	-16.8	18.6	3.9	0.1	12.815	0.100	0.100	0	1	64
J074521+473436	3.05358	Fe II	-20.0	20.0	999.0	999.0	11.705	0.176	0.301	-1	3	64
J074521+473436	3.05358	H I	-59.8	29.6	-14.3	0.6	16.726	0.012	0.013	0	2	64
J074521+473436	3.05358	O I	-20.0	20.0	999.0	999.0	11.922	0.176	0.301	-1	3	64
J074521+473436	3.05358	Si II	-20.0	20.0	0.4	2.1	10.752	0.074	0.089	-1	3	64
J074521+473436	3.12615	C II	-15.0	15.0	999.0	999.0	11.327	0.176	0.301	-1	3	65
J074521+473436	3.12615	C IV	-15.0	15.0	-0.5	0.7	11.939	0.033	0.036	0	3	65

Table 2 continued

Table 2 (*continued*)

Target	z_{abs}	Ion	v_1	v_2	v	σ_v	$\log N$	$\sigma_{\log N}^1$	$\sigma_{\log N}^2$	Detection	Reliability	Unique
			(km s $^{-1}$)	(km s $^{-1}$)	(km s $^{-1}$)	[cm $^{-2}$]	Flag	Flag	ID			
J074521+473436	3.12615	H I	-55.0	27.0	-14.6	0.2	15.076	0.003	0.003	0	3	65
J074521+473436	3.12615	O I	-15.0	15.0	999.0	999.0	11.941	0.176	0.301	-1	3	65
J074521+473436	3.12615	Si II	-15.0	15.0	1.4	3.6	11.666	0.138	0.203	-1	3	65
J074521+473436	3.12615	Si IV	-15.0	15.0	-3.6	3.1	11.328	0.134	0.194	-1	3	65
J074749+443417	4.35301	Al II	-15.0	17.0	999.0	999.0	11.674	0.176	0.301	-1	3	66
J074749+443417	4.35301	C II	-15.0	17.0	999.0	999.0	12.403	0.176	0.301	-1	3	66
J074749+443417	4.35301	C III	-15.0	17.0	3.0	0.5	13.220	0.035	0.038	-1	3	66
J074749+443417	4.35301	C IV	-15.0	17.0	12.1	5.4	12.785	0.147	0.224	-1	3	66
J074749+443417	4.35301	H I	-44.8	39.0	0.2	0.7	15.902	0.011	0.011	0	3	66
J074749+443417	4.35301	O I	-15.0	17.0	2.6	3.9	12.991	0.146	0.222	-1	3	66
J074749+443417	4.35301	O VI	-15.0	17.0	-3.9	1.4	13.101	0.056	0.064	-1	3	66
J074749+443417	4.35301	Si II	-15.0	17.0	999.0	999.0	11.213	0.176	0.301	-1	3	66
J074749+443417	4.35301	Si IV	-15.0	17.0	999.0	999.0	11.856	0.176	0.301	-1	3	66
J080117+521034	3.04028	Al II	-200.0	50.0	-27.0	3.7	12.085	0.018	0.019	0	1	67
J080117+521034	3.04028	C IV	-200.0	50.0	-75.4	0.2	13.968	0.002	0.002	0	3	67
J080117+521034	3.04028	Fe II	-200.0	50.0	-34.0	16.1	12.629	0.078	0.096	0	1	67
J080117+521034	3.04028	H I	-403.5	126.3	-78.4	0.9	19.690	0.150	0.150	0	3	67
J080117+521034	3.04028	N I	-200.0	50.0	999.0	999.0	12.748	0.176	0.301	-1	3	67
J080117+521034	3.04028	O I	-200.0	50.0	-8.5	1.3	13.972	0.006	0.006	0	1	67
J080117+521034	3.04028	O VI	-200.0	50.0	-62.2	1.9	14.545	0.012	0.013	0	1	67
J080117+521034	3.04028	Si II	-200.0	50.0	-35.3	3.2	13.080	0.017	0.017	0	1	67
J080117+521034	3.04028	Si IV	-200.0	50.0	-65.6	0.5	13.481	0.003	0.003	0	3	67
J080117+521034	3.04464	Al II	-15.0	15.0	999.0	999.0	10.580	0.176	0.301	-1	3	68
J080117+521034	3.04464	C II	-15.0	15.0	-13.8	2.2	12.079	0.065	0.076	-1	3	68
J080117+521034	3.04464	C IV	-15.0	15.0	999.0	999.0	11.729	0.176	0.301	-1	3	68
J080117+521034	3.04464	Fe II	-15.0	15.0	999.0	999.0	11.753	0.176	0.301	-1	3	68
J080117+521034	3.04464	H I	-168.0	105.0	-26.3	70.4	19.250	0.250	0.250	0	3	68
J080117+521034	3.04464	N I	-15.0	15.0	999.0	999.0	12.017	0.176	0.301	-1	3	68
J080117+521034	3.04464	O I	-15.0	15.0	999.0	999.0	11.971	0.176	0.301	-1	3	68
J080117+521034	3.04464	O VI	-15.0	15.0	1.5	3.9	12.699	0.150	0.230	-1	3	68
J080117+521034	3.04464	S II	-15.0	15.0	999.0	999.0	12.648	0.176	0.301	-1	3	68
J080117+521034	3.04464	Si II	-15.0	15.0	999.0	999.0	11.205	0.176	0.301	-1	3	68
J080117+521034	3.04464	Si III	-15.0	15.0	-4.9	0.3	11.858	0.013	0.013	-1	3	68
J080117+521034	3.04464	Si IV	-15.0	15.0	999.0	999.0	10.969	0.176	0.301	-1	3	68
J081240+320808	2.58869	Al II	-15.0	15.0	2.0	3.9	10.582	0.155	0.243	-1	3	69
J081240+320808	2.58869	Al III	-15.0	15.0	3.4	2.4	11.478	0.098	0.127	-1	3	69
J081240+320808	2.58869	C II	-15.0	15.0	0.3	4.2	11.801	0.166	0.272	-1	3	69
J081240+320808	2.58869	C IV	-15.0	15.0	999.0	999.0	11.433	0.176	0.301	-1	3	69
J081240+320808	2.58869	Fe II	-15.0	15.0	999.0	999.0	11.890	0.176	0.301	-1	3	69
J081240+320808	2.58869	Fe III	-15.0	15.0	999.0	999.0	12.468	0.176	0.301	-1	3	69
J081240+320808	2.58869	H I	-50.2	30.3	-2.7	4.0	15.931	0.011	0.008	0	2	69
J081240+320808	2.58869	O I	-15.0	15.0	999.0	999.0	12.282	0.176	0.301	-1	3	69
J081240+320808	2.58869	Si II	-15.0	15.0	999.0	999.0	10.720	0.176	0.301	-1	3	69
J081240+320808	2.58869	Si IV	-15.0	15.0	999.0	999.0	11.095	0.176	0.301	-1	3	69
J082107+310751	2.24571	Al II	-15.0	15.0	999.0	999.0	10.711	0.176	0.301	-1	3	70
J082107+310751	2.24571	C IV	-15.0	15.0	-6.2	4.1	11.777	0.124	0.174	-1	3	70
J082107+310751	2.24571	Fe II	-15.0	15.0	-6.0	3.2	12.376	0.126	0.179	-1	3	70

Table 2 continued

Table 2 (*continued*)

Target	z_{abs}	Ion	v_1	v_2	v	σ_v	$\log N$	$\sigma_{\log N}^1$	$\sigma_{\log N}^2$	Detection	Reliability	Unique
			(km s $^{-1}$)	(km s $^{-1}$)	(km s $^{-1}$)	[cm $^{-2}$]	Flag	Flag	ID			
J082107+310751	2.24571	H I	-70.0	70.0	-7.4	0.5	14.861	0.011	0.012	0	2	70
J082107+310751	2.24571	O I	-15.0	15.0	3.2	1.4	12.840	0.059	0.068	-1	3	70
J082107+310751	2.24571	Si II	-15.0	15.0	999.0	999.0	11.784	0.176	0.301	-1	3	70
J082107+310751	2.24571	Si III	-15.0	15.0	-1.8	0.3	12.108	0.015	0.015	-1	3	70
J082107+310751	2.24571	Si IV	-15.0	15.0	999.0	999.0	11.522	0.176	0.301	-1	3	70
J082107+310751	2.55190	Al II	-75.0	5.0	-44.5	5.5	11.286	0.086	0.107	-1	3	71
J082107+310751	2.55190	C II	-75.0	5.0	999.0	999.0	12.108	0.176	0.301	-1	3	71
J082107+310751	2.55190	C IV	-75.0	5.0	-33.7	0.4	13.279	0.008	0.008	0	3	71
J082107+310751	2.55190	Fe II	-75.0	5.0	999.0	999.0	12.369	0.176	0.301	-1	3	71
J082107+310751	2.55190	H I	-80.6	0.9	-41.2	0.4	15.612	0.005	0.005	0	3	71
J082107+310751	2.55190	O I	-75.0	5.0	999.0	999.0	12.527	0.176	0.301	-1	3	71
J082107+310751	2.55190	O VI	-60.0	5.0	-22.4	0.2	13.953	0.005	0.005	0	3	71
J082107+310751	2.55190	Si II	-75.0	5.0	999.0	999.0	10.920	0.176	0.301	-1	3	71
J082107+310751	2.55190	Si III	-75.0	5.0	999.0	999.0	11.356	0.176	0.301	-1	3	71
J082107+310751	2.55190	Si IV	-75.0	5.0	-53.1	7.7	12.049	0.099	0.129	-1	3	71
J082107+310751	2.55652	Al II	-15.0	15.0	999.0	999.0	10.683	0.176	0.301	-1	3	72
J082107+310751	2.55652	C II	-15.0	15.0	999.0	999.0	11.880	0.176	0.301	-1	3	72
J082107+310751	2.55652	C IV	-15.0	15.0	-2.6	3.1	12.126	0.130	0.185	-1	3	72
J082107+310751	2.55652	Fe II	-15.0	15.0	999.0	999.0	12.137	0.176	0.301	-1	3	72
J082107+310751	2.55652	H I	-38.0	22.0	-10.2	0.3	15.177	0.007	0.007	0	3	72
J082107+310751	2.55652	O I	-15.0	15.0	999.0	999.0	12.354	0.176	0.301	-1	3	72
J082107+310751	2.55652	Si II	-15.0	15.0	999.0	999.0	11.886	0.176	0.301	-1	3	72
J082107+310751	2.55652	Si III	-15.0	15.0	999.0	999.0	11.854	0.176	0.301	-1	3	72
J082107+310751	2.55652	Si IV	-15.0	15.0	999.0	999.0	11.532	0.176	0.301	-1	3	72
J083102+335803	2.41864	Al II	-15.0	15.0	999.0	999.0	11.249	0.176	0.301	-1	3	73
J083102+335803	2.41864	C II	-15.0	15.0	999.0	999.0	12.400	0.176	0.301	-1	3	73
J083102+335803	2.41864	C III	-15.0	15.0	3.4	1.4	12.540	0.060	0.070	-1	3	73
J083102+335803	2.41864	C IV	-15.0	15.0	999.0	999.0	12.047	0.176	0.301	-1	3	73
J083102+335803	2.41864	Fe II	-15.0	15.0	999.0	999.0	12.618	0.176	0.301	-1	3	73
J083102+335803	2.41864	H I	-46.1	46.1	-8.0	1.7	15.304	0.016	0.016	0	3	73
J083102+335803	2.41864	O I	-15.0	15.0	2.9	2.8	13.109	0.108	0.144	-1	3	73
J083102+335803	2.41864	O VI	-15.0	15.0	999.0	999.0	12.813	0.176	0.301	-1	3	73
J083102+335803	2.41864	Si II	-15.0	15.0	999.0	999.0	12.274	0.176	0.301	-1	3	73
J083102+335803	2.41864	Si IV	-15.0	15.0	999.0	999.0	11.654	0.176	0.301	-1	3	73
J090033+421546	3.08569	Al II	-50.0	-1.0	999.0	999.0	10.735	0.176	0.301	-1	3	74
J090033+421546	3.08569	C II	-50.0	-1.0	999.0	999.0	11.864	0.176	0.301	-1	3	74
J090033+421546	3.08569	C IV	-50.0	-1.0	-22.1	1.2	12.544	0.033	0.035	0	3	74
J090033+421546	3.08569	H I	-49.5	46.1	-8.0	1.0	14.994	0.006	0.006	0	3	74
J090033+421546	3.08569	O I	-50.0	-1.0	999.0	999.0	13.111	0.176	0.301	-1	3	74
J090033+421546	3.08569	O VI	-50.0	-1.0	-26.9	2.4	13.202	0.069	0.082	0	1	74
J090033+421546	3.08569	Si II	-50.0	-1.0	999.0	999.0	11.750	0.176	0.301	-1	3	74
J090033+421546	3.08569	Si IV	-50.0	-1.0	999.0	999.0	11.294	0.176	0.301	-1	3	74
J090033+421546	3.15992	Al II	-15.0	15.0	999.0	999.0	10.733	0.176	0.301	-1	3	75
J090033+421546	3.15992	C II	-15.0	15.0	999.0	999.0	11.726	0.176	0.301	-1	3	75
J090033+421546	3.15992	C III	-15.0	15.0	2.7	1.4	12.316	0.056	0.065	-1	3	75
J090033+421546	3.15992	C IV	-15.0	15.0	999.0	999.0	11.723	0.176	0.301	-1	3	75
J090033+421546	3.15992	Fe II	-15.0	15.0	999.0	999.0	11.999	0.176	0.301	-1	3	75

Table 2 continued

Table 2 (*continued*)

Target	z_{abs}	Ion	v_1	v_2	v	σ_v	$\log N$	$\sigma_{\log N}^1$	$\sigma_{\log N}^2$	Detection	Reliability	Unique
			(km s $^{-1}$)	(km s $^{-1}$)	(km s $^{-1}$)	[cm $^{-2}$]	Flag	Flag	ID			
J090033+421546	3.15992	H I	-84.6	29.7	-21.5	0.7	15.054	0.007	0.010	0	2	75
J090033+421546	3.15992	O I	-15.0	15.0	0.8	2.3	12.393	0.092	0.117	-1	3	75
J090033+421546	3.15992	O VI	-15.0	15.0	-1.5	1.2	12.838	0.063	0.073	-1	3	75
J090033+421546	3.15992	Si II	-15.0	15.0	999.0	999.0	10.475	0.176	0.301	-1	3	75
J090033+421546	3.15992	Si IV	-15.0	15.0	999.0	999.0	11.367	0.176	0.301	-1	3	75
J093337+284532	3.37217	C II	-15.0	15.0	999.0	999.0	11.877	0.176	0.301	-1	3	76
J093337+284532	3.37217	C III	-15.0	15.0	999.0	999.0	12.269	0.176	0.301	-1	3	76
J093337+284532	3.37217	C IV	-15.0	15.0	999.0	999.0	11.768	0.176	0.301	-1	3	76
J093337+284532	3.37217	H I	-50.5	34.2	-8.3	2.8	15.312	0.022	0.022	0	2	76
J093337+284532	3.37217	O I	-15.0	15.0	-6.2	3.7	12.707	0.121	0.169	-1	3	76
J093337+284532	3.37217	O VI	-15.0	15.0	4.4	2.2	13.032	0.093	0.119	-1	3	76
J093337+284532	3.37217	Si II	-15.0	15.0	999.0	999.0	10.985	0.176	0.301	-1	3	76
J093337+284532	3.37217	Si IV	-15.0	15.0	999.0	999.0	11.425	0.176	0.301	-1	3	76
J093643+292713	2.40065	Al II	-15.0	15.0	999.0	999.0	11.187	0.176	0.301	-1	3	77
J093643+292713	2.40065	C II	-15.0	15.0	999.0	999.0	12.295	0.176	0.301	-1	3	77
J093643+292713	2.40065	C IV	-40.0	130.0	38.8	1.2	14.095	0.016	0.016	0	3	77
J093643+292713	2.40065	Fe II	-15.0	15.0	999.0	999.0	13.449	0.176	0.301	-1	3	77
J093643+292713	2.40065	H I	-83.6	119.4	21.7	10.6	15.852	0.009	0.010	0	2	77
J093643+292713	2.40065	O I	-15.0	15.0	999.0	999.0	12.718	0.176	0.301	-1	3	77
J093643+292713	2.40065	O VI	-40.0	130.0	48.4	2.2	14.609	0.018	0.019	0	3	77
J093643+292713	2.40065	Si II	-15.0	15.0	999.0	999.0	12.345	0.176	0.301	-1	3	77
J093643+292713	2.40065	Si IV	-40.0	130.0	58.8	1.9	12.809	0.015	0.016	0	3	77
J093643+292713	2.41258	Al II	-15.0	15.0	999.0	999.0	11.176	0.176	0.301	-1	3	78
J093643+292713	2.41258	C II	-15.0	15.0	999.0	999.0	12.377	0.176	0.301	-1	3	78
J093643+292713	2.41258	C IV	-15.0	15.0	-0.9	3.1	12.249	0.144	0.217	-1	3	78
J093643+292713	2.41258	Fe II	-15.0	15.0	999.0	999.0	12.535	0.176	0.301	-1	3	78
J093643+292713	2.41258	Fe III	-15.0	15.0	999.0	999.0	12.860	0.176	0.301	-1	3	78
J093643+292713	2.41258	H I	-84.3	74.5	-10.4	4.6	16.169	0.099	0.080	0	2	78
J093643+292713	2.41258	O I	-15.0	15.0	4.1	1.3	13.369	0.060	0.070	-1	3	78
J093643+292713	2.41258	O VI	-15.0	15.0	999.0	999.0	12.902	0.176	0.301	-1	3	78
J093643+292713	2.41258	Si II	-15.0	15.0	999.0	999.0	11.572	0.176	0.301	-1	3	78
J093643+292713	2.41258	Si III	-30.0	10.0	999.0	999.0	11.365	0.176	0.301	-1	3	78
J093643+292713	2.41258	Si IV	-15.0	15.0	999.0	999.0	11.538	0.176	0.301	-1	3	78
J093643+292713	2.54337	C IV	-15.0	15.0	0.8	2.5	12.357	0.101	0.132	-1	3	79
J093643+292713	2.54337	Fe III	-15.0	15.0	999.0	999.0	12.974	0.176	0.301	-1	3	79
J093643+292713	2.54337	H I	-40.0	40.0	3.4	0.9	15.863	0.009	0.009	0	3	79
J093643+292713	2.54337	O I	-15.0	15.0	999.0	999.0	13.664	0.176	0.301	-1	3	79
J093643+292713	2.54337	O VI	-15.0	15.0	999.0	999.0	12.911	0.176	0.301	-1	3	79
J093643+292713	2.54337	Si II	-15.0	15.0	999.0	999.0	11.825	0.180	0.300	-1	3	79
J093643+292713	2.54337	Si III	-15.0	15.0	999.0	999.0	11.279	0.176	0.301	-1	3	79
J093643+292713	2.54337	Si IV	-15.0	15.0	999.0	999.0	12.108	0.176	0.301	-1	3	79
J093643+292713	2.58243	C II	-15.0	15.0	999.0	999.0	11.797	0.176	0.301	-1	3	80
J093643+292713	2.58243	C IV	-15.0	15.0	999.0	999.0	12.154	0.176	0.301	-1	3	80
J093643+292713	2.58243	Fe II	-15.0	15.0	999.0	999.0	12.636	0.176	0.301	-1	3	80
J093643+292713	2.58243	H I	-51.2	17.0	-16.7	0.8	15.152	0.008	0.007	0	3	80
J093643+292713	2.58243	O I	-15.0	15.0	999.0	999.0	13.051	0.176	0.301	-1	3	80
J093643+292713	2.58243	Si II	-15.0	15.0	999.0	999.0	11.430	0.176	0.301	-1	3	80

Table 2 continued

Table 2 (*continued*)

Target	z_{abs}	Ion	v_1	v_2	v	σ_v	$\log N$	$\sigma_{\log N}^1$	$\sigma_{\log N}^2$	Detection	Reliability	Unique
			(km s $^{-1}$)	(km s $^{-1}$)	(km s $^{-1}$)	[cm $^{-2}$]	Flag	Flag	ID			
J093643+292713	2.58243	Si III	-15.0	15.0	-1.7	1.4	11.791	0.067	0.079	-1	3	80
J093643+292713	2.58243	Si IV	-15.0	15.0	999.0	999.0	11.739	0.176	0.301	-1	3	80
J093643+292713	2.59624	C II	23.0	55.0	46.9	4.6	12.181	0.139	0.205	-1	3	81
J093643+292713	2.59624	C III	23.0	55.0	37.3	0.5	13.268	0.038	0.042	0	1	81
J093643+292713	2.59624	C IV	23.0	55.0	37.4	0.6	13.001	0.030	0.032	0	3	81
J093643+292713	2.59624	Fe II	23.0	55.0	999.0	999.0	12.811	0.176	0.301	-1	3	81
J093643+292713	2.59624	H I	-5.0	92.0	37.6	1.1	16.009	0.006	0.008	0	3	81
J093643+292713	2.59624	Si II	23.0	55.0	999.0	999.0	11.355	0.176	0.301	-1	3	81
J093643+292713	2.59624	Si IV	23.0	55.0	39.0	2.8	12.014	0.110	0.148	0	2	81
J093643+292713	2.69883	C III	20.0	60.0	41.3	0.5	13.432	0.061	0.071	0	1	82
J093643+292713	2.69883	C IV	20.0	60.0	39.3	0.7	13.154	0.027	0.029	0	3	82
J093643+292713	2.69883	H I	-22.7	68.2	33.7	0.7	15.620	0.017	0.018	0	3	82
J093643+292713	2.69883	Si II	20.0	60.0	999.0	999.0	11.345	0.176	0.301	-1	3	82
J093643+292713	2.69883	Si III	20.0	60.0	41.9	1.7	11.915	0.064	0.076	0	1	82
J093643+292713	2.69883	Si IV	20.0	60.0	999.0	999.0	11.849	0.176	0.301	-1	3	82
J094202+042244	2.60246	Al II	-15.0	15.0	999.0	999.0	10.787	0.176	0.301	-1	3	83
J094202+042244	2.60246	C II	-15.0	15.0	999.0	999.0	12.283	0.176	0.301	-1	3	83
J094202+042244	2.60246	C IV	-15.0	15.0	999.0	999.0	11.766	0.176	0.301	-1	3	83
J094202+042244	2.60246	Fe II	-15.0	15.0	15.8	10.7	12.463	0.162	0.260	-1	3	83
J094202+042244	2.60246	H I	-63.0	22.7	-14.9	0.5	15.167	0.006	0.007	0	3	83
J094202+042244	2.60246	O I	-15.0	15.0	999.0	999.0	12.507	0.176	0.301	-1	3	83
J094202+042244	2.60246	Si II	-15.0	15.0	1.1	2.9	11.288	0.115	0.157	-1	3	83
J094202+042244	2.60246	Si IV	-15.0	15.0	999.0	999.0	11.655	0.176	0.301	-1	3	83
J094202+042244	2.72833	C III	-35.0	35.0	1.2	0.6	13.788	0.012	0.012	0	1	84
J094202+042244	2.72833	C IV	-35.0	35.0	-1.6	0.3	13.727	0.006	0.006	0	3	84
J094202+042244	2.72833	Fe II	-35.0	35.0	999.0	999.0	12.543	0.176	0.301	-1	3	84
J094202+042244	2.72833	H I	-50.0	50.0	6.9	0.3	14.945	0.005	0.004	0	3	84
J094202+042244	2.72833	N V	-35.0	35.0	999.0	999.0	12.216	0.176	0.301	-1	3	84
J094202+042244	2.72833	O VI	-35.0	35.0	2.4	0.3	14.025	0.006	0.006	0	1	84
J094202+042244	2.72833	Si II	-35.0	35.0	999.0	999.0	12.227	0.176	0.301	-1	3	84
J094202+042244	2.72833	Si III	-35.0	35.0	4.6	1.2	12.198	0.026	0.027	0	1	84
J094202+042244	2.72833	Si IV	-35.0	35.0	-0.3	0.5	12.566	0.011	0.012	0	1	84
J094202+042244	2.72984	C IV	-50.0	32.0	1.6	0.2	14.207	0.005	0.005	0	3	85
J094202+042244	2.72984	Fe II	-50.0	32.0	999.0	999.0	13.332	0.176	0.301	-1	3	85
J094202+042244	2.72984	H I	-29.9	22.6	-0.1	0.2	16.183	0.005	0.006	0	3	85
J094202+042244	2.72984	N V	-50.0	32.0	2.6	0.7	13.563	0.013	0.013	0	1	85
J094202+042244	2.72984	O VI	-50.0	32.0	-3.2	0.2	14.385	0.004	0.004	0	3	85
J094202+042244	2.72984	Si IV	-50.0	32.0	2.5	0.1	13.528	0.002	0.002	0	1	85
J094202+042244	2.73088	C II	-19.0	50.0	7.3	0.2	13.999	0.005	0.005	0	1	86
J094202+042244	2.73088	C IV	-19.0	50.0	11.6	0.3	14.717	0.033	0.035	-2	1	86
J094202+042244	2.73088	Fe II	-19.0	50.0	999.0	999.0	12.495	0.176	0.301	-1	3	86
J094202+042244	2.73088	H I	-44.7	51.3	-1.7	0.4	17.102	0.005	0.005	0	3	86
J094202+042244	2.73088	O I	-19.0	50.0	18.6	5.1	12.913	0.108	0.144	-1	3	86
J094202+042244	2.73088	O VI	-19.0	50.0	13.9	0.2	14.335	0.004	0.004	0	3	86
J094202+042244	2.73088	Si II	-19.0	50.0	8.8	1.8	13.014	0.035	0.038	0	3	86
J094202+042244	2.73088	Si IV	-19.0	50.0	8.5	0.1	14.150	0.004	0.004	-2	1	86
J094202+042244	2.81325	C II	-17.0	18.0	999.0	999.0	12.335	0.176	0.301	-1	3	87

Table 2 continued

Table 2 (*continued*)

Target	z_{abs}	Ion	v_1	v_2	v	σ_v	$\log N$	$\sigma_{\log N}^1$	$\sigma_{\log N}^2$	Detection	Reliability	Unique
			(km s $^{-1}$)	(km s $^{-1}$)	(km s $^{-1}$)	[cm $^{-2}$]	Flag	Flag	ID			
J094202+042244	2.81325	C IV	-17.0	18.0	-1.8	0.3	13.146	0.012	0.013	0	3	87
J094202+042244	2.81325	H I	-25.0	25.0	1.1	0.5	15.226	0.018	0.019	0	3	87
J094202+042244	2.81325	Si II	-17.0	18.0	999.0	999.0	11.997	0.176	0.301	-1	3	87
J094202+042244	2.81325	Si IV	-17.0	18.0	-1.3	1.7	12.482	0.065	0.076	0	1	87
J094202+042244	2.81407	C III	-18.0	16.0	0.4	0.5	13.876	0.051	0.058	-2	1	88
J094202+042244	2.81407	C IV	-18.0	16.0	0.3	0.1	13.508	0.007	0.007	0	3	88
J094202+042244	2.81407	Fe II	-18.0	16.0	999.0	999.0	12.369	0.176	0.301	-1	3	88
J094202+042244	2.81407	H I	-25.0	14.0	-5.1	0.2	15.730	0.011	0.011	0	3	88
J094202+042244	2.81407	Si II	-18.0	16.0	999.0	999.0	12.088	0.176	0.301	-1	3	88
J094202+042244	2.81407	Si III	-18.0	16.0	-0.8	0.1	12.873	0.007	0.007	0	1	88
J094202+042244	2.81407	Si IV	-18.0	16.0	0.0	0.9	12.747	0.047	0.052	0	1	88
J094202+042244	2.81450	C III	-14.0	15.0	-1.7	0.3	13.693	0.026	0.028	-2	1	89
J094202+042244	2.81450	C IV	-14.0	15.0	-2.1	0.1	13.350	0.009	0.009	0	3	89
J094202+042244	2.81450	Fe II	-14.0	15.0	999.0	999.0	12.296	0.176	0.301	-1	3	89
J094202+042244	2.81450	H I	-17.0	17.0	-4.3	0.4	15.242	0.029	0.031	0	3	89
J094202+042244	2.81450	Si II	-14.0	15.0	-6.6	2.9	12.145	0.124	0.175	-1	3	89
J094202+042244	2.81450	Si III	-14.0	15.0	1.4	0.1	12.830	0.006	0.006	0	1	89
J094202+042244	2.81450	Si IV	-14.0	15.0	-2.4	1.1	12.545	0.055	0.063	0	1	89
J094202+042244	2.84851	C IV	-42.5	30.9	-0.9	1.1	12.952	0.023	0.024	0	3	90
J094202+042244	2.84851	Fe II	-50.0	30.0	999.0	999.0	12.637	0.176	0.301	-1	3	90
J094202+042244	2.84851	H I	-66.8	13.1	-6.1	0.5	15.363	0.008	0.008	0	3	90
J094202+042244	2.84851	O I	-50.0	30.0	999.0	999.0	12.903	0.176	0.301	-1	3	90
J094202+042244	2.84851	Si II	-50.0	30.0	999.0	999.0	12.217	0.176	0.301	-1	3	90
J094202+042244	2.84851	Si IV	-50.0	30.0	999.0	999.0	11.592	0.176	0.301	-1	3	90
J094202+042244	3.09385	C II	-15.0	15.0	999.0	999.0	12.139	0.176	0.301	-1	3	91
J094202+042244	3.09385	H I	-79.1	-3.4	-45.6	0.2	15.855	0.001	0.001	0	3	91
J094202+042244	3.09385	Si II	-15.0	15.0	999.0	999.0	10.817	0.176	0.301	-1	3	91
J094202+042244	3.09385	Si III	-15.0	15.0	-1.6	0.9	11.804	0.036	0.040	-1	3	91
J094202+042244	3.09385	Si IV	-15.0	15.0	999.0	999.0	11.420	0.176	0.301	-1	3	91
J095852+120245	3.09623	Al II	-15.0	15.0	999.0	999.0	11.147	0.176	0.301	-1	3	92
J095852+120245	3.09623	C II	-15.0	15.0	999.0	999.0	12.116	0.176	0.301	-1	3	92
J095852+120245	3.09623	C IV	-15.0	15.0	999.0	999.0	11.816	0.176	0.301	-1	3	92
J095852+120245	3.09623	Fe II	-15.0	15.0	999.0	999.0	12.202	0.176	0.301	-1	3	92
J095852+120245	3.09623	Fe III	-15.0	15.0	-1.2	1.8	12.798	0.085	0.106	-1	3	92
J095852+120245	3.09623	H I	-30.7	40.9	2.2	1.8	17.146	0.065	0.047	0	3	92
J095852+120245	3.09623	O I	-15.0	15.0	999.0	999.0	12.156	0.176	0.301	-1	3	92
J095852+120245	3.09623	O VI	-15.0	15.0	999.0	999.0	12.213	0.176	0.301	-1	3	92
J095852+120245	3.09623	Si II	-15.0	15.0	999.0	999.0	11.848	0.176	0.301	-1	3	92
J095852+120245	3.09623	Si III	-15.0	15.0	999.0	999.0	10.977	0.176	0.301	-1	3	92
J095852+120245	3.09623	Si IV	-15.0	15.0	999.0	999.0	11.410	0.176	0.301	-1	3	92
J095852+120245	3.09623	Zn II	-15.0	15.0	999.0	999.0	11.718	0.176	0.301	-1	3	92
J095852+120245	3.09691	Al II	-17.0	38.0	999.0	999.0	11.278	0.176	0.301	-1	3	93
J095852+120245	3.09691	C II	-17.0	38.0	13.3	5.1	12.386	0.107	0.143	-1	3	93
J095852+120245	3.09691	C IV	-19.1	56.6	10.6	2.0	12.805	0.038	0.042	0	1	93
J095852+120245	3.09691	Fe II	-17.0	38.0	999.0	999.0	12.326	0.176	0.301	-1	3	93
J095852+120245	3.09691	H I	-21.0	21.0	-2.3	0.7	16.349	0.033	0.038	0	3	93
J095852+120245	3.09691	O I	-17.0	38.0	999.0	999.0	12.355	0.176	0.301	-1	3	93

Table 2 continued

Table 2 (*continued*)

Target	z_{abs}	Ion	v_1	v_2	v	σ_v	$\log N$	$\sigma_{\log N}^1$	$\sigma_{\log N}^2$	Detection	Reliability	Unique
			(km s $^{-1}$)	(km s $^{-1}$)	(km s $^{-1}$)	[cm $^{-2}$]	Flag	Flag	ID			
J095852+120245	3.09691	O VI	-17.0	38.0	999.0	999.0	12.281	0.176	0.301	-1	3	93
J095852+120245	3.09691	Si II	-17.0	38.0	6.6	8.7	12.025	0.164	0.266	-1	3	93
J095852+120245	3.09691	Si IV	-17.0	38.0	12.9	3.8	11.899	0.080	0.099	0	3	93
J095852+120245	3.09691	Zn II	-17.0	38.0	999.0	999.0	11.943	0.176	0.301	-1	3	93
J095852+120245	3.15768	C II	-15.0	15.0	999.0	999.0	12.256	0.176	0.301	-1	3	94
J095852+120245	3.15768	C IV	-15.0	15.0	999.0	999.0	11.959	0.176	0.301	-1	3	94
J095852+120245	3.15768	Fe II	-15.0	15.0	999.0	999.0	12.454	0.176	0.301	-1	3	94
J095852+120245	3.15768	H I	-73.4	39.2	-13.1	0.2	15.491	0.003	0.002	0	3	94
J095852+120245	3.15768	O I	-15.0	15.0	999.0	999.0	12.351	0.176	0.301	-1	3	94
J095852+120245	3.15768	O VI	-15.0	15.0	999.0	999.0	12.521	0.176	0.301	-1	3	94
J095852+120245	3.15768	Si II	-15.0	15.0	999.0	999.0	10.714	0.176	0.301	-1	3	94
J095852+120245	3.15768	Si III	-15.0	15.0	999.0	999.0	11.276	0.176	0.301	-1	3	94
J095852+120245	3.15768	Si IV	-15.0	15.0	999.0	999.0	11.467	0.176	0.301	-1	3	94
J095852+120245	3.15768	Zn II	-15.0	15.0	999.0	999.0	11.816	0.176	0.301	-1	3	94
J095852+120245	3.22317	Al II	-50.0	25.0	999.0	999.0	11.288	0.176	0.301	-1	3	95
J095852+120245	3.22317	Al III	-50.0	25.0	999.0	999.0	12.209	0.176	0.301	-1	3	95
J095852+120245	3.22317	C II	-50.0	25.0	-6.6	9.1	12.329	0.145	0.219	0	1	95
J095852+120245	3.22317	C IV	-50.0	25.0	-10.8	0.3	13.760	0.007	0.008	0	3	95
J095852+120245	3.22317	H I	-27.6	38.2	2.2	0.1	17.356	0.003	0.003	0	3	95
J095852+120245	3.22317	O I	-50.0	25.0	999.0	999.0	12.574	0.176	0.301	-1	3	95
J095852+120245	3.22317	Si II	-50.0	25.0	-4.4	4.3	11.402	0.074	0.090	0	2	95
J095852+120245	3.22317	Si III	-50.0	25.0	-6.5	0.2	13.080	0.004	0.004	0	1	95
J095852+120245	3.22317	Si IV	-50.0	25.0	-11.6	0.3	13.133	0.007	0.007	0	3	95
J100841+362319	2.76763	Al II	-15.0	15.0	999.0	999.0	10.863	0.176	0.301	-1	3	96
J100841+362319	2.76763	Al III	-15.0	15.0	999.0	999.0	11.602	0.176	0.301	-1	3	96
J100841+362319	2.76763	C III	-15.0	15.0	999.0	999.0	12.258	0.176	0.301	-1	3	96
J100841+362319	2.76763	C IV	-15.0	15.0	-0.5	3.0	11.975	0.136	0.198	-1	3	96
J100841+362319	2.76763	H I	-119.5	58.0	-10.5	0.6	14.948	0.008	0.008	0	3	96
J100841+362319	2.76763	O I	-15.0	15.0	999.0	999.0	13.202	0.176	0.301	-1	3	96
J100841+362319	2.76763	Si II	-15.0	15.0	999.0	999.0	11.954	0.176	0.301	-1	3	96
J100841+362319	2.76763	Si IV	-15.0	15.0	2.3	4.4	11.482	0.165	0.270	-1	3	96
J100841+362319	2.76763	Zn II	-15.0	15.0	999.0	999.0	11.677	0.176	0.301	-1	3	96
J100841+362319	2.94749	Al II	-20.0	45.0	5.1	0.5	12.429	0.013	0.013	0	1	97
J100841+362319	2.94749	Al III	-20.0	45.0	999.0	999.0	11.579	0.176	0.301	-1	3	97
J100841+362319	2.94749	C II	-20.0	45.0	7.3	0.3	14.628	0.018	0.019	-2	2	97
J100841+362319	2.94749	C IV	-20.0	45.0	19.1	0.4	13.482	0.009	0.009	0	3	97
J100841+362319	2.94749	H I	-46.3	84.7	12.9	5.9	19.725	0.002	0.002	0	3	97
J100841+362319	2.94749	O I	-20.0	45.0	3.4	0.4	15.068	0.030	0.033	0	3	97
J100841+362319	2.94749	Si II	-20.0	45.0	4.2	0.3	13.858	0.010	0.010	0	2	97
J100841+362319	2.94749	Si IV	-20.0	45.0	18.5	0.3	13.200	0.008	0.008	0	3	97
J100841+362319	3.01081	Al II	-15.0	15.0	999.0	999.0	10.807	0.176	0.301	-1	3	98
J100841+362319	3.01081	Al III	-15.0	15.0	999.0	999.0	11.436	0.176	0.301	-1	3	98
J100841+362319	3.01081	C II	-15.0	15.0	999.0	999.0	12.153	0.176	0.301	-1	3	98
J100841+362319	3.01081	C IV	-15.0	15.0	999.0	999.0	11.880	0.176	0.301	-1	3	98
J100841+362319	3.01081	Fe II	-15.0	15.0	999.0	999.0	12.308	0.176	0.301	-1	3	98
J100841+362319	3.01081	H I	-67.7	37.1	-17.6	1.2	15.161	0.010	0.010	0	3	98
J100841+362319	3.01081	O I	-15.0	15.0	999.0	999.0	12.507	0.176	0.301	-1	3	98

Table 2 continued

Table 2 (*continued*)

Target	z_{abs}	Ion	v_1	v_2	v	σ_v	$\log N$	$\sigma_{\log N}^1$	$\sigma_{\log N}^2$	Detection	Reliability	Unique
			(km s $^{-1}$)	(km s $^{-1}$)	(km s $^{-1}$)	[cm $^{-2}$]	Flag	Flag	ID			
J100841+362319	3.01081	O VI	-15.0	15.0	-2.9	3.6	12.596	0.131	0.188	-1	3	98
J100841+362319	3.01081	Si II	-15.0	15.0	999.0	999.0	11.026	0.176	0.301	-1	3	98
J100841+362319	3.01081	Si IV	-15.0	15.0	0.3	4.3	11.495	0.172	0.289	-1	3	98
J100841+362319	3.03460	Al II	-50.0	20.0	999.0	999.0	10.983	0.176	0.301	-1	3	99
J100841+362319	3.03460	Al III	-50.0	20.0	999.0	999.0	11.749	0.176	0.301	-1	3	99
J100841+362319	3.03460	C II	-50.0	20.0	999.0	999.0	12.288	0.176	0.301	-1	3	99
J100841+362319	3.03460	C IV	-57.3	20.5	-20.5	2.5	12.646	0.046	0.052	0	3	99
J100841+362319	3.03460	Fe II	-50.0	20.0	999.0	999.0	12.494	0.176	0.301	-1	3	99
J100841+362319	3.03460	H I	-54.3	17.2	-19.1	0.4	15.301	0.006	0.006	0	3	99
J100841+362319	3.03460	O I	-50.0	20.0	999.0	999.0	12.712	0.176	0.301	-1	3	99
J100841+362319	3.03460	O VI	-50.0	20.0	-11.6	0.6	13.578	0.012	0.013	0	3	99
J100841+362319	3.03460	Si II	-50.0	20.0	999.0	999.0	12.485	0.176	0.301	-1	3	99
J100841+362319	3.03460	Si IV	-50.0	20.0	999.0	999.0	11.745	0.176	0.301	-1	3	99
J100841+362319	3.07200	Al II	-70.0	10.0	999.0	999.0	11.111	0.176	0.301	-1	3	100
J100841+362319	3.07200	Al III	-70.0	10.0	999.0	999.0	11.798	0.180	0.300	-1	3	100
J100841+362319	3.07200	C II	-70.0	10.0	999.0	999.0	12.377	0.176	0.301	-1	3	100
J100841+362319	3.07200	C III	-93.2	9.5	-39.3	1.0	13.169	0.017	0.017	0	1	100
J100841+362319	3.07200	C IV	-74.0	13.0	-41.5	1.8	13.052	0.030	0.032	0	3	100
J100841+362319	3.07200	Fe II	-70.0	10.0	999.0	999.0	12.684	0.176	0.301	-1	3	100
J100841+362319	3.07200	H I	-72.0	11.0	-25.8	0.5	15.502	0.009	0.010	0	3	100
J100841+362319	3.07200	O I	-70.0	10.0	-51.7	14.3	12.829	0.159	0.254	-1	3	100
J100841+362319	3.07200	O VI	-70.2	17.6	-39.7	0.9	13.767	0.017	0.017	0	1	100
J100841+362319	3.07200	Si II	-70.0	10.0	999.0	999.0	11.178	0.176	0.301	-1	3	100
J100841+362319	3.07200	Si IV	-70.0	10.0	-45.1	10.2	11.849	0.138	0.203	-1	3	100
J100841+362319	3.10854	Al II	-60.0	5.0	999.0	999.0	11.005	0.176	0.301	-1	3	101
J100841+362319	3.10854	C II	-60.0	5.0	999.0	999.0	12.273	0.176	0.301	-1	3	101
J100841+362319	3.10854	C III	-60.0	5.0	-22.1	0.3	13.284	0.009	0.009	0	1	101
J100841+362319	3.10854	C IV	-60.0	5.0	-25.9	0.5	13.182	0.011	0.011	0	3	101
J100841+362319	3.10854	Fe II	-60.0	5.0	999.0	999.0	12.589	0.176	0.301	-1	3	101
J100841+362319	3.10854	H I	-44.4	11.9	-15.4	0.3	15.356	0.006	0.006	0	3	101
J100841+362319	3.10854	O I	-60.0	5.0	999.0	999.0	12.761	0.176	0.301	-1	3	101
J100841+362319	3.10854	Si II	-60.0	5.0	999.0	999.0	11.290	0.176	0.301	-1	3	101
J100841+362319	3.10854	Si IV	-60.0	5.0	999.0	999.0	11.616	0.176	0.301	-1	3	101
J101155+294141	2.42901	Al II	-50.0	15.0	-15.2	0.3	11.987	0.006	0.006	0	1	102
J101155+294141	2.42901	Al III	-50.0	15.0	-11.4	0.8	12.091	0.017	0.018	0	3	102
J101155+294141	2.42901	C II	-50.0	15.0	-13.7	0.1	13.697	0.003	0.003	0	3	102
J101155+294141	2.42901	C IV	-50.0	15.0	-17.2	0.4	13.749	0.009	0.010	0	3	102
J101155+294141	2.42901	H I	-50.0	14.0	-17.2	0.4	17.750	0.150	0.150	0	3	102
J101155+294141	2.42901	O I	-50.0	14.0	999.0	999.0	12.100	0.176	0.301	-1	3	102
J101155+294141	2.42901	Si II	-50.0	15.0	-12.1	0.1	12.713	0.003	0.003	0	3	102
J101155+294141	2.42901	Si III	-50.0	15.0	-16.1	0.4	13.575	0.012	0.012	0	1	102
J101155+294141	2.42901	Si IV	-50.0	15.0	-16.9	0.1	13.627	0.002	0.002	0	1	102
J101155+294141	2.42901	Zn II	-50.0	15.0	999.0	999.0	11.193	0.176	0.301	-1	3	102
J101155+294141	2.50364	Al II	-20.0	20.0	-1.3	1.6	10.829	0.057	0.066	0	1	103
J101155+294141	2.50364	Al III	-20.0	20.0	999.0	999.0	10.979	0.176	0.301	-1	3	103
J101155+294141	2.50364	C II	-20.0	20.0	0.2	0.4	12.723	0.017	0.017	0	1	103
J101155+294141	2.50364	C III	-20.0	20.0	0.2	0.1	13.862	0.016	0.016	-2	1	103

Table 2 continued

Table 2 (*continued*)

Target	z_{abs}	Ion	v_1	v_2	v	σ_v	$\log N$	$\sigma_{\log N}^1$	$\sigma_{\log N}^2$	Detection	Reliability	Unique
			(km s $^{-1}$)	(km s $^{-1}$)	(km s $^{-1}$)	[cm $^{-2}$]	Flag	Flag	ID			
J101155+294141	2.50364	C IV	-20.0	20.0	-1.7	0.1	12.998	0.005	0.005	0	3	103
J101155+294141	2.50364	Fe II	-20.0	20.0	999.0	999.0	11.782	0.176	0.301	-1	3	103
J101155+294141	2.50364	H I	-20.5	17.0	-0.8	0.1	17.355	0.001	0.001	0	3	103
J101155+294141	2.50364	Si II	-20.0	20.0	-2.6	4.5	11.629	0.146	0.221	0	1	103
J101155+294141	2.50364	Si III	-20.0	20.0	1.1	0.0	12.977	0.003	0.003	0	1	103
J101155+294141	2.50364	Si IV	-20.0	20.0	-1.3	0.1	12.636	0.004	0.004	0	3	103
J101447+430030	2.84090	Al II	-30.0	20.0	2.0	5.2	10.986	0.119	0.164	-1	3	104
J101447+430030	2.84090	C II	-30.0	20.0	999.0	999.0	11.870	0.176	0.301	-1	3	104
J101447+430030	2.84090	C IV	-30.0	20.0	-8.9	1.4	12.448	0.040	0.044	0	3	104
J101447+430030	2.84090	Fe II	-30.0	20.0	999.0	999.0	12.324	0.176	0.301	-1	3	104
J101447+430030	2.84090	H I	-49.6	28.6	-16.7	0.2	15.316	0.003	0.003	0	3	104
J101447+430030	2.84090	O VI	-30.0	20.0	-5.8	0.6	13.389	0.018	0.019	0	1	104
J101447+430030	2.84090	Si II	-30.0	20.0	999.0	999.0	11.928	0.176	0.301	-1	3	104
J101447+430030	2.84090	Si IV	-30.0	20.0	999.0	999.0	11.406	0.176	0.301	-1	3	104
J101447+430030	2.98705	Al II	-45.0	1.0	999.0	999.0	10.858	0.176	0.301	-1	3	105
J101447+430030	2.98705	C II	-45.0	1.0	999.0	999.0	12.007	0.176	0.301	-1	3	105
J101447+430030	2.98705	C III	-45.0	1.0	-26.8	1.0	12.363	0.029	0.031	-1	3	105
J101447+430030	2.98705	C IV	-45.0	1.0	-26.2	1.3	12.521	0.036	0.039	0	3	105
J101447+430030	2.98705	Fe II	-45.0	1.0	999.0	999.0	12.315	0.176	0.301	-1	3	105
J101447+430030	2.98705	H I	-79.0	24.0	-20.0	0.3	15.188	0.002	0.002	0	3	105
J101447+430030	2.98705	Si II	-45.0	1.0	-32.7	4.3	11.308	0.098	0.126	-1	3	105
J101447+430030	2.98705	Si IV	-45.0	1.0	999.0	999.0	11.358	0.176	0.301	-1	3	105
J101447+430030	3.01439	C II	-43.0	37.0	-38.5	2.8	12.885	0.029	0.031	-1	3	106
J101447+430030	3.01439	C IV	-43.0	37.0	-5.1	0.3	13.425	0.006	0.006	0	3	106
J101447+430030	3.01439	Fe II	-43.0	37.0	999.0	999.0	12.511	0.176	0.301	-1	3	106
J101447+430030	3.01439	Fe III	-43.0	37.0	999.0	999.0	12.496	0.176	0.301	-1	3	106
J101447+430030	3.01439	H I	-42.6	39.6	-2.0	0.2	16.681	0.004	0.002	0	3	106
J101447+430030	3.01439	O I	-43.0	37.0	999.0	999.0	12.500	0.176	0.301	-1	3	106
J101447+430030	3.01439	O VI	-43.0	37.0	-0.5	0.1	14.388	0.002	0.002	0	3	106
J101447+430030	3.01439	Si II	-43.0	37.0	999.0	999.0	10.980	0.176	0.301	-1	3	106
J101447+430030	3.01439	Si IV	-43.0	37.0	999.0	999.0	11.500	0.176	0.301	-1	3	106
J101447+430030	3.11460	C II	-30.0	5.0	999.0	999.0	12.134	0.176	0.301	-1	3	107
J101447+430030	3.11460	C IV	-30.0	5.0	-12.0	0.3	12.878	0.012	0.012	0	3	107
J101447+430030	3.11460	Fe II	-30.0	5.0	999.0	999.0	12.336	0.176	0.301	-1	3	107
J101447+430030	3.11460	H I	-50.7	22.0	-12.9	0.1	15.974	0.001	0.001	0	3	107
J101447+430030	3.11460	O I	-30.0	5.0	999.0	999.0	12.264	0.176	0.301	-1	3	107
J101447+430030	3.11460	O VI	-30.0	5.0	-8.8	0.6	12.980	0.022	0.024	-1	3	107
J101447+430030	3.11460	Si II	-30.0	5.0	999.0	999.0	10.970	0.176	0.301	-1	3	107
J101447+430030	3.11460	Si III	-20.5	1.1	-11.1	0.1	12.180	0.010	0.010	0	1	107
J101447+430030	3.11460	Si IV	-30.0	5.0	-11.7	0.9	12.090	0.037	0.040	0	3	107
J101723-204658	2.45051	Al II	-25.0	30.0	-1.6	3.0	11.178	0.076	0.092	0	1	108
J101723-204658	2.45051	C II	-25.0	30.0	-2.2	0.7	12.985	0.018	0.018	0	3	108
J101723-204658	2.45051	C IV	-25.0	30.0	0.1	0.3	13.176	0.010	0.010	0	3	108
J101723-204658	2.45051	Fe II	-25.0	30.0	999.0	999.0	12.189	0.176	0.301	-1	3	108
J101723-204658	2.45051	H I	-45.2	48.3	-0.6	1.0	17.284	0.200	0.014	0	3	108
J101723-204658	2.45051	O I	-25.0	30.0	999.0	999.0	12.367	0.176	0.301	-1	3	108
J101723-204658	2.45051	Si II	-25.0	30.0	-4.0	1.3	11.721	0.033	0.036	0	2	108

Table 2 continued

Table 2 (*continued*)

Target	z_{abs}	Ion	v_1	v_2	v	σ_v	$\log N$	$\sigma_{\log N}^1$	$\sigma_{\log N}^2$	Detection	Reliability	Unique
			(km s $^{-1}$)	(km s $^{-1}$)	(km s $^{-1}$)	[cm $^{-2}$]	Flag	Flag	ID			
J101723–204658	2.45051	Si III	−25.0	30.0	4.5	0.7	13.334	0.026	0.028	−2	1	108
J101723–204658	2.45051	Si IV	−25.0	30.0	3.9	0.2	12.942	0.007	0.007	0	3	108
J102009+104002	3.05421	C II	−25.0	32.0	999.0	999.0	12.229	0.176	0.301	−1	3	109
J102009+104002	3.05421	C IV	−25.0	32.0	17.6	1.0	12.856	0.021	0.022	0	1	109
J102009+104002	3.05421	Fe II	−25.0	32.0	999.0	999.0	12.376	0.176	0.301	−1	3	109
J102009+104002	3.05421	H I	−50.6	33.2	−2.8	0.6	17.268	0.015	0.016	0	3	109
J102009+104002	3.05421	O I	−25.0	32.0	999.0	999.0	12.566	0.176	0.301	−1	3	109
J102009+104002	3.05421	Si II	−25.0	32.0	999.0	999.0	12.373	0.176	0.301	−1	3	109
J102009+104002	3.05421	Si III	−25.0	32.0	11.4	0.1	12.973	0.005	0.005	0	1	109
J102009+104002	3.05421	Si IV	−25.0	32.0	12.3	0.7	12.596	0.017	0.018	0	3	109
J102009+104002	3.05498	C II	−24.0	25.0	−2.2	3.1	12.564	0.085	0.106	0	1	110
J102009+104002	3.05498	C IV	−24.0	25.0	−1.6	0.5	13.090	0.014	0.015	0	3	110
J102009+104002	3.05498	Fe II	−24.0	25.0	999.0	999.0	12.442	0.176	0.301	−1	3	110
J102009+104002	3.05498	H I	−20.9	21.8	6.2	0.2	16.330	0.039	0.043	0	3	110
J102009+104002	3.05498	O I	−24.0	25.0	999.0	999.0	12.540	0.176	0.301	−1	3	110
J102009+104002	3.05498	Si II	−24.0	25.0	−16.1	10.4	12.589	0.161	0.258	−1	3	110
J102009+104002	3.05498	Si III	−24.0	25.0	−2.5	0.1	13.013	0.005	0.005	0	1	110
J102009+104002	3.05498	Si IV	−24.0	25.0	−3.5	0.4	12.743	0.013	0.013	0	3	110
J104018+572448	3.26628	C II	−25.0	35.0	6.1	0.7	14.021	0.025	0.027	0	1	111
J104018+572448	3.26628	C IV	−25.0	35.0	−5.1	1.8	13.205	0.035	0.038	0	3	111
J104018+572448	3.26628	H I	−61.5	78.5	2.9	17.8	18.600	0.200	0.200	0	3	111
J104018+572448	3.26628	O I	−25.0	35.0	−1.9	1.0	13.920	0.026	0.027	0	1	111
J104018+572448	3.26628	O VI	−25.0	35.0	999.0	999.0	12.790	0.176	0.301	−1	3	111
J104018+572448	3.26628	Si II	−25.0	35.0	6.0	0.3	13.202	0.014	0.014	0	3	111
J104018+572448	3.26628	Si III	−25.0	35.0	9.2	0.9	13.492	0.044	0.049	−2	1	111
J104018+572448	3.26628	Si IV	−25.0	35.0	3.3	1.2	12.987	0.028	0.030	0	3	111
J104018+572448	3.27747	C III	−25.0	25.0	−2.9	0.4	13.477	0.046	0.051	0	1	112
J104018+572448	3.27747	C IV	−25.0	25.0	−0.2	0.9	13.275	0.027	0.029	0	3	112
J104018+572448	3.27747	H I	−68.0	30.9	−5.2	0.5	15.803	0.009	0.009	0	3	112
J104018+572448	3.27747	O I	−25.0	25.0	999.0	999.0	12.876	0.176	0.301	−1	3	112
J104018+572448	3.27747	O VI	−25.0	25.0	1.5	2.3	13.299	0.071	0.085	0	1	112
J104018+572448	3.27747	Si II	−25.0	25.0	999.0	999.0	11.443	0.176	0.301	−1	3	112
J104018+572448	3.27747	Si IV	−22.3	22.8	−2.2	2.0	12.597	0.059	0.069	0	3	112
J104018+572448	3.32379	H I	−55.7	30.5	−11.1	0.8	15.743	0.015	0.013	0	3	113
J104018+572448	3.32379	O I	−25.0	25.0	999.0	999.0	12.982	0.176	0.301	−1	3	113
J104018+572448	3.32379	Si II	−25.0	25.0	999.0	999.0	11.464	0.176	0.301	−1	3	113
J104018+572448	3.32379	Si IV	−25.0	25.0	−0.2	1.4	12.689	0.041	0.046	0	3	113
J104018+572448	3.34454	C II	−30.0	1.0	999.0	999.0	12.566	0.176	0.301	−1	3	114
J104018+572448	3.34454	H I	−46.1	22.2	−15.2	0.7	16.053	0.009	0.010	0	3	114
J104018+572448	3.34454	O I	−30.0	1.0	999.0	999.0	12.879	0.176	0.301	−1	3	114
J104018+572448	3.34454	Si II	−30.0	1.0	999.0	999.0	11.387	0.176	0.301	−1	3	114
J104018+572448	3.34454	Si III	−30.0	1.0	−15.7	0.6	12.209	0.032	0.035	0	1	114
J104018+572448	3.34454	Si IV	−30.0	1.0	999.0	999.0	11.934	0.176	0.301	−1	3	114
J104018+572448	3.36421	C III	−19.0	25.0	0.8	0.7	13.082	0.023	0.024	0	1	115
J104018+572448	3.36421	H I	−47.3	28.7	−6.8	0.4	15.603	0.008	0.009	0	3	115
J104018+572448	3.36421	O I	−19.0	25.0	999.0	999.0	12.990	0.176	0.301	−1	3	115
J104018+572448	3.36421	O VI	−15.4	38.2	5.4	0.5	13.829	0.018	0.019	0	3	115

Table 2 continued

Table 2 (*continued*)

Target	z_{abs}	Ion	v_1	v_2	v	σ_v	$\log N$	$\sigma_{\log N}^1$	$\sigma_{\log N}^2$	Detection	Reliability	Unique
			(km s $^{-1}$)	(km s $^{-1}$)	(km s $^{-1}$)	[cm $^{-2}$]	Flag	Flag	ID			
J104018+572448	3.36421	Si II	-19.0	25.0	999.0	999.0	11.488	0.176	0.301	-1	3	115
J104018+572448	3.36421	Si IV	-19.0	25.0	999.0	999.0	12.098	0.176	0.301	-1	3	115
J105756+455553	3.69194	Al II	-25.0	25.0	-7.4	4.5	10.874	0.112	0.151	-1	3	116
J105756+455553	3.69194	C IV	-25.0	25.0	12.2	8.2	11.807	0.133	0.192	-1	3	116
J105756+455553	3.69194	Fe II	-25.0	25.0	999.0	999.0	12.061	0.176	0.301	-1	3	116
J105756+455553	3.69194	H I	-54.0	19.6	-16.2	0.2	14.698	0.003	0.003	0	3	116
J105756+455553	3.69194	Si II	-25.0	25.0	999.0	999.0	11.592	0.176	0.301	-1	3	116
J105756+455553	3.69194	Si IV	-25.0	25.0	999.0	999.0	11.266	0.176	0.301	-1	3	116
J113418+574204	3.34514	Al II	-15.0	15.0	999.0	999.0	10.975	0.176	0.301	-1	3	117
J113418+574204	3.34514	C II	-15.0	15.0	999.0	999.0	12.223	0.176	0.301	-1	3	117
J113418+574204	3.34514	C IV	-15.0	15.0	999.0	999.0	11.978	0.176	0.301	-1	3	117
J113418+574204	3.34514	Fe II	-15.0	15.0	999.0	999.0	12.530	0.176	0.301	-1	3	117
J113418+574204	3.34514	Fe III	-15.0	15.0	999.0	999.0	12.747	0.176	0.301	-1	3	117
J113418+574204	3.34514	H I	-56.3	46.1	-12.9	0.5	15.134	0.004	0.004	0	3	117
J113418+574204	3.34514	O I	-15.0	15.0	999.0	999.0	13.586	0.176	0.301	-1	3	117
J113418+574204	3.34514	O VI	-15.0	15.0	999.0	999.0	12.430	0.176	0.301	-1	3	117
J113418+574204	3.34514	Si II	-15.0	15.0	999.0	999.0	11.033	0.176	0.301	-1	3	117
J113418+574204	3.34514	Si IV	-15.0	15.0	999.0	999.0	11.567	0.176	0.301	-1	3	117
J113418+574204	3.46347	Al II	-30.0	-5.0	-19.4	3.5	10.949	0.155	0.244	-1	3	118
J113418+574204	3.46347	Al III	-30.0	-5.0	-21.9	3.5	11.477	0.143	0.215	-1	3	118
J113418+574204	3.46347	C II	-30.0	-5.0	999.0	999.0	12.122	0.176	0.301	-1	3	118
J113418+574204	3.46347	C III	-30.0	-5.0	-18.9	0.3	12.817	0.022	0.023	0	1	118
J113418+574204	3.46347	C IV	-30.0	-5.0	-20.0	0.7	12.608	0.045	0.051	0	1	118
J113418+574204	3.46347	Fe II	-30.0	-5.0	999.0	999.0	12.436	0.176	0.301	-1	3	118
J113418+574204	3.46347	H I	-52.9	23.9	-20.3	0.4	15.136	0.008	0.006	0	3	118
J113418+574204	3.46347	O I	-30.0	-5.0	-20.1	3.0	12.897	0.131	0.188	-1	3	118
J113418+574204	3.46347	O VI	-30.0	-5.0	999.0	999.0	12.760	0.176	0.301	-1	3	118
J113418+574204	3.46347	Si II	-30.0	-5.0	999.0	999.0	12.077	0.176	0.301	-1	3	118
J113418+574204	3.46347	Si III	-30.0	-5.0	999.0	999.0	11.132	0.176	0.301	-1	3	118
J113418+574204	3.46347	Si IV	-30.0	-5.0	999.0	999.0	11.500	0.176	0.301	-1	3	118
J113508+222715	2.74242	Al II	-15.0	15.0	6.3	4.2	11.151	0.137	0.202	-1	3	119
J113508+222715	2.74242	C III	-15.0	15.0	2.2	2.7	11.900	0.124	0.175	-1	3	119
J113508+222715	2.74242	C IV	-15.0	15.0	999.0	999.0	11.883	0.176	0.301	-1	3	119
J113508+222715	2.74242	Fe II	-15.0	15.0	999.0	999.0	12.022	0.176	0.301	-1	3	119
J113508+222715	2.74242	Fe III	-15.0	15.0	999.0	999.0	12.563	0.176	0.301	-1	3	119
J113508+222715	2.74242	H I	-56.3	32.4	-14.4	1.2	15.055	0.009	0.010	0	2	119
J113508+222715	2.74242	O I	-15.0	15.0	999.0	999.0	12.360	0.176	0.301	-1	3	119
J113508+222715	2.74242	Si II	-15.0	15.0	4.0	2.9	10.990	0.107	0.143	-1	3	119
J113508+222715	2.74242	Si IV	-15.0	15.0	999.0	999.0	11.362	0.176	0.301	-1	3	119
J120006+312630	2.84264	C II	-30.0	25.0	999.0	999.0	12.398	0.176	0.301	-1	3	120
J120006+312630	2.84264	C IV	-30.0	25.0	-0.9	0.2	13.250	0.005	0.005	0	3	120
J120006+312630	2.84264	H I	-66.6	34.1	-19.5	0.3	14.804	0.011	0.008	0	3	120
J120006+312630	2.84264	O I	-30.0	25.0	-11.9	8.5	12.381	0.150	0.232	-1	3	120
J120006+312630	2.84264	O VI	-30.0	25.0	-3.3	0.2	14.058	0.007	0.007	0	3	120
J120006+312630	2.84264	Si II	-30.0	25.0	-5.7	1.6	11.677	0.038	0.042	-1	3	120
J120006+312630	2.84264	Si III	-30.0	25.0	-4.2	0.5	12.071	0.014	0.015	0	1	120
J120006+312630	2.84264	Si IV	-30.0	25.0	-3.0	3.0	11.729	0.080	0.098	0	3	120

Table 2 continued

Table 2 (*continued*)

Target	z_{abs}	Ion	v_1	v_2	v	σ_v	$\log N$	$\sigma_{\log N}^1$	$\sigma_{\log N}^2$	Detection	Reliability	Unique
			(km s $^{-1}$)	(km s $^{-1}$)	(km s $^{-1}$)	[cm $^{-2}$]	Flag	Flag	ID			
J120006+312630	2.87577	C II	-50.0	55.0	5.3	2.3	12.809	0.032	0.034	0	1	121
J120006+312630	2.87577	C IV	-50.0	55.0	0.4	0.2	13.563	0.003	0.003	0	3	121
J120006+312630	2.87577	H I	-46.2	16.0	-13.3	2.3	16.561	0.020	0.022	0	3	121
J120006+312630	2.87577	O I	-50.0	55.0	999.0	999.0	12.472	0.176	0.301	-1	3	121
J120006+312630	2.87577	Si II	-50.0	55.0	-15.7	15.1	11.040	0.150	0.231	-1	3	121
J120006+312630	2.87577	Si IV	-50.0	55.0	-3.0	1.4	12.941	0.020	0.021	0	1	121
J121930+494052	2.22541	Al II	-2.0	45.0	999.0	999.0	10.491	0.176	0.301	-1	3	122
J121930+494052	2.22541	C IV	-2.0	45.0	15.2	1.3	12.393	0.035	0.038	0	1	122
J121930+494052	2.22541	Fe II	-2.0	45.0	999.0	999.0	11.976	0.176	0.301	-1	3	122
J121930+494052	2.22541	H I	-151.9	71.7	-12.9	0.3	15.109	0.005	0.005	0	3	122
J121930+494052	2.22541	O I	-2.0	45.0	23.0	2.4	12.802	0.064	0.076	-1	3	122
J121930+494052	2.22541	O VI	-87.0	56.3	-3.7	1.4	14.043	0.016	0.016	0	1	122
J121930+494052	2.22541	Si II	-2.0	45.0	17.0	2.7	11.379	0.072	0.086	-1	3	122
J121930+494052	2.22541	Si III	-2.0	45.0	999.0	999.0	10.810	0.176	0.301	-1	3	122
J121930+494052	2.22541	Si IV	-2.0	45.0	999.0	999.0	11.386	0.176	0.301	-1	3	122
J121930+494052	2.22541	Zn II	-2.0	45.0	999.0	999.0	11.209	0.176	0.301	-1	3	122
J121930+494052	2.27897	Al II	-29.0	15.0	999.0	999.0	10.475	0.176	0.301	-1	3	123
J121930+494052	2.27897	Al III	-29.0	15.0	999.0	999.0	11.183	0.176	0.301	-1	3	123
J121930+494052	2.27897	C IV	-29.0	15.0	-11.0	0.2	12.901	0.008	0.008	0	3	123
J121930+494052	2.27897	Fe II	-29.0	15.0	999.0	999.0	12.893	0.176	0.301	-1	3	123
J121930+494052	2.27897	H I	-47.0	41.6	-6.4	0.3	14.960	0.010	0.010	0	3	123
J121930+494052	2.27897	O VI	-22.5	10.2	-7.8	0.1	13.777	0.007	0.007	0	3	123
J121930+494052	2.27897	Si II	-29.0	15.0	999.0	999.0	11.668	0.176	0.301	-1	3	123
J121930+494052	2.27897	Si III	-29.0	15.0	999.0	999.0	11.074	0.176	0.301	-1	3	123
J121930+494052	2.27897	Si IV	-29.0	15.0	999.0	999.0	11.072	0.176	0.301	-1	3	123
J121930+494052	2.27897	Zn II	-29.0	15.0	999.0	999.0	11.294	0.176	0.301	-1	3	123
J121930+494052	2.47346	Al II	-15.0	15.0	999.0	999.0	10.517	0.176	0.301	-1	3	124
J121930+494052	2.47346	Al III	-15.0	15.0	-7.9	6.4	11.311	0.158	0.251	-1	3	124
J121930+494052	2.47346	C II	-15.0	15.0	999.0	999.0	11.577	0.176	0.301	-1	3	124
J121930+494052	2.47346	C III	-15.0	15.0	999.0	999.0	11.440	0.176	0.301	-1	3	124
J121930+494052	2.47346	C IV	-15.0	15.0	0.2	0.9	12.085	0.046	0.052	0	3	124
J121930+494052	2.47346	Fe II	-15.0	15.0	999.0	999.0	11.899	0.176	0.301	-1	3	124
J121930+494052	2.47346	H I	-34.6	22.3	-2.3	0.2	15.046	0.004	0.003	0	3	124
J121930+494052	2.47346	O I	-15.0	15.0	999.0	999.0	12.023	0.176	0.301	-1	3	124
J121930+494052	2.47346	O VI	-15.0	15.0	2.1	0.5	12.874	0.024	0.026	0	3	124
J121930+494052	2.47346	Si II	-15.0	15.0	999.0	999.0	11.760	0.176	0.301	-1	3	124
J121930+494052	2.47346	Si III	-15.0	15.0	999.0	999.0	10.744	0.176	0.301	-1	3	124
J121930+494052	2.47346	Si IV	-15.0	15.0	999.0	999.0	11.022	0.176	0.301	-1	3	124
J121930+494052	2.47346	Zn II	-15.0	15.0	999.0	999.0	11.176	0.176	0.301	-1	3	124
J121930+494052	2.47816	Al II	-57.0	46.0	999.0	999.0	10.780	0.176	0.301	-1	3	125
J121930+494052	2.47816	Al III	-57.0	46.0	999.0	999.0	11.433	0.176	0.301	-1	3	125
J121930+494052	2.47816	C II	-57.0	46.0	-6.2	10.8	12.006	0.137	0.202	-1	3	125
J121930+494052	2.47816	C III	-57.0	46.0	-10.0	0.7	13.839	0.018	0.019	0	1	125
J121930+494052	2.47816	C IV	-57.0	46.0	-6.5	0.3	13.443	0.004	0.004	0	3	125
J121930+494052	2.47816	Fe II	-57.0	46.0	999.0	999.0	12.172	0.176	0.301	-1	3	125
J121930+494052	2.47816	Fe III	-57.0	46.0	16.6	4.0	13.147	0.046	0.052	-1	3	125
J121930+494052	2.47816	H I	-30.7	35.8	0.9	0.3	16.021	0.004	0.004	0	3	125

Table 2 continued

Table 2 (*continued*)

Target	z_{abs}	Ion	v_1	v_2	v	σ_v	$\log N$	$\sigma_{\log N}^1$	$\sigma_{\log N}^2$	Detection	Reliability	Unique
			(km s $^{-1}$)	(km s $^{-1}$)	(km s $^{-1}$)	[cm $^{-2}$]	Flag	Flag	ID			
J121930+494052	2.47816	O I	-57.0	46.0	999.0	999.0	12.339	0.176	0.301	-1	3	125
J121930+494052	2.47816	Si II	-57.0	46.0	999.0	999.0	12.534	0.176	0.301	-1	3	125
J121930+494052	2.47816	Si III	-57.0	46.0	-13.1	0.4	12.542	0.007	0.007	0	1	125
J121930+494052	2.47816	Si IV	-57.0	46.0	-21.0	0.4	12.849	0.006	0.007	0	3	125
J121930+494052	2.47816	Zn II	-57.0	46.0	999.0	999.0	11.440	0.176	0.301	-1	3	125
J121930+494052	2.52850	Al II	-35.0	5.0	999.0	999.0	10.639	0.176	0.301	-1	3	126
J121930+494052	2.52850	Al III	-35.0	5.0	-34.9	7.8	11.303	0.137	0.200	-1	3	126
J121930+494052	2.52850	C II	-35.0	5.0	999.0	999.0	11.715	0.176	0.301	-1	3	126
J121930+494052	2.52850	C III	-35.0	5.0	-9.0	0.2	12.874	0.008	0.009	0	1	126
J121930+494052	2.52850	C IV	-35.0	5.0	-12.2	0.4	12.569	0.017	0.018	0	3	126
J121930+494052	2.52850	Fe II	-35.0	5.0	999.0	999.0	11.878	0.176	0.301	-1	3	126
J121930+494052	2.52850	H I	-20.5	20.5	-5.6	0.1	15.091	0.002	0.004	0	3	126
J121930+494052	2.52850	O I	-35.0	5.0	999.0	999.0	12.080	0.176	0.301	-1	3	126
J121930+494052	2.52850	Si II	-35.0	5.0	999.0	999.0	11.850	0.176	0.301	-1	3	126
J121930+494052	2.52850	Si III	-35.0	5.0	999.0	999.0	10.916	0.176	0.301	-1	3	126
J121930+494052	2.52850	Si IV	-35.0	5.0	999.0	999.0	11.164	0.176	0.301	-1	3	126
J121930+494052	2.54882	Al II	-41.0	5.0	999.0	999.0	10.551	0.176	0.301	-1	3	127
J121930+494052	2.54882	Al III	-41.0	5.0	999.0	999.0	11.060	0.176	0.301	-1	3	127
J121930+494052	2.54882	C II	-41.0	5.0	-13.4	4.9	11.909	0.138	0.205	-1	3	127
J121930+494052	2.54882	C III	-41.0	5.0	-21.7	0.1	13.156	0.006	0.006	0	1	127
J121930+494052	2.54882	C IV	-41.0	5.0	-19.1	0.1	13.139	0.005	0.005	0	3	127
J121930+494052	2.54882	Fe II	-41.0	5.0	999.0	999.0	12.039	0.176	0.301	-1	3	127
J121930+494052	2.54882	H I	-55.3	23.7	-21.9	0.2	15.572	0.004	0.002	0	3	127
J121930+494052	2.54882	O I	-41.0	5.0	999.0	999.0	12.134	0.176	0.301	-1	3	127
J121930+494052	2.54882	O VI	-41.0	5.0	-19.9	0.3	13.754	0.009	0.009	0	1	127
J121930+494052	2.54882	Si II	-41.0	5.0	999.0	999.0	11.880	0.176	0.301	-1	3	127
J121930+494052	2.54882	Si III	-41.0	5.0	-21.6	0.9	11.729	0.028	0.030	0	1	127
J121930+494052	2.54882	Si IV	-41.0	5.0	999.0	999.0	11.199	0.176	0.301	-1	3	127
J121930+494052	2.57078	Al II	-50.0	25.0	-28.2	5.5	11.100	0.077	0.094	-1	3	128
J121930+494052	2.57078	Al III	-50.0	25.0	999.0	999.0	11.241	0.176	0.301	-1	3	128
J121930+494052	2.57078	C II	-50.0	25.0	999.0	999.0	11.840	0.176	0.301	-1	3	128
J121930+494052	2.57078	C III	-50.0	25.0	999.0	999.0	11.894	0.176	0.301	-1	3	128
J121930+494052	2.57078	C IV	-50.0	25.0	999.0	999.0	12.003	0.176	0.301	-1	3	128
J121930+494052	2.57078	Fe II	-50.0	25.0	999.0	999.0	12.009	0.176	0.301	-1	3	128
J121930+494052	2.57078	H I	-80.2	71.7	-8.6	0.2	15.114	0.001	0.001	0	3	128
J121930+494052	2.57078	O I	-50.0	25.0	999.0	999.0	12.249	0.176	0.301	-1	3	128
J121930+494052	2.57078	O VI	-50.0	25.0	-1.9	0.3	13.676	0.006	0.006	0	3	128
J121930+494052	2.57078	Si II	-50.0	25.0	999.0	999.0	11.872	0.176	0.301	-1	3	128
J121930+494052	2.57078	Si IV	-50.0	25.0	999.0	999.0	11.277	0.176	0.301	-1	3	128
J121930+494052	2.57761	Al II	-25.0	30.0	999.0	999.0	10.771	0.176	0.301	-1	3	129
J121930+494052	2.57761	Al III	-25.0	30.0	999.0	999.0	11.254	0.176	0.301	-1	3	129
J121930+494052	2.57761	C II	-25.0	30.0	-7.8	7.1	11.965	0.135	0.197	-1	3	129
J121930+494052	2.57761	C IV	-25.0	30.0	3.4	2.0	12.291	0.047	0.053	0	2	129
J121930+494052	2.57761	Fe II	-25.0	30.0	999.0	999.0	11.953	0.176	0.301	-1	3	129
J121930+494052	2.57761	Fe III	-25.0	30.0	999.0	999.0	12.345	0.176	0.301	-1	3	129
J121930+494052	2.57761	H I	-58.0	73.4	-0.8	0.1	15.025	0.001	0.001	0	3	129
J121930+494052	2.57761	O I	-25.0	30.0	999.0	999.0	12.199	0.176	0.301	-1	3	129

Table 2 continued

Table 2 (*continued*)

Target	z_{abs}	Ion	v_1	v_2	v	σ_v	$\log N$	$\sigma_{\log N}^1$	$\sigma_{\log N}^2$	Detection	Reliability	Unique
			(km s $^{-1}$)	(km s $^{-1}$)	(km s $^{-1}$)	[cm $^{-2}$]	Flag	Flag	ID			
J121930+494052	2.57761	O VI	-25.0	30.0	5.7	0.4	13.324	0.012	0.012	0	3	129
J121930+494052	2.57761	Si II	-25.0	30.0	999.0	999.0	10.774	0.176	0.301	-1	3	129
J121930+494052	2.57761	Si IV	-25.0	30.0	999.0	999.0	11.208	0.176	0.301	-1	3	129
J121930+494052	2.62063	Al II	-45.0	5.0	999.0	999.0	10.600	0.176	0.301	-1	3	130
J121930+494052	2.62063	Al III	-45.0	5.0	999.0	999.0	11.043	0.180	0.300	-1	3	130
J121930+494052	2.62063	C II	-45.0	5.0	999.0	999.0	11.740	0.176	0.301	-1	3	130
J121930+494052	2.62063	C III	-45.0	5.0	-13.9	0.2	13.767	0.014	0.015	-2	1	130
J121930+494052	2.62063	C IV	-45.0	5.0	-15.8	0.1	13.333	0.004	0.004	0	3	130
J121930+494052	2.62063	Fe II	-45.0	5.0	999.0	999.0	11.993	0.176	0.301	-1	3	130
J121930+494052	2.62063	H I	-70.0	13.6	-13.6	0.1	15.903	0.001	0.003	0	3	130
J121930+494052	2.62063	O I	-45.0	5.0	-11.4	5.5	12.362	0.130	0.186	-1	3	130
J121930+494052	2.62063	O VI	-45.0	5.0	-20.1	0.3	13.387	0.011	0.011	0	1	130
J121930+494052	2.62063	Si II	-45.0	5.0	999.0	999.0	10.806	0.176	0.301	-1	3	130
J121930+494052	2.62063	Si III	-45.0	5.0	-10.0	0.2	12.422	0.005	0.005	0	1	130
J121930+494052	2.62063	Si IV	-45.0	5.0	-12.2	0.3	12.566	0.010	0.010	0	3	130
J124610+303131	2.46655	Al II	-15.0	15.0	999.0	999.0	11.081	0.176	0.301	-1	3	131
J124610+303131	2.46655	C II	-15.0	15.0	999.0	999.0	12.517	0.176	0.301	-1	3	131
J124610+303131	2.46655	C IV	-15.0	15.0	1.4	2.3	12.277	0.094	0.119	-1	3	131
J124610+303131	2.46655	Fe II	-15.0	15.0	999.0	999.0	12.462	0.176	0.301	-1	3	131
J124610+303131	2.46655	H I	-78.5	61.4	-8.6	0.6	15.224	0.005	0.005	0	3	131
J124610+303131	2.46655	Si II	-15.0	15.0	999.0	999.0	11.077	0.176	0.301	-1	3	131
J124610+303131	2.46655	Si IV	-15.0	15.0	999.0	999.0	11.910	0.176	0.301	-1	3	131
J130411+295348	2.57585	C II	-15.0	15.0	-0.5	1.2	12.550	0.058	0.067	0	3	132
J130411+295348	2.57585	C III	-15.0	15.0	1.2	0.4	13.272	0.052	0.059	0	1	132
J130411+295348	2.57585	C IV	-15.0	15.0	3.6	3.0	12.250	0.123	0.172	0	1	132
J130411+295348	2.57585	Fe II	-15.0	15.0	999.0	999.0	12.459	0.176	0.301	-1	3	132
J130411+295348	2.57585	Fe III	-15.0	15.0	999.0	999.0	12.695	0.176	0.301	-1	3	132
J130411+295348	2.57585	H I	-30.7	44.4	1.2	0.7	15.618	0.007	0.009	0	3	132
J130411+295348	2.57585	O VI	-15.0	15.0	999.0	999.0	12.406	0.176	0.301	-1	3	132
J130411+295348	2.57585	Si II	-15.0	15.0	-4.2	2.9	11.814	0.118	0.162	-1	3	132
J130411+295348	2.57585	Si III	-15.0	15.0	1.9	0.3	12.357	0.018	0.019	0	1	132
J130411+295348	2.57585	Si IV	-15.0	15.0	1.4	1.0	12.190	0.049	0.055	0	3	132
J130411+295348	2.57726	C II	-15.0	15.0	-13.6	6.5	12.209	0.117	0.161	-1	3	133
J130411+295348	2.57726	C IV	-15.0	15.0	999.0	999.0	12.033	0.176	0.301	-1	3	133
J130411+295348	2.57726	Fe II	-15.0	15.0	999.0	999.0	14.171	0.176	0.301	-1	3	133
J130411+295348	2.57726	H I	-31.0	24.5	-1.6	0.8	15.047	0.009	0.009	0	3	133
J130411+295348	2.57726	O VI	-15.0	15.0	0.9	1.4	12.930	0.064	0.075	-1	3	133
J130411+295348	2.57726	Si II	-15.0	15.0	999.0	999.0	11.563	0.176	0.301	-1	3	133
J130411+295348	2.57726	Si III	-15.0	15.0	2.4	0.5	12.082	0.024	0.025	-1	3	133
J130411+295348	2.57726	Si IV	-15.0	15.0	999.0	999.0	11.652	0.176	0.301	-1	3	133
J130411+295348	2.75550	C II	-15.0	45.0	999.0	999.0	12.410	0.176	0.301	-1	3	134
J130411+295348	2.75550	C IV	-15.0	45.0	9.0	1.4	12.944	0.033	0.036	0	3	134
J130411+295348	2.75550	H I	-29.1	47.8	6.6	0.3	15.072	0.007	0.007	0	3	134
J130411+295348	2.75550	O I	-15.0	45.0	999.0	999.0	12.694	0.176	0.301	-1	3	134
J130411+295348	2.75550	O VI	-15.0	45.0	12.2	0.3	13.978	0.008	0.008	0	3	134
J130411+295348	2.75550	Si II	-15.0	45.0	999.0	999.0	11.179	0.176	0.301	-1	3	134
J130411+295348	2.75550	Si IV	-15.0	45.0	999.0	999.0	11.754	0.176	0.301	-1	3	134

Table 2 continued

Table 2 (*continued*)

Target	z_{abs}	Ion	v_1	v_2	v	σ_v	$\log N$	$\sigma_{\log N}^1$	$\sigma_{\log N}^2$	Detection	Reliability	Unique
			(km s $^{-1}$)	(km s $^{-1}$)	(km s $^{-1}$)	[cm $^{-2}$]	Flag	Flag	ID			
J130411+295348	2.79811	C II	-15.0	15.0	999.0	999.0	12.298	0.176	0.301	-1	3	135
J130411+295348	2.79811	H I	-51.0	10.4	-25.9	0.4	15.897	0.005	0.005	0	3	135
J130411+295348	2.79811	O I	-15.0	15.0	999.0	999.0	12.801	0.176	0.301	-1	3	135
J130411+295348	2.79811	Si II	-15.0	15.0	5.1	5.3	11.030	0.171	0.285	-1	3	135
J130411+295348	2.79811	Si III	-15.0	15.0	0.5	0.5	12.002	0.024	0.025	-1	3	135
J130411+295348	2.79811	Si IV	-15.0	15.0	999.0	999.0	11.660	0.176	0.301	-1	3	135
J130411+295348	2.82924	C II	-15.0	15.0	-1.2	3.9	12.289	0.164	0.267	-1	3	136
J130411+295348	2.82924	H I	-25.1	12.0	-1.5	0.2	16.378	0.004	0.004	0	3	136
J130411+295348	2.82924	O I	-15.0	15.0	6.3	3.6	12.816	0.130	0.186	-1	3	136
J130411+295348	2.82924	Si II	-15.0	15.0	5.4	2.9	11.382	0.108	0.145	-1	3	136
J130411+295348	2.82924	Si IV	-15.0	15.0	999.0	999.0	11.585	0.176	0.301	-1	3	136
J131215+423900	2.41504	Al II	-15.0	15.0	18.7	7.2	10.904	0.143	0.215	-1	1	137
J131215+423900	2.41504	C III	-4.1	21.5	5.7	0.5	12.577	0.029	0.031	0	1	137
J131215+423900	2.41504	C IV	-19.5	21.5	2.1	0.9	12.671	0.033	0.036	0	3	137
J131215+423900	2.41504	Fe II	-15.0	15.0	999.0	999.0	12.022	0.176	0.301	-1	3	137
J131215+423900	2.41504	H I	-42.7	44.4	-0.2	1.3	15.598	0.008	0.008	0	3	137
J131215+423900	2.41504	O I	-15.0	15.0	-5.9	3.3	12.466	0.109	0.146	-1	3	137
J131215+423900	2.41504	O VI	-15.0	15.0	0.9	0.7	13.408	0.030	0.033	-1	3	137
J131215+423900	2.41504	Si II	-15.0	15.0	999.0	999.0	11.510	0.176	0.301	-1	3	137
J131215+423900	2.41504	Si III	-15.0	15.0	999.0	999.0	11.323	0.176	0.301	-1	3	137
J131215+423900	2.41504	Si IV	-15.0	15.0	999.0	999.0	11.292	0.176	0.301	-1	3	137
J131215+423900	2.48998	Al II	-20.0	20.0	999.0	999.0	10.888	0.176	0.301	-1	3	138
J131215+423900	2.48998	C II	-20.0	20.0	6.8	4.7	12.207	0.133	0.192	0	3	138
J131215+423900	2.48998	C III	-20.0	20.0	0.6	0.3	13.718	0.024	0.025	-2	1	138
J131215+423900	2.48998	C IV	-20.0	20.0	-2.1	0.6	13.084	0.042	0.046	0	3	138
J131215+423900	2.48998	Fe II	-20.0	20.0	999.0	999.0	12.207	0.176	0.301	-1	3	138
J131215+423900	2.48998	Fe III	-20.0	20.0	999.0	999.0	12.648	0.176	0.301	-1	3	138
J131215+423900	2.48998	H I	-35.7	35.7	0.8	0.3	16.796	0.005	0.005	0	3	138
J131215+423900	2.48998	O I	-20.0	20.0	999.0	999.0	12.382	0.176	0.301	-1	3	138
J131215+423900	2.48998	O VI	-20.0	20.0	999.0	999.0	13.500	0.176	0.301	-1	3	138
J131215+423900	2.48998	Si II	-20.0	20.0	2.9	1.6	11.529	0.054	0.062	-1	3	138
J131215+423900	2.48998	Si III	-20.0	20.0	3.7	0.2	12.833	0.009	0.009	-2	1	138
J131215+423900	2.48998	Si IV	-20.0	20.0	1.5	0.5	12.568	0.018	0.019	0	3	138
J134328+572147	2.79941	C II	-15.0	15.0	999.0	999.0	12.171	0.176	0.301	-1	3	139
J134328+572147	2.79941	C IV	-15.0	15.0	-13.0	6.3	12.375	0.150	0.231	-1	3	139
J134328+572147	2.79941	Fe II	-15.0	15.0	999.0	999.0	12.730	0.176	0.301	-1	3	139
J134328+572147	2.79941	H I	-37.5	18.8	-13.0	0.9	15.309	0.010	0.011	0	3	139
J134328+572147	2.79941	O I	-15.0	15.0	999.0	999.0	12.342	0.176	0.301	-1	3	139
J134328+572147	2.79941	O VI	-15.0	10.0	999.0	999.0	12.647	0.176	0.301	-1	3	139
J134328+572147	2.79941	Si II	-15.0	15.0	999.0	999.0	12.109	0.176	0.301	-1	3	139
J134328+572147	2.79941	Si III	-15.0	15.0	999.0	999.0	11.341	0.176	0.301	-1	3	139
J134328+572147	2.79941	Si IV	-15.0	15.0	999.0	999.0	11.685	0.176	0.301	-1	3	139
J134328+572147	2.83437	C II	-30.0	30.0	-2.4	0.4	14.402	0.047	0.053	-2	1	140
J134328+572147	2.83437	C IV	-30.0	30.0	-7.3	1.3	13.141	0.029	0.031	0	3	140
J134328+572147	2.83437	Fe II	-30.0	30.0	-6.1	5.6	12.900	0.128	0.183	-1	3	140
J134328+572147	2.83437	Fe III	-30.0	30.0	-16.4	7.7	13.104	0.117	0.161	-1	3	140
J134328+572147	2.83437	H I	-40.0	35.0	-0.8	18.8	17.780	0.300	0.300	0	3	140

Table 2 continued

Table 2 (*continued*)

Target	z_{abs}	Ion	v_1	v_2	v	σ_v	$\log N$	$\sigma_{\log N}^1$	$\sigma_{\log N}^2$	Detection	Reliability	Unique
			(km s $^{-1}$)	(km s $^{-1}$)	(km s $^{-1}$)	[cm $^{-2}$]	Flag	Flag	ID			
J134328+572147	2.83437	O I	-30.0	30.0	-1.5	0.5	13.856	0.012	0.012	0	1	140
J134328+572147	2.83437	Si II	-30.0	30.0	-1.7	0.3	13.430	0.016	0.017	0	3	140
J134328+572147	2.83437	Si III	-30.0	30.0	-6.6	1.1	13.577	0.004	0.004	-2	1	140
J134328+572147	2.83437	Si IV	-30.0	30.0	-7.9	1.1	12.805	0.027	0.029	0	3	140
J134328+572147	2.87056	C IV	-42.0	30.0	-17.8	1.3	13.855	0.032	0.034	0	3	141
J134328+572147	2.87056	H I	-37.5	8.0	-12.0	0.6	16.254	0.009	0.009	0	3	141
J134328+572147	2.87056	O I	-42.0	30.0	999.0	999.0	12.854	0.176	0.301	-1	3	141
J134328+572147	2.87056	O VI	-42.0	30.0	-21.5	0.8	14.276	0.016	0.016	0	1	141
J134328+572147	2.87056	Si II	-42.0	30.0	999.0	999.0	12.524	0.176	0.301	-1	3	141
J134328+572147	2.87056	Si III	-42.0	30.0	-5.5	0.6	12.796	0.012	0.012	0	1	141
J134328+572147	2.87056	Si IV	-42.0	30.0	-17.2	1.1	13.000	0.021	0.022	0	3	141
J134544+262506	2.86367	C II	-20.0	20.0	3.7	2.1	12.615	0.071	0.085	0	3	142
J134544+262506	2.86367	C IV	-20.0	20.0	-0.3	0.6	13.027	0.026	0.027	0	3	142
J134544+262506	2.86367	Fe II	-20.0	20.0	999.0	999.0	12.576	0.176	0.301	-1	3	142
J134544+262506	2.86367	Fe III	-20.0	20.0	999.0	999.0	12.716	0.176	0.301	-1	3	142
J134544+262506	2.86367	H I	-13.7	23.9	2.0	0.3	16.267	0.008	0.007	0	3	142
J134544+262506	2.86367	O I	-20.0	20.0	999.0	999.0	12.721	0.176	0.301	-1	3	142
J134544+262506	2.86367	Si II	-20.0	20.0	-1.6	3.3	11.384	0.106	0.141	0	1	142
J134544+262506	2.86367	Si III	-20.0	20.0	2.9	0.1	13.026	0.021	0.023	0	1	142
J134544+262506	2.86367	Si IV	-20.0	20.0	-0.0	0.6	12.707	0.022	0.024	0	2	142
J135038-251216	2.37059	Al II	-70.0	-1.0	999.0	999.0	10.945	0.176	0.301	-1	3	143
J135038-251216	2.37059	C II	-70.0	-1.0	999.0	999.0	12.093	0.176	0.301	-1	3	143
J135038-251216	2.37059	C III	-70.0	-1.0	-41.9	1.5	12.767	0.032	0.035	0	1	143
J135038-251216	2.37059	C IV	-70.0	-1.0	-39.0	1.1	12.921	0.022	0.023	0	3	143
J135038-251216	2.37059	Fe II	-70.0	-1.0	999.0	999.0	12.377	0.176	0.301	-1	3	143
J135038-251216	2.37059	H I	-101.4	52.6	-3.6	0.4	14.969	0.009	0.009	0	3	143
J135038-251216	2.37059	O I	-70.0	-1.0	999.0	999.0	12.451	0.176	0.301	-1	3	143
J135038-251216	2.37059	O VI	-70.0	-1.0	-29.6	0.6	14.026	0.013	0.014	0	1	143
J135038-251216	2.37059	Si II	-70.0	-1.0	999.0	999.0	12.159	0.176	0.301	-1	3	143
J135038-251216	2.37059	Si IV	-70.0	-1.0	-42.5	8.3	11.586	0.150	0.231	-1	3	143
J135038-251216	2.44516	Al II	1.0	50.0	999.0	999.0	10.872	0.176	0.301	-1	3	144
J135038-251216	2.44516	C II	1.0	50.0	999.0	999.0	12.012	0.176	0.301	-1	3	144
J135038-251216	2.44516	C III	1.0	50.0	28.3	1.0	12.702	0.034	0.037	0	1	144
J135038-251216	2.44516	C IIS	1.0	50.0	13.3	4.4	12.671	0.086	0.107	0	1	144
J135038-251216	2.44516	C IV	1.0	50.0	21.8	1.8	12.445	0.049	0.055	0	3	144
J135038-251216	2.44516	Fe II	1.0	50.0	999.0	999.0	12.320	0.176	0.301	-1	3	144
J135038-251216	2.44516	Fe III	1.0	50.0	999.0	999.0	12.529	0.176	0.301	-1	3	144
J135038-251216	2.44516	H I	-46.3	52.8	13.6	0.6	15.235	0.013	0.013	0	3	144
J135038-251216	2.44516	O I	1.0	50.0	999.0	999.0	12.391	0.176	0.301	-1	3	144
J135038-251216	2.44516	O VI	1.0	50.0	25.1	0.4	13.587	0.012	0.012	0	3	144
J135038-251216	2.44516	Si II	1.0	50.0	999.0	999.0	12.022	0.176	0.301	-1	3	144
J135038-251216	2.44516	Si III	1.0	50.0	999.0	999.0	10.997	0.176	0.301	-1	3	144
J135038-251216	2.44516	Si IV	1.0	50.0	999.0	999.0	11.457	0.176	0.301	-1	3	144
J135038-251216	2.57299	Al II	-42.0	35.0	-2.8	10.3	11.048	0.162	0.261	-1	3	145
J135038-251216	2.57299	C II	-42.0	35.0	999.0	999.0	12.138	0.176	0.301	-1	3	145
J135038-251216	2.57299	C III	-42.0	35.0	-7.3	0.5	13.134	0.010	0.010	0	1	145
J135038-251216	2.57299	C IV	-42.0	35.0	-12.3	2.8	12.450	0.047	0.052	0	3	145

Table 2 continued

Table 2 (*continued*)

Target	z_{abs}	Ion	v_1	v_2	v	σ_v	$\log N$	$\sigma_{\log N}^1$	$\sigma_{\log N}^2$	Detection	Reliability	Unique
			(km s $^{-1}$)	(km s $^{-1}$)	(km s $^{-1}$)	[cm $^{-2}$]	Flag	Flag	ID			
J135038–251216	2.57299	Fe II	–42.0	35.0	–0.7	7.1	12.656	0.117	0.160	–1	3	145
J135038–251216	2.57299	H I	–46.6	27.9	–1.1	0.4	16.319	0.007	0.007	0	3	145
J135038–251216	2.57299	Si II	–42.0	35.0	0.2	8.6	11.268	0.145	0.220	–1	3	145
J135038–251216	2.57299	Si III	–42.0	35.0	–2.5	0.5	12.310	0.011	0.011	0	1	145
J135038–251216	2.57299	Si IV	–42.0	35.0	–14.3	5.6	11.812	0.091	0.116	0	2	145
J135038–251216	2.57455	Al II	–25.0	25.0	999.0	999.0	10.903	0.176	0.301	–1	3	146
J135038–251216	2.57455	C II	–25.0	25.0	–1.6	0.7	13.108	0.020	0.020	–1	3	146
J135038–251216	2.57455	C III	–25.0	25.0	–3.3	0.5	13.566	0.026	0.028	0	1	146
J135038–251216	2.57455	C IV	–25.0	25.0	–4.0	0.2	13.455	0.006	0.006	0	3	146
J135038–251216	2.57455	Fe II	–25.0	25.0	999.0	999.0	12.335	0.176	0.301	–1	3	146
J135038–251216	2.57455	H I	–29.0	23.9	–2.1	0.2	15.065	0.005	0.003	0	3	146
J135038–251216	2.57455	O I	–25.0	25.0	999.0	999.0	12.427	0.176	0.301	–1	3	146
J135038–251216	2.57455	O VI	–25.0	25.0	–2.0	0.4	13.432	0.013	0.013	0	3	146
J135038–251216	2.57455	Si II	–25.0	25.0	999.0	999.0	11.961	0.180	0.300	–1	3	146
J135038–251216	2.57455	Si III	–24.9	18.2	–3.8	0.2	12.432	0.008	0.008	0	1	146
J135038–251216	2.57455	Si IV	–25.0	25.0	–7.0	0.7	12.437	0.020	0.021	0	1	146
J142438+225600	3.33427	C II	–25.0	15.0	999.0	999.0	11.198	0.176	0.301	–1	3	147
J142438+225600	3.33427	C IV	–25.0	15.0	–15.0	4.5	11.457	0.127	0.181	0	1	147
J142438+225600	3.33427	Fe III	–25.0	15.0	–0.8	3.6	12.168	0.103	0.135	–1	3	147
J142438+225600	3.33427	H I	–102.4	49.5	–15.6	0.1	14.990	0.002	0.002	0	3	147
J142438+225600	3.33427	O I	–25.0	15.0	999.0	999.0	11.319	0.176	0.301	–1	3	147
J142438+225600	3.33427	O VI	–25.0	15.0	–4.3	0.5	12.947	0.020	0.021	0	1	147
J142438+225600	3.33427	Si II	–25.0	15.0	999.0	999.0	11.078	0.176	0.301	–1	3	147
J142438+225600	3.33427	Si IV	–25.0	15.0	999.0	999.0	11.018	0.176	0.301	–1	3	147
J142438+225600	3.38281	C II	–20.0	10.0	–2.6	0.4	12.148	0.017	0.018	–1	1	148
J142438+225600	3.38281	C III	–20.0	10.0	–4.6	0.1	13.191	0.005	0.005	0	1	148
J142438+225600	3.38281	C IV	–20.0	10.0	–8.2	0.1	12.672	0.006	0.006	0	3	148
J142438+225600	3.38281	Fe II	–20.0	10.0	999.0	999.0	11.636	0.176	0.301	–1	3	148
J142438+225600	3.38281	H I	–21.7	20.5	–2.6	0.3	16.984	0.100	0.100	0	3	148
J142438+225600	3.38281	O I	–20.0	10.0	–15.0	8.2	11.550	0.168	0.278	–1	3	148
J142438+225600	3.38281	Si II	–20.0	10.0	999.0	999.0	11.275	0.176	0.301	–1	3	148
J142438+225600	3.38281	Si III	–20.0	10.0	–4.0	0.1	12.092	0.004	0.004	0	1	148
J142438+225600	3.38281	Si IV	–20.0	10.0	–9.4	0.4	11.795	0.017	0.018	0	3	148
J142438+225600	3.44848	C II	–15.0	30.0	7.7	1.1	11.955	0.037	0.041	0	1	149
J142438+225600	3.44848	C III	–15.0	30.0	8.7	0.1	13.435	0.005	0.005	0	1	149
J142438+225600	3.44848	C IV	–15.0	30.0	6.8	0.4	12.446	0.014	0.015	0	1	149
J142438+225600	3.44848	H I	–25.6	40.9	8.4	0.1	16.132	0.008	0.004	0	3	149
J142438+225600	3.44848	O I	–15.0	30.0	999.0	999.0	11.665	0.176	0.301	–1	3	149
J142438+225600	3.44848	Si III	–15.0	30.0	7.8	0.1	12.534	0.002	0.002	0	1	149
J142438+225600	3.44848	Si IV	–15.0	30.0	6.2	0.1	12.323	0.005	0.005	0	3	149
J142438+225600	3.53989	C II	–17.0	39.0	4.1	0.1	13.391	0.002	0.002	0	1	150
J142438+225600	3.53989	C III	–17.0	39.0	14.1	0.1	13.890	0.009	0.009	–2	1	150
J142438+225600	3.53989	C IV	–17.0	39.0	5.6	0.2	12.838	0.005	0.005	0	3	150
J142438+225600	3.53989	H I	–15.0	41.0	10.0	0.1	16.064	0.002	0.004	0	3	150
J142438+225600	3.53989	O I	–24.6	30.6	4.5	0.1	12.382	0.002	0.002	0	1	150
J142438+225600	3.53989	Si II	–17.0	39.0	10.3	0.0	12.878	0.001	0.001	0	1	150
J142438+225600	3.53989	Si III	–17.0	39.0	8.3	0.2	12.411	0.005	0.005	0	3	150

Table 2 continued

Table 2 (*continued*)

Target	z_{abs}	Ion	v_1	v_2	v	σ_v	$\log N$	$\sigma_{\log N}^1$	$\sigma_{\log N}^2$	Detection	Reliability	Unique
			(km s $^{-1}$)	(km s $^{-1}$)	(km s $^{-1}$)	[cm $^{-2}$]	Flag	Flag	ID			
J142438+225600	3.56653	C II	-15.0	30.0	999.0	999.0	11.338	0.176	0.301	-1	3	151
J142438+225600	3.56653	C IV	-15.0	30.0	10.8	0.7	12.121	0.023	0.024	0	1	151
J142438+225600	3.56653	H I	-47.8	40.9	8.8	0.1	15.556	0.001	0.001	0	3	151
J142438+225600	3.56653	O I	-15.0	30.0	999.0	999.0	11.632	0.176	0.301	-1	3	151
J142438+225600	3.56653	Si II	-15.0	30.0	999.0	999.0	10.091	0.176	0.301	-1	3	151
J143316+313126	2.58177	Al II	-15.0	15.0	999.0	999.0	10.835	0.176	0.301	-1	3	152
J143316+313126	2.58177	C II	-15.0	15.0	999.0	999.0	11.746	0.176	0.301	-1	3	152
J143316+313126	2.58177	C III	-15.0	15.0	0.4	0.4	12.846	0.018	0.019	-1	3	152
J143316+313126	2.58177	C IV	-15.0	15.0	-2.3	1.9	12.141	0.083	0.103	0	2	152
J143316+313126	2.58177	H I	-35.8	34.1	-1.9	0.2	15.877	0.002	0.002	0	3	152
J143316+313126	2.58177	O I	-15.0	15.0	0.3	2.4	12.621	0.106	0.141	-1	3	152
J143316+313126	2.58177	Si II	-15.0	15.0	999.0	999.0	11.402	0.176	0.301	-1	3	152
J143316+313126	2.58177	Si III	-15.0	15.0	2.5	0.5	11.871	0.025	0.027	-1	3	152
J143316+313126	2.58177	Si IV	-15.0	15.0	-2.2	4.3	11.299	0.170	0.283	-1	3	152
J143316+313126	2.58591	C II	-70.7	30.7	-2.4	1.1	13.370	0.016	0.016	0	1	153
J143316+313126	2.58591	C III	-55.0	55.0	17.9	0.6	13.406	0.009	0.009	0	1	153
J143316+313126	2.58591	C IV	-55.0	55.0	999.0	999.0	12.050	0.176	0.301	-1	3	153
J143316+313126	2.58591	Fe II	-55.0	55.0	999.0	999.0	13.480	0.176	0.301	-1	3	153
J143316+313126	2.58591	H I	-92.2	80.2	-18.8	43.7	18.150	0.150	0.150	0	3	153
J143316+313126	2.58591	O I	-55.0	55.0	-49.7	11.3	13.045	0.080	0.098	-1	3	153
J143316+313126	2.58591	O VI	-55.0	55.0	999.0	999.0	12.802	0.176	0.301	-1	3	153
J143316+313126	2.58591	Si II	-70.0	30.0	-5.8	2.0	12.604	0.032	0.035	0	1	153
J143316+313126	2.58591	Si III	-55.0	55.0	11.4	0.6	12.739	0.008	0.009	0	1	153
J143316+313126	2.58591	Si IV	-55.0	55.0	999.0	999.0	11.713	0.176	0.301	-1	3	153
J143316+313126	2.58814	Al II	-15.0	15.0	-4.2	4.7	10.868	0.174	0.294	-1	3	154
J143316+313126	2.58814	C II	-15.0	15.0	2.6	3.0	11.956	0.126	0.177	-1	3	154
J143316+313126	2.58814	C IV	-15.0	15.0	-3.8	2.5	12.111	0.110	0.147	-1	3	154
J143316+313126	2.58814	Fe II	-15.0	15.0	999.0	999.0	12.291	0.176	0.301	-1	3	154
J143316+313126	2.58814	H I	-35.0	40.0	2.0	0.5	15.254	0.007	0.007	0	3	154
J143316+313126	2.58814	O VI	-15.0	15.0	1.5	2.7	12.366	0.114	0.156	-1	3	154
J143316+313126	2.58814	Si II	-15.0	15.0	999.0	999.0	11.395	0.176	0.301	-1	3	154
J143316+313126	2.58814	Si III	-15.0	15.0	999.0	999.0	10.911	0.176	0.301	-1	3	154
J143316+313126	2.58814	Si IV	-15.0	15.0	999.0	999.0	11.399	0.176	0.301	-1	3	154
J143316+313126	2.61282	Al II	-51.0	51.0	999.0	999.0	11.048	0.176	0.301	-1	3	155
J143316+313126	2.61282	C II	-51.0	51.0	999.0	999.0	13.062	0.176	0.301	-1	3	155
J143316+313126	2.61282	C IV	-51.0	51.0	-0.3	0.6	13.476	0.011	0.011	0	3	155
J143316+313126	2.61282	H I	-80.0	70.0	-20.5	0.3	15.516	0.004	0.004	0	3	155
J143316+313126	2.61282	Si II	-51.0	51.0	999.0	999.0	12.270	0.176	0.301	-1	3	155
J143316+313126	2.61282	Si IV	-51.0	51.0	999.0	999.0	11.610	0.176	0.301	-1	3	155
J143316+313126	2.64432	Al II	-51.0	-2.0	999.0	999.0	10.896	0.176	0.301	-1	3	156
J143316+313126	2.64432	C II	-51.0	-2.0	999.0	999.0	13.135	0.176	0.301	-1	3	156
J143316+313126	2.64432	C III	-51.0	-2.0	-20.0	0.2	13.542	0.011	0.012	0	1	156
J143316+313126	2.64432	C IV	-51.0	-2.0	-18.4	0.4	13.181	0.012	0.012	0	3	156
J143316+313126	2.64432	Fe II	-51.0	-2.0	999.0	999.0	12.486	0.176	0.301	-1	3	156
J143316+313126	2.64432	H I	-51.2	27.3	-12.5	0.2	16.117	0.003	0.003	0	3	156
J143316+313126	2.64432	Si II	-51.0	-2.0	-28.8	4.0	11.387	0.103	0.135	-1	3	156
J143316+313126	2.64432	Si III	-51.0	-2.0	-17.9	1.6	11.884	0.038	0.042	0	1	156

Table 2 continued

Table 2 (*continued*)

Target	z_{abs}	Ion	v_1	v_2	v	σ_v	$\log N$	$\sigma_{\log N}^1$	$\sigma_{\log N}^2$	Detection	Reliability	Unique
			(km s $^{-1}$)	(km s $^{-1}$)	(km s $^{-1}$)	[cm $^{-2}$]	Flag	Flag	ID			
J143316+313126	2.64432	Si IV	-51.0	-2.0	-22.7	3.3	11.790	0.085	0.106	0	3	156
J143316+313126	2.73377	C II	-51.0	10.0	999.0	999.0	12.033	0.176	0.301	-1	3	157
J143316+313126	2.73377	C IV	-51.0	10.0	-14.3	1.1	12.920	0.028	0.030	0	3	157
J143316+313126	2.73377	H I	-42.7	27.3	-9.0	0.3	15.552	0.004	0.005	0	3	157
J143316+313126	2.73377	O I	-51.0	10.0	999.0	999.0	12.473	0.176	0.301	-1	3	157
J143316+313126	2.73377	Si II	-51.0	10.0	-16.5	9.2	12.295	0.164	0.265	-1	3	157
J143316+313126	2.73377	Si III	-51.0	10.0	-29.5	0.9	12.292	0.016	0.017	-1	3	157
J143316+313126	2.73377	Si IV	-51.0	10.0	999.0	999.0	11.578	0.176	0.301	-1	3	157
J143316+313126	2.74931	C II	-40.0	20.0	999.0	999.0	12.204	0.176	0.301	-1	3	158
J143316+313126	2.74931	C IV	-40.0	20.0	999.0	999.0	12.298	0.180	0.300	-1	3	158
J143316+313126	2.74931	Fe II	-40.0	20.0	999.0	999.0	13.543	0.176	0.301	-1	3	158
J143316+313126	2.74931	H I	-45.5	38.6	-2.4	0.1	15.280	0.004	0.004	0	3	158
J143316+313126	2.74931	O I	-40.0	20.0	-3.0	4.9	12.758	0.090	0.113	-1	3	158
J143316+313126	2.74931	Si II	-40.0	20.0	999.0	999.0	12.135	0.176	0.301	-1	3	158
J143316+313126	2.74931	Si IV	-40.0	20.0	999.0	999.0	11.609	0.176	0.301	-1	3	158
J143316+313126	2.77502	C II	-70.0	-5.0	999.0	999.0	12.192	0.176	0.301	-1	3	159
J143316+313126	2.77502	C III	-70.0	-5.0	-41.9	0.3	13.171	0.007	0.007	0	1	159
J143316+313126	2.77502	C IV	-70.0	-5.0	-37.7	1.2	12.852	0.027	0.029	0	3	159
J143316+313126	2.77502	Fe II	-70.0	-5.0	999.0	999.0	12.460	0.176	0.301	-1	3	159
J143316+313126	2.77502	H I	-119.5	75.1	-20.4	0.2	15.078	0.002	0.002	0	3	159
J143316+313126	2.77502	O I	-70.0	-5.0	999.0	999.0	12.445	0.176	0.301	-1	3	159
J143316+313126	2.77502	Si II	-70.0	-5.0	999.0	999.0	12.186	0.176	0.301	-1	3	159
J143316+313126	2.77502	Si IV	-70.0	-5.0	999.0	999.0	11.618	0.176	0.301	-1	3	159
J143316+313126	2.88759	C II	-45.0	-10.0	999.0	999.0	12.192	0.176	0.301	-1	3	160
J143316+313126	2.88759	C III	-45.0	-10.0	-21.4	0.3	12.842	0.014	0.014	0	1	160
J143316+313126	2.88759	C IV	-45.0	-10.0	999.0	999.0	12.119	0.180	0.300	-1	3	160
J143316+313126	2.88759	H I	-74.5	29.0	-15.7	0.2	15.276	0.002	0.002	0	3	160
J143316+313126	2.88759	O I	-45.0	-10.0	999.0	999.0	12.430	0.176	0.301	-1	3	160
J143316+313126	2.88759	O VI	-45.0	-10.0	-25.7	3.4	12.447	0.113	0.153	-1	3	160
J143316+313126	2.88759	Si II	-45.0	-10.0	999.0	999.0	10.920	0.176	0.301	-1	3	160
J143316+313126	2.88759	Si IV	-45.0	-10.0	999.0	999.0	11.763	0.176	0.301	-1	3	160
J143316+313126	2.89093	C II	-80.0	35.0	999.0	999.0	12.357	0.176	0.301	-1	3	161
J143316+313126	2.89093	C III	-80.0	35.0	-19.6	0.6	13.251	0.008	0.008	0	1	161
J143316+313126	2.89093	C IV	-80.0	35.0	-23.9	1.1	13.173	0.015	0.016	0	3	161
J143316+313126	2.89093	H I	-56.3	27.3	-15.4	0.1	15.930	0.003	0.003	0	3	161
J143316+313126	2.89093	O I	-80.0	35.0	999.0	999.0	12.730	0.176	0.301	-1	3	161
J143316+313126	2.89093	O VI	-80.0	35.0	-13.2	0.6	13.885	0.008	0.008	0	1	161
J143316+313126	2.89093	Si II	-80.0	35.0	999.0	999.0	11.254	0.176	0.301	-1	3	161
J143316+313126	2.89093	Si IV	-80.0	35.0	999.0	999.0	12.068	0.176	0.301	-1	3	161
J143316+313126	2.90116	C II	-15.0	15.0	-0.4	1.5	12.426	0.075	0.091	0	1	162
J143316+313126	2.90116	C III	-15.0	15.0	-0.3	0.1	13.274	0.007	0.007	0	1	162
J143316+313126	2.90116	C IV	-15.0	15.0	-0.6	1.1	12.265	0.054	0.062	0	3	162
J143316+313126	2.90116	H I	-25.0	25.0	-0.3	0.1	16.176	0.004	0.002	0	3	162
J143316+313126	2.90116	O I	-15.0	15.0	999.0	999.0	12.476	0.176	0.301	-1	3	162
J143316+313126	2.90116	Si II	-15.0	15.0	3.2	2.5	11.195	0.100	0.131	0	2	162
J143316+313126	2.90116	Si IV	-15.0	15.0	-0.7	0.9	12.109	0.043	0.047	0	3	162
J143316+313126	2.90184	C II	-25.0	20.0	999.0	999.0	12.161	0.176	0.301	-1	3	163

Table 2 continued

Table 2 (*continued*)

Target	z_{abs}	Ion	v_1	v_2	v	σ_v	$\log N$	$\sigma_{\log N}^1$	$\sigma_{\log N}^2$	Detection	Reliability	Unique
			(km s $^{-1}$)	(km s $^{-1}$)	(km s $^{-1}$)	[cm $^{-2}$]	Flag	Flag	ID			
J143316+313126	2.90184	C III	-25.0	20.0	1.8	0.2	13.205	0.007	0.007	0	1	163
J143316+313126	2.90184	C IV	-25.0	20.0	1.0	0.5	12.879	0.017	0.018	0	3	163
J143316+313126	2.90184	H I	-25.0	15.0	-2.8	0.1	15.598	0.014	0.015	0	3	163
J143316+313126	2.90184	O I	-25.0	20.0	999.0	999.0	12.552	0.176	0.301	-1	3	163
J143316+313126	2.90184	Si II	-25.0	20.0	999.0	999.0	10.969	0.176	0.301	-1	3	163
J143316+313126	2.90184	Si IV	-25.0	20.0	999.0	999.0	11.747	0.176	0.301	-1	3	163
J143316+313126	2.90227	C II	-12.0	50.0	999.0	999.0	12.182	0.176	0.301	-1	3	164
J143316+313126	2.90227	C IV	-12.0	50.0	17.0	0.3	13.331	0.008	0.008	0	3	164
J143316+313126	2.90227	H I	-17.0	32.0	1.8	0.2	15.642	0.009	0.011	0	3	164
J143316+313126	2.90227	O I	-12.0	50.0	999.0	999.0	13.846	0.176	0.301	-1	3	164
J143316+313126	2.90227	Si II	-12.0	50.0	999.0	999.0	11.074	0.176	0.301	-1	3	164
J143316+313126	2.90227	Si IV	-12.0	50.0	999.0	999.0	11.510	0.176	0.301	-1	3	164
J143316+313126	2.90645	C II	-35.0	8.0	-16.6	2.3	12.597	0.073	0.088	-1	3	165
J143316+313126	2.90645	C IV	-35.0	8.0	-11.0	1.7	12.483	0.055	0.064	0	1	165
J143316+313126	2.90645	H I	-44.0	44.0	-7.8	0.1	15.271	0.004	0.004	0	3	165
J143316+313126	2.90645	O I	-35.0	8.0	999.0	999.0	12.496	0.176	0.301	-1	3	165
J143316+313126	2.90645	O VI	-35.0	8.0	-16.1	0.6	13.146	0.020	0.020	0	1	165
J143316+313126	2.90645	Si II	-35.0	8.0	999.0	999.0	10.985	0.176	0.301	-1	3	165
J143316+313126	2.90645	Si III	-35.0	8.0	-1.1	3.5	11.356	0.078	0.095	0	1	165
J143316+313126	2.90645	Si IV	-35.0	8.0	999.0	999.0	11.420	0.176	0.301	-1	3	165
J143316+313126	2.92832	C IV	-39.0	15.0	-11.3	2.2	12.917	0.056	0.065	0	1	166
J143316+313126	2.92832	H I	-80.3	48.6	-12.2	0.2	15.099	0.001	0.001	0	3	166
J143316+313126	2.92832	O I	-50.0	20.0	999.0	999.0	13.635	0.176	0.301	-1	3	166
J143316+313126	2.92832	O VI	-50.0	20.0	-12.7	0.3	13.742	0.007	0.007	0	3	166
J143316+313126	2.92832	Si II	-50.0	20.0	-17.9	7.5	11.337	0.145	0.218	-1	3	166
J143316+313126	2.92832	Si IV	-50.0	20.0	999.0	999.0	11.556	0.176	0.301	-1	3	166
J144453+291905	2.32985	Al II	-12.0	100.0	999.0	999.0	10.567	0.176	0.301	-1	3	167
J144453+291905	2.32985	C III	-12.0	100.0	41.8	0.2	13.892	0.006	0.006	0	1	167
J144453+291905	2.32985	C IV	-12.0	100.0	38.5	0.1	13.852	0.002	0.002	0	1	167
J144453+291905	2.32985	Fe II	-12.0	100.0	999.0	999.0	12.126	0.176	0.301	-1	3	167
J144453+291905	2.32985	H I	-31.7	117.3	29.9	0.2	15.128	0.004	0.004	0	3	167
J144453+291905	2.32985	O I	-12.0	100.0	999.0	999.0	13.340	0.176	0.301	-1	3	167
J144453+291905	2.32985	Si II	-12.0	100.0	999.0	999.0	11.746	0.176	0.301	-1	3	167
J144453+291905	2.32985	Si III	-12.0	100.0	45.0	0.7	12.221	0.010	0.010	0	1	167
J144453+291905	2.32985	Si IV	-12.0	100.0	37.6	1.0	12.391	0.013	0.014	0	1	167
J144453+291905	2.37869	Al II	-58.0	5.0	999.0	999.0	16.168	0.176	0.301	-1	3	168
J144453+291905	2.37869	C II	-58.0	5.0	999.0	999.0	16.963	0.176	0.301	-1	3	168
J144453+291905	2.37869	C IV	-58.0	5.0	-30.6	3.2	11.912	0.068	0.080	0	3	168
J144453+291905	2.37869	Fe II	-58.0	5.0	999.0	999.0	12.060	0.176	0.301	-1	3	168
J144453+291905	2.37869	Fe III	-58.0	5.0	999.0	999.0	12.175	0.176	0.301	-1	3	168
J144453+291905	2.37869	H I	-90.9	10.5	-34.8	0.2	15.668	0.002	0.005	0	2	168
J144453+291905	2.37869	O VI	-58.0	5.0	-20.8	0.4	13.391	0.009	0.010	0	1	168
J144453+291905	2.37869	Si II	-58.0	5.0	-24.1	7.5	11.761	0.134	0.195	-1	3	168
J144453+291905	2.37869	Si III	-45.0	15.0	-55.2	17.5	10.822	0.149	0.228	-1	3	168
J144453+291905	2.37869	Si IV	-60.0	1.0	-30.2	5.9	11.221	0.144	0.216	-1	3	168
J144453+291905	2.46741	Al II	-50.0	15.0	-12.1	5.9	10.840	0.120	0.166	-1	3	169
J144453+291905	2.46741	C II	-50.0	15.0	-7.4	0.8	12.769	0.017	0.017	0	1	169

Table 2 continued

Table 2 (*continued*)

Target	z_{abs}	Ion	v_1	v_2	v	σ_v	$\log N$	$\sigma_{\log N}^1$	$\sigma_{\log N}^2$	Detection	Reliability	Unique
			(km s $^{-1}$)	(km s $^{-1}$)	(km s $^{-1}$)	[cm $^{-2}$]	Flag	Flag	ID			
J144453+291905	2.46741	C IV	-50.0	15.0	-9.4	0.2	13.310	0.004	0.004	0	3	169
J144453+291905	2.46741	Fe II	-50.0	15.0	999.0	999.0	11.925	0.176	0.301	-1	3	169
J144453+291905	2.46741	H I	-74.3	8.0	-28.8	0.2	16.802	0.002	0.002	0	3	169
J144453+291905	2.46741	Si II	-50.0	15.0	30.9	20.7	10.714	0.141	0.211	-1	3	169
J144453+291905	2.46741	Si IV	-50.0	15.0	-9.3	0.6	12.689	0.012	0.013	0	1	169
J144453+291905	2.47417	C II	-15.0	15.0	3.0	0.1	13.038	0.006	0.007	0	3	170
J144453+291905	2.47417	C III	-15.0	15.0	1.8	0.1	13.699	0.018	0.019	-2	1	170
J144453+291905	2.47417	C IV	-15.0	15.0	1.9	0.0	13.519	0.003	0.003	0	3	170
J144453+291905	2.47417	Fe II	-15.0	15.0	999.0	999.0	11.770	0.176	0.301	-1	3	170
J144453+291905	2.47417	H I	-15.0	30.0	2.9	0.1	15.209	0.004	0.003	0	3	170
J144453+291905	2.47417	O I	-15.0	15.0	999.0	999.0	11.807	0.176	0.301	-1	3	170
J144453+291905	2.47417	Si II	-15.0	15.0	5.1	3.2	11.762	0.112	0.151	0	1	170
J144453+291905	2.47417	Si III	-6.3	18.6	4.4	0.1	12.782	0.006	0.006	-2	1	170
J144453+291905	2.47417	Si IV	-15.0	15.0	2.2	0.1	12.759	0.007	0.007	0	1	170
J144453+291905	2.55484	Al II	-15.0	15.0	-7.1	3.3	10.641	0.112	0.151	-1	3	171
J144453+291905	2.55484	C II	-15.0	15.0	999.0	999.0	11.522	0.176	0.301	-1	3	171
J144453+291905	2.55484	C III	-15.0	15.0	-0.8	0.1	12.709	0.006	0.006	0	1	171
J144453+291905	2.55484	C IV	-15.0	15.0	-0.3	0.3	12.401	0.015	0.016	0	3	171
J144453+291905	2.55484	Fe II	-15.0	15.0	999.0	999.0	11.814	0.176	0.301	-1	3	171
J144453+291905	2.55484	H I	-40.0	40.0	1.0	0.1	15.618	0.001	0.001	0	3	171
J144453+291905	2.55484	Si II	-15.0	15.0	999.0	999.0	11.509	0.176	0.301	-1	3	171
J144453+291905	2.55484	Si III	-15.0	15.0	4.4	1.3	11.038	0.057	0.065	-1	3	171
J144453+291905	2.55484	Si IV	-15.0	15.0	-1.3	3.0	11.210	0.118	0.162	-1	3	171
J155152+191104	2.35276	Al II	-25.0	12.0	999.0	999.0	9.989	0.176	0.301	-1	3	172
J155152+191104	2.35276	C IV	-25.0	12.0	-8.5	0.6	11.880	0.024	0.025	0	3	172
J155152+191104	2.35276	Fe II	-25.0	12.0	999.0	999.0	11.399	0.176	0.301	-1	3	172
J155152+191104	2.35276	H I	-20.0	20.0	-6.4	0.2	14.990	0.002	0.004	0	3	172
J155152+191104	2.35276	O VI	-25.0	12.0	-8.2	1.4	12.947	0.057	0.066	0	1	172
J155152+191104	2.35276	Si II	-25.0	12.0	2.0	3.5	10.840	0.101	0.132	-1	3	172
J155152+191104	2.35276	Si III	-25.0	12.0	999.0	999.0	10.406	0.176	0.301	-1	3	172
J155152+191104	2.35276	Si IV	-25.0	12.0	999.0	999.0	10.513	0.176	0.301	-1	3	172
J155152+191104	2.69270	C II	-40.0	30.0	2.3	2.0	12.154	0.038	0.041	0	1	173
J155152+191104	2.69270	C III	-40.0	30.0	0.4	0.3	14.161	0.018	0.019	-2	1	173
J155152+191104	2.69270	C IV	-40.0	30.0	-0.0	0.0	13.833	0.001	0.001	0	3	173
J155152+191104	2.69270	H I	-37.0	47.0	1.5	0.1	15.411	0.002	0.002	0	3	173
J155152+191104	2.69270	O I	-40.0	30.0	999.0	999.0	11.867	0.176	0.301	-1	3	173
J155152+191104	2.69270	Si II	-40.0	-1.0	999.0	999.0	10.487	0.176	0.301	-1	3	173
J155152+191104	2.69270	Si III	-40.0	30.0	2.8	0.0	12.822	0.001	0.001	0	1	173
J155152+191104	2.69270	Si IV	-40.0	30.0	0.9	0.1	13.007	0.001	0.001	0	3	173
J155152+191104	2.69478	C II	-30.0	29.0	6.4	3.3	11.834	0.068	0.081	0	1	174
J155152+191104	2.69478	C III	-30.0	29.0	0.1	0.1	13.628	0.004	0.004	0	1	174
J155152+191104	2.69478	C IV	-30.0	29.0	0.8	0.1	13.135	0.002	0.002	0	3	174
J155152+191104	2.69478	H I	-35.0	35.0	-3.3	0.1	16.253	0.002	0.002	0	3	174
J155152+191104	2.69478	O I	-30.0	29.0	999.0	999.0	11.701	0.176	0.301	-1	3	174
J155152+191104	2.69478	O VI	-30.0	29.0	-4.4	0.3	13.412	0.007	0.007	0	1	174
J155152+191104	2.69478	Si II	-30.0	29.0	999.0	999.0	11.195	0.176	0.301	-1	3	174
J155152+191104	2.69478	Si III	-30.0	29.0	2.6	0.1	12.432	0.002	0.002	0	1	174

Table 2 continued

Table 2 (*continued*)

Target	z_{abs}	Ion	v_1	v_2	v	σ_v	$\log N$	$\sigma_{\log N}^1$	$\sigma_{\log N}^2$	Detection	Reliability	Unique
			(km s $^{-1}$)	(km s $^{-1}$)	(km s $^{-1}$)	[cm $^{-2}$]	Flag	Flag	ID			
J155152+191104	2.69478	Si IV	-36.9	24.6	3.3	0.2	12.443	0.004	0.004	0	3	174
J160455+381201	2.53794	Al II	-28.0	20.0	999.0	999.0	10.573	0.176	0.301	-1	3	175
J160455+381201	2.53794	Al III	-28.0	20.0	8.0	8.2	10.942	0.165	0.270	-1	3	175
J160455+381201	2.53794	C II	-28.0	20.0	999.0	999.0	11.747	0.176	0.301	-1	3	175
J160455+381201	2.53794	C IV	-28.0	20.0	-5.4	0.1	13.366	0.002	0.002	0	3	175
J160455+381201	2.53794	H I	-27.3	40.9	-3.7	0.3	15.368	0.005	0.005	0	3	175
J160455+381201	2.53794	O I	-28.0	20.0	999.0	999.0	12.207	0.176	0.301	-1	3	175
J160455+381201	2.53794	O VI	-28.0	20.0	2.5	1.1	13.385	0.030	0.032	0	1	175
J160455+381201	2.53794	Si II	-28.0	20.0	999.0	999.0	10.875	0.176	0.301	-1	3	175
J160455+381201	2.53794	Si IV	-28.0	20.0	-12.1	3.1	11.582	0.069	0.083	0	3	175
J160843+071508	2.42112	Al II	-30.0	20.0	-15.0	4.8	11.040	0.098	0.127	-1	3	176
J160843+071508	2.42112	Al III	-30.0	20.0	999.0	999.0	11.533	0.176	0.301	-1	3	176
J160843+071508	2.42112	C III	-30.0	20.0	-5.1	0.4	13.483	0.037	0.041	0	1	176
J160843+071508	2.42112	C IV	-30.0	20.0	-6.2	0.2	13.363	0.006	0.006	0	3	176
J160843+071508	2.42112	Fe II	-30.0	20.0	999.0	999.0	12.202	0.176	0.301	-1	3	176
J160843+071508	2.42112	H I	-25.0	23.0	1.7	0.5	14.911	0.023	0.019	0	3	176
J160843+071508	2.42112	O I	-30.0	20.0	999.0	999.0	12.440	0.176	0.301	-1	3	176
J160843+071508	2.42112	O VI	-30.0	20.0	1.0	0.9	13.321	0.027	0.029	0	3	176
J160843+071508	2.42112	Si II	-30.0	20.0	-15.1	1.9	11.688	0.046	0.051	-1	3	176
J160843+071508	2.42112	Si III	-30.0	20.0	-3.1	0.6	12.089	0.017	0.018	0	1	176
J160843+071508	2.42112	Si IV	-20.5	3.4	-4.1	0.4	12.054	0.022	0.023	0	1	176
J160843+071508	2.42219	Al II	-30.0	20.0	0.6	5.6	10.865	0.136	0.199	0	1	177
J160843+071508	2.42219	Al III	-30.0	20.0	-5.9	3.7	11.804	0.105	0.139	-1	3	177
J160843+071508	2.42219	C III	-30.0	20.0	0.1	49.3	13.844	0.007	0.007	-2	1	177
J160843+071508	2.42219	C IV	-30.0	20.0	-2.7	0.1	13.389	0.006	0.006	0	3	177
J160843+071508	2.42219	Fe II	-30.0	20.0	999.0	999.0	12.206	0.176	0.301	-1	3	177
J160843+071508	2.42219	H I	-30.0	30.0	1.9	3.9	16.211	0.017	0.013	0	3	177
J160843+071508	2.42219	O I	-30.0	20.0	999.0	999.0	12.410	0.176	0.301	-1	3	177
J160843+071508	2.42219	Si II	-30.0	20.0	-1.6	0.3	12.434	0.010	0.010	0	3	177
J160843+071508	2.42219	Si III	-30.0	20.0	1.6	0.1	13.146	0.012	0.012	-2	1	177
J160843+071508	2.42219	Si IV	-18.4	8.2	-1.1	0.1	12.916	0.004	0.004	0	3	177
J162557+264448	2.53680	Al II	-15.0	15.0	999.0	999.0	10.928	0.176	0.301	-1	3	178
J162557+264448	2.53680	Al III	-15.0	15.0	999.0	999.0	11.536	0.176	0.301	-1	3	178
J162557+264448	2.53680	C II	-15.0	15.0	999.0	999.0	12.304	0.176	0.301	-1	3	178
J162557+264448	2.53680	C III	-15.0	15.0	999.0	999.0	12.010	0.176	0.301	-1	3	178
J162557+264448	2.53680	C IV	-15.0	15.0	999.0	999.0	11.818	0.176	0.301	-1	3	178
J162557+264448	2.53680	Fe II	-15.0	15.0	999.0	999.0	12.421	0.176	0.301	-1	3	178
J162557+264448	2.53680	H I	-55.3	10.8	-24.4	0.8	15.348	0.012	0.013	0	3	178
J162557+264448	2.53680	O I	-15.0	15.0	999.0	999.0	12.755	0.176	0.301	-1	3	178
J162557+264448	2.53680	Si II	-15.0	15.0	999.0	999.0	11.094	0.176	0.301	-1	3	178
J162557+264448	2.53680	Si IV	-15.0	15.0	999.0	999.0	11.665	0.176	0.301	-1	3	178
J162557+264448	2.53680	Zn II	-15.0	15.0	999.0	999.0	11.527	0.176	0.301	-1	3	178
J162557+264448	2.55094	Al II	-50.0	35.0	5.2	1.9	11.981	0.030	0.032	0	1	179
J162557+264448	2.55094	Al III	-50.0	35.0	999.0	999.0	11.756	0.176	0.301	-1	3	179
J162557+264448	2.55094	C II	-50.0	35.0	6.3	0.8	13.816	0.016	0.016	0	1	179
J162557+264448	2.55094	C III	-50.0	35.0	0.4	9.1	14.174	0.008	0.009	-2	1	179
J162557+264448	2.55094	C IV	-50.0	35.0	-1.9	0.3	13.651	0.006	0.006	0	3	179

Table 2 continued

Table 2 (*continued*)

Target	z_{abs}	Ion	v_1	v_2	v	σ_v	$\log N$	$\sigma_{\log N}^1$	$\sigma_{\log N}^2$	Detection	Reliability	Unique
			(km s $^{-1}$)	(km s $^{-1}$)	(km s $^{-1}$)	[cm $^{-2}$]	Flag	Flag	ID			
J162557+264448	2.55094	Fe II	-50.0	35.0	999.0	999.0	12.674	0.176	0.301	-1	3	179
J162557+264448	2.55094	Fe III	-50.0	35.0	999.0	999.0	13.088	0.176	0.301	-1	3	179
J162557+264448	2.55094	H I	-52.9	78.5	9.8	7.8	17.750	0.100	0.100	0	3	179
J162557+264448	2.55094	O I	-50.0	35.0	999.0	999.0	12.962	0.176	0.301	-1	3	179
J162557+264448	2.55094	O VI	-50.0	35.0	999.0	999.0	13.040	0.176	0.301	-1	3	179
J162557+264448	2.55094	Si II	-50.0	35.0	10.7	0.9	12.585	0.014	0.015	0	3	179
J162557+264448	2.55094	Si III	-50.0	35.0	3.8	0.9	13.653	0.026	0.028	-2	1	179
J162557+264448	2.55094	Si IV	-50.0	35.0	3.9	0.4	13.430	0.009	0.010	0	3	179
J162557+264448	2.55094	Zn II	-50.0	35.0	999.0	999.0	12.076	0.176	0.301	-1	3	179
J170100+641209	2.37993	Al II	-25.0	25.0	0.0	2.8	10.550	0.079	0.097	0	1	180
J170100+641209	2.37993	C III	-25.0	25.0	0.4	0.2	13.407	0.010	0.011	0	1	180
J170100+641209	2.37993	C IV	-51.1	23.8	-3.3	0.2	13.091	0.004	0.004	0	3	180
J170100+641209	2.37993	Fe II	-25.0	25.0	999.0	999.0	11.123	0.176	0.301	-1	3	180
J170100+641209	2.37993	H I	-37.5	29.0	-1.2	0.3	15.507	0.005	0.005	0	3	180
J170100+641209	2.37993	O VI	-25.0	25.0	3.0	0.2	13.532	0.007	0.007	0	3	180
J170100+641209	2.37993	Si II	-25.0	25.0	999.0	999.0	10.746	0.176	0.301	-1	3	180
J170100+641209	2.37993	Si III	-25.0	25.0	-0.7	0.4	11.748	0.014	0.014	0	1	180
J170100+641209	2.37993	Si IV	-25.0	25.0	-1.9	0.7	11.732	0.021	0.022	0	3	180
J170100+641209	2.37993	Zn II	-25.0	25.0	999.0	999.0	10.853	0.176	0.301	-1	3	180
J170100+641209	2.43307	Al II	-20.0	12.0	-2.9	0.6	10.897	0.027	0.029	0	1	181
J170100+641209	2.43307	Al III	-20.0	12.0	999.0	999.0	10.626	0.176	0.301	-1	3	181
J170100+641209	2.43307	C II	-20.0	12.0	-2.3	0.1	12.804	0.005	0.005	0	1	181
J170100+641209	2.43307	C III	-20.0	12.0	-1.9	0.8	13.899	0.037	0.041	-2	1	181
J170100+641209	2.43307	C IV	-20.0	12.0	-3.4	0.0	13.272	0.002	0.002	0	1	181
J170100+641209	2.43307	Fe II	-20.0	12.0	999.0	999.0	11.662	0.176	0.301	-1	3	181
J170100+641209	2.43307	Fe III	-20.0	12.0	-10.9	1.8	12.447	0.065	0.076	0	1	181
J170100+641209	2.43307	H I	-34.1	23.9	-4.1	0.3	16.288	0.008	0.008	0	3	181
J170100+641209	2.43307	O I	-20.0	12.0	999.0	999.0	15.011	0.176	0.301	-1	3	181
J170100+641209	2.43307	O VI	-20.0	12.0	-2.4	0.2	13.415	0.007	0.007	0	1	181
J170100+641209	2.43307	Si II	-12.0	12.0	-0.1	0.1	12.015	0.006	0.007	0	3	181
J170100+641209	2.43307	Si III	-20.0	12.0	-0.9	0.0	12.944	0.003	0.003	0	1	181
J170100+641209	2.43307	Si IV	-20.0	12.0	-2.7	0.1	12.632	0.003	0.003	0	1	181
J170100+641209	2.43359	Al II	-28.0	30.0	-16.9	3.6	10.700	0.054	0.062	0	1	182
J170100+641209	2.43359	Al III	-28.0	30.0	999.0	999.0	10.746	0.176	0.301	-1	3	182
J170100+641209	2.43359	C II	-28.0	30.0	-5.4	0.3	12.802	0.007	0.007	0	1	182
J170100+641209	2.43359	C IV	-28.0	30.0	-6.4	0.1	13.126	0.003	0.003	0	1	182
J170100+641209	2.43359	Fe II	-28.0	30.0	999.0	999.0	11.817	0.176	0.301	-1	3	182
J170100+641209	2.43359	Fe III	-28.0	30.0	999.0	999.0	12.069	0.176	0.301	-1	3	182
J170100+641209	2.43359	H I	-22.0	35.0	1.3	0.3	16.401	0.006	0.006	0	3	182
J170100+641209	2.43359	O VI	-28.0	30.0	-3.2	0.3	13.531	0.006	0.006	0	3	182
J170100+641209	2.43359	Si II	-28.0	30.0	-4.5	0.4	12.039	0.008	0.008	0	1	182
J170100+641209	2.43359	Si III	-28.0	30.0	-2.2	0.0	13.145	0.002	0.002	0	1	182
J170100+641209	2.43359	Si IV	-28.0	30.0	-4.9	0.1	12.662	0.003	0.003	0	1	182
J170100+641209	2.43979	Al III	-29.0	15.0	0.0	3.3	11.011	0.094	0.120	-1	3	183
J170100+641209	2.43979	C II	-29.0	15.0	999.0	999.0	11.299	0.176	0.301	-1	3	183
J170100+641209	2.43979	C III	-29.0	15.0	-4.0	0.5	12.614	0.014	0.015	0	1	183
J170100+641209	2.43979	C IV	-29.0	15.0	-8.8	0.2	12.642	0.007	0.007	0	3	183

Table 2 continued

Table 2 (*continued*)

Target	z_{abs}	Ion	v_1	v_2	v	σ_v	$\log N$	$\sigma_{\log N}^1$	$\sigma_{\log N}^2$	Detection	Reliability	Unique
			(km s $^{-1}$)	(km s $^{-1}$)	(km s $^{-1}$)	[cm $^{-2}$]	Flag	Flag	ID			
J170100+641209	2.43979	Fe II	-29.0	15.0	999.0	999.0	11.625	0.176	0.301	-1	3	183
J170100+641209	2.43979	H I	-38.4	38.3	1.4	0.2	15.402	0.004	0.004	0	3	183
J170100+641209	2.43979	O I	-29.0	15.0	999.0	999.0	14.955	0.176	0.301	-1	3	183
J170100+641209	2.43979	O VI	-29.0	15.0	-4.5	0.3	13.746	0.009	0.009	0	1	183
J170100+641209	2.43979	Si II	-29.0	15.0	999.0	999.0	11.256	0.176	0.301	-1	3	183
J170100+641209	2.43979	Si III	-29.0	15.0	-10.6	2.0	11.041	0.055	0.062	-1	1	183
J170100+641209	2.43979	Si IV	-29.0	15.0	999.0	999.0	10.771	0.176	0.301	-1	3	183
J170100+641209	2.43979	Zn II	-29.0	15.0	999.0	999.0	10.774	0.176	0.301	-1	3	183
J170100+641209	2.49647	Al II	-15.0	15.0	999.0	999.0	10.050	0.176	0.301	-1	3	184
J170100+641209	2.49647	Al III	-15.0	15.0	999.0	999.0	10.963	0.176	0.301	-1	3	184
J170100+641209	2.49647	C II	-15.0	15.0	999.0	999.0	11.233	0.176	0.301	-1	3	184
J170100+641209	2.49647	C IV	-20.0	20.0	-0.7	0.4	12.246	0.016	0.017	0	3	184
J170100+641209	2.49647	Fe II	-15.0	15.0	-0.6	2.6	11.842	0.103	0.135	-1	3	184
J170100+641209	2.49647	Fe III	-15.0	15.0	999.0	999.0	12.020	0.176	0.301	-1	3	184
J170100+641209	2.49647	H I	-30.7	27.3	-1.9	0.1	14.622	0.006	0.009	0	3	184
J170100+641209	2.49647	Si II	-15.0	15.0	-8.2	3.8	10.619	0.107	0.143	-1	3	184
J170100+641209	2.49647	Si IV	-15.0	15.0	-4.1	5.9	10.745	0.173	0.291	-1	3	184
J170100+641209	2.49647	Zn II	-15.0	15.0	999.0	999.0	10.737	0.176	0.301	-1	3	184
J170100+641209	2.51255	Al II	-15.0	15.0	-7.1	3.8	10.247	0.129	0.185	-1	3	185
J170100+641209	2.51255	C II	-15.0	15.0	999.0	999.0	11.232	0.176	0.301	-1	3	185
J170100+641209	2.51255	C III	-15.0	15.0	1.4	0.7	12.127	0.032	0.035	-1	3	185
J170100+641209	2.51255	C IV	-15.0	15.0	999.0	999.0	11.351	0.176	0.301	-1	3	185
J170100+641209	2.51255	Fe II	-15.0	15.0	-10.2	3.6	11.829	0.098	0.127	-1	3	185
J170100+641209	2.51255	H I	-88.8	64.8	-14.0	0.2	15.152	0.004	0.004	0	3	185
J170100+641209	2.51255	Si II	-15.0	15.0	-13.1	6.2	10.750	0.146	0.221	-1	3	185
J170100+641209	2.51255	Si III	-15.0	15.0	999.0	999.0	10.436	0.176	0.301	-1	3	185
J170100+641209	2.51255	Si IV	-15.0	15.0	999.0	999.0	10.732	0.176	0.301	-1	3	185
J170100+641209	2.51255	Zn II	-15.0	15.0	999.0	999.0	10.669	0.176	0.301	-1	3	185
J170100+641209	2.59668	Al II	-15.0	15.0	999.0	999.0	10.192	0.176	0.301	-1	3	186
J170100+641209	2.59668	Al III	-15.0	15.0	999.0	999.0	10.678	0.176	0.301	-1	3	186
J170100+641209	2.59668	C II	-15.0	15.0	999.0	999.0	11.336	0.176	0.301	-1	3	186
J170100+641209	2.59668	C III	-15.0	15.0	-0.7	2.8	11.411	0.120	0.167	-1	3	186
J170100+641209	2.59668	C IV	-15.0	15.0	999.0	999.0	11.082	0.176	0.301	-1	3	186
J170100+641209	2.59668	Fe II	-15.0	15.0	999.0	999.0	11.579	0.176	0.301	-1	3	186
J170100+641209	2.59668	H I	-105.8	66.5	-9.4	0.1	15.043	0.004	0.004	0	3	186
J170100+641209	2.59668	O I	-15.0	15.0	999.0	999.0	11.689	0.176	0.301	-1	3	186
J170100+641209	2.59668	O VI	-15.0	15.0	0.0	1.8	12.279	0.090	0.114	-1	3	186
J170100+641209	2.59668	Si II	-15.0	15.0	-5.8	2.7	10.456	0.096	0.124	-1	3	186
J170100+641209	2.59668	Si IV	-15.0	15.0	999.0	999.0	10.728	0.176	0.301	-1	3	186
J170100+641209	2.59668	Zn II	-15.0	15.0	999.0	999.0	10.879	0.176	0.301	-1	3	186
J171227+575507	2.81553	C III	-40.0	20.0	-11.6	1.4	14.074	0.035	0.038	-2	1	187
J171227+575507	2.81553	C IV	-40.0	20.0	-13.4	0.2	13.849	0.005	0.005	0	3	187
J171227+575507	2.81553	Fe II	-40.0	20.0	-8.6	5.2	12.502	0.111	0.150	-1	3	187
J171227+575507	2.81553	H I	-56.3	20.5	-13.6	0.3	15.055	0.004	0.004	0	3	187
J171227+575507	2.81553	Si II	-40.0	20.0	3.7	1.9	11.699	0.038	0.042	-1	3	187
J171227+575507	2.81553	Si III	-44.0	9.2	-11.1	0.3	12.769	0.007	0.008	0	1	187
J171227+575507	2.81553	Si IV	-46.1	36.8	-14.8	1.1	12.610	0.019	0.020	0	3	187

Table 2 continued

Table 2 (*continued*)

Target	z_{abs}	Ion	v_1	v_2	v	σ_v	$\log N$	$\sigma_{\log N}^1$	$\sigma_{\log N}^2$	Detection	Reliability	Unique
			(km s $^{-1}$)	(km s $^{-1}$)	(km s $^{-1}$)	[cm $^{-2}$]	Flag	Flag	ID			
J171227+575507	2.88991	C II	-10.0	15.0	999.0	999.0	11.929	0.176	0.301	-1	3	188
J171227+575507	2.88991	C III	-10.0	15.0	2.0	0.2	13.350	0.016	0.017	0	1	188
J171227+575507	2.88991	C IV	-10.0	15.0	1.5	0.8	12.355	0.049	0.055	0	1	188
J171227+575507	2.88991	Fe II	-10.0	15.0	999.0	999.0	12.149	0.176	0.301	-1	3	188
J171227+575507	2.88991	H I	-48.5	32.9	-2.2	0.2	16.735	0.005	0.005	0	3	188
J171227+575507	2.88991	O I	-10.0	15.0	999.0	999.0	12.270	0.176	0.301	-1	3	188
J171227+575507	2.88991	Si II	-10.0	15.0	999.0	999.0	10.751	0.176	0.301	-1	3	188
J171227+575507	2.88991	Si III	-10.0	15.0	3.4	0.1	12.395	0.008	0.008	0	1	188
J171227+575507	2.88991	Si IV	-10.0	15.0	999.0	999.0	11.697	0.176	0.301	-1	3	188
J171227+575507	2.97141	C II	-30.5	10.9	-9.3	0.7	13.018	0.023	0.024	0	3	189
J171227+575507	2.97141	C III	-37.3	23.2	-4.9	23.0	14.132	0.002	0.002	-2	1	189
J171227+575507	2.97141	C IV	-35.0	20.0	-4.7	0.1	14.202	0.005	0.005	0	3	189
J171227+575507	2.97141	H I	-27.3	15.4	-7.1	0.1	15.454	0.002	0.002	0	3	189
J171227+575507	2.97141	O I	-35.0	20.0	999.0	999.0	12.574	0.176	0.301	-1	3	189
J171227+575507	2.97141	Si II	-35.0	20.0	-12.9	1.5	11.854	0.037	0.041	0	2	189
J171227+575507	2.97141	Si III	-18.7	6.0	-6.1	0.0	13.045	0.006	0.006	0	1	189
J171227+575507	2.97141	Si IV	-35.0	20.0	-6.6	0.2	13.190	0.007	0.007	0	3	189
J173352+540030	3.20694	Al III	-5.0	15.0	4.5	1.5	11.410	0.093	0.119	-1	3	190
J173352+540030	3.20694	C II	-5.0	15.0	5.8	1.2	12.199	0.075	0.091	-1	3	190
J173352+540030	3.20694	C III	-5.0	15.0	3.5	0.2	12.585	0.014	0.015	0	1	190
J173352+540030	3.20694	C IV	-5.0	15.0	999.0	999.0	11.887	0.180	0.300	-1	3	190
J173352+540030	3.20694	Fe II	-5.0	15.0	999.0	999.0	12.057	0.176	0.301	-1	3	190
J173352+540030	3.20694	H I	-54.0	22.0	-8.5	0.2	15.790	0.004	0.004	0	3	190
J173352+540030	3.20694	O I	-5.0	15.0	999.0	999.0	12.270	0.176	0.301	-1	3	190
J173352+540030	3.20694	O VI	-5.0	15.0	5.6	1.9	12.203	0.158	0.250	-1	3	190
J173352+540030	3.20694	Si II	-5.0	15.0	4.0	3.2	11.976	0.171	0.287	-1	3	190
J173352+540030	3.20694	Si IV	-5.0	15.0	4.1	1.2	11.902	0.074	0.089	0	1	190
J173352+540030	3.20694	Zn II	-5.0	15.0	999.0	999.0	11.306	0.176	0.301	-1	3	190
J173352+540030	3.28216	Al II	-15.0	11.0	999.0	999.0	10.594	0.176	0.301	-1	3	191
J173352+540030	3.28216	Al III	-15.0	11.0	999.0	999.0	11.322	0.180	0.300	-1	3	191
J173352+540030	3.28216	C II	-15.0	11.0	999.0	999.0	11.961	0.176	0.301	-1	3	191
J173352+540030	3.28216	C IV	-15.0	11.0	-2.7	0.6	12.721	0.035	0.038	0	1	191
J173352+540030	3.28216	H I	-30.7	52.9	6.1	0.2	16.476	0.002	0.004	0	3	191
J173352+540030	3.28216	O I	-15.0	11.0	999.0	999.0	12.211	0.176	0.301	-1	3	191
J173352+540030	3.28216	Si II	-15.0	11.0	999.0	999.0	10.666	0.176	0.301	-1	3	191
J173352+540030	3.28216	Si III	-15.0	11.0	-0.3	0.2	12.084	0.013	0.014	0	1	191
J173352+540030	3.28216	Si IV	-15.0	11.0	0.8	1.5	11.923	0.080	0.098	0	1	191
J173352+540030	3.30295	C II	-30.0	30.0	999.0	999.0	11.985	0.176	0.301	-1	3	192
J173352+540030	3.30295	C III	-30.0	30.0	-6.3	0.4	12.917	0.012	0.012	-1	3	192
J173352+540030	3.30295	C IV	-30.0	30.0	999.0	999.0	12.147	0.176	0.301	-1	3	192
J173352+540030	3.30295	H I	-37.5	35.8	-2.9	0.2	15.723	0.004	0.002	0	3	192
J173352+540030	3.30295	O I	-30.0	30.0	999.0	999.0	12.523	0.176	0.301	-1	3	192
J173352+540030	3.30295	O VI	-30.0	30.0	-3.5	0.4	13.600	0.009	0.009	0	3	192
J173352+540030	3.30295	Si II	-30.0	30.0	999.0	999.0	10.971	0.176	0.301	-1	3	192
J173352+540030	3.30295	Si III	-30.0	30.0	-0.6	0.3	12.508	0.010	0.010	-1	3	192
J173352+540030	3.30295	Si IV	-30.0	30.0	999.0	999.0	11.483	0.176	0.301	-1	3	192
J193957-100241	3.61935	C II	-30.0	5.0	999.0	999.0	11.755	0.176	0.301	-1	3	193

Table 2 continued

Table 2 (*continued*)

Target	z_{abs}	Ion	v_1	v_2	v	σ_v	$\log N$	$\sigma_{\log N}^1$	$\sigma_{\log N}^2$	Detection	Reliability	Unique
			(km s $^{-1}$)	(km s $^{-1}$)	(km s $^{-1}$)	[cm $^{-2}$]	Flag	Flag	ID			
J193957–100241	3.61935	H I	−39.3	34.1	−12.1	0.1	15.727	0.001	0.001	0	3	193
J193957–100241	3.61935	O I	−30.0	5.0	999.0	999.0	12.225	0.176	0.301	−1	3	193
J193957–100241	3.61935	Si II	−30.0	5.0	999.0	999.0	11.960	0.176	0.301	−1	3	193
J193957–100241	3.61935	Si IV	−30.0	5.0	−10.0	0.3	12.460	0.011	0.012	0	3	193
J212912–153841	2.95558	C II	−20.0	20.0	999.0	999.0	11.986	0.176	0.301	−1	3	194
J212912–153841	2.95558	C IV	−20.0	20.0	0.1	1.1	12.335	0.041	0.045	0	1	194
J212912–153841	2.95558	Fe II	−20.0	20.0	999.0	999.0	12.491	0.176	0.301	−1	3	194
J212912–153841	2.95558	H I	−50.9	21.6	−11.3	0.6	15.220	0.006	0.005	0	3	194
J212912–153841	2.95558	O VI	−20.0	20.0	−5.9	1.7	12.983	0.057	0.065	−1	3	194
J212912–153841	2.95558	Si II	−20.0	20.0	999.0	999.0	11.714	0.176	0.301	−1	3	194
J212912–153841	2.95558	Si IV	−20.0	20.0	999.0	999.0	11.308	0.176	0.301	−1	3	194
J212912–153841	2.96755	C II	−13.0	30.0	4.1	0.5	12.888	0.018	0.019	0	1	195
J212912–153841	2.96755	C IV	−13.0	30.0	8.6	0.2	13.132	0.006	0.006	0	3	195
J212912–153841	2.96755	Fe II	−13.0	30.0	999.0	999.0	12.530	0.176	0.301	−1	3	195
J212912–153841	2.96755	H I	−23.5	27.3	2.2	0.6	17.339	0.087	0.108	0	3	195
J212912–153841	2.96755	Si II	−13.0	30.0	18.5	4.6	12.006	0.109	0.146	0	1	195
J212912–153841	2.96755	Si III	−13.0	30.0	4.2	0.1	12.857	0.007	0.007	0	1	195
J212912–153841	2.96755	Si IV	−13.0	30.0	4.7	0.4	12.500	0.015	0.015	0	3	195
J212912–153841	3.04863	C II	−15.0	15.0	999.0	999.0	11.727	0.176	0.301	−1	3	196
J212912–153841	3.04863	C III	−15.0	15.0	0.6	0.5	12.680	0.026	0.028	−1	3	196
J212912–153841	3.04863	C IV	−15.0	15.0	−1.3	3.9	12.002	0.156	0.247	−1	3	196
J212912–153841	3.04863	H I	−41.4	25.7	−8.1	0.5	15.538	0.009	0.006	0	3	196
J212912–153841	3.04863	O I	−15.0	15.0	999.0	999.0	12.169	0.176	0.301	−1	3	196
J212912–153841	3.04863	O VI	−15.0	15.0	−6.3	3.5	12.739	0.115	0.157	−1	3	196
J212912–153841	3.04863	Si II	−15.0	15.0	999.0	999.0	11.295	0.176	0.301	−1	3	196
J212912–153841	3.04863	Si IV	−15.0	15.0	999.0	999.0	11.484	0.176	0.301	−1	3	196
J212912–153841	3.21670	C II	−25.0	15.0	−8.5	4.0	12.120	0.123	0.173	−1	3	197
J212912–153841	3.21670	H I	−64.6	10.7	−14.1	0.4	15.852	0.004	0.004	0	3	197
J212912–153841	3.21670	O I	−25.0	15.0	999.0	999.0	12.241	0.176	0.301	−1	3	197
J212912–153841	3.21670	O VI	−25.0	15.0	−1.6	0.6	13.185	0.021	0.022	−1	3	197
J212912–153841	3.21670	Si II	−25.0	15.0	999.0	999.0	10.784	0.176	0.301	−1	3	197
J212912–153841	3.21670	Si III	−25.0	15.0	−6.9	0.2	12.334	0.007	0.007	0	1	197
J212912–153841	3.21670	Si IV	−25.0	15.0	−9.0	0.8	12.215	0.026	0.028	0	1	197
J220852–194400	2.54217	C IV	−35.0	50.0	−3.1	1.4	12.690	0.024	0.025	0	3	198
J220852–194400	2.54217	Fe II	−35.0	5.0	999.0	999.0	12.199	0.176	0.301	−1	3	198
J220852–194400	2.54217	Fe III	−35.0	5.0	999.0	999.0	12.473	0.176	0.301	−1	3	198
J220852–194400	2.54217	H I	−83.6	46.1	−3.8	0.1	14.903	0.004	0.004	0	3	198
J220852–194400	2.54217	O I	−35.0	5.0	999.0	999.0	12.169	0.176	0.301	−1	3	198
J220852–194400	2.54217	Si II	−35.0	5.0	999.0	999.0	10.715	0.176	0.301	−1	3	198
J220852–194400	2.54217	Si III	−35.0	50.0	14.1	5.4	11.245	0.098	0.127	−1	3	198
J220852–194400	2.54217	Si IV	−35.0	5.0	999.0	999.0	11.244	0.176	0.301	−1	3	198
J222256–094636	2.86475	C IV	−35.0	50.0	0.6	1.3	13.619	0.022	0.023	0	1	199
J222256–094636	2.86475	H I	−37.5	32.4	−1.0	2.5	17.300	0.200	0.050	0	3	199
J222256–094636	2.86475	O I	−35.0	50.0	999.0	999.0	12.896	0.176	0.301	−1	3	199
J222256–094636	2.86475	Si II	−35.0	50.0	999.0	999.0	12.506	0.176	0.301	−1	3	199
J222256–094636	2.86475	Si IV	−35.0	50.0	1.6	0.8	13.225	0.013	0.013	0	1	199
J222256–094636	2.87419	C IV	−15.0	15.0	1.7	2.1	12.437	0.087	0.109	−1	3	200

Table 2 continued

Table 2 (*continued*)

Target	z_{abs}	Ion	v_1	v_2	v	σ_v	$\log N$	$\sigma_{\log N}^1$	$\sigma_{\log N}^2$	Detection	Reliability	Unique
			(km s $^{-1}$)	(km s $^{-1}$)	(km s $^{-1}$)	[cm $^{-2}$]	Flag	Flag	ID			
J222256–094636	2.87419	H I	−32.4	45.5	9.1	1.1	15.755	0.015	0.016	0	3	200
J222256–094636	2.87419	O I	−15.0	15.0	999.0	999.0	12.686	0.176	0.301	−1	3	200
J222256–094636	2.87419	O VI	−15.0	15.0	999.0	999.0	12.419	0.176	0.301	−1	3	200
J222256–094636	2.87419	Si II	−15.0	15.0	999.0	999.0	11.215	0.176	0.301	−1	3	200
J222256–094636	2.87419	Si IV	−15.0	15.0	999.0	999.0	11.597	0.176	0.301	−1	3	200
J234628+124859	2.54133	Al II	−40.0	1.0	999.0	999.0	10.482	0.176	0.301	−1	3	201
J234628+124859	2.54133	Al III	−40.0	1.0	999.0	999.0	11.017	0.176	0.301	−1	3	201
J234628+124859	2.54133	C II	−40.0	1.0	999.0	999.0	11.636	0.176	0.301	−1	3	201
J234628+124859	2.54133	C IV	−40.0	1.0	−21.4	1.2	12.329	0.047	0.053	0	1	201
J234628+124859	2.54133	Fe II	−40.0	1.0	999.0	999.0	11.923	0.176	0.301	−1	3	201
J234628+124859	2.54133	Fe III	−40.0	1.0	−23.6	2.6	12.680	0.079	0.097	0	1	201
J234628+124859	2.54133	H I	−12.0	23.9	−19.4	0.2	15.122	0.004	0.004	0	3	201
J234628+124859	2.54133	O I	−40.0	1.0	−18.9	7.2	12.111	0.172	0.289	−1	3	201
J234628+124859	2.54133	Si II	−40.0	1.0	999.0	999.0	11.521	0.176	0.301	−1	3	201
J234628+124859	2.54133	Si IV	−40.0	1.0	999.0	999.0	10.968	0.176	0.301	−1	3	201
J234628+124859	2.54133	Zn II	−40.0	1.0	999.0	999.0	11.146	0.176	0.301	−1	3	201
J234856–104131	3.15981	C II	−8.0	31.0	999.0	999.0	12.506	0.176	0.301	−1	3	202
J234856–104131	3.15981	H I	−39.0	30.0	7.2	0.4	16.287	0.006	0.006	0	3	202
J234856–104131	3.15981	O I	−8.0	31.0	999.0	999.0	12.889	0.176	0.301	−1	3	202
J234856–104131	3.15981	Si II	−8.0	31.0	999.0	999.0	11.459	0.176	0.301	−1	3	202
J234856–104131	3.15981	Si III	−8.0	31.0	10.8	0.4	12.401	0.017	0.017	0	1	202
J234856–104131	3.15981	Si IV	−8.0	31.0	−2.1	3.8	12.227	0.085	0.106	0	2	202

NOTE—A 999.0 value corresponds to a non-detection and the upper limit on the column density is quoted at the 2σ level. The detection flag has the following definition: 0 = detection; −1 = upper limit (non-detection); −2 = detection but a lower limit owing to saturation of the line. Depending if a single or several transitions were detected, a reliability flag is assigned as follows: 1 = most reliable: results based on several transitions or a non-detection (a non-detection always reliable since it is estimated in an uncontaminated region of the spectrum); 2 = reliable: results based on at least two transitions, but where only one transition is detected at the 2σ level and the upper limits agree with that detection; 3 = less reliable: results based only on a single transition or several saturated transitions.

Table 3. Summary of the H I Fit Results

Target	z_{abs}	Comp.	v	σ_v	b	σ_b	$\log N$	$\sigma_{\log N}$
			(km s $^{-1}$)	[cm $^{-2}$]				
J002127–020333	2.54918	1	−5.6	0.2	32.5	0.2	15.672	0.016
J003501–091817	2.35342	1	9.1	0.6	29.1	0.7	15.560	0.030
J004530–261709	2.81907	1	−25.8	1.1	74.0	0.5	19.664	0.010
J004530–261709	3.24823	1	−2.1	0.2	25.1	0.2	15.081	0.016
J004530–261709	3.36517	1	−18.6	0.4	53.2	0.6	15.538	0.016
J004530–261709	3.36517	2	5.3	1.4	16.0	1.3	15.368	0.055
J005700+143737	2.54721	1	−30.9	1.4	55.8	1.9	15.062	0.018
J010311+131617	2.54303	1	−0.5	0.1	27.9	0.1	15.629	0.010
J010311+131617	2.55125	1	11.5	0.6	31.9	0.5	14.900	0.010
J010311+131617	2.55125	2	76.9	0.2	28.9	0.3	15.502	0.010
J010806+163550	2.31582	1	−12.1	0.1	28.3	0.1	14.540	0.010
J010806+163550	2.46164	1	4.7	0.1	29.7	0.1	14.721	0.010
J010806+163550	2.48359	1	1.6	0.4	30.3	0.5	15.318	0.010

Table 3 continued

Table 3 (*continued*)

Target	z_{abs}	Comp.	v	σ_v	b	σ_b	$\log N$	$\sigma_{\log N}$
			(km s $^{-1}$)	[cm $^{-2}$]				
J010806+163550	2.50561	1	-0.9	0.1	23.9	0.1	15.901	0.010
J010925-210257	2.96546	1	-7.4	0.3	24.4	0.3	14.744	0.013
J010925-210257	3.14253	1	-1.3	0.4	23.1	0.5	16.147	0.013
J011150+140141	2.42374	1	0.8	1.3	36.0	1.7	14.818	0.026
J012156+144823	2.41837	1	-15.7	0.1	31.4	0.2	14.824	0.010
J012156+144823	2.46812	1	-13.1	0.1	26.2	0.1	14.903	0.011
J012156+144823	2.53765	1	-20.2	0.1	29.3	0.1	15.086	0.010
J012156+144823	2.62486	1	-18.8	0.1	28.5	0.1	14.973	0.010
J012156+144823	2.66022	1	0.0	0.1	29.7	0.1	14.788	0.010
J012156+144823	2.66022	2	164.9	0.1	26.0	0.1	19.084	0.010
J012156+144823	2.66022	3	188.4	0.1	54.2	0.1	17.021	0.010
J012156+144823	2.66022	4	318.4	0.1	48.3	0.1	17.257	0.010
J012156+144823	2.66022	5	463.8	0.1	28.9	0.1	16.232	0.010
J012156+144823	2.81222	1	-24.9	0.1	34.6	0.1	14.606	0.010
J014516-094517	2.49969	1	-8.8	0.1	32.8	0.1	15.045	0.010
J014516-094517	2.58808	1	-12.8	0.1	34.5	0.1	15.083	0.010
J014516-094517	2.66513	1	1.9	0.1	25.7	0.1	16.169	0.010
J014516-094517	2.66911	1	-21.0	0.1	31.9	0.1	15.449	0.010
J014516-094517	2.69212	1	-30.8	0.1	30.0	0.1	15.444	0.010
J014516-094517	2.69430	1	-5.4	0.1	25.8	0.1	14.711	0.010
J014516-094517	2.70685	1	-10.2	0.1	32.5	0.1	15.112	0.010
J015741-010629	3.36274	1	-10.9	0.3	27.0	0.3	15.109	0.019
J020455+364917	2.53103	1	-15.5	0.2	31.9	0.3	14.449	0.011
J020950-000506	2.41125	1	-39.6	1.2	42.5	0.7	14.810	0.014
J020950-000506	2.41125	2	17.2	1.0	32.2	0.5	14.591	0.023
J020950-000506	2.57449	1	-1.8	0.1	25.6	0.1	16.853	0.010
J020950-000506	2.64137	1	-11.2	0.2	26.9	0.3	15.362	0.010
J020950-000506	2.76903	1	-0.5	0.1	24.4	0.1	15.781	0.010
J023359+004938	2.48836	1	-14.9	1.3	28.1	1.6	14.628	0.029
J025905+001121	3.12722	1	-10.9	0.1	26.4	0.1	15.019	0.012
J025905+001121	3.22368	1	-11.2	0.3	32.1	0.4	15.115	0.010
J025905+001121	3.30796	1	-9.4	0.4	25.7	0.5	15.780	0.015
J030341-002321	2.44326	1	-4.2	1.1	80.7	0.6	19.866	0.010
J030341-002321	2.93700	1	-16.4	0.3	38.1	0.3	15.683	0.010
J030341-002321	2.95653	1	-13.5	1.2	19.8	1.5	15.793	0.054
J030341-002321	2.95653	2	7.1	1.3	38.1	0.7	15.998	0.032
J030341-002321	2.99495	1	-14.8	0.3	37.9	0.4	16.177	0.010
J030341-002321	3.10354	1	-3.1	0.4	26.1	0.6	15.506	0.017
J030341-002321	3.10937	1	-10.5	0.1	24.5	0.1	14.795	0.010
J030341-002321	3.15168	1	-5.2	0.1	22.8	0.1	15.447	0.010
J033900-013318	3.11542	1	-13.7	1.3	65.8	0.8	19.600	0.010
J045213-164012	2.39910	1	-13.5	0.2	38.1	0.3	15.182	0.010
J045213-164012	2.44044	1	1.9	0.1	24.9	0.1	14.595	0.010
J045213-164012	2.53542	1	-15.7	0.1	28.1	0.1	14.682	0.010
J064204+675835	2.86842	1	-46.4	1.6	33.5	0.8	14.857	0.027
J064204+675835	2.86842	2	16.7	0.5	30.1	0.2	15.854	0.016
J064204+675835	3.01338	1	-5.6	0.6	18.1	0.6	15.386	0.022
J064204+675835	3.01338	2	11.7	0.2	37.9	0.2	15.653	0.010

Table 3 continued

Table 3 (*continued*)

Target	z_{abs}	Comp.	v	σ_v	b	σ_b	$\log N$	$\sigma_{\log N}$
			(km s $^{-1}$)	[cm $^{-2}$]				
J064204+675835	3.06746	1	0.8	0.1	25.4	0.2	15.302	0.010
J073149+285448	3.42673	1	-13.0	0.3	24.5	0.2	14.663	0.012
J074521+473436	2.85216	1	1.8	0.1	35.0	0.1	14.623	0.010
J074521+473436	2.85216	2	7.8	0.4	18.2	0.6	14.275	0.021
J074521+473436	2.96558	1	-11.9	0.2	60.8	0.4	14.578	0.010
J074521+473436	2.96558	2	0.8	0.2	22.3	0.3	14.503	0.010
J074521+473436	3.03515	1	13.2	0.9	37.4	3.1	16.150	0.116
J074521+473436	3.03515	2	17.1	0.3	21.5	0.8	16.598	0.041
J074521+473436	3.05358	1	-17.8	0.4	21.5	0.4	16.532	0.019
J074521+473436	3.05358	2	-9.3	0.1	32.9	0.1	16.349	0.017
J074521+473436	3.12615	1	-15.9	0.1	24.7	0.1	15.076	0.010
J074749+443417	4.35301	1	-4.4	0.2	28.1	0.1	15.915	0.013
J080117+521034	3.04028	1	-541.5	0.2	40.5	0.4	15.054	0.025
J080117+521034	3.04028	2	-78.4	0.9	51.7	0.4	19.689	0.010
J080117+521034	3.04028	3	290.2	1.0	35.4	0.4	19.255	0.024
J080117+521034	3.04028	4	497.1	0.9	19.3	0.3	19.116	0.012
J080117+521034	3.04028	5	633.6	0.7	14.6	1.1	15.790	0.289
J080117+521034	3.04028	6	823.7	0.2	31.6	0.4	13.873	0.010
J081240+320808	2.58869	1	-4.2	0.1	23.8	0.1	15.912	0.014
J082107+310751	2.24571	1	-8.3	0.1	31.9	0.1	14.839	0.010
J082107+310751	2.55190	1	-42.8	0.5	26.9	0.3	15.579	0.010
J082107+310751	2.55190	2	9.3	2.9	37.5	1.8	14.818	0.043
J082107+310751	2.55652	1	-9.7	0.2	27.9	0.3	15.186	0.010
J083102+335803	2.41864	1	-4.5	0.2	31.0	0.3	15.206	0.022
J090033+421546	3.08569	1	-11.5	0.2	27.1	0.2	15.011	0.013
J090033+421546	3.15992	1	-20.6	0.3	28.4	0.4	15.048	0.012
J093337+284532	3.37217	1	-10.2	0.5	27.5	0.7	15.294	0.035
J093643+292713	2.40065	1	8.4	0.4	64.7	0.4	15.850	0.016
J093643+292713	2.41258	1	-4.0	0.3	28.5	0.3	16.152	0.032
J093643+292713	2.54337	1	4.5	0.7	34.5	0.8	15.888	0.015
J093643+292713	2.58243	1	-15.1	0.4	32.5	0.5	15.191	0.015
J093643+292713	2.59624	1	-11.1	0.7	55.1	0.4	15.534	0.019
J093643+292713	2.59624	2	32.6	0.8	27.4	0.6	15.855	0.018
J093643+292713	2.69883	1	29.2	0.5	33.6	0.5	15.600	0.011
J094202+042244	2.60246	1	-15.3	0.2	27.8	0.2	15.187	0.010
J094202+042244	2.60246	2	53.4	1.0	27.4	0.9	13.635	0.019
J094202+042244	2.72833	1	-13.8	0.6	20.0	0.4	14.648	0.013
J094202+042244	2.72833	2	19.7	0.5	13.3	0.6	14.517	0.018
J094202+042244	2.72833	3	122.2	0.4	19.7	0.3	16.171	0.011
J094202+042244	2.72833	4	162.7	0.8	79.0	1.3	15.656	0.028
J094202+042244	2.72833	5	203.6	0.2	27.2	0.2	17.087	0.010
J094202+042244	2.81325	1	-0.7	0.8	16.7	1.3	15.238	0.023
J094202+042244	2.81325	2	57.7	1.0	17.0	1.1	15.750	0.026
J094202+042244	2.81325	3	90.2	2.5	15.5	2.4	15.222	0.082
J094202+042244	2.84851	1	-8.4	0.6	27.0	1.0	15.151	0.025
J094202+042244	2.84851	2	29.5	5.0	76.5	4.5	15.235	0.021
J094202+042244	3.09385	1	-43.3	0.1	30.8	0.2	15.875	0.010
J095852+120245	3.09623	1	-1.3	0.7	21.4	0.6	17.134	0.033

Table 3 continued

Table 3 (*continued*)

Target	z_{abs}	Comp.	v	σ_v	b	σ_b	$\log N$	$\sigma_{\log N}$
			(km s $^{-1}$)	[cm $^{-2}$]				
J095852+120245	3.09623	2	55.7	2.6	28.7	1.9	16.374	0.037
J095852+120245	3.15768	1	-12.0	0.1	33.6	0.1	15.511	0.010
J095852+120245	3.22317	1	0.8	0.1	22.9	0.2	17.354	0.010
J100841+362319	2.76763	1	-10.1	0.2	34.3	0.2	14.950	0.010
J100841+362319	2.94749	1	-79.0	0.1	23.6	0.1	15.250	0.010
J100841+362319	2.94749	2	11.0	0.1	19.4	0.1	19.721	0.010
J100841+362319	2.94749	3	130.9	0.1	29.2	0.1	16.565	0.010
J100841+362319	3.01081	1	-15.5	0.2	36.5	0.2	15.147	0.012
J100841+362319	3.03460	1	-20.6	0.5	31.6	0.7	15.341	0.010
J100841+362319	3.07200	1	-26.0	0.3	36.8	0.4	15.485	0.010
J100841+362319	3.10854	1	-14.9	0.4	21.3	0.5	15.389	0.010
J101155+294141	2.50364	1	-0.2	0.1	20.3	0.1	17.414	0.010
J101447+430030	2.84090	1	-17.6	0.1	26.9	0.1	15.333	0.010
J101447+430030	2.98705	1	-18.2	0.1	34.0	0.1	15.182	0.010
J101447+430030	3.01439	1	0.2	0.1	23.5	0.1	16.670	0.010
J101447+430030	3.11460	1	-12.7	0.1	22.0	0.1	15.991	0.010
J101723-204658	2.45051	1	0.0	0.1	23.6	0.2	17.279	0.010
J102009+104002	3.05498	1	-62.8	0.4	22.1	0.3	17.294	0.028
J102009+104002	3.05498	2	-3.3	0.9	32.8	0.5	16.457	0.013
J104018+572448	3.27747	1	-5.2	0.4	27.0	0.5	15.786	0.012
J104018+572448	3.32379	1	-10.2	0.6	26.2	0.8	15.709	0.014
J104018+572448	3.34454	1	-16.0	0.9	34.4	1.1	16.083	0.013
J104018+572448	3.36421	1	-5.6	0.4	26.5	0.5	15.598	0.010
J105756+455553	3.69194	1	-13.7	0.1	25.6	0.1	14.714	0.010
J113418+574204	3.34514	1	-12.6	0.3	32.6	0.4	15.196	0.010
J113418+574204	3.46347	1	-16.7	0.2	28.3	0.3	15.146	0.010
J113508+222715	2.74242	1	-16.6	0.3	29.3	0.4	15.044	0.013
J120006+312630	2.84264	1	-20.0	0.3	27.7	0.4	14.779	0.010
J120006+312630	2.87577	1	-15.2	0.4	24.1	0.4	16.549	0.037
J121930+494052	2.22541	1	-15.0	0.7	68.5	0.9	15.009	0.010
J121930+494052	2.22541	2	6.3	1.1	26.8	1.8	14.420	0.041
J121930+494052	2.27897	1	-11.6	0.2	27.3	0.3	14.944	0.010
J121930+494052	2.47346	1	3.9	0.1	23.3	0.1	15.074	0.010
J121930+494052	2.47816	1	0.8	0.2	28.2	0.3	16.016	0.010
J121930+494052	2.52850	1	-9.1	0.1	27.2	0.1	15.101	0.010
J121930+494052	2.54882	1	-18.2	0.1	27.8	0.1	15.594	0.010
J121930+494052	2.57078	1	-7.9	0.1	33.6	0.1	15.106	0.010
J121930+494052	2.57761	1	1.0	0.1	29.5	0.1	15.057	0.010
J121930+494052	2.62063	1	-14.8	0.1	24.9	0.1	15.917	0.010
J124610+303131	2.46655	1	-9.4	0.3	33.3	0.3	15.270	0.010
J130411+295348	2.57585	1	0.1	0.1	18.2	0.1	15.550	0.014
J130411+295348	2.57726	1	-2.5	0.5	21.2	0.6	15.038	0.017
J130411+295348	2.75550	1	4.5	0.4	32.2	0.5	15.087	0.010
J130411+295348	2.79811	1	-20.8	0.3	34.0	0.3	15.918	0.010
J130411+295348	2.82924	1	-1.5	0.1	18.8	0.2	16.385	0.010
J131215+423900	2.41504	1	0.0	0.3	25.8	0.3	15.610	0.011
J131215+423900	2.48998	1	0.7	0.2	21.3	0.2	16.791	0.010
J134328+572147	2.79941	1	-10.2	0.8	38.3	1.0	15.338	0.012

Table 3 continued

Table 3 (*continued*)

Target	z_{abs}	Comp.	v	σ_v	b	σ_b	$\log N$	$\sigma_{\log N}$
			(km s $^{-1}$)	[cm $^{-2}$]				
J134328+572147	2.83437	1	1.2	0.1	17.7	0.1	18.180	0.010
J134328+572147	2.87056	1	-9.4	1.1	32.6	1.4	16.301	0.017
J134544+262506	2.86367	1	-3.7	0.3	24.8	0.3	16.333	0.011
J135038-251216	2.37059	1	-15.6	0.8	44.5	0.9	14.839	0.025
J135038-251216	2.37059	2	-2.9	0.9	21.6	1.4	14.562	0.049
J135038-251216	2.44516	1	13.4	0.8	36.0	1.1	15.267	0.011
J135038-251216	2.57299	1	-0.8	0.3	34.8	0.4	16.335	0.010
J135038-251216	2.57455	1	-3.9	0.1	15.5	0.1	15.045	0.010
J142438+225600	3.33427	1	-39.9	0.3	42.9	0.2	14.461	0.010
J142438+225600	3.33427	2	-10.7	0.1	23.2	0.1	14.862	0.010
J142438+225600	3.38281	1	-2.5	0.4	14.9	0.5	17.006	0.013
J142438+225600	3.44848	1	7.9	0.1	21.8	0.2	16.103	0.010
J142438+225600	3.53989	1	7.1	0.1	21.9	0.1	16.128	0.010
J142438+225600	3.56653	1	8.6	0.1	23.1	0.1	15.569	0.010
J143316+313126	2.58177	1	-3.6	0.1	25.7	0.1	15.885	0.010
J143316+313126	2.58591	1	-3.3	0.1	33.5	0.1	18.152	0.010
J143316+313126	2.58591	2	179.1	0.2	37.1	0.2	15.278	0.010
J143316+313126	2.61282	1	-18.6	0.3	46.2	0.3	15.536	0.010
J143316+313126	2.64432	1	-18.5	0.1	24.1	0.1	16.135	0.010
J143316+313126	2.73377	1	-12.5	0.1	30.9	0.1	15.564	0.010
J143316+313126	2.74931	1	-5.1	0.2	28.7	0.2	15.321	0.010
J143316+313126	2.77502	1	-17.9	0.1	49.9	0.1	15.087	0.010
J143316+313126	2.88759	1	-11.2	0.1	34.6	0.1	15.314	0.010
J143316+313126	2.89093	1	-16.9	0.2	35.1	0.2	15.956	0.010
J143316+313126	2.90116	1	-0.6	0.2	21.0	0.3	16.211	0.010
J143316+313126	2.90116	2	48.0	0.7	15.5	1.1	15.556	0.032
J143316+313126	2.90116	3	84.3	0.9	21.1	1.0	15.705	0.020
J143316+313126	2.90645	1	-8.9	0.2	32.2	0.3	15.291	0.010
J143316+313126	2.92832	1	-11.0	0.1	30.5	0.1	15.099	0.010
J144453+291905	2.32985	1	28.1	0.1	40.0	0.2	15.154	0.010
J144453+291905	2.37869	1	-36.3	0.2	25.6	0.1	15.602	0.010
J144453+291905	2.37869	2	22.0	0.5	30.0	0.3	14.908	0.010
J144453+291905	2.46741	1	-23.2	0.1	26.9	0.1	16.799	0.010
J144453+291905	2.47417	1	2.4	0.1	15.0	0.1	15.211	0.010
J144453+291905	2.55484	1	2.1	0.1	28.5	0.1	15.612	0.010
J155152+191104	2.35276	1	-6.6	0.2	28.2	0.2	14.990	0.010
J155152+191104	2.69270	1	-5.0	0.3	50.0	0.6	15.073	0.010
J155152+191104	2.69270	2	3.2	0.1	20.8	0.2	15.241	0.010
J155152+191104	2.69478	1	3.6	0.3	30.1	0.5	16.249	0.010
J160455+381201	2.53794	1	-2.3	0.1	25.6	0.1	15.374	0.010
J160843+071508	2.42112	1	-3.1	0.2	19.2	0.3	14.640	0.010
J160843+071508	2.42219	1	-0.7	0.3	17.1	0.3	16.179	0.016
J162557+264448	2.53680	1	-86.0	2.3	14.9	3.3	14.246	0.089
J162557+264448	2.53680	2	-21.8	1.1	35.9	1.4	15.335	0.017
J162557+264448	2.55094	1	2.1	0.1	25.0	0.1	17.750	0.010
J170100+641209	2.37993	1	-2.1	0.2	26.2	0.3	15.528	0.010
J170100+641209	2.43307	1	-0.0	1.2	28.8	1.0	16.317	0.020
J170100+641209	2.43307	2	49.2	0.8	24.1	0.6	16.388	0.017

Table 3 continued

Table 3 (*continued*)

Target	z_{abs}	Comp.	v	σ_v	b	σ_b	$\log N$	$\sigma_{\log N}$
			(km s $^{-1}$)	[cm $^{-2}$]				
J170100+641209	2.43979	1	-4.5	0.4	37.4	0.5	15.462	0.010
J170100+641209	2.49647	1	-2.0	0.2	31.5	0.4	14.689	0.010
J170100+641209	2.51255	1	-16.5	0.1	31.0	0.1	15.180	0.010
J170100+641209	2.59668	1	-49.7	1.5	56.6	1.0	14.480	0.015
J170100+641209	2.59668	2	-4.4	0.1	27.3	0.2	15.027	0.010
J171227+575507	2.81553	1	-13.7	0.2	29.8	0.2	15.060	0.010
J171227+575507	2.88991	1	-2.9	0.1	23.4	0.1	16.757	0.010
J171227+575507	2.97141	1	-8.0	0.1	18.6	0.1	15.478	0.010
J173352+540030	3.20694	1	-7.5	0.1	25.2	0.1	15.750	0.010
J173352+540030	3.28216	1	5.1	0.1	23.5	0.1	16.476	0.010
J173352+540030	3.30295	1	-3.9	0.2	26.8	0.2	15.781	0.010
J193957-100241	3.61935	1	-11.8	0.1	24.9	0.1	15.735	0.010
J212912-153841	2.95558	1	-8.2	0.1	28.1	0.1	15.206	0.010
J212912-153841	2.96755	1	0.2	0.1	26.0	0.1	17.320	0.010
J212912-153841	3.04863	1	-12.1	0.2	28.4	0.2	15.462	0.010
J212912-153841	3.21670	1	-12.7	0.3	35.0	0.3	15.846	0.010
J220852-194400	2.54217	1	-3.2	0.1	28.7	0.1	14.901	0.010
J222256-094636	2.86475	1	-10.1	0.6	37.0	0.8	16.913	0.031
J222256-094636	2.86475	2	-9.7	0.3	57.4	0.8	15.921	0.056
J222256-094636	2.86475	3	0.7	0.6	16.8	0.9	17.224	0.047
J222256-094636	2.87419	1	9.0	0.8	34.4	1.1	15.787	0.014
J234628+124859	2.54133	1	-21.4	0.2	28.0	0.2	15.096	0.010
J234856-104131	3.15981	1	7.2	0.5	31.5	0.5	16.336	0.011

NOTE—The redshift between parentheses in the second column indicates the actual redshift of the absorber associated with that velocity component.

Table 4. Metallicities of the Absorbers in KODIAQ-Z Sample

QSO Name	z_{abs}	$\log N_{\text{H I}}$	[X/H]	$\log U$	[C/ α]
		[cm $^{-2}$]			
J010806+163550	2.31582	14.574 ± 0.004	$<-4.738, <-3.675, <-2.475$	-2.117, -1.521:, -0.945	...
J045213-164012	2.44044	14.611 ± 0.004	$<-4.739, <-3.688, <-2.568$	-2.141, -1.540:, -0.910	...
J170100+641209	2.49647	14.622 ± 0.007	-2.425, -2.069, -1.776	-1.743, -1.470, -1.222	-0.460, -0.099:, +0.264
J023359+004938	2.48836	14.640 ± 0.019	$<-4.723, <-3.594, <-2.517$	-2.098, -1.503:, -0.942	...
J073149+285448	3.42673	14.653 ± 0.008	$<-4.743, <-3.677, <-2.418$	-2.165, -1.557:, -0.954	...
J045213-164012	2.53542	14.674 ± 0.003	$<-4.790, <-3.922, <-3.079$	-2.109, -1.492:, -0.914	...
J012156+144823	2.81222	14.683 ± 0.002	$<-4.777, <-3.941, <-3.014$	-2.126, -1.567:, -0.976	...
J105756+455553	3.69194	14.698 ± 0.003	$<-4.754, <-3.776, <-2.567$	-2.198, -1.603:, -1.011	...
J010925-210257	2.96546	14.706 ± 0.008	-2.840, -2.632, -2.263	-0.797, -0.561, -0.362	-0.754, -0.428:, -0.071
J014516-094517	2.69430	14.708 ± 0.002	-2.809, -2.269, -1.832	-2.031, -1.685, -1.335	-0.291, +0.020:, +0.355
J074521+473436	2.85216	14.723 ± 0.004	-2.590, -2.205, -1.890	-1.660, -1.395:, -1.134	-0.499, -0.122:, +0.251
J010806+163550	2.46164	14.754 ± 0.002	$<-4.722, <-3.651, <-2.500$	-2.138, -1.515:, -0.913	...
J074521+473436	2.96558	14.761 ± 0.003	-1.021, -0.868, -0.692	-2.560, -2.544, -2.527	+0.629, +0.785:, +0.918
J030341-002321	3.10937	14.766 ± 0.004	$<-4.789, <-3.992, <-3.158$	-2.125, -1.520:, -0.921	...
J011150+140141	2.42374	14.803 ± 0.020	-0.572, -0.476, -0.376	-1.635, -1.598, -1.559	-0.977, -0.914:, -0.799
J120006+312630	2.84264	14.804 ± 0.010	-0.594, -0.578, -0.564	-1.272, -1.269, -1.266	-1.000, -1.000, -0.999

Table 4 continued

Table 4 (*continued*)

QSO Name	z_{abs}	$\log N_{\text{HI}}$ [cm $^{-2}$]	[X/H]	$\log U$	[C/ α]
J012156+144823	2.66022	14.828 ± 0.021	<-4.791, <-4.012, <-2.977	-2.231, -1.626:, -0.987	...
J012156+144823	2.41837	14.829 ± 0.007	-1.737, -1.581, -1.447	-1.819, -1.585, -1.449	<-0.945, <-0.668, <-0.091
J082107+310751	2.24571	14.861 ± 0.012	<-4.755, <-3.820, <-2.790	-2.186, -1.558:, -0.933	...
J010311+131617	2.55125	14.862 ± 0.003	-2.221, -1.824, -1.481	-1.190, -1.159:, -1.133	-0.598, -0.261:, +0.128
J220852-194400	2.54217	14.903 ± 0.004	-2.320, -1.965, -1.653	-1.610, -1.360:, -1.063	-0.522, -0.143:, +0.247
J160843+071508	2.42112	14.911 ± 0.021	-0.971, -0.943, -0.915	-1.895, -1.870, -1.846	-0.105, -0.055, -0.005
J094202+042244	2.72833	14.945 ± 0.004	-0.347, -0.338, -0.329	-1.355, -1.352, -1.349	-0.783, -0.775, -0.765
J100841+362319	2.76763	14.948 ± 0.008	<-4.780, <-3.890, <-2.913	-2.140, -1.541:, -0.926	...
J121930+494052	2.27897	14.960 ± 0.010	-2.052, -2.040, -2.028	-0.769, -0.763, -0.757	...
J012156+144823	2.46812	14.962 ± 0.010	-2.730, -2.335, -1.997	-1.840, -1.477, -1.134	-0.526, -0.122:, +0.306
J012156+144823	2.62486	14.966 ± 0.007	-3.090, -2.663, -2.286	-1.936, -1.687, -1.444	-0.617, -0.261:, +0.123
J135038-251216	2.37059	14.969 ± 0.009	-1.866, -1.849, -1.831	-0.750, -0.740, -0.729	...
J142438+225600	3.33427	14.990 ± 0.002	-3.316, -3.278, -3.218	-0.409, -0.355, -0.329	...
J155152+191104	2.35276	14.990 ± 0.003	-3.126, -2.838, -2.485	-0.997, -0.796, -0.580	-0.658, -0.276:, +0.094
J090033+421546	3.08569	14.994 ± 0.006	-2.683, -2.324, -1.940	-1.034, -0.853, -0.648	-0.674, -0.299:, +0.097
J020950-000506	2.41125	15.009 ± 0.006	<-4.637, <-3.248, <-1.763	-1.981, -1.340:, -0.760	...
J121930+494052	2.57761	15.025 ± 0.001	-2.757, -2.721, -2.685	-0.646, -0.613, -0.581	...
J014516-094517	2.49969	15.026 ± 0.001	<-4.823, <-4.119, <-3.115	-2.218, -1.617:, -1.022	...
J025905+001121	3.12722	15.035 ± 0.009	<-4.790, <-3.972, <-3.102	-2.136, -1.571:, -0.966	...
J005700+143737	2.54721	15.040 ± 0.010	<-4.749, <-3.711, <-2.731	-2.069, -1.442:, -0.846	...
J170100+641209	2.59668	15.043 ± 0.004	<-4.864, <-4.332, <-3.608	-2.230, -1.636:, -0.975	...
J121930+494052	2.47346	15.046 ± 0.004	-3.040, -2.998, -2.956	-0.795, -0.767, -0.739	...
J130411+295348	2.57726	15.047 ± 0.009	<-4.776, <-3.836, <-2.711	-2.191, -1.583:, -0.963	...
J090033+421546	3.15992	15.054 ± 0.009	<-4.788, <-3.997, <-3.003	-2.174, -1.592:, -0.985	...
J113508+222715	2.74242	15.055 ± 0.009	<-4.790, <-3.995, <-3.205	-2.122, -1.510:, -0.898	...
J171227+575507	2.81553	15.055 ± 0.004	-0.326, -0.296, -0.276	-2.439, -2.416, -2.383	+0.674, +0.729, +0.770
J014516-094517	2.58808	15.065 ± 0.001	-3.091, -2.700, -2.377	-1.652, -1.239, -0.725	-0.598, -0.212:, +0.214
J135038-251216	2.57455	15.065 ± 0.004	-0.754, -0.738, -0.720	-1.921, -1.907, -1.892	-0.293, -0.259, -0.227
J130411+295348	2.75550	15.072 ± 0.007	-2.174, -2.148, -2.121	-0.590, -0.570, -0.549	...
J074521+473436	3.12615	15.076 ± 0.003	-3.111, -2.604, -2.173	-1.941, -1.611:, -1.303	-0.566, -0.193:, +0.187
J143316+313126	2.77502	15.078 ± 0.002	-2.131, -1.819, -1.553	-1.817, -1.776, -1.737	-0.202, +0.033:, +0.326
J121930+494052	2.52850	15.091 ± 0.003	-2.627, -2.378, -2.155	-1.810, -1.784, -1.758	+0.086, +0.300:, +0.544
J014516-094517	2.70685	15.097 ± 0.001	-1.311, -1.264, -1.228	-1.292, -1.278, -1.261	-0.955, -0.925, -0.885
J143316+313126	2.92832	15.099 ± 0.001	-2.097, -1.830, -1.539	-1.040, -0.901, -0.769	-0.764, -0.480:, -0.217
J121930+494052	2.22541	15.109 ± 0.005	-2.387, -2.370, -2.354	-0.261, -0.227, -0.197	...
J025905+001121	3.22368	15.113 ± 0.005	<-4.805, <-4.054, <-3.192	-2.159, -1.577:, -0.982	...
J121930+494052	2.57078	15.114 ± 0.001	-2.535, -2.337, -2.122	-0.838, -0.717, -0.547	-0.918, -0.738:, -0.506
J004530-261709	3.24823	15.120 ± 0.010	<-4.762, <-3.821, <-2.573	-2.164, -1.589:, -0.977	...
J234628+124859	2.54133	15.122 ± 0.004	-2.879, -2.465, -2.140	-1.674, -1.310:, -0.922	-0.570, -0.192:, +0.215
J012156+144823	2.53765	15.124 ± 0.004	-2.090, -1.973, -1.858	-1.894, -1.840, -1.787	-0.591, -0.464:, -0.332
J144453+291905	2.32985	15.128 ± 0.004	-0.772, -0.762, -0.753	-1.696, -1.690, -1.684	-0.192, -0.180, -0.167
J113418+574204	3.34514	15.134 ± 0.004	<-4.788, <-3.932, <-2.740	-2.209, -1.638:, -1.064	...
J113418+574204	3.46347	15.136 ± 0.007	-2.703, -2.385, -2.125	-1.566, -1.506, -1.444	-0.269, -0.013:, +0.301
J015741-010629	3.36274	15.145 ± 0.015	<-4.602, <-3.054, <-1.488	-2.006, -1.393:, -0.828	...
J093643+292713	2.58243	15.152 ± 0.008	<-4.769, <-3.826, <-2.736	-2.155, -1.556:, -0.954	...
J170100+641209	2.51255	15.152 ± 0.004	<-4.843, <-4.267, <-3.505	-2.153, -1.579:, -0.943	...
J045213-164012	2.39910	15.161 ± 0.004	-1.417, -1.271, -1.079	-1.852, -1.639, -1.431	-0.449, -0.075, +0.273
J100841+362319	3.01081	15.161 ± 0.010	<-4.787, <-3.977, <-2.866	-2.235, -1.650:, -1.044	...

Table 4 continued

Table 4 (*continued*)

QSO Name	z_{abs}	$\log N_{\text{HI}}$ [cm $^{-2}$]	[X/H]	$\log U$	[C/ α]
J094202+042244	2.60246	15.167 ± 0.007	$<-4.807, <-3.997, <-2.942$	-2.196, -1.597:, -0.959	...
J082107+310751	2.55652	15.177 ± 0.007	$<-4.757, <-3.822, <-2.831$	-2.156, -1.551:, -0.910	...
J101447+430030	2.98705	15.188 ± 0.002	-2.932, -2.522, -2.139	-1.099, -0.936:, -0.653	-0.661, -0.280:, +0.126
J144453+291905	2.47417	15.209 ± 0.004	-0.432, -0.360, -0.295	-2.450, -2.395, -2.328	+0.271, +0.340, +0.418
J212912-153841	2.95558	15.220 ± 0.005	-2.958, -2.513, -2.139	-1.822, -1.475:, -1.168	-0.534, -0.161:, +0.229
J124610+303131	2.46655	15.224 ± 0.005	$<-4.743, <-3.756, <-2.705$	-2.174, -1.577:, -0.935	...
J094202+042244	2.81325	15.226 ± 0.019	-0.995, -0.915, -0.817	-2.194, -1.989, -1.784	-0.674, -0.381:, -0.131
J135038-251216	2.44516	15.235 ± 0.013	-2.308, -2.284, -2.260	-0.902, -0.890, -0.877	...
J094202+042244	2.81450	15.242 ± 0.030	-0.510, -0.416, -0.316	-2.593, -2.517, -2.431	+0.188, +0.329, +0.456
J143316+313126	2.58814	15.254 ± 0.007	$<-4.789, <-3.978, <-3.086$	-2.110, -1.560:, -1.027	...
J143316+313126	2.90645	15.271 ± 0.004	-1.679, -1.634, -1.590	-1.339, -1.321, -1.303	-0.996, -0.985, -0.960
J143316+313126	2.88759	15.276 ± 0.002	-2.373, -1.960, -1.601	-2.469, -2.133:, -1.693	-0.350, -0.074:, +0.250
J143316+313126	2.74931	15.280 ± 0.004	$<-4.752, <-3.793, <-2.676$	-2.163, -1.564:, -0.945	...
J100841+362319	3.03460	15.301 ± 0.006	-2.723, -2.456, -2.128	-0.918, -0.757, -0.585	-0.693, -0.359:, -0.041
J083102+335803	2.41864	15.304 ± 0.016	$<-4.812, <-4.017, <-3.015$	-2.158, -1.553:, -0.967	...
J134328+572147	2.79941	15.309 ± 0.010	$<-4.768, <-3.894, <-2.882$	-2.121, -1.563:, -1.015	...
J093337+284532	3.37217	15.312 ± 0.022	$<-4.831, <-4.159, <-3.267$	-2.196, -1.614:, -0.999	...
J010806+163550	2.48359	15.315 ± 0.010	-2.139, -1.753, -1.380	-1.033, -0.999, -0.970	-0.665, -0.294:, +0.087
J101447+430030	2.84090	15.316 ± 0.003	-2.916, -2.545, -2.180	-1.020, -0.840, -0.611	$<-0.887, <-0.452, <+0.098$
J064204+675835	3.06746	15.332 ± 0.006	$<-4.855, <-4.321, <-3.319$	-2.292, -1.696:, -1.041	...
J162557+264448	2.53680	15.348 ± 0.013	$<-4.814, <-4.130, <-3.377$	-2.172, -1.575:, -0.923	...
J100841+362319	3.10854	15.356 ± 0.006	-2.375, -2.043, -1.774	-1.466, -1.445, -1.425	-0.320, -0.066:, +0.253
J020950-000506	2.64137	15.360 ± 0.003	-0.875, -0.846, -0.833	-1.261, -1.236, -1.222	-0.995, -0.980, -0.936
J094202+042244	2.84851	15.363 ± 0.008	-2.519, -2.140, -1.809	-1.786, -1.461, -1.170	-0.467, -0.078:, +0.323
J160455+381201	2.53794	15.368 ± 0.005	-2.056, -2.049, -2.041	-1.222, -1.208, -1.193	...
J014516-094517	2.69212	15.395 ± 0.001	$<-4.899, <-4.511, <-3.979$	$>-2.362, >-1.513:, >-0.678$...
J170100+641209	2.43979	15.402 ± 0.004	-1.763, -1.754, -1.746	-1.165, -1.159, -1.154	-0.999, -0.997, -0.992
J155152+191104	2.69270	15.411 ± 0.002	-0.720, -0.687, -0.636	-2.535, -2.484, -2.426	-0.530, -0.470, -0.412
J014516-094517	2.66911	15.412 ± 0.001	$<-4.891, <-4.454, <-3.932$	-2.183, -1.525:, -0.894	...
J030341-002321	3.15168	15.436 ± 0.004	$<-4.764, <-3.783, <-2.629$	-2.042, -1.491:, -1.040	...
J030341-002321	3.10354	15.449 ± 0.010	$<-4.801, <-4.045, <-3.246$	-2.125, -1.574:, -0.966	...
J171227+575507	2.97141	15.454 ± 0.002	-0.522, -0.515, -0.508	-2.081, -2.071, -2.062	+0.179, +0.193, +0.207
J095852+120245	3.15768	15.491 ± 0.002	$<-4.822, <-4.127, <-3.204$	-2.206, -1.642:, -1.042	...
J100841+362319	3.07200	15.502 ± 0.009	-1.427, -1.385, -1.355	-1.252, -1.239, -1.222	-0.993, -0.972:, -0.931
J010311+131617	2.55216	15.505 ± 0.007	-2.541, -2.200, -1.925	-1.488, -1.475:, -1.463	-0.375, -0.114:, +0.220
J170100+641209	2.37993	15.507 ± 0.005	-1.376, -1.366, -1.356	-1.462, -1.459, -1.456	-0.912, -0.904, -0.896
J143316+313126	2.61282	15.516 ± 0.004	-2.256, -1.948, -1.663	-1.625, -1.396, -1.188	-0.347, +0.004:, +0.369
J212912-153841	3.04863	15.538 ± 0.007	$<-4.830, <-4.128, <-3.121$	-2.201, -1.615:, -1.008	...
J143316+313126	2.73377	15.552 ± 0.004	-2.731, -2.337, -2.012	-1.719, -1.422:, -1.133	-0.525, -0.148:, +0.247
J142438+225600	3.56653	15.556 ± 0.001	-3.387, -2.935, -2.583	-1.845, -1.579:, -1.319	-0.618, -0.233:, +0.175
J121930+494052	2.54882	15.572 ± 0.003	-2.311, -2.306, -2.301	-1.093, -1.089, -1.086	...
J143316+313126	2.90184	15.598 ± 0.014	-2.597, -2.277, -2.007	-1.768, -1.743, -1.717	-0.309, -0.049:, +0.261
J131215+423900	2.41504	15.598 ± 0.008	-3.056, -2.642, -2.284	-1.368, -1.316, -1.264	-0.627, -0.272:, +0.136
J104018+572448	3.36421	15.603 ± 0.009	-2.353, -2.334, -2.315	-0.802, -0.793, -0.783	...
J003501-091817	2.35342	15.610 ± 0.045	$<-4.786, <-3.933, <-2.870$	-2.182, -1.567:, -0.924	...
J082107+310751	2.55190	15.612 ± 0.005	-2.176, -1.897, -1.636	-1.182, -1.065, -0.936	-0.761, -0.521, -0.256
J130411+295348	2.57585	15.618 ± 0.008	-1.345, -1.293, -1.239	-2.691, -2.635, -2.579	...
J144453+291905	2.55484	15.618 ± 0.001	-3.140, -2.892, -2.750	-1.796, -1.776, -1.756	-0.041, +0.102:, +0.347

Table 4 continued

Table 4 (*continued*)

QSO Name	z_{abs}	$\log N_{\text{HI}}$ [cm $^{-2}$]	[X/H]	$\log U$	[C/ α]
J093643+292713	2.69883	15.620 ± 0.018	-1.971, -1.868, -1.754	-1.840, -1.755, -1.677	-0.383, -0.191, -0.003
J010311+131617	2.54303	15.621 ± 0.002	-2.447, -2.191, -1.930	-1.175, -1.058, -0.940	-0.489, -0.247, -0.005
J143316+313126	2.90227	15.642 ± 0.010	-2.554, -2.248, -1.986	-1.657, -1.449, -1.278	-0.269, +0.066:, +0.400
J030341-002321	2.93700	15.648 ± 0.006	<-4.886, <-4.413, <-3.812	-2.176, -1.518:, -0.854	...
J144453+291905	2.37869	15.668 ± 0.004	-3.318, -3.153, -2.953	-0.867, -0.747, -0.623	-0.839, -0.610:, -0.390
J002127-020333	2.54918	15.680 ± 0.021	-2.634, -2.112, -1.662	-2.047, -1.674, -1.295	-0.304, +0.011:, +0.361
J173352+540030	3.30295	15.723 ± 0.003	-3.344, -3.194, -2.947	-0.657, -0.500, -0.371	-0.880, -0.662:, -0.399
J193957-100241	3.61935	15.727 ± 0.001	-1.580, -1.555, -1.481	-2.052, -1.852, -1.628	-0.838, -0.602:, -0.362
J094202+042244	2.81407	15.730 ± 0.011	-1.169, -1.151, -1.128	-2.105, -2.032, -1.971	-0.368, -0.250, -0.123
J104018+572448	3.32379	15.743 ± 0.014	-1.330, -1.246, -1.029	-2.031, -1.664, -1.286	...
J025905+001121	3.30796	15.744 ± 0.012	-1.710, -1.677, -1.643	-1.666, -1.643, -1.620	-0.593, -0.552, -0.510
J222256-094636	2.87419	15.755 ± 0.015	<-4.812, <-4.037, <-2.985	-2.218, -1.664:, -1.118	...
J004530-261709	3.36517	15.770 ± 0.015	<-4.675, <-3.379, <-2.048	-2.029, -1.408:, -0.840	...
J020950-000506	2.76903	15.773 ± 0.002	<-4.908, <-4.494, <-3.813	-2.230, -1.725:, -1.177	...
J173352+540030	3.20694	15.790 ± 0.004	-2.043, -1.707, -1.320	-2.717, -2.440, -2.116	-0.948, -0.867, -0.772
J104018+572448	3.27747	15.803 ± 0.009	-1.445, -1.411, -1.376	-1.531, -1.506, -1.481	-0.994, -0.978, -0.949
J064204+675835	3.01338	15.819 ± 0.004	<-4.751, <-3.854, <-2.880	-2.138, -1.563:, -0.941	...
J212912-153841	3.21670	15.852 ± 0.004	-1.899, -1.881, -1.844	-1.856, -1.808, -1.766	-0.701, -0.390:, -0.129
J093643+292713	2.40065	15.852 ± 0.009	-0.832, -0.818, -0.805	-1.353, -1.347, -1.341	-0.934, -0.914, -0.893
J094202+042244	3.09385	15.855 ± 0.001	<-4.709, <-3.547, <-2.289	-1.999, -1.344:, -0.791	...
J093643+292713	2.54337	15.863 ± 0.009	<-4.826, <-4.166, <-3.351	-2.150, -1.590:, -1.006	...
J143316+313126	2.58177	15.877 ± 0.002	-3.826, -3.364, -2.952	-1.768, -1.374:, -0.912	-0.618, -0.239:, +0.164
J064204+675835	2.86842	15.894 ± 0.006	<-4.859, <-4.325, <-3.620	-2.254, -1.649:, -0.972	...
J130411+295348	2.79811	15.897 ± 0.005	<-4.678, <-3.405, <-2.051	-1.984, -1.348:, -0.778	...
J074749+443417	4.35301	15.902 ± 0.011	<-4.777, <-3.960, <-2.966	-2.155, -1.607:, -1.055	...
J121930+494052	2.62063	15.903 ± 0.002	-1.536, -1.518, -1.501	-1.718, -1.704, -1.692	-0.735, -0.706, -0.672
J010806+163550	2.50561	15.914 ± 0.004	-2.607, -2.429, -2.257	-2.205, -1.937, -1.677	-0.771, -0.340, +0.048
J143316+313126	2.89093	15.930 ± 0.003	-2.576, -2.569, -2.563	-0.889, -0.885, -0.882	...
J081240+320808	2.58869	15.931 ± 0.010	<-4.906, <-4.500, <-3.527	-2.407, -1.856:, -1.172	...
J101447+430030	3.11460	15.974 ± 0.001	-2.148, -2.099, -2.029	-1.828, -1.755, -1.692	-0.734, -0.577, -0.424
J093643+292713	2.59624	16.009 ± 0.007	-2.175, -2.046, -1.919	-1.771, -1.707, -1.644	-0.779, -0.629, -0.474
J121930+494052	2.47816	16.021 ± 0.004	-1.301, -1.294, -1.289	-1.648, -1.644, -1.641	-1.000, -0.998, -0.995
J104018+572448	3.34454	16.053 ± 0.009	-2.317, -2.234, -2.036	-2.500, -2.145:, -1.772	...
J142438+225600	3.53989	16.064 ± 0.003	-0.658, -0.655, -0.652	-3.178, -3.176, -3.173	+0.132, +0.135, +0.138
J143316+313126	2.64432	16.117 ± 0.003	-2.468, -2.428, -2.387	-1.802, -1.779, -1.756	-0.138, -0.083, -0.027
J142438+225600	3.44848	16.132 ± 0.006	-2.088, -2.081, -2.075	-2.066, -2.057, -2.047	-0.412, -0.401, -0.389
J010925-210257	3.14253	16.147 ± 0.013	<-4.715, <-3.586, <-2.381	-2.664, -2.102:, -1.500	...
J014516-094517	2.66513	16.156 ± 0.001	-2.446, -2.401, -2.354	-1.881, -1.823, -1.761	-0.340, -0.204, -0.075
J030341-002321	2.95653	16.161 ± 0.010	-1.574, -1.528, -1.499	-1.503, -1.476, -1.458	-0.982, -0.940, -0.869
J093643+292713	2.41258	16.169 ± 0.089	<-4.835, <-4.151, <-3.278	-2.699, -2.184:, -1.689	...
J030341-002321	2.99495	16.170 ± 0.004	-1.893, -1.878, -1.859	-2.118, -2.042, -1.969	-0.017, +0.116, +0.233
J143316+313126	2.90116	16.176 ± 0.003	-1.791, -1.702, -1.623	-2.653, -2.605, -2.551	-0.425, -0.377, -0.332
J094202+042244	2.72984	16.183 ± 0.005	-0.758, -0.749, -0.744	-1.506, -1.504, -1.503	-1.000, -1.000, -0.997
J160843+071508	2.42219	16.211 ± 0.015	-0.730, -0.715, -0.699	-2.754, -2.748, -2.743	+0.074, +0.083, +0.092
J155152+191104	2.69478	16.253 ± 0.002	-2.039, -2.035, -2.031	-1.800, -1.795, -1.790	-0.623, -0.613, -0.603
J134328+572147	2.87056	16.254 ± 0.009	-1.203, -1.190, -1.177	-1.393, -1.388, -1.383	-0.999, -0.996, -0.989
J012156+144823	2.66593	16.259 ± 0.023	-0.743, -0.724, -0.704	-2.532, -2.530, -2.527	-0.110, -0.106, -0.101
J134544+262506	2.86367	16.267 ± 0.008	-1.573, -1.536, -1.497	-2.381, -2.343, -2.304	-0.359, -0.315, -0.270

Table 4 continued

Table 4 (*continued*)

QSO Name	z_{abs}	$\log N_{\text{H I}}$ [cm $^{-2}$]	[X/H]	$\log U$	[C/ α]
J234856–104131	3.15981	16.287 ± 0.006	−2.344, −2.301, −2.175	−2.059, −1.843, −1.661	−0.660, −0.302:, +0.022
J170100+641209	2.43307	16.288 ± 0.008	−1.458, −1.450, −1.441	−2.465, −2.462, −2.459	+0.010, +0.013, +0.017
J135038–251216	2.57299	16.319 ± 0.007	−2.398, −2.380, −2.356	−2.283, −2.223, −2.159	−0.444, −0.382, −0.341
J102009+104002	3.05498	16.330 ± 0.041	−1.545, −1.449, −1.391	−2.465, −2.452, −2.438	...
J095852+120245	3.09691	16.349 ± 0.035	−2.749, −2.628, −2.463	−2.220, −1.934, −1.708	−0.524, −0.184:, +0.119
J130411+295348	2.82924	16.378 ± 0.004	<−4.759, <−3.810, <−2.845	−2.664, −2.100:, −1.500	...
J170100+641209	2.43359	16.401 ± 0.006	−1.430, −1.421, −1.413	−2.553, −2.550, −2.546	−0.139, −0.135, −0.130
J173352+540030	3.28216	16.476 ± 0.003	−2.910, −2.888, −2.834	−1.994, −1.843, −1.705	−0.578, −0.307:, −0.048
J120006+312630	2.87577	16.561 ± 0.021	−1.778, −1.737, −1.696	−2.295, −2.277, −2.260	...
J101447+430030	3.01439	16.681 ± 0.003	−3.341, −3.339, −3.336	−0.271, −0.271, −0.271	...
J074521+473436	3.05358	16.726 ± 0.013	−4.209, −3.719, −3.302	−1.662, −1.429:, −1.126	−0.616, −0.253:, +0.127
J074521+473436	3.03515	16.727 ± 0.014	−3.209, −3.160, −3.103	−1.935, −1.800, −1.681	−0.466, −0.307, −0.133
J171227+575507	2.88991	16.735 ± 0.005	−2.704, −2.652, −2.605	−2.513, −2.448, −2.366	−0.163, −0.117, −0.084
J020950–000506	2.57449	16.777 ± 0.003	−1.803, −1.788, −1.774	−2.018, −1.994, −1.969	−0.040, −0.032, −0.024
J131215+423900	2.48998	16.796 ± 0.005	−2.398, −2.369, −2.332	−2.167, −2.102, −2.045	−0.465, −0.399, −0.323
J144453+291905	2.46741	16.802 ± 0.002	−2.088, −2.071, −2.053	−2.351, −2.339, −2.328	−0.088, −0.073, −0.057
J142438+225600	3.38281	16.984 ± 0.100	−3.662, −3.533, −3.403	−1.835, −1.825, −1.815	−0.275, −0.241, −0.208
J094202+042244	2.73088	17.102 ± 0.005	−1.123, −1.049, −0.906	−2.416, −1.994, −1.749	−0.092, −0.021, +0.028
J095852+120245	3.09623	17.146 ± 0.056	<−4.946, <−4.699, <−4.182	>−3.103, >−2.523:, >−2.028	...
J025905+001121	3.08465	17.250 ± 0.250	−2.560, −2.292, −1.979	−2.212, −2.139, −2.059	−0.207, −0.141, −0.069
J012156+144823	2.66416	17.260 ± 0.100	−1.433, −1.281, −1.237	−1.662, −1.605, −1.580	...
J102009+104002	3.05421	17.268 ± 0.015	−2.825, −2.796, −2.768	−2.236, −2.200, −2.163	−0.474, −0.425, −0.379
J101723–204658	2.45051	17.284 ± 0.107	−2.079, −1.975, −1.882	−2.499, −2.485, −2.470	−0.292, −0.281, −0.269
J222256–094636	2.86475	17.300 ± 0.125	−2.668, −2.254, −1.826	−2.483, −2.135, −1.729	−0.636, −0.345, −0.105
J212912–153841	2.96755	17.339 ± 0.097	−2.748, −2.652, −2.550	−2.456, −2.443, −2.429	+0.204, +0.217, +0.231
J101155+294141	2.50364	17.355 ± 0.001	−2.758, −2.751, −2.743	−2.300, −2.293, −2.285	−0.238, −0.229, −0.221
J095852+120245	3.22317	17.356 ± 0.003	−3.055, −3.050, −3.045	−1.466, −1.455, −1.443	−0.592, −0.573, −0.554
J025905+001121	3.08204	17.500 ± 0.250	<−4.912, <−4.514, <−3.844	>−3.018, >−2.506:, >−2.071	...
J162557+264448	2.55094	17.750 ± 0.100	−1.478, −1.441, −1.397	−2.643, −2.634, −2.624	−0.128, −0.118, −0.107
J101155+294141	2.42901	17.750 ± 0.150	−0.513, −0.399, −0.378	−2.500, −2.490, −2.486	...
J134328+572147	2.83437	17.780 ± 0.300	−1.778, −1.751, −1.722	−2.996, −2.974, −2.953	+0.167, +0.208, +0.251
J143316+313126	2.58591	18.150 ± 0.150	−1.793, −1.656, −1.588	<−3.641, <−3.617, <−3.576	...
J064204+675835	2.90469	18.420 ± 0.225	−1.567, −1.546, −1.387	−1.968, −0.952, −0.667	+0.023, +0.166:, +0.393
J104018+572448	3.26628	18.600 ± 0.200	−2.266, −2.238, −2.209	−2.650, −2.631, −2.612	−0.043, −0.018, +0.006
J030341–002321	2.94069	18.650 ± 0.225	−2.373, −2.247, −2.058	−2.140, −2.012, −1.915	+0.141, +0.222, +0.263
J012156+144823	2.66241	19.100 ± 0.350	−0.885, −0.834, −0.784	−4.011, −3.951, −3.893	...
J080117+521034	3.04464	19.250 ± 0.250	<−4.949, <−4.727, <−4.398	−2.316, −1.701:, −1.049	...
J033900–013318	3.11542	19.600 ± 0.050	−1.670, −1.620, −1.569	−2.552, −2.425, −2.290	...
J004530–261709	2.81907	19.660 ± 0.010	−0.553, −0.493, −0.434	<−4.739, <−4.717, <−4.657	...
J080117+521034	3.04028	19.690 ± 0.150	−2.719, −2.710, −2.697	−1.972, −1.961, −1.954	...
J100841+362319	2.94749	19.725 ± 0.002	−1.853, −1.845, −1.837	−2.725, −2.720, −2.714	...
J030341–002321	2.44326	19.866 ± 0.010	−2.290, −2.280, −2.270	−2.705, −2.698, −2.690	−0.096, −0.083, −0.070

NOTE— The lower to upper bounds for each quantity represent the 68% CI for detections and the 80% CI for the upper or lower limits; the middle number is the median metallicity. When a colon is present after the median value of $\log U$, this implies that a $\log U$ Gaussian prior was used to determine the properties of the absorber.

Table 5. Metallicity Statistics at $2.2 \leq z \leq 3.6$

Abs.	Type	N_{abs}	$\widetilde{[\text{X}/\text{H}]}$	$\overline{[\text{X}/\text{H}]}$	IQR
KODIAQ-Z sample					
SLFs	Ss	155	-2.42	-2.62 ± 1.23	$[-3.61, -1.76]$
pLLs	Ss	24	-2.09	-2.27 ± 1.04	$[-2.91, -1.45]$
LLs	Ss	16	-2.16	-2.17 ± 0.90	$[-2.75, -1.58]$
pLLSs+LLSs		40	-2.13	-2.23 ± 0.99	$[-2.78, -1.51]$
SLFs+pLLs+LLs		195	-2.36	-2.54 ± 1.20	$[-3.37, -1.69]$
SLLSs		7	-2.09	-2.11 ± 1.29	$[-2.70, -0.87]$
HD-LLS sample					
LLSs		46	-2.22	-2.28 ± 0.78	$[-2.77, -1.71]$
SLLSs		73	-1.89	-1.91 ± 0.84	$[-2.46, -1.33]$
KODIAQ-Z+HD-LLS sample					
LLSs		62	-2.20	-2.25 ± 0.81	$[-2.75, -1.69]$
pLLSs+LLSs		86	-2.19	-2.26 ± 0.88	$[-2.77, -1.66]$
SLFs+pLLs+LLs		241	-2.34	-2.49 ± 1.13	$[-3.23, -1.70]$
SLLSs		80	-1.90	-1.93 ± 0.89	$[-2.47, -1.33]$
R12-DLA sample					
DLAs		101	-1.41	-1.41 ± 0.50	$[-1.70, -1.05]$

NOTE—The tilde and bar above $[\text{X}/\text{H}]$ represent the median and mean (with the standard deviation), respectively. To derive the mean, median, standard deviation, and IQR we directly use the walkers for the KODIAQ-Z and HD-LLS absorbers. Note that these are means, standard deviations, and IQRs in logarithmic space.

Table 6. Fraction of very and extremely metal-poor absorbers at $2.2 \leq z \leq 3.6$

Abs.	N_{abs}	Fraction with $[\text{X}/\text{H}] < -2.4$	Fraction with $[\text{X}/\text{H}] < -3.0$	Fraction with $[\text{X}/\text{H}] < -3.5$
Type				
SLFs	155	>41.2%–54.3%	>14.7%–25.1%	>2.9%–8.9%
pLLs	24	23.3%–54.2%	10.5%–37.1%	5.1%–27.5%
LLs	62	26.3%–45.9%	8.6%–23.3%	2.0%–11.5%
SLLs	80	20.1%–36.5%	3.1%–12.3%	0.3%–5.4%
DLAs	101	0.2%–4.3%	0.0%–2.6%	0.0%–2.6%

NOTE—The SLFs and pLLs are from KODIAQ-Z; the LLs and SLLs are from KODIAQ-Z+HD-LLS; the DLAs are from R12-DLA. The percentage ranges are estimated using the Wilson score with 90% confidence intervals. For upper limits, we use the 90th percentile to define the metallicity values. The SLFs have an important fraction of upper limits, which is the reason that we mark them with a $>$ sign in that table.

Table 7. Physical Properties of the KODIAQ-Z Sample

QSO Name	z_{abs}	$\log N_{\text{HI}}$	$\log N_{\text{H}}$	$\log n_{\text{H}}$	$\log T$	l (kpc)
		[cm $^{-2}$]	[cm $^{-2}$]	[cm $^{-3}$]	[K]	
J010806+163550	2.31582	14.574 ± 0.004	17.935, 18.635, 19.305	-3.737, -3.161:, -2.565	4.387, 4.521, 4.644	0.1, 2.0, 35.7
J045213-164012	2.44044	14.611 ± 0.004	17.944, 18.649, 19.378	-3.785, -3.155:, -2.554	4.381, 4.516, 4.645	0.1, 2.1, 47.2
J170100+641209	2.49647	14.622 ± 0.007	18.409, 18.725, 19.013	-3.479, -3.231, -2.958	4.456, 4.513, 4.566	0.8, 2.9, 10.1
J023359+004938	2.48836	14.640 ± 0.019	18.025, 18.721, 19.371	-3.758, -3.197:, -2.602	4.391, 4.524, 4.638	0.1, 2.7, 43.8
J073149+285448	3.42673	14.653 ± 0.008	17.955, 18.665, 19.333	-3.880, -3.277:, -2.670	4.363, 4.502, 4.584	0.1, 2.8, 52.9
J045213-164012	2.53542	14.674 ± 0.003	18.047, 18.769, 19.434	-3.792, -3.214:, -2.597	4.389, 4.527, 4.640	0.1, 3.1, 54.5
J012156+144823	2.81222	14.683 ± 0.002	18.034, 18.687, 19.368	-3.765, -3.174:, -2.616	4.382, 4.508, 4.621	0.1, 2.4, 44.0
J105756+455553	3.69194	14.698 ± 0.003	17.959, 18.656, 19.307	-3.865, -3.273:, -2.678	4.352, 4.485, 4.564	0.1, 2.8, 48.1
J010925-210257	2.96546	14.706 ± 0.008	19.558, 19.789, 19.956	-4.401, -4.202, -3.967	4.580, 4.612, 4.621	108.6, 318.0, 737.9
J014516-094517	2.69430	14.708 ± 0.002	18.159, 18.564, 18.980	-3.390, -3.040, -2.695	4.392, 4.472, 4.554	0.2, 1.3, 7.6
J074521+473436	2.85216	14.723 ± 0.004	18.607, 18.914, 19.212	-3.613, -3.352:, -3.087	4.473, 4.528, 4.580	1.6, 6.0, 21.6
J010806+163550	2.46164	14.754 ± 0.002	18.091, 18.821, 19.517	-3.784, -3.182:, -2.559	4.381, 4.521, 4.642	0.1, 3.3, 64.7
J074521+473436	2.96558	14.761 ± 0.003	17.537, 17.568, 17.599	-2.237, -2.219, -2.203	4.181, 4.214, 4.238	0.0, 0.0, 0.0
J030341-002321	3.10937	14.766 ± 0.004	18.117, 18.826, 19.495	-3.864, -3.266:, -2.660	4.378, 4.516, 4.608	0.2, 4.0, 74.1
J011150+140141	2.42374	14.803 ± 0.020	18.533, 18.586, 18.638	-3.134, -3.095, -3.058	4.243, 4.273, 4.299	1.3, 1.6, 1.9
J120006+312630	2.84264	14.804 ± 0.010	19.037, 19.051, 19.069	-3.480, -3.477, -3.474	4.332, 4.336, 4.340	10.6, 10.9, 11.4
J012156+144823	2.66022	14.828 ± 0.021	18.057, 18.764, 19.503	-3.734, -3.095:, -2.490	4.361, 4.495, 4.624	0.1, 2.3, 56.0
J012156+144823	2.41837	14.829 ± 0.007	18.518, 18.776, 18.921	-3.244, -3.108, -2.874	4.431, 4.464, 4.481	0.8, 2.5, 4.7
J082107+310751	2.24571	14.861 ± 0.012	18.145, 18.883, 19.609	-3.744, -3.120:, -2.491	4.374, 4.513, 4.647	0.1, 3.3, 73.1
J010311+131617	2.55125	14.862 ± 0.003	19.253, 19.312, 19.354	-3.574, -3.548:, -3.518	4.526, 4.562, 4.585	19.2, 23.5, 27.4
J220852-194400	2.54217	14.903 ± 0.004	18.840, 19.126, 19.464	-3.644, -3.347:, -3.097	4.475, 4.526, 4.586	2.8, 9.7, 41.5
J160843+071508	2.42112	14.911 ± 0.021	18.447, 18.486, 18.525	-2.847, -2.823, -2.798	4.336, 4.341, 4.346	0.6, 0.7, 0.8
J094202+042244	2.72833	14.945 ± 0.004	18.968, 18.974, 18.981	-3.381, -3.378, -3.376	4.256, 4.259, 4.262	7.2, 7.3, 7.4
J100841+362319	2.76763	14.948 ± 0.008	18.285, 18.985, 19.688	-3.810, -3.194:, -2.595	4.379, 4.513, 4.625	0.2, 4.9, 101.6
J121930+494052	2.27897	14.960 ± 0.010	19.856, 19.869, 19.881	-3.922, -3.917, -3.911	4.642, 4.643, 4.644	190.4, 197.7, 205.1
J012156+144823	2.46812	14.962 ± 0.010	18.641, 19.066, 19.465	-3.564, -3.221, -2.858	4.440, 4.519, 4.592	1.0, 6.3, 34.7
J012156+144823	2.62486	14.966 ± 0.007	18.537, 18.827, 19.112	-3.273, -3.029, -2.781	4.422, 4.477, 4.531	0.7, 2.3, 7.9
J135038-251216	2.37059	14.969 ± 0.009	19.873, 19.889, 19.904	-3.959, -3.948, -3.937	4.628, 4.630, 4.633	210.3, 222.5, 235.6
J142438+225600	3.33427	14.990 ± 0.002	20.154, 20.195, 20.215	-4.491, -4.465, -4.411	4.506, 4.514, 4.529	1190.2, 1479.1, 1646.1
J155152+191104	2.35276	14.990 ± 0.003	19.652, 19.879, 20.107	-4.106, -3.890, -3.689	4.622, 4.657, 4.675	71.0, 190.3, 529.4
J090033+421546	3.08569	14.994 ± 0.006	19.579, 19.783, 19.987	-4.134, -3.928, -3.747	4.571, 4.602, 4.612	68.6, 166.8, 427.9
J020950-000506	2.41125	15.009 ± 0.006	18.530, 19.277, 19.914	-3.932, -3.352:, -2.711	4.416, 4.542, 4.641	0.6, 13.8, 228.3
J121930+494052	2.57761	15.025 ± 0.001	20.059, 20.092, 20.123	-4.130, -4.098, -4.065	4.655, 4.655, 4.656	431.8, 501.0, 580.5
J014516-094517	2.49969	15.026 ± 0.001	18.273, 18.974, 19.667	-3.679, -3.084:, -2.483	4.365, 4.497, 4.624	0.2, 3.7, 71.8
J025905+001121	3.12722	15.035 ± 0.009	18.376, 19.036, 19.717	-3.822, -3.217:, -2.652	4.375, 4.503, 4.601	0.3, 5.8, 112.2
J005700+143737	2.54721	15.040 ± 0.010	18.458, 19.193, 19.872	-3.861, -3.265:, -2.638	4.397, 4.536, 4.641	0.4, 9.3, 175.1
J170100+641209	2.59668	15.043 ± 0.004	18.276, 18.968, 19.736	-3.738, -3.077:, -2.483	4.362, 4.493, 4.628	0.2, 3.6, 96.3
J121930+494052	2.47346	15.046 ± 0.004	19.933, 19.963, 19.994	-3.959, -3.931, -3.903	4.653, 4.657, 4.660	222.0, 253.8, 290.6
J130411+295348	2.57726	15.047 ± 0.009	18.325, 19.036, 19.753	-3.748, -3.128:, -2.520	4.369, 4.504, 4.630	0.2, 4.7, 102.6
J090033+421546	3.15992	15.054 ± 0.009	18.349, 19.029, 19.717	-3.808, -3.201:, -2.619	4.366, 4.498, 4.598	0.3, 5.5, 108.6
J113508+222715	2.74242	15.055 ± 0.009	18.413, 19.128, 19.824	-3.834, -3.222:, -2.610	4.384, 4.520, 4.627	0.3, 7.2, 147.5

Table 7 continued

Table 7 (continued)

QSO Name	z_{abs}	$\log N_{\text{HI}}$ [cm $^{-2}$]	$\log N_{\text{H}}$ [cm $^{-2}$]	$\log n_{\text{H}}$ [cm $^{-3}$]	$\log T$ [K]	l (kpc)
J171227+575507	2.81553	15.055 ± 0.004	17.869, 17.898, 17.942	-2.359, -2.326, -2.303	4.077, 4.086, 4.101	0.0, 0.1, 0.1
J014516-094517	2.58808	15.065 ± 0.001	18.969, 19.452, 20.018	-3.987, -3.473, -3.060	4.485, 4.575, 4.642	3.5, 27.2, 328.0
J135038-251216	2.57455	15.065 ± 0.004	18.544, 18.559, 18.574	-2.818, -2.804, -2.789	4.290, 4.293, 4.296	0.7, 0.7, 0.8
J130411+295348	2.75550	15.072 ± 0.007	20.135, 20.157, 20.179	-4.185, -4.164, -4.144	4.626, 4.627, 4.628	617.5, 678.6, 748.7
J074521+473436	3.12615	15.076 ± 0.003	18.637, 19.024, 19.384	-3.485, -3.177; -2.847	4.413, 4.488, 4.556	1.0, 5.1, 23.9
J143316+313126	2.77502	15.078 ± 0.002	18.764, 18.818, 18.869	-3.000, -2.960, -2.919	4.418, 4.438, 4.454	1.6, 1.9, 2.4
J121930+494052	2.52850	15.091 ± 0.003	18.807, 18.838, 18.869	-2.946, -2.921, -2.895	4.447, 4.454, 4.461	1.6, 1.9, 2.1
J014516-094517	2.70685	15.097 ± 0.001	19.337, 19.357, 19.382	-3.467, -3.449, -3.436	4.469, 4.477, 4.486	19.2, 20.7, 22.9
J143316+313126	2.92832	15.099 ± 0.001	19.651, 19.824, 19.977	-3.989, -3.857, -3.719	4.544, 4.586, 4.613	76.0, 155.6, 299.9
J121930+494052	2.22541	15.109 ± 0.005	20.535, 20.567, 20.595	-4.479, -4.449, -4.415	4.665, 4.667, 4.670	2893.6, 3364.9, 3837.5
J025905+001121	3.22368	15.113 ± 0.005	18.425, 19.107, 19.775	-3.821, -3.226; -2.643	4.369, 4.500, 4.594	0.4, 7.0, 127.9
J121930+494052	2.57078	15.114 ± 0.001	19.934, 20.072, 20.243	-4.163, -3.993, -3.872	4.625, 4.646, 4.652	207.3, 376.5, 825.9
J004530-261709	3.24823	15.120 ± 0.010	18.425, 19.099, 19.787	-3.829, -3.218; -2.642	4.365, 4.497, 4.591	0.4, 6.7, 133.5
J234628+124859	2.54133	15.122 ± 0.004	18.997, 19.423, 19.865	-3.784, -3.397; -3.032	4.477, 4.556, 4.627	3.5, 21.4, 145.0
J012156+144823	2.53765	15.124 ± 0.004	18.736, 18.798, 18.860	-2.918, -2.866, -2.812	4.422, 4.433, 4.445	1.1, 1.5, 1.9
J144453+291905	2.32985	15.128 ± 0.004	18.856, 18.864, 18.872	-2.999, -2.994, -2.988	4.331, 4.332, 4.334	2.3, 2.3, 2.4
J113418+574204	3.34514	15.134 ± 0.004	18.389, 19.056, 19.708	-3.758, -3.184; -2.613	4.355, 4.485, 4.581	0.3, 5.6, 94.7
J113418+574204	3.46347	15.136 ± 0.007	19.132, 19.201, 19.272	-3.396, -3.334, -3.274	4.489, 4.502, 4.516	8.3, 11.1, 15.1
J015741-010629	3.36274	15.145 ± 0.015	18.631, 19.336, 19.925	-3.996, -3.431; -2.819	4.392, 4.505, 4.579	0.9, 18.9, 271.2
J093643+292713	2.58243	15.152 ± 0.008	18.471, 19.172, 19.868	-3.757, -3.155; -2.556	4.377, 4.510, 4.630	0.3, 6.9, 136.6
J170100+641209	2.51255	15.152 ± 0.004	18.475, 19.146, 19.882	-3.760, -3.124; -2.550	4.379, 4.506, 4.635	0.3, 6.0, 141.9
J045213-164012	2.39910	15.161 ± 0.004	18.793, 19.021, 19.234	-3.260, -3.051, -2.839	4.396, 4.419, 4.438	1.4, 3.8, 10.1
J100841+362319	3.01081	15.161 ± 0.010	18.389, 19.070, 19.766	-3.726, -3.120; -2.535	4.355, 4.486, 4.599	0.3, 5.0, 100.7
J094202+042244	2.60246	15.167 ± 0.007	18.439, 19.140, 19.877	-3.755, -3.117; -2.518	4.368, 4.501, 4.628	0.3, 5.8, 138.7
J082107+310751	2.55652	15.177 ± 0.007	18.496, 19.205, 19.941	-3.798, -3.158; -2.552	4.377, 4.511, 4.635	0.4, 7.5, 178.2
J101447+430030	2.98705	15.188 ± 0.002	19.721, 19.899, 20.182	-4.114, -3.830; -3.668	4.581, 4.603, 4.617	79.2, 173.9, 641.2
J144453+291905	2.47417	15.209 ± 0.004	18.021, 18.097, 18.187	-2.370, -2.304, -2.248	4.092, 4.122, 4.156	0.1, 0.1, 0.1
J212912-153841	2.95558	15.220 ± 0.005	18.921, 19.327, 19.681	-3.594, -3.287; -2.940	4.440, 4.517, 4.580	2.4, 13.3, 61.0
J124610+303131	2.46655	15.224 ± 0.005	18.521, 19.221, 19.964	-3.763, -3.121; -2.523	4.373, 4.506, 4.637	0.4, 7.1, 172.8
J094202+042244	2.81325	15.226 ± 0.019	18.418, 18.659, 18.884	-2.957, -2.752, -2.547	4.265, 4.314, 4.347	0.3, 0.8, 2.2
J135038-251216	2.44516	15.235 ± 0.013	19.991, 20.011, 20.030	-3.818, -3.806, -3.794	4.627, 4.629, 4.631	198.5, 212.3, 227.5
J094202+042244	2.81450	15.242 ± 0.030	17.896, 18.015, 18.141	-2.311, -2.225, -2.149	4.069, 4.113, 4.154	0.0, 0.1, 0.1
J143316+313126	2.58814	15.254 ± 0.007	18.627, 19.271, 19.888	-3.685, -3.152; -2.602	4.387, 4.509, 4.619	0.5, 8.6, 121.6
J143316+313126	2.90645	15.271 ± 0.004	19.495, 19.519, 19.543	-3.452, -3.434, -3.416	4.501, 4.509, 4.516	26.4, 29.1, 32.0
J143316+313126	2.88759	15.276 ± 0.002	18.224, 18.611, 19.121	-3.059, -2.620; -2.284	4.294, 4.368, 4.463	0.1, 0.6, 4.9
J143316+313126	2.74931	15.280 ± 0.004	18.590, 19.292, 20.000	-3.788, -3.170; -2.570	4.373, 4.507, 4.621	0.5, 9.4, 198.8
J100841+362319	3.03460	15.301 ± 0.006	20.020, 20.195, 20.357	-4.189, -4.017, -3.855	4.591, 4.608, 4.614	243.4, 527.3, 1141.1
J083102+335803	2.41864	15.304 ± 0.016	18.623, 19.330, 20.010	-3.726, -3.140; -2.535	4.378, 4.511, 4.634	0.5, 9.6, 177.0
J134328+572147	2.79941	15.309 ± 0.010	18.668, 19.322, 19.952	-3.724, -3.177; -2.619	4.382, 4.506, 4.612	0.6, 10.2, 153.8
J093337+284532	3.37217	15.312 ± 0.022	18.581, 19.261, 19.953	-3.827, -3.211; -2.630	4.358, 4.490, 4.581	0.5, 9.7, 195.2
J010806+163550	2.48359	15.315 ± 0.010	19.872, 19.943, 19.992	-3.729, -3.701, -3.667	4.536, 4.582, 4.609	112.6, 142.6, 169.8
J101447+430030	2.84090	15.316 ± 0.003	19.934, 20.136, 20.366	-4.135, -3.906, -3.725	4.594, 4.621, 4.633	148.0, 357.0, 1026.7

Table 7 continued

Table 7 (continued)

QSO Name	z_{abs}	$\log N_{\text{H I}}$	$\log N_{\text{H}}$	$\log n_{\text{H}}$	$\log T$	l
		[cm $^{-2}$]	[cm $^{-2}$]	[cm $^{-3}$]	[K]	(kpc)
J064204+675835	3.06746	15.332 ± 0.006	18.494, 19.188, 19.940	-3.737, -3.083; -2.487	4.342, 4.475, 4.593	0.3, 6.0, 154.2
J162557+264448	2.53680	15.348 ± 0.013	18.651, 19.347, 20.098	-3.783, -3.131; -2.534	4.375, 4.506, 4.634	0.5, 9.7, 246.9
J100841+362319	3.10854	15.356 ± 0.006	19.452, 19.487, 19.517	-3.360, -3.340, -3.319	4.492, 4.510, 4.522	19.1, 21.8, 24.3
J020950-000506	2.64137	15.360 ± 0.003	19.580, 19.605, 19.621	-3.497, -3.483, -3.458	4.403, 4.406, 4.409	35.4, 39.6, 42.5
J094202+042244	2.84851	15.363 ± 0.008	19.101, 19.480, 19.813	-3.576, -3.285, -2.960	4.441, 4.511, 4.570	3.7, 18.9, 79.4
J160455+381201	2.53794	15.368 ± 0.005	19.760, 19.777, 19.795	-3.513, -3.498, -3.484	4.560, 4.563, 4.566	56.8, 61.1, 65.8
J014516-094517	2.69212	15.395 ± 0.001	18.690, 19.469, 20.226	<-4.047, <-3.213; <-2.363	4.371, 4.519, 4.631	0.6, 15.6, 413.9
J170100+641209	2.43979	15.402 ± 0.004	19.844, 19.852, 19.860	-3.541, -3.535, -3.530	4.554, 4.555, 4.557	76.8, 79.0, 81.4
J155152+191104	2.69270	15.411 ± 0.002	18.204, 18.268, 18.337	-2.300, -2.242, -2.191	4.175, 4.195, 4.212	0.1, 0.1, 0.1
J014516-094517	2.66911	15.412 ± 0.001	18.702, 19.472, 20.191	-3.828, -3.197; -2.539	4.370, 4.516, 4.629	0.6, 15.1, 339.0
J030341-002321	3.15168	15.436 ± 0.004	18.887, 19.530, 20.045	-3.752, -3.300; -2.750	4.395, 4.516, 4.595	1.4, 21.9, 203.0
J030341-002321	3.10354	15.449 ± 0.010	18.804, 19.450, 20.136	-3.818, -3.210; -2.659	4.378, 4.501, 4.602	0.9, 14.8, 291.3
J171227+575507	2.97141	15.454 ± 0.002	18.709, 18.721, 18.732	-2.702, -2.693, -2.684	4.198, 4.201, 4.204	0.8, 0.8, 0.9
J095852+120245	3.15768	15.491 ± 0.002	18.753, 19.413, 20.099	-3.751, -3.151; -2.587	4.359, 4.486, 4.594	0.7, 11.9, 229.1
J100841+362319	3.07200	15.502 ± 0.009	19.799, 19.819, 19.845	-3.557, -3.540, -3.528	4.483, 4.489, 4.497	68.9, 74.2, 81.6
J010311+131617	2.55216	15.505 ± 0.007	19.588, 19.613, 19.633	-3.245, -3.233; -3.219	4.502, 4.514, 4.523	20.8, 22.7, 24.4
J170100+641209	2.37993	15.507 ± 0.005	19.586, 19.593, 19.600	-3.233, -3.230, -3.227	4.461, 4.463, 4.465	21.1, 21.6, 22.0
J143316+313126	2.61282	15.516 ± 0.004	19.440, 19.702, 19.937	-3.527, -3.319, -3.090	4.472, 4.514, 4.556	11.0, 34.0, 94.2
J212912-153841	3.04863	15.538 ± 0.007	18.807, 19.493, 20.187	-3.768, -3.161; -2.575	4.362, 4.493, 4.602	0.8, 14.6, 292.8
J143316+313126	2.73377	15.552 ± 0.004	19.376, 19.722, 20.056	-3.598, -3.309; -3.012	4.461, 4.525, 4.584	7.9, 34.8, 145.6
J142438+225600	3.56653	15.556 ± 0.001	19.237, 19.550, 19.852	-3.538, -3.278; -3.012	4.432, 4.494, 4.550	5.8, 21.8, 79.5
J121930+494052	2.54882	15.572 ± 0.003	20.120, 20.125, 20.130	-3.621, -3.618, -3.615	4.593, 4.593, 4.594	176.0, 179.3, 182.7
J143316+313126	2.90184	15.598 ± 0.014	19.360, 19.396, 19.432	-3.038, -3.012, -2.986	4.447, 4.457, 4.465	7.2, 8.3, 9.5
J131215+423900	2.41504	15.598 ± 0.008	19.837, 19.900, 19.962	-3.428, -3.377, -3.325	4.543, 4.556, 4.569	47.1, 61.3, 79.4
J104018+572448	3.36421	15.603 ± 0.009	20.435, 20.449, 20.462	-4.041, -4.032, -4.022	4.592, 4.593, 4.594	932.8, 979.9, 1028.9
J003501-091817	2.35342	15.610 ± 0.045	18.903, 19.624, 20.368	-3.762, -3.119; -2.505	4.373, 4.508, 4.641	0.8, 17.9, 440.8
J082107+310751	2.55190	15.612 ± 0.005	20.027, 20.178, 20.336	-3.772, -3.643, -3.526	4.537, 4.578, 4.614	115.7, 214.4, 414.8
J130411+295348	2.57585	15.618 ± 0.008	18.307, 18.373, 18.438	-2.132, -2.076, -2.020	4.240, 4.253, 4.265	0.1, 0.1, 0.1
J144453+291905	2.55484	15.618 ± 0.001	19.362, 19.385, 19.409	-2.952, -2.932, -2.912	4.454, 4.459, 4.463	6.1, 6.7, 7.4
J093643+292713	2.69883	15.620 ± 0.018	19.296, 19.395, 19.482	-3.049, -2.971, -2.886	4.429, 4.444, 4.455	4.9, 7.5, 11.0
J010311+131617	2.54303	15.621 ± 0.002	20.065, 20.210, 20.349	-3.766, -3.649, -3.531	4.562, 4.595, 4.623	128.0, 233.8, 423.3
J143316+313126	2.90227	15.642 ± 0.010	19.540, 19.782, 19.978	-3.476, -3.306, -3.098	4.473, 4.517, 4.552	14.1, 39.6, 92.2
J030341-002321	2.93700	15.648 ± 0.006	18.950, 19.721, 20.467	-3.906, -3.242; -2.584	4.369, 4.517, 4.619	1.1, 29.8, 764.7
J144453+291905	2.37869	15.668 ± 0.004	20.487, 20.619, 20.747	-4.065, -3.942, -3.821	4.644, 4.661, 4.670	659.3, 1178.6, 2100.4
J002127-020333	2.54918	15.680 ± 0.021	19.115, 19.555, 20.007	-3.413, -3.033, -2.661	4.382, 4.468, 4.559	1.9, 12.5, 85.3
J173352+540030	3.30295	15.723 ± 0.003	20.709, 20.842, 20.940	-4.444, -4.315, -4.158	4.536, 4.571, 4.598	2385.3, 4655.2, 7840.0
J193957-100241	3.61935	15.727 ± 0.001	19.142, 19.375, 19.629	-3.237, -3.013, -2.813	4.352, 4.397, 4.441	2.9, 7.9, 23.8
J094202+042244	2.81407	15.730 ± 0.011	19.062, 19.145, 19.213	-2.771, -2.710, -2.637	4.325, 4.337, 4.344	1.6, 2.3, 3.1
J104018+572448	3.32379	15.743 ± 0.014	19.169, 19.580, 19.969	-3.533, -3.155, -2.787	4.342, 4.402, 4.426	2.9, 17.6, 103.3
J025905+001121	3.30796	15.744 ± 0.012	19.608, 19.638, 19.669	-3.196, -3.173, -3.150	4.445, 4.450, 4.456	18.6, 21.0, 23.7
J222256-094636	2.87419	15.755 ± 0.015	19.008, 19.658, 20.295	-3.632, -3.086; -2.532	4.359, 4.484, 4.598	1.1, 18.0, 273.3
J004530-261709	3.36517	15.770 ± 0.015	19.242, 19.977, 20.584	-3.984, -3.417; -2.796	4.394, 4.530, 4.600	3.5, 80.5, 1202.6

Table 7 continued

Table 7 (continued)

QSO Name	z_{abs}	$\log N_{\text{HI}}$ [cm $^{-2}$]	$\log N_{\text{H}}$ [cm $^{-2}$]	$\log n_{\text{H}}$ [cm $^{-3}$]	$\log T$ [K]	l (kpc)
J020950-000506	2.76903	15.773 ± 0.002	19.015, 19.606, 20.248	-3.559, -3.011:, -2.506	4.359, 4.472, 4.591	1.1, 13.4, 207.8
J173352+540030	3.20694	15.790 ± 0.004	18.455, 18.777, 19.155	-2.684, -2.360, -2.083	4.231, 4.295, 4.369	0.1, 0.4, 2.2
J104018+572448	3.27747	15.803 ± 0.009	19.802, 19.834, 19.866	-3.331, -3.306, -3.280	4.444, 4.451, 4.459	39.3, 44.6, 50.9
J064204+675835	3.01338	15.819 ± 0.004	19.167, 19.847, 20.555	-3.830, -3.207:, -2.633	4.376, 4.510, 4.620	2.0, 36.7, 785.7
J212912-153841	3.21670	15.852 ± 0.004	19.516, 19.572, 19.620	-3.035, -2.993, -2.945	4.422, 4.432, 4.439	9.4, 11.9, 14.7
J093643+292713	2.40065	15.852 ± 0.009	19.970, 19.983, 19.995	-3.350, -3.344, -3.338	4.382, 4.384, 4.387	66.2, 68.8, 71.4
J094202+042244	3.09385	15.855 ± 0.001	19.367, 20.144, 20.741	-3.992, -3.439:, -2.784	4.406, 4.555, 4.622	4.6, 124.1, 1751.7
J093643+292713	2.54337	15.863 ± 0.009	19.199, 19.858, 20.539	-3.700, -3.116:, -2.556	4.379, 4.504, 4.627	1.8, 30.5, 561.7
J143316+313126	2.58177	15.877 ± 0.002	19.663, 20.127, 20.657	-3.799, -3.337:, -2.943	4.463, 4.553, 4.639	13.1, 94.4, 925.1
J064204+675835	2.86842	15.894 ± 0.006	19.111, 19.825, 20.608	-3.778, -3.100:, -2.496	4.353, 4.492, 4.624	1.3, 27.3, 784.2
J130411+295348	2.79811	15.897 ± 0.005	19.428, 20.180, 20.798	-3.962, -3.392:, -2.755	4.413, 4.549, 4.630	4.9, 121.1, 1872.0
J074749+443417	4.35301	15.902 ± 0.011	19.226, 19.886, 20.509	-3.926, -3.374:, -2.826	4.352, 4.490, 4.582	3.6, 59.0, 886.8
J121930+494052	2.62063	15.903 ± 0.002	19.710, 19.725, 19.738	-3.024, -3.012, -2.998	4.434, 4.436, 4.437	16.5, 17.7, 18.7
J010806+163550	2.50561	15.914 ± 0.004	19.188, 19.499, 19.805	-3.025, -2.765, -2.497	4.364, 4.422, 4.479	1.6, 6.0, 21.9
J143316+313126	2.89093	15.930 ± 0.003	20.727, 20.732, 20.738	-3.871, -3.868, -3.864	4.634, 4.634, 4.635	1264.5, 1289.9, 1315.3
J081240+320808	2.58869	15.931 ± 0.010	18.974, 19.616, 20.423	-3.541, -2.856:, -2.305	4.324, 4.444, 4.599	0.6, 9.6, 298.4
J101447+430030	3.11460	15.974 ± 0.001	19.686, 19.770, 19.844	-3.094, -3.031, -2.958	4.439, 4.455, 4.468	14.3, 20.5, 28.1
J093643+292713	2.59624	16.009 ± 0.007	19.785, 19.861, 19.934	-3.069, -3.006, -2.942	4.451, 4.465, 4.478	17.3, 23.9, 32.6
J121930+494052	2.47816	16.021 ± 0.004	19.883, 19.889, 19.895	-3.058, -3.054, -3.051	4.422, 4.423, 4.424	27.9, 28.5, 29.0
J104018+572448	3.34454	16.053 ± 0.009	18.986, 19.399, 19.842	-3.049, -2.676:, -2.322	4.290, 4.366, 4.457	0.7, 3.8, 25.3
J142438+225600	3.53989	16.064 ± 0.003	18.179, 18.182, 18.185	-1.679, -1.676, -1.674	4.092, 4.093, 4.094	0.0, 0.0, 0.0
J143316+313126	2.64432	16.117 ± 0.003	19.876, 19.902, 19.930	-2.963, -2.940, -2.917	4.458, 4.463, 4.469	20.1, 22.5, 25.3
J142438+225600	3.44848	16.132 ± 0.006	19.568, 19.582, 19.596	-2.791, -2.781, -2.771	4.380, 4.382, 4.384	7.1, 7.5, 7.9
J010925-210257	3.14253	16.147 ± 0.013	18.901, 19.552, 20.295	-3.290, -2.688:, -2.126	4.266, 4.385, 4.551	0.3, 5.6, 124.6
J014516-094517	2.66513	16.156 ± 0.001	19.823, 19.893, 19.966	-2.960, -2.899, -2.840	4.440, 4.454, 4.469	14.9, 20.1, 27.3
J030341-002321	2.95653	16.161 ± 0.010	20.240, 20.272, 20.295	-3.304, -3.287, -3.259	4.492, 4.495, 4.498	102.6, 117.3, 128.3
J093643+292713	2.41258	16.169 ± 0.089	18.878, 19.480, 20.078	-3.003, -2.508:, -1.993	4.268, 4.375, 4.493	0.2, 3.2, 38.5
J030341-002321	2.99495	16.170 ± 0.004	19.545, 19.636, 19.723	-2.799, -2.726, -2.650	4.370, 4.387, 4.404	5.1, 7.5, 10.8
J143316+313126	2.90116	16.176 ± 0.003	18.934, 18.989, 19.052	-2.204, -2.149, -2.102	4.259, 4.269, 4.281	0.4, 0.4, 0.6
J094202+042244	2.72984	16.183 ± 0.005	20.116, 20.123, 20.134	-3.228, -3.226, -3.224	4.346, 4.348, 4.350	71.1, 72.4, 74.1
J160843+071508	2.42219	16.211 ± 0.015	18.787, 18.805, 18.822	-1.950, -1.945, -1.939	4.163, 4.167, 4.171	0.2, 0.2, 0.2
J155152+191104	2.69478	16.253 ± 0.002	20.019, 20.026, 20.033	-2.935, -2.930, -2.925	4.457, 4.458, 4.459	28.5, 29.3, 30.1
J134328+572147	2.87056	16.254 ± 0.009	20.415, 20.429, 20.445	-3.367, -3.362, -3.357	4.465, 4.468, 4.472	192.1, 200.2, 209.4
J012156+144823	2.66593	16.259 ± 0.023	18.960, 18.984, 19.008	-2.194, -2.192, -2.190	4.189, 4.193, 4.198	0.5, 0.5, 0.5
J134544+262506	2.86367	16.267 ± 0.008	19.330, 19.377, 19.423	-2.445, -2.406, -2.368	4.304, 4.313, 4.322	1.6, 2.0, 2.4
J234856-104131	3.15981	16.287 ± 0.006	19.749, 20.012, 20.238	-3.132, -2.950, -2.734	4.393, 4.450, 4.500	9.9, 29.6, 76.0
J170100+641209	2.43307	16.288 ± 0.008	19.208, 19.218, 19.226	-2.235, -2.232, -2.229	4.291, 4.292, 4.293	0.9, 0.9, 0.9
J135038-251216	2.57299	16.319 ± 0.007	19.519, 19.591, 19.668	-2.552, -2.487, -2.427	4.349, 4.362, 4.378	2.9, 3.9, 5.4
J102009+104002	3.05498	16.330 ± 0.041	19.138, 19.198, 19.295	-2.339, -2.325, -2.312	4.278, 4.284, 4.291	0.9, 1.1, 1.4
J095852+120245	3.09691	16.349 ± 0.035	19.622, 19.970, 20.255	-3.075, -2.849, -2.564	4.357, 4.431, 4.497	4.9, 21.4, 69.2
J130411+295348	2.82924	16.378 ± 0.004	19.144, 19.805, 20.558	-3.244, -2.644:, -2.080	4.271, 4.395, 4.570	0.5, 9.1, 206.0
J170100+641209	2.43359	16.401 ± 0.006	19.269, 19.278, 19.287	-2.148, -2.144, -2.141	4.274, 4.275, 4.276	0.8, 0.9, 0.9

Table 7 continued

Table 7 (continued)

QSO Name	z_{abs}	$\log N_{\text{HI}}$ [cm $^{-2}$]	$\log N_{\text{H}}$ [cm $^{-2}$]	$\log n_{\text{H}}$ [cm $^{-3}$]	$\log T$ [K]	l (kpc)
J173352+540030	3.28216	16.476 ± 0.003	20.031, 20.218, 20.393	-3.107, -2.969, -2.818	4.413, 4.455, 4.496	22.9, 49.9, 102.3
J120006+312630	2.87577	16.561 ± 0.021	19.735, 19.769, 19.802	-2.491, -2.474, -2.456	4.329, 4.334, 4.339	5.1, 5.7, 6.3
J101447+430030	3.01439	16.681 ± 0.003	21.994, 21.995, 21.997	-4.500, -4.500, -4.500	4.695, 4.695, 4.696	100916.0, 101284.1, 101680.1
J074521+473436	3.05358	16.726 ± 0.013	20.708, 21.000, 21.353	-3.651, -3.348:, -3.115	4.507, 4.571, 4.630	215.5, 721.4, 3288.5
J074521+473436	3.03515	16.727 ± 0.014	20.365, 20.535, 20.688	-3.093, -2.974, -2.839	4.429, 4.466, 4.501	51.9, 104.7, 195.7
J171227+575507	2.88991	16.735 ± 0.005	19.687, 19.762, 19.859	-2.387, -2.305, -2.240	4.296, 4.310, 4.328	2.7, 3.8, 5.7
J020950-000506	2.57449	16.777 ± 0.003	20.308, 20.337, 20.368	-2.741, -2.716, -2.693	4.398, 4.404, 4.410	32.4, 36.7, 41.7
J131215+423900	2.48998	16.796 ± 0.005	20.162, 20.242, 20.312	-2.655, -2.598, -2.533	4.377, 4.394, 4.408	16.1, 22.4, 30.0
J144453+291905	2.46741	16.802 ± 0.002	19.945, 19.960, 19.973	-2.370, -2.359, -2.347	4.332, 4.335, 4.337	6.4, 6.7, 7.1
J142438+225600	3.38281	16.984 ± 0.100	20.620, 20.716, 20.812	-3.012, -3.002, -2.993	4.426, 4.433, 4.440	135.9, 169.8, 211.5
J094202+042244	2.73088	17.102 ± 0.005	20.107, 20.574, 20.814	-2.982, -2.737, -2.315	4.234, 4.288, 4.312	8.6, 66.2, 203.1
J095852+120245	3.09623	17.146 ± 0.056	19.561, 20.067, 20.530	<-2.756, <-2.260:, <-1.681	4.212, 4.284, 4.362	0.8, 6.9, 49.7
J025905+001121	3.08465	17.250 ± 0.250	20.306, 20.570, 20.808	-2.722, -2.642, -2.570	4.331, 4.346, 4.363	26.1, 54.2, 104.1
J012156+144823	2.66416	17.260 ± 0.100	21.231, 21.244, 21.283	-3.141, -3.116, -3.060	4.367, 4.371, 4.379	697.8, 748.6, 809.4
J102009+104002	3.05421	17.268 ± 0.015	20.510, 20.554, 20.599	-2.614, -2.577, -2.541	4.331, 4.339, 4.346	36.5, 43.8, 52.9
J101723-204658	2.45051	17.284 ± 0.107	20.001, 20.094, 20.198	-2.226, -2.211, -2.197	4.290, 4.293, 4.295	5.2, 6.5, 8.5
J222256-094636	2.86475	17.300 ± 0.125	20.241, 20.655, 21.145	-3.020, -2.614, -2.266	4.276, 4.348, 4.439	10.6, 60.1, 473.1
J212912-153841	2.96755	17.339 ± 0.097	20.129, 20.227, 20.321	-2.335, -2.321, -2.308	4.293, 4.296, 4.298	9.0, 11.4, 14.5
J101155+294141	2.50364	17.355 ± 0.001	20.511, 20.520, 20.529	-2.417, -2.409, -2.402	4.325, 4.326, 4.328	26.5, 27.5, 28.6
J095852+120245	3.22317	17.356 ± 0.003	21.488, 21.502, 21.516	-3.360, -3.348, -3.336	4.486, 4.489, 4.491	2160.6, 2292.1, 2430.5
J025905+001121	3.08204	17.500 ± 0.250	19.851, 20.323, 20.736	<-2.710, <-2.275:, <-1.763	4.214, 4.275, 4.340	1.8, 12.9, 70.4
J162557+264448	2.55094	17.750 ± 0.100	19.972, 20.018, 20.055	-2.084, -2.074, -2.065	4.242, 4.245, 4.247	3.5, 4.0, 4.4
J101155+294141	2.42901	17.750 ± 0.150	18.977, 19.001, 19.123	-2.208, -2.204, -2.194	4.108, 4.114, 4.148	0.5, 0.5, 0.7
J134328+572147	2.83437	17.780 ± 0.300	20.155, 20.180, 20.204	-1.791, -1.770, -1.749	4.158, 4.161, 4.164	2.6, 2.9, 3.2
J143316+313126	2.58591	18.150 ± 0.150	18.934, 19.000, 19.137	>-1.136, >-1.095, >-1.071	4.119, 4.121, 4.124	0.0, 0.0, 0.1
J064204+675835	2.90469	18.420 ± 0.225	21.247, 22.375, 22.657	-4.088, -3.803, -2.787	4.284, 4.413, 4.419	347.4, 48767.9, 180386.5
J104018+572448	3.26628	18.600 ± 0.200	20.556, 20.578, 20.601	-2.198, -2.178, -2.159	4.199, 4.201, 4.204	16.8, 18.5, 20.4
J030341-002321	2.94069	18.650 ± 0.225	21.060, 21.228, 21.348	-2.845, -2.749, -2.620	4.299, 4.319, 4.335	154.9, 307.0, 506.4
J012156+144823	2.66241	19.100 ± 0.350	19.220, 19.278, 19.340	-0.828, -0.770, -0.710	4.018, 4.025, 4.031	0.0, 0.0, 0.0
J080117+521034	3.04464	19.250 ± 0.250	20.903, 21.606, 22.348	-3.726, -3.075:, -2.460	4.264, 4.380, 4.482	74.7, 1552.4, 38417.4
J033900-013318	3.11542	19.600 ± 0.050	20.657, 20.792, 20.935	-2.497, -2.361, -2.234	4.200, 4.221, 4.244	25.2, 46.1, 87.6
J004530-261709	2.81907	19.660 ± 0.010	19.683, 19.693, 19.703	>-0.086, >-0.025, >-0.004	3.295, 3.347, 3.397	0.0, 0.0, 0.0
J080117+521034	3.04028	19.690 ± 0.150	21.310, 21.323, 21.331	-2.821, -2.814, -2.803	4.313, 4.315, 4.316	420.4, 443.7, 459.5
J100841+362319	2.94749	19.725 ± 0.002	20.519, 20.524, 20.529	-2.047, -2.042, -2.036	4.169, 4.170, 4.171	11.6, 11.9, 12.2
J030341-002321	2.44326	19.866 ± 0.010	20.577, 20.585, 20.592	-2.005, -1.997, -1.990	4.166, 4.167, 4.169	12.0, 12.4, 12.8

NOTE— The lower and upper bounds for each quantity represent the 68% CI, while the middle value is the median value. When a colon is present after the median value of $\log n_{\text{H}}$, this implies that a log U Gaussian prior was used to determine the properties of the absorber (see §5.2).

Table 8. Statistical Physical Properties of the Absorbers

Absorber Type	$\widetilde{\log N_{\text{HI}}}$ [cm $^{-2}$]	$\overline{\log N_{\text{HI}}}$ [cm $^{-2}$]	$\widetilde{\log n_{\text{H}}}$ [cm $^{-3}$]	$\overline{\log n_{\text{H}}}$ [cm $^{-3}$]	$\widetilde{\log N_{\text{H}}}$ [cm $^{-2}$]	$\overline{\log N_{\text{H}}}$ [cm $^{-2}$]	$\widetilde{\log l}$ [kpc]	$\overline{\log l}$ [kpc]	$\widetilde{\log T}$ [K]	$\overline{\log T}$ [K]
Entire sample										
SLFs	15.36	15.41 ± 0.42	-3.23	-3.25 ± 0.57	19.59	19.47 ± 0.68	1.31	1.23 ± 1.19	4.46	4.46 ± 0.14
pLLSs	16.40	16.52 ± 0.27	-2.60	-2.69 ± 0.54	19.97	19.95 ± 0.70	1.33	1.15 ± 1.21	4.36	4.37 ± 0.11
LLSs	18.10	17.97 ± 0.43	-2.56	-2.55 ± 0.50	20.78	20.80 ± 0.64	1.86	1.85 ± 1.12	4.29	4.29 ± 0.09
SLLSs	19.58	19.50 ± 0.31	-2.25	-2.26 ± 0.76	20.69	20.80 ± 0.68	1.41	1.57 ± 1.43	4.19	4.19 ± 0.15
Restricted sample without the $\log U$ constraint										
SLFs	15.30	15.35 ± 0.42	-3.20	-3.22 ± 0.44	19.41	19.38 ± 0.58	1.05	1.12 ± 0.94	4.50	4.48 ± 0.11
pLLSs	16.44	16.55 ± 0.28	-2.62	-2.70 ± 0.53	19.99	19.99 ± 0.60	1.14	1.20 ± 1.19	4.38	4.38 ± 0.11
LLSs	18.10	17.96 ± 0.42	-2.56	-2.55 ± 0.49	20.80	20.80 ± 0.63	1.86	1.86 ± 1.10	4.29	4.30 ± 0.08
SLLSs	19.54	19.49 ± 0.31	-2.26	-2.28 ± 0.75	20.71	20.81 ± 0.68	1.46	1.60 ± 1.42	4.20	4.19 ± 0.15

NOTE—The tilde and bar above each parameter represent the median and mean (with the standard deviation), respectively, of the logarithmic values of the parameter. The entire sample consists of 321 absorbers: 155 SLFs, 24 pLLSs, 62 LLSs, and 80 SLLSs. The restricted sample without the $\log U$ constraint contains 243 absorbers (i.e., absorbers that were modeled with a flat prior on $\log U$): 85 SLFs, 21 pLLSs, 59 LLSs, and 78 SLLSs. Note that N_{HI} is estimated directly from the data, while all other quantities are estimated from our photoionization modeling. We include the results from the HD-LLS survey for the LLSs and SLLSs.

Table 9. Metallicity statistics of the FOGGIE absorbers at $2 \leq z \leq 3$

Abs. Type	$\widetilde{[X/H]}$	$\overline{[X/H]}$	IQR
SLFs _s	-2.43	-2.87 ± 1.68	[-3.22, -1.86]
pLLs _s	-1.98	-2.13 ± 1.09	[-2.49, -1.56]
LLs _s	-1.62	-1.73 ± 0.92	[-2.10, -1.18]
SLLs _s	-1.41	-1.45 ± 0.76	[-1.87, -0.96]
DLA	-0.96	-1.19 ± 1.00	[-1.57, -0.60]

NOTE—The tilde and bar above [X/H] represent the median and mean (with the standard deviation), respectively.